UNIVERSITA DEGLI STUDI

DI MODENA E REGGIO EMILIA

in convenzione con l'Università degli Studi di Parma

Dottorato di ricerca in NEUROSCIENZE

Ciclo XXXIV

Advanced Multimodal Neuroimaging in Epilepsy

Candidato: Francesca Talami

Relatore (Tutor): Prof. Stefano Meletti

Correlatore: Dott.ssa Anna Vaudano

Coordinatore del Corso di Dottorato: Prof. Sandro Rubichi

ABSTRACT

This PhD thesis titled "Multimodal Neuroimaging in Epilepsy" focuses on the use of multimodal neuroimaging techniques, namely simultaneous EEG-fMRI, in the study of epilepsy.

The first section of the thesis provides a literature review to multimodal neuroimaging. In particular, Chapters 2 and 3 cover the principles and methods of EEG and fMRI, including statistical analysis and functional connectivity, while Chapter 4 discusses the integration of EEG and fMRI focusing in particular on EEG-informed fMRI analysis.

The second section of the thesis is focused on epilepsy, including its epidemiology, classification, clinical aspects, and treatment. Chapters 6 and 7 are a brief introduction on temporal lobe epilepsy and benign rolandic epilepsy with center-temporal spikes (SeLECTS), respectively, covering the electrophysiology, neuroimaging, and treatment of each disorder. Chapter 8 discusses epilepsy surgery and the pre-surgical evaluation process.

The third and final section of the thesis presents three experimental studies. Chapter 9 examines the effect of temporal lobe spikes on intrinsic connectivity networks (ICN), suggesting the use of EEG–fMRI co-registration for TLE patients, not only for localizing purposes but also to investigate ICN alterations.

Chapter 10 explores fMRI-based effective connectivity in surgical remediable epilepsies providing preliminary evidence to support the applicability of DCM on fMRI data to investigate the epileptic networks and, particularly, to identify the EZ in complex cases.

Lastly, Chapter 11 investigates the influence of wakefulness on the brain networks involved in centrotemporal spike generation in SeLECTS. Overall, this thesis provides valuable insights into the use of multimodal neuroimaging techniques in the study of epilepsy, including the potential for more precise localization of epileptic foci and improved surgical outcomes.

***

In questa tesi, intitolata "Neuroimaging Avanzato Multimodale nello Studio dell'Epilessia", è un approfondimento sull'uso di tecniche di neuroimaging multimodali, in particolare co-registrazioni simultanee di EEG-fMRI, nello studio dell'epilessia.

La prima sezione della tesi fornisce una rassegna della letteratura sul neuroimaging multimodale. In particolare, i capitoli 2 e 3 trattano i principi e i metodi dell'EEG e della fMRI, compresa l'analisi statistica e la connettività funzionale e effettiva, mentre il capitolo 4 discute delle tecniche di integrazione dei dati EEG e fMRI, concentrandosi in particolare sull'analisi dei dati fMRI a partire dalle informaioni fornite dall'EEG.

La seconda sezione è un'introduzione al macro-tema dell''epilessia, compresa la sua epidemiologia, la classificazione, gli aspetti clinici e il trattamento. I capitoli 6 e 7 sono una breve introduzione all'epilessia del lobo temporale e alla Self Limited Epilepsy with Cetrotemporal Spikes (SeLECTS), rispettivamente, e trattano l'elettrofisiologia, le neuroimmagini e il trattamento di ciascun disturbo. Il capitolo 8, invece presenta una rapida disamina del percorso di valutazione prechirurgica delle epilessie farmaco-resistenti.

La terza e ultima sezione della tesi presenta tre studi sperimentali. Il capitolo 9 esamina l'effetto delle anomalie epilettiche su Intrinsic Connectivity Networks (ICN), suggerendo l'utilità delle coregistrazioni EEG-fMRI per i pazienti affetti da TLE, non solo a scopi localizzatori nella valutazione prechirurgica, ma anche per indagare le alterazioni di ICNs.

Il capitolo 10 esplora la connettività effettiva dei dati di fMRI nelle epilessie rimediabili chirurgicamente, fornendo prove preliminari a sostegno dell'applicabilità della DCM sui dati fMRI per indagare le reti epilettiche e, in particolare, per identificare l'EZ nei casi complessi.

Infine, il Capitolo 11 indaga l'influenza delle oscillazioni dello stato di veglia sulle reti cerebrali coinvolte nella generazione di spike centrotemporali in pazienti SeLECTS. Nel complesso, questa tesi fornisce preziose indicazioni sull'uso di tecniche di neuroimaging multimodale nello studio dell'epilessia, compreso il potenziale per una localizzazione più precisa dei focolai epilettici e un miglioramento dei risultati chirurgici.

TABLE OF CONTENTS

LIST OF ABBREVIATIONS

ATLR	Anterior Temporal Lobe Resection
BCG	Ballistocardiogram
BECTS	Benign Epilepsy with Centro-Temporal Spikes
BOLD	Blood Oxygenation Level Dependent
CBF	Cerebral Blood Flow
CBV	Cerebral Blood Volume
CMRO2	Cerebral Metabolic Rate of Oxygen
CT	Computerised Tomography
DCM	Dynamic Causal Modelling
DMN	Default Mode Network
ECG	Electrocardiogram
EEG	Electroencephalography
EIT	Electrical Impedance Tomography
ERP	Event-Related Potentials
EZ	Epileptic Zone
FE	Frequency Encoding
FWE	Family Wise Error
FIR	Finite Impulse Response
fMRI	Functional Magnatic Resonance Imaging
GLM	General Linear Model
HRF	Haemodynamic Response Function
HS	Hippocampal Sclerosis
ICA	Independent Component Analysis
ICN	Intrinsically Connected Networks
IED	Inter-ictal Epileptic Discharge
LFPs	Local Field Potentials
MEG	Magnetoencephalography

MRI	Magnetic Resonance Imaging
NIRS	Near Infrared Spectroscopy
PE	Phase Encoding
PET	Positron Emission Tomography
PPI	Psychophysiological Interaction
(E/I) PSP	(Excitatory/Inhibitory) Postsynaptic Potentials
N/REM	Non/Rapid Eye Movement
RF	Radiofrequency
RSN	Resting State Networks
SS	Slice Selection
SUDEP	Sudden Unexpected Death in Epilepsy
TE	Echo Time
TLE	Temporal Lobe Epilepsy
TMS	Transcranial Magnetic Stimulation
TR	Repetition Time

ACKNOWLEDGMENTS

I would like to express my deepest gratitude to my PhD supervisor Professor Stefano Meletti for his guidance and mentorship. I am grateful for the opportunity to learn from his vast knowledge, brilliant insight and clarity of thought.

I am extremely grateful to Dott.ssa Anna Elisabetta Vaudano for teaching me something new every day and being a continuing source of inspiration, not only for her indefatigable dedication to science, but also for her kindness, generosity and strength of character. I am lucky to say that without her I wouldn't be the person I am today.

I am also grateful to Professor Louis Lemieux for his prompt and invaluable advice on all my projects, for his wittiness and expertise.

I am greatly indebted to all patients, controls and friends who generously participated to the experiments and to all the staff, dotctors and researchers that made the research possible. Dott.ssa Alice Ballerini, dott.ssa Simona Scolastico, dott.ssa Elisa Micalizzi, dott.ssa Giada Giovannini, dott.ssa Alessandra Arriatti, dott.ssa Giulia Turchi and dott.ssa Daniela Ballotta, thanks for making my time at Ospedale Civile di Baggiovara rewarding and enjoyable.

I am particularly grateful to my parents, Andrea e Chiara, my brother Marco and my sister Sofia for nurturing my curiosity and their constant encouragement.

Finally, Jacopo and Ada for being my home and solace.

FUNDING

This work was supported by a grant Dipartimenti di eccellenza 2018-2022, MIUR, Italy, to the Department of Biomedical, Metabolic and Neural Sciences.
The studies “Temporal Lobe Spikes Affect Distant Intrinsic Connectivity Networks” in Chapter 10 and “fMRI-Based Effective Connectivity in Surgical Remediable Epilepsies: A Pilot Study” in Chapter 11 were also supported by Finalizzata, project codeNET-2013-02355313, Ministry of Health to the Azienda Ospedaliera-Universitaria di Modena Centro hub chirurgia epilessia (DGR 1172/18).

LIST OF TABLES

LIST OF FIGURES

PUBLICATIONS

The studies reported in Chapter 9 and 10 have been published in international peer-reviewed journals:

- Vaudano AE, Mirandola L, Talami F, Giovannini G, Monti G, Riguzzi P, Volpi L, Michelucci R, Bisulli F, Pasini E, Tinuper P, Di Vito L, Gessaroli G, Malagoli M, G. Pavesi G, Cardinale F, Tassi, Lemieux LL, Meletti S (2021) fMRI-Based Effective Connectivity in Surgical Remediable Epilepsies: A Pilot Study. Brain Topography 34:632–650 https://doi.org/10.1007/s10548-021-00857-x

- Mirandola L, Ballotta D, Talami F, Giovannini G, Pavesi G, Vaudano AE, Meletti S (2021) Temporal lobe spikes affect distant intrinsic connectivity networks. Frontiers in Neurology 21: 746468. 10.3389/fneur.2021.746468

SECTION I: MULTIMODAL NEUROIMAGING

Chapter 1: Multimodal Neuroimaging

1.1. INTRODUCTION

The human brain is a highly complex systems and cannot be understood by studying changes in a single observable physiological parameter. The exploration of brain activity requires the integration of various observations, methodologies and parameters. Multimodal neuroimaging has emerged as a way to combine different physiological data acquired from different types of instruments and answer questions about brain activity.

As perfectly summarized by Lemieux, Villringer and Mulert: “multimodal imaging should allow the investigator to address the question: what happens to brain observable Z when observable X changes (or event Y occurs)?” (Villringer, Mulert and Lemieux, 2022).

In the last century, the development of noninvasive brain imaging methodologies and their integration has been exponential and had a major impact in the field of neuroscience.

A summary of available noninvasive brain imaging methods and the principles they use is provided in **Table 1.1**.

***Table 1.1**: Noninvasive brain imaging methods and the principle they use (Villringer, Mulert and Lemieux, 2022).*

Method	Physical principle
Computerised tomography (CT)	Absorption of X-rays
Positron emission tomography (PET)	Emission/detection of positrons
Magnetic resonance imaging (MRI)	Nuclear magnetic resonance (NMR)
Optical imaging	Light absorption, scattering, fluorescence
Electroencephalography (EEG)	Electrical potentials
Magnetoencephalography (MEG)	Magnetic fields
Electrical impedance tomography (EIT)	Changes in electrical impedance
Ultrasound	Doppler effect in ultrasound

Different neuroimaging modalities measure different neurophysiological processes and can be combined to provide complementary information, depending on the characteristics of the phenomena of interest and the research question. **Table 1.2** categorizes methods according to the neurophysiological processes they reflect and shows how the combination and integration of different techniques can provide complementary information about neurophysiology.

***Table 1.2**: Noninvasive brain imaging methods and the physiological parameters they reflect*
(Villringer, Mulert and Lemieux, 2022).

Physiological parameters	**Technique**	**Method**
Oxygen consumption	PET	O2 PET
	MRI	BOLD and CBF–MRI (calibrated with CO2 challenge)
Electrophysiological markers of brain activity		
"Field potentials" (presumably reflecting synaptic activity)	EEG	Event-related evoked potentials
Action potentials (high-frequency	EEG–MEG	High-frequency oscillations

bursts)		
Evoked fields (presumably reflecting synaptic activity)	MEG	Event-related evoked magnetic fields
Assessment of background rhythms and evoked rhythms	EEG, MEG	Assessment of occipital alpha rhythms
Molecular markers		
Various markers of energy metabolism containing phosphorus: ATP, ADP, creatinine phosphate	MR	P31 magnetic resonance spectroscopy
Various molecules in millimolar concentration range: lactate, *N*-acetyl-aspartate, glutamate, GABA, etc.	MR	H1 magnetic resonance spectroscopy
Other molecular markers at smaller concentrations	PET	PET of various positron-emitting tracers
	Optical	Fluorescence detection of various fluorescent/phosphorescent tracers
Brain morphology/volumetry		
Volumes of brain areas	MRI	Voxel-based morphometry (VBM)
Orientation of nerve fibres	MRI	Diffusion tensor imaging
Others		
Cell volume	MRI	Diffusion imaging
	Optical	Scattering

The integration of multimodal measurements comes with different degrees of technical difficulties, **Table 1.3** summarizes which imaging techniques have been successfully combined in order to perform simultaneous observations (Villringer, Mulert and Lemieux, 2022

Table 1.3*: Multimodal noninvasive neuroimaging techniques (Villringer, Mulert and Lemieux, 2022).*

Combination	References
EEG–MRI	Ives et al. (1993), Busch et al. (1995), Bonmassar et al. (1999, 2001), Allen et al. (1998, 2000), Lemieux et al. (1997, 2001a, b), Goldman et al. (2000), Krakow et al. (2000), Vasios et al. (2006), Neuner et al. (2013)

NIRS–MRI	Kleinschmidt et al. (1996), Kida et al. (1996), Punwani et al. (1998), Toronov et al. (2001), Mehagnoul-Schipper et al. (2002), Strangman et al. (2002)
TES–MRI	Brandt et al. (1996)
MRI–MEG	Zotev et al. (2008)
fTCD–MRI	Probably feasible, since combined ultrasound and MRI systems have been demonstrated (McDannold et al. 2003)
PET–NIRS	Villringer et al. (1997), Polinder-Bos et al. (2020)
PET–fTCD	Sabri et al. (2003)
PET–EEG	Buchsbaum et al. (1984), Sadato et al. (1998), Barrington et al. (1998), Gamma et al. (2004)
PET–MEG	Feasible in principle, but no example of a successful combination was found
PET–CT	Mainly used in clinical oncology (Beyer et al. 2000)
PET–MRI	Catana et al. (2008), Judenhofer et al. (2008), Kim et al. (2020)
EEG–MEG	Salustri and Chapman (1989), Buchner et al. (1994), Plummer et al. (2019)
EEG–NIRS	Hoshi et al. (1994), Steinhoff et al. (1996), Kirkpatrick et al. (1998), Obrig et al. (2002), Shin et al. (2018)
MEG–NIRS	Mackert et al. (2004), Seki et al. (2012)
NIRS–TCD	Terborg et al. (2003)

It is worth mentioning that all the techniques listed in **Tables 1.1**, **1.2** and **1.3** only measure brain activity, while another set of multimodal approaches combines techniques which stimulate/modulate brain activity with methods which measure brain activity (e.g., transcranial magnetic stimulation (TMS) with PET). The precise description of these methods is beyond the scope of this thesis, which will be focusing on the different applications of EEG-fMRI in the study of epilepsy.

1.2. MULTIMODAL DATA INTEGRATION

There are different ways to integrate various modalities, depending on the level of synchrony between the acquired data and the methods used to analyze and interpret them.

There are two important aspects to keep in mind when defining the analytical strategies for multimodal datasets: firstly, it is important that all signals obtained with multiple modalities relate to the same phenomenon of interest; secondly, it is the nature and the characteristics of the phenomenon of interest that must determine the useful ways in which the data can be acquired and integrated.

In fact, as anticipated, simultaneous multimodal measurements carry a number of practical difficulties that need to be carefully considered in relation to the expected benefits for the data. Increased costs (e.g., the need for adapting instruments to the new environment to ensure MR compatibility), potential interactions between instruments that can result in degradation of data quality (e.g., EEG artifacts during MRI data acquisition), and increased health risks for subjects (e.g., higher risk of introducing magnetic materials into the MR environment) are only some of the issues that have to be addressed in order to perform simultaneous multimodal neuroimaging.

However, there are some experimental contexts in which simultaneous multimodal acquisitions can be rather beneficial, making the technical challenges worth tackling.

The central consideration, when planning a multimodal study, is whether the same brain activity will occur if the experiment is repeated across modalities.

For instance, if individual events are being studied, then simultaneous measurements from a single session is necessary to ensure the same behaviour of interest is acquired. Similarly, the study of unpredictable events or the study of effects averaged over multiple events also require simultaneous data acquisitions.

On the other hand, in experimental studies with controlled tasks or stimuli, serial single-modality acquisitions may be sufficient, and the advantages of simultaneously acquiring multimodal data may not be straightforward. Once the multimodal data is acquired, it can be combined in different ways, ranging from simple comparisons in time and space, to complex models that aim to explain the underlying neuronal activity and biophysical processes. The degree to which the relationship between signals is incorporated into a model determines the approach used (Villringer, Mulert and Lemieux, 2022).

1.2.1. Spatial Coregistration

This approach involves the direct comparison of information obtained from multiple modalities (Villringer, Mulert and Lemieux, 2022). One of its typical applications is the evaluation of a new localization technique.

For example, the comparison between the EEG source reconstruction of the generators of interictal spikes or event-related potentials with the localizing information of EEG informed fMRI (Lemieux et al. 2001a, b; Benar et al. 2003; Mulert et al. 2004). Another example are the studies that comparing fMRI and NIRS confirmed that T2*-weighted fMRI signal increases during functional activation correlate with local drops in [deoxy-Hb] (Kleinschmidt et al. 1996; Kida et al. 1996; Punwani et al. 1998; Toronov et al. 2001; Mehagnoul-Schipper et al. 2002; Strangman et al. 2002).

1.2.2. Asymmetric Integration

Asymmetric integration implies the use of data from one modality to analyze data from other modalities (Villringer, Mulert and Lemieux, 2022). This can be done either in the spatial domain (e.g., when regions of interest identified by PET or fMRI are used as priors to solve the EEG-MEG inverse problem (Heinze et al. 1994; Liu et al. 1998; Daunizeau et al. 2006; Stancak et al. 2005; Babiloni et al. 2003) or temporal domain (e.g., EEG-derived hypothesis-driven approach to fMRI analysis).

This latter case is particularly important for the scope of this thesis as the paradigmatic example for the EEG-derived hypothesis-driven approach to fMRI analysis is the study of the haemodynamic correlates of epileptic spikes recorded noninvasively (Warach et al. 1996; Lemieux et al. 2001a, b; Krakow et al. 2001a, b).

The experimental studies presented in Section III, adopt this mode of data integration.

1.2.3. Symmetrical Data Fusion

Symmetrical data fusion represents the next frontier in multimodal neuroimaging. It will require a better understanding of the relationship between signals acquired from different modalities and their underlying generative mechanisms, as well as new computational models that link neuronal activity to haemodynamic, electrical and magnetic parameters in order to create biophysical models that relate the data from each modality within a unified framework. (See Chapters. 25, 28 and 29 of Mulert and Lemieux, 2022).

In this thesis, we will only delve into the main applications of simultaneous EEG-fMRI. Specifically, we will focus on the use of EEG-informed fMRI in the study of temporal lobe epilepsy and benign epilepsy with centro-temporal spikes (BECTS).

Chapter 2: EEG

2.1. INTRODUCTION

The electroencephalogram (EEG) is the summed electrical activity of populations of neurons, with contributions from glial cells. The electrical activity of the brain was discovered by Caton in 1875 who explored the electrical phenomena of the exposed cerebral hemispheres of rabbits and monkeys using a galvanometer. In 1929 Berger demonstrated that the EEG could be recorded from the human scalp, but despite being a meticulous scientist in his EEG work, Berger also developed very unscientific ideas about its nature. He believed in a powerful force that he called *Psychische Energie* with EEG waves acting as messengers even capable of transmitting thoughts and emotions between individuals. This contributed to slowing down the diffusion of EEG as a scientific tool and it was only after Adrian and Mathews' 1934 demonstration that the alpha rhythm was likely generated in the occipital lobes in humans, and not an artifact, that it was accepted as a method for analysing brain functions in health and disease.

Since then, the development of clinical and experimental EEG work opened the doors to extensive studies of brain functions, and it became a standard instrument in clinical and research settings over time, reaching a high point around 1960 and then starting to slow down. Epileptology remains an exception and keeps using the tool of EEG video monitoring to its full extent (Niedermeyer E and Schomer DL, 2018; Lopes da Silva, 2022).

2.2. THE CELLULAR BASIS OF EEG

We can distinguish two main forms of neuronal activation (Lopes da Silva and van Rotterdam 2018; Lopes da Silva 2002; Nunez 1995):

- the action potential is a rapid change in membrane potential, mediated by sodium and potassium voltage-dependent ionic conductance gNa and gK. The intracellular potential jumps from negative to positive and in 1 or 2 ms returns to the resting intracellular negativity, generating an impulse that propagates along axons and dendrites without loss of amplitude (Lopes da Silva, 2022).
- postsynaptic potentials (PSPs) are slower changes in membrane potential due to synaptic activation, mediated by several neurotransmitter systems. Postsynaptic potentials can be distinguished in excitatory (EPSPs) and the inhibitory (IPSPs), depending on the nature of the neurotransmitter involved, the corresponding receptor and their interactions with specific ionic channels and/or intracellular second messengers. During an EPSP the positive electric current is directed by positive ions inwards (e.g., Na+) generating an active sink in the extracellular medium. In IPSP the positive electric current is directed from the inside of the neuron to the outside, by negative ions inwards (e.g., Cl−) or positive ions (e.g., K+) outwards, generating an active source in the extracellular medium. Since there is no accumulation of charge anywhere in the medium, the trans membrane currents that flow in or out at the active synaptic sites are compensated by currents that flow in the opposite direction along the neuronal membrane. In the case of an EPSP, besides the active sink at the level of the synapse, there are distributed passive sources along the soma-dendritic membrane and the opposite occurs in the case of an IPSP (Lopes da Silva, 2018a) (**Figure 2.1)**.

Electrical activity of neurons can then be regarded as a combination of action and postsynaptic potentials. However, macroscopic monitoring of these electrical fields require that a large population of neurons is synchronously activated, and orthogonally orientated in relation to the skull.

The neurons that mainly contribute to the EEG (or MEG) are the pyramidal neurons of the cortex, since they are arranged in palisades, with the apical dendrites aligned perpendicularly to the cortical surface and, when activated with a certain degree of synchrony, generate coherent electric/magnetic fields (Local Field Potentials, LFPs), which can be detected by electrodes placed at relatively small distances. Thus, the main contribution underlying scalp EEG measures is the LFP fluctuations resulting from postsynaptic activity within a large population of cortical pyramidal cells, with a modest contribution from the glial cells (Dale and Halgren, 2001; Nunez and Silberstein, 2000, Akay, 2006; Amzica and Lopes Da Silva, 2018).

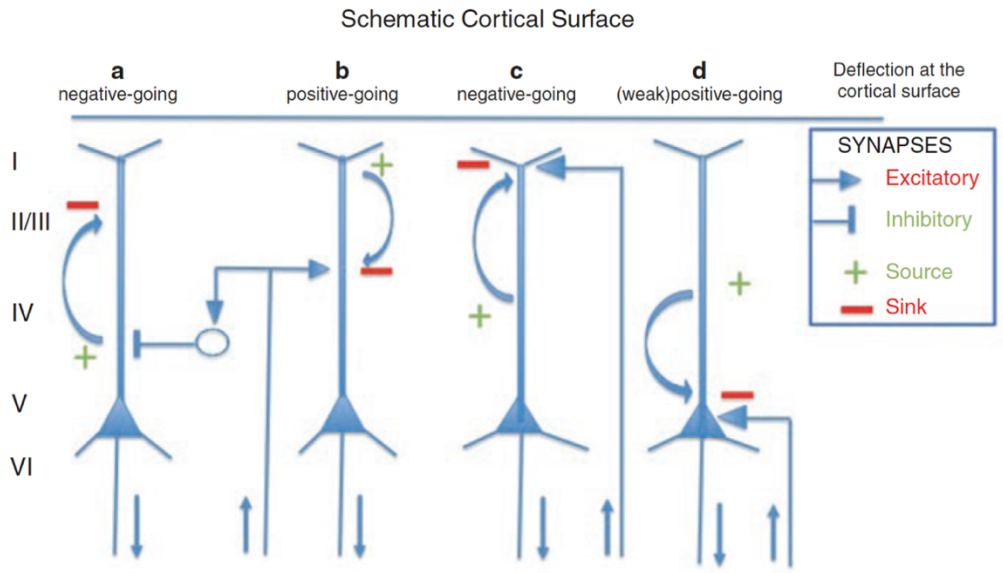

***Figure 2.1**: Representation of four typical cases of cortical generators of LFPs. Example of inhibitory LFP(a) and excitatory synaptic activity (b, c, d) at different sites of the soma-dendritic membrane of a pyramidal cell. The direction of extracellular currents is indicated by the curved arrows. The interneuron (circle) represents a stellate cell that would generate an approximately closed field and would not generate a field potential measurable far from its source. (Lopes da Silva, 2022).*

2.3. EEG ACTIVITIES

As stated in the previous paragraph, given the complexity of the brain electrical activity and the numerous factors that concur in the determination of the signal registered by scalp EEG, it is clear that scalp EEG is a mixture of LFPs generated by several brain sources. Such mixture gives rise to two main types of electrical activity— rhythmical and arhythmic (He et al., 2010).

2.3.1. EEG rhythmic activity

The power spectra of LFPs and scalp EEG signals follow a 1= f b power law distribution, characteristic of most of the scale-free dynamics in nature, and their peaks are associated with EEG rhythmic activity: delta (0.5-4 Hz), theta (4-8 Hz), alpha (8-13 Hz), beta (13-30 Hz), and gamma (above 30 Hz).

The delta rhythm is mostly observed in adults during deep stages of sleep, displaying a high coherence across the scalp, and is thought to reflect various interactions within the cortex or thalamus. Theta rhythm plays a significant role in infancy, childhood, and states of drowsiness and sleep. It is also considered a biomarker of various forms of pathology that involve the slowing of alpha rhythms. However, Theta rhythms are highly abundant in the hippocampus of many animal species, particularly rodents, and are thought to be related to the regulatory aspect of information transfer between different regions of the brain.

The alpha rhythm is predominantly observed in the posterior regions of the brain. It is most prominent when the subject is instructed to close their eyes and relax, but it disappears when the subject is engaged in a task. The alpha rhythm originates in the cortex, but strongly influences thalamo-cortical interactions.

Beta rhythm are associated with states of alertness and focused attention and its spatial distribution and physiological origin vary depending on the type of beta activity, which can be classified as frontal, central, posterior, or diffuse.

Gamma rhythm, on the other hand, is associated with information processing and the initiation of voluntary movements.

In addition to individual differences between subjects, the impact of brain rhythms on EEG signals is influenced by the subject's age and behavioural state, with alertness level being a particularly important factor (Akay, 2006; Amzica and Lopes da Silva, 2005).

2.3.2. EEG Arrythmic Activity

In addition to the described peaks in the EEG power spectrum, the rest of the power law distribution represents the brain's arrhythmic activity, which is characterized by fluctuations appearing at specific time-points on the EEG traces, without apparent periodicity. This arrhythmic activity can be spontaneous, such as EEG microstates and epileptic activity, or can result

from the brain's response to certain stimuli, inducing time-locked activation of specific neuronal populations or reorganization of ongoing EEG activity (Lopes da Silva, 2018b).

Stimuli time-locked electrical potentials, event-related potentials (ERPs), are electrical manifestations of great physiological relevance and have been widely studied, also in the context of multimodal neuroimaging. Although, ERPs are beyond the scope of this dissertation and will not be further discussed.

Instead, a brief analysis will be dedicated to EEG epileptic activity, in particular inter-ictal epileptic discharge (IEDs). For a deeper insight into epilepsy, see Section II.

2.3.3. EEG Epileptic Activity: Interictal activity

EEG epileptic activity can be roughly categorized into two types: interictal and ictal paroxysmal activity. Ictal paroxysmal activity will not be further discussed in this thesis. Please refer to Chang BS, Schomer DL and Niedermeyer E (2018) Epilepsy in Adults and the Elderly [In: Niedermeyer E, Lopes da Silva F (eds) Electroencephalography: basic principles, clinical applications and related fields, 6th edn. Lippincott, Williams & Wilkins, New York] for a complete review of EEG epileptic activity.

Epileptiform interictal EEG abnormalities comprise spikes, which are brief electrographic transients lasting less than 70 ms, with a negative main component and variable amplitude, and sharp waves, which last 70-120 ms, due to their prolonged descending phase (Figure 2.2) (de Curtis and Avanzini, 2001).

(A)

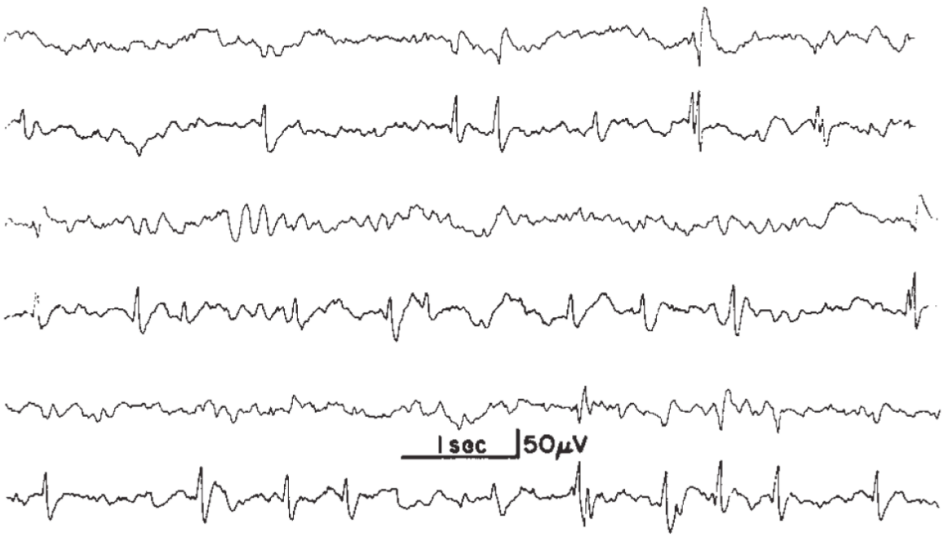

(B)

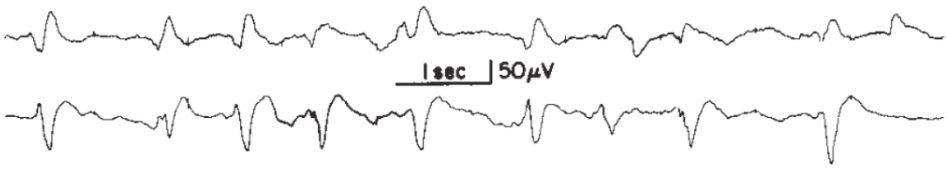

***Figure 2.2**: Example of epileptiform interictal EEG abnormalities.*
*(**A**) Various wave morphologies of spikes recorded from the same patient (age 6 years). (**B**) Recurrent sharp wave recorded from a 61-year-old patient. (Chang, Schomer and Niedermeyer, 2018).*

IEDs are considered pathological due to their rare occurrence (<1%) in healthy individuals (Gregory et al., 1993) and their strong association with epilepsy (Marsan and Zivin, 1970).

Various pathological mechanisms have been proposed to underlie the interictal spike, including the intrinsic burst properties of neurons and the synchronisation of neuronal populations.

The activation of hyperpolarising GABA(A) and GABA(B) receptor-mediated currents and calcium-dependent potassium currents terminates the interictal spike (de Curtis and Avanzini, 2001; McCormick and Contreras, 2001),

resulting in a post-spike refractory period during which neuronal activity is inhibited (de Curtis and Avanzini, 2001).

Spikes appear to be intrinsically different from a seizure, which not necessarily evolve from spike discharges but may begin as a distinct high-frequency rhythm. Although, spike discharges can precede the seizure with progressively less effective after hyperpolarisations in mesial temporal lobe epilepsy (King and Spencer, 1995), but ictal activity remains a distinct phenomenon

Moreover, IEDs are not necessarily indicative of the area from which seizures arise and the predictive value of IEDs depends on epilepsy type and aetiology. This is of great importance in the field of epilepsy surgery, where the definition and identification of the full extent of the irritative zone is critical to directing surgery and predicting surgical outcome (see Section II, Chapter 8). Presurgical planning played a central role in the development of simultaneous EEG and fMRI (see Section I, Chapter 4).

2.4. THE PROBLEM OF EEG SOURCE RECONSTRUCTION

Given the aforementioned considerations, it becomes evident that scalp EEG signals are a complex mixture of LFPs generated by various sources in the brain. This poses a challenge for localizing these sources in space by means of EEG alone, which, again, is particularly important in cases of focal epilepsy where the aim is to identify the location of the epileptogenic focus or foci. The process of EEG source reconstruction involves formulating the "forward problem," which describes the electrical potential on the scalp as a function of dipole sources in the brain, and then solving the "inverse problem," which estimates the current dipole sources given a certain potential scalp distribution.

The problem of EEG source reconstruction is very complex and this dissertation is not going to describe it further. However, it is worth mentioning because of the importance of this EEG limitation in the development of multimodal neuroimaging techniques.

For a detailed account of the inverse problem in EEG refer to Mulert 2022 What Can fMRI Add to the ERP Story? [In: Mulert C., Lemieux L (eds) EEG-fMRI: Physiological basis, Techniques, and Applications. 7th Edition. Springer Nature Switzerland https://doi.org/10.1007/978-3-031-07121-8].

Chapter 3: fMRI

3.1. MR PHYSICS

3.1.1. Nuclear magnetic resonance

The signal measured during MRI arises from atomic nuclei of the tissue's hydrogen atoms (i.e., protons), being hydrogen the most abundant and therefore producing the strongest signal. A proton possesses a physical property, its spin, which behaves roughly speaking like a compass needle: each spin has a small magnetic dipole moment and aligns in an external magnetic field.

When an external magnetic *B0* field is applied, such as inside the magnetic resonance scanner bore, spins align either antiparallel or parallel to the magnetic field *B0*, with a majority of nuclei aligning along *B0*, a 'low energy' state. Only a small population of nuclei are anti-aligned in the 'high energy' state and the sum of all the individual magnetic moments precessing around *B0* yield a single magnetisation vector, *M* aligned along *B0* (z axis) **(Figure 3.1 (a)).**

When a radiofrequency (RF) pulse *B1,* at a specific frequency known as the Larmor frequency *w0* (that specific for hydrogen and directly proportional to the field strength), is applied perpendicular to the magnetic field, the protons are excited from the low to the 'high energy' state. This has the effect of tilting *M* away from the *B0* axis, and towards the transverse **(Figure 3.1 (b)).** The tilted magnetisation then rotates around the magnetic field vector. During this movement, called precession, the protons send out an electromagnetic wave,

returning to their original energy state, that has the Larmor frequency **(Figure 3.1 (c))** and that is measured by the receiver coil.

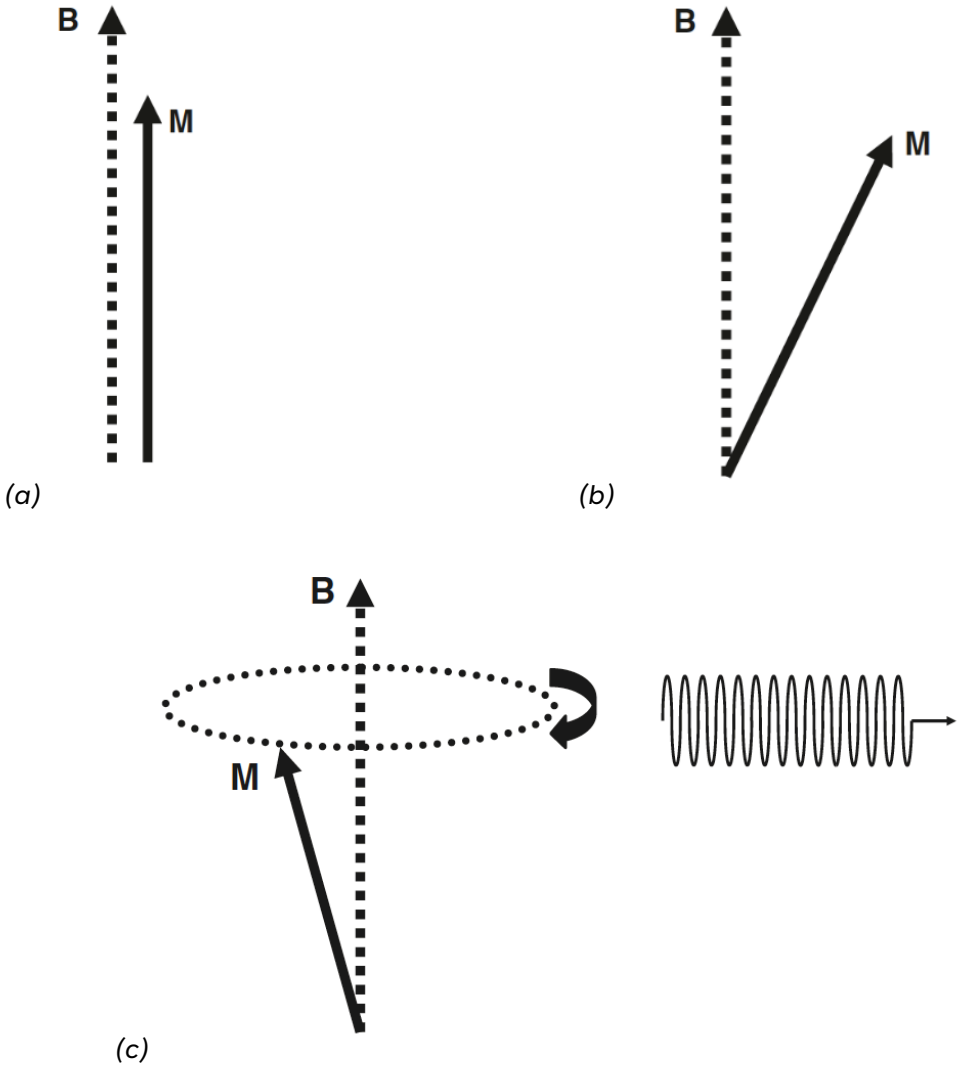

***Figure 3.1**: The Magnetic Resonance Effect*

*(**a**) Spins align in an external magnetic field B, giving rise to a macroscopic magnetisation M which is parallel to B. (**b**) If the protons inside the magnetic field B are exposed to an electromagnetic wave with the Larmor frequency, the magnetisation M is tilted. (**c**) The tilted magnetisation rotates around the magnetic field vector, sending out an electro-magnetic wave with the Larmor frequency (Deichmann, Nöth, Merola and Weiskopf, 2022)*

The signal decay that is measured by the receiver coil is characterised by T1 or spin-lattice relaxation (recovery in the z direction) and T2 or spin-spin relaxation (decay of the magnetisation in the x-y plane). The effect of these

relaxation processes is highly dependent on the local physical and chemical environments that dictate the properties of the surrounding tissues. Ultimately, MRI relies on the differences in relaxation properties of tissues, as it allows tissue differentiation reflected by different contrasts in the MR images, and ultimately changes in tissue compositions associated with disease, hence the increasingly wider application of MRI in medicine. Specifically, different tissues can be found in the brain, namely blood, grey matter, white matter and cerebrospinal fluid, each with distinct biochemical and biophysical properties, and consequently nuclear magnetic resonance relaxation properties (Huettel et al., 2004; McRobbie et al., 2007; Deichmann, Nöth, Merola and Weiskopf, 2022).

3.1.2. Image Formation

As previously mentioned, in MRI, the detection of an MR signal requires the frequency of *B1* to match that of the precessing nuclear spins, which depends on the strength of the magnetic field, *B0*. However, if the *B0* field were perfectly homogeneous, all spins within the sample being imaged would precess at the same frequency, making it impossible to determine the location from which the signal originated. To address this, MRI techniques use magnetic field gradients that vary the strength of the resulting field linearly along the direction of the gradient, providing spatial encoding.

The combination of the RF pulse and gradient fields, applied at very specific times, is used to obtain slice selection (SS), frequency encoding (FE) and phase encoding (PE) as desired. The application of an RF pulse of the appropriate frequency and bandwidth in the presence of a slice select gradient excites a small slice of the sample, allowing the sample to be studied slice by slice.

The repetition time (TR) is the interval between two successive pulse cycles in milliseconds (ms) and the echo time (TE) is the time taken from the application of the RF pulse to the measurement of the MR signal in ms. A combination of three gradient fields; slice selection, frequency encoding and phase encoding, are used to spatially encode the protons.

K-space is a mathematical representation of the raw data collected during an MRI scan. Every point in k-space includes information from all locations in the MR image. Points in the centre of k-space have low spatial frequencies and represent the overall image shape, while points near the edge have high spatial frequencies and convey fine details. The k-space matrix is then transformed into an image by applying Fourier transformation. After Fourier transformation, the image is composed of small cubes called voxels. The size of the voxels determines the resolution of the image and is determined by the step size of the gradients. A typical 128 x 128 matrix is obtained by performing 128 phase encoding steps, with frequency encoding carried out at 128 points for each step. The number of steps determines voxel size, with larger voxels having greater signal to noise and increased partial volume effect. Signal to noise is proportional to voxel volume to the square root of the number of phase encoding steps (Deichmann, Nöth, Merola and Weiskopf, 2022).

3.2. THE BOLD CONTRAST AND THE HEMODYNAMIC RESPONSE FUNCTION

The BOLD (Blood Oxygenation Level Dependent) contrast mechanism is commonly used in functional MRI studies to image the brain (Ogawa et al. 1990; Kwong et al. 1992). Here the classic stimulus-induced activation model (see **Figure 3.2**) will be used to explain the BOLD effect. Although, it's important to note that investigations that seek to reveal patterns of signal change related to spontaneous fluctuations in brain activity, such as resting state and epilepsy EEG-fMRI studies, may not correspond to effects here described. For a brief introduction to this type of modelling see Chapter 4, Paragraph 4.4.

When using gradient echo techniques with a suitable echo time, signal amplitudes are temporarily enhanced in regions of neuronal activation, this relies on the fact that cerebral blood flow and neuronal activation are

coupled. In other words; when an area of the brain is in use, blood flow to that region increases.

When the brain is at rest, there is a high concentration of deoxyhaemoglobin in the blood due to low local oxygen concentrations, making it paramagnetic and leading to magnetic field inhomogeneities at vessel and brain tissue interfaces. This causes T2* to be shortened and a signal reduction in T2*-weighted gradient echo images. However, when there is neuronal activation, more oxygen is delivered to the site of activation through an increased cerebral blood flow, leading to a decrease in deoxyhaemoglobin and an increase in oxyhaemoglobin, which is diamagnetic. In other words, following increased neuronal activity, CBF overcompensates for the increased need for oxygenated blood. As a result, deoxyHb content drops within local capillaries, venules, and draining veins. This causes the magnetic properties of blood and brain tissue to become more similar, reducing field inhomogeneities and increasing local image intensity. This mechanism is termed the blood oxygenation level-dependent (BOLD) effect. The BOLD effect mainly represents synaptic activity (local field potentials) (Logothetis, 2003; Deichmann, Nöth, Merola and Weiskopf, 2022) and is inversely proportional to the local content of deoxyhemoglobin (deoxyHb).

The typical haemodynamic response following neuronal activation associated with a stimulus or spontaneous brain activity is shown in **Figure 3.2** and is called *haemodynamic response function* (HRF).

It starts with a slight signal decrease, but this initial dip is not always observed and depends on the field strength used. After that, a positive BOLD response is observed, which lasts for about 5-10 seconds. However, in the remaining time up to 30 seconds after the stimulus, a signal undershoot is observed (van Zijl et al. 2012). The important physiological parameters that influence the BOLD effect are the cerebral metabolic rate of oxygen consumption (CMRO2), the cerebral blood flow (CBF) and the cerebral blood volume (CBV) (**Figure 3.2**)

The underlying physiology of these effects is not fully understood, particularly how the coupling between neuronal activity and blood flow occurs and which aspect of neuronal activity it reflects best. EEG-fMRI studies may help answer some of these questions (Logothetis et al. 2001; Shmuel et al. 2006; Laufs et al. 2003; Moosmann et al. 2003; Siero et al. 2014; Deichmann, Nöth, Merola and Weiskopf, 2).

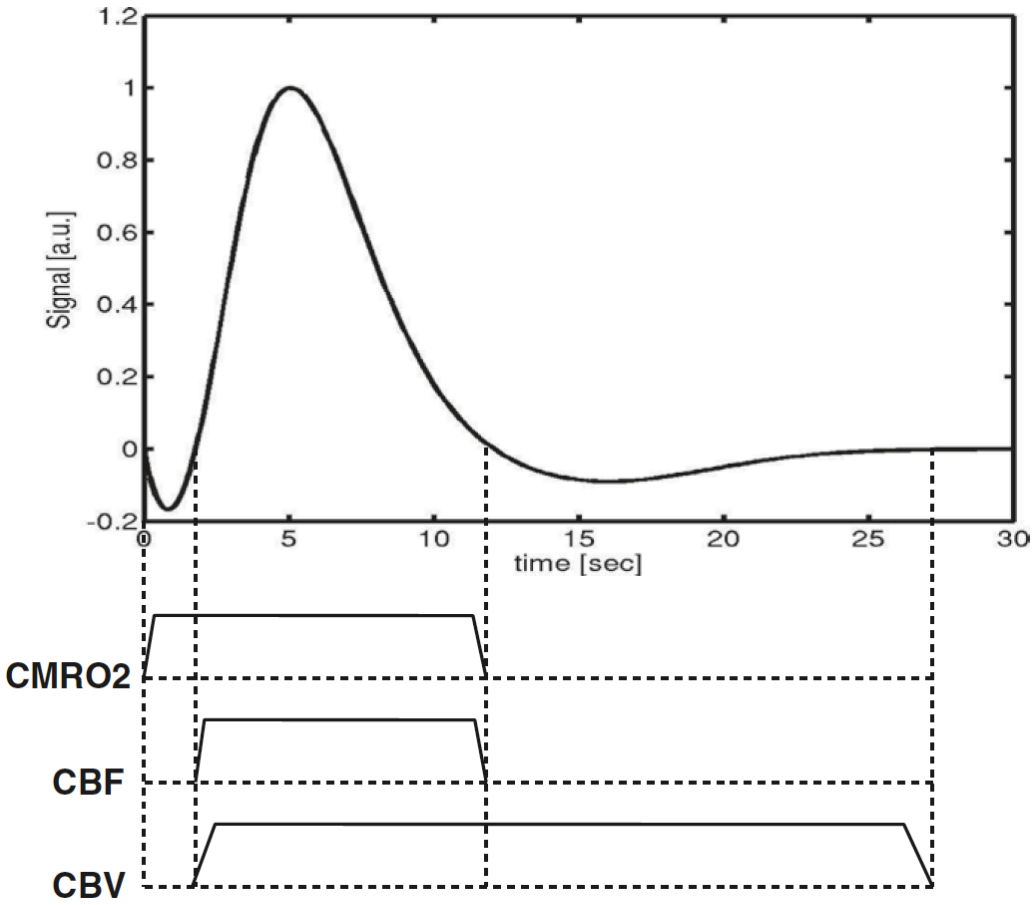

***Figure 3.2**: The haemodynamic response function*
Following a stimulus, the typical haemodynamic response function shows a negative initial dip, a strong positive BOLD response and a subsequent negative undershoot. These phenomena can be explained with the different time constants of the underlying physiological parameters: the cerebral metabolic rate of oxygen consumption (CMRO2), the cerebral blood flow (CBF) and the cerebral blood volume (CBV) (Deichmann, Nöth, Merola and Weiskopf, 2022)

Given what has been said, the BOLD response appears to be a slower, low-pass filtered version of the neurophysiological response in the temporal domain. This can be explained by the fact that changes in blood flow occur on a much slower time scale compared to changes in neuronal activity. While BOLD responses to brief and discrete stimulation occur within hundreds of milliseconds to seconds, neurophysiological responses generally occur within milliseconds or tens of milliseconds. Typically, the highest level of blood flow and the maximum BOLD response are observed 5-6 seconds after exposure to a short stimulus. Therefore, the vascular response to a synaptic input may still be developing by the time a second stimulus is presented. In cases where such temporal overlap between responses happens, the vascular response to a stimulus may be influenced by preceding stimuli (Lauritzen, 2005).

Negative BOLD

It is worth noting that the BOLD response curve can be inverted, meaning that the large BOLD change that occurs after 5-10 seconds can be negative. This has been observed in various fMRI and EEG-fMRI studies, where a decrease in blood flow and neuronal activity in the cortex can lead to a negative BOLD response (Hamandi et al. 2008; Carmichael et al. 2008; Havlicek et al. 2015). There are several hypotheses regarding the origin of negative responses, with some suggesting that it may be purely vascular in nature, such as the "vascular blood steal" hypothesis. This view concludes that the negative BOLD response (NBR) may not be closely related to the underlying neuronal activity (Harel et al. 2002; Kannurpatti and Biswal 2004). However, there are robust evidence suggesting that the NBR is associated with reductions in local neuronal activity (Shmuel and Maier, 2022).

3.3. STATISTICAL ANALYSIS OF FMRI DATA

A fundamental bases for fMRI data analysis is the identification of the voxels where the BOLD signal is significantly correlated with a given timecourse.

As a large proportion of the variance in fMRI timeseries can be attributed to head motion (Friston et al. 1996), in order to analyze fMRI data, a set of pre-processing steps are initially performed to correct for motion and align the images to a standard anatomical space. Various software packages, such as statistical parametric mapping (SPM), are available for carrying out these steps (Friston, 1995).

3.3.1. Spatial preprocessing

Realignment

The initial step in fMRI data processing is to align the whole brain volumes to correct for any head motion, which can lead to artefacts in the data. A typical fMRI data series contains multiple 3D volumes, one for each time point. To align the data, a common reference frame is chosen (usually the first slice), and the time series is realigned to this reference frame.

The statistical analysis of fMRI data is carried out using a t-test, where the signal change is measured relative to the residual variance. The residual variance is computed from the sum of squared differences between the data and the linear model it is fitted to. Head motion artefacts will contribute to the residual variance, which can reduce the sensitivity of the analysis.

Normalisation

Following the realignment step, the fMRI data is then mapped into a standard anatomical space, which enables group-level analyses and facilitates reporting of the data in a consistent reference coordinate system. Specifically, the functional mean realigned image is warped to the SPM EPI template, which is in standard anatomical space (Talairach and Tournoux, 1988). The transformation parameters obtained are then applied to all images in the time series.

Smoothing

The primary purpose of spatial smoothing is to increase the signal-to-noise ratio and to comply with the assumptions of Gaussian field theory. A set of data points, such as a time series or an image, are averaged with their neighbours, which reduces the variation in high-frequency data and produces a smoothing effect. In SPM, spatial smoothing is achieved by applying a Gaussian kernel with a known width to each voxel. The width of the Gaussian is often measured in terms of the Full Width at Half Maximum (FWHM), which represents the width of the kernel at half the maximum height of the Gaussian. Smoothing also enables averaging across subjects.

3.3.2. The general linear model

The standard approach for fMRI data analysis involves the application of a general linear model (GLM) to the data, which expresses the predicted fMRI signal timecourse as a sum of linear terms representing both the experimental effects of interest and confounding effects (e.g., movement) (Worsley and Friston 1995) (**Figure 3.3**). This assumes that fMRI changes are linearly related to experimental effects at every voxel. The same GLM is applied to every voxel in the brain. The null hypothesis is that there is no effect at each voxel, generating a t-statistic for each voxel. Variability in the resulting weights across voxels provides information on the localization of the effect. A Z-score equivalent is then computed before an image of t-statistics is generated. This is called a statistical parametric map. Finally, an inference is drawn from this SPM, reliably locating voxels where an effect is present limiting the possibility of false positives. SPM uses much of the same underlying mathematics as other statistics packages and commonly used statistical tests such as linear regression, t-tests and analysis of variance (ANOVA).

The fMRI signal at any given voxel is represented as a vector of weighted “regressors”, that are categorized as effects of interest or of no interest/confounds, in order to separate signal from noise in all its forms, such

as noise associated with instrumental, physiological or other effects (body motion) not related to the specific experimental question. The regressors are convolved with the haemodynamic response function (HRF) or other basis set (see paragraph 3.2) of the BOLD effect in order to account for the lag of the response described above. The general linear model imposes a temporal smoothing function on the time-series as data from one scan to the next are correlated.

The choice of a specific mathematical representation for the events of interest is dictated by the nature of the events. When selecting a haemodynamic basis set for fMRI data analysis, several factors need to be taken into account. For example, if the goal is to accurately estimate the shape of the BOLD response to an event, a flexible basis set comprising multiple functions covering a shorter or longer time window than the standard HRF may be required. On the other hand, if the aim is to detect effects that match a specific function with maximum sensitivity, a basis set restricted to a single function may be more appropriate (Josephs and Henson, 1999).

For a comprehensive explanation of model estimation and statistical models please see Worsley et al. 2002, Lindquist 2008 or the open-source SPM software manuals http://www.fil.ion.ucl.ac.uk/spm/doc/manual.pdf.

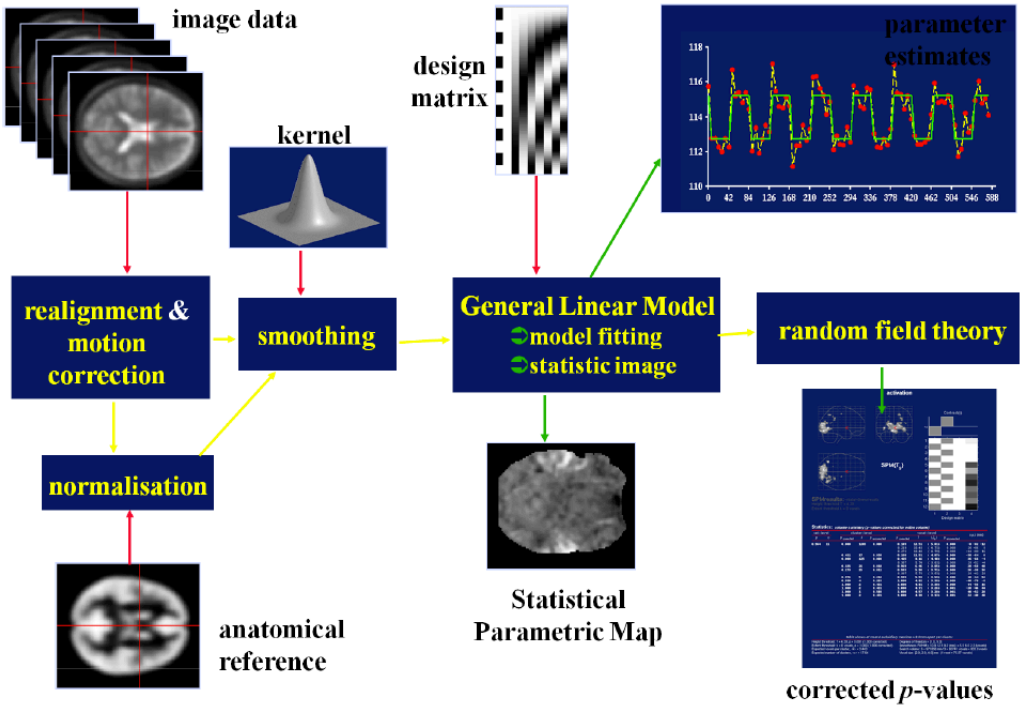

***Figure 3.3**: Schematic of fMRI statistical analysis (http://www.fil.ion.ucl.ac.uk/spm/doc/manual.pdf)*

3.3.3. Significance and random field theory

The null hypothesis of a statistical comparison in fMRI is that there is no change in any voxel in the brain. Since each SPM map computes a statistic for every voxel, there is a likelihood of false positives at standard statistical thresholds, such as $p<0.05$ or $p<0.01$, due to the problem of multiple comparisons. To address this, a correction is necessary for the number of statistical tests performed. The Bonferroni correction is one approach, but it can be overly conservative for most SPMs. Instead, SPM uses a correction based on Gaussian field theory, which takes into account the correlation between neighbouring voxels and the smoothing of data using FWHM kernel to create resells, which are used to correct for multiple comparisons. This correction is less conservative than the Bonferroni correction, provided that the data is sufficiently smooth. Small volume correction can be used to

appropriately correct data for a priori identified regions of interest. (Brett et al., 2003).

3.3.4. Functional Connectivity

Functional connectivity refers to statistical associations among spatially distributed neurophysiological time series (Friston, 2011), not only fMRI data, but also obtained from EEG or MEG. Although fMRI has relatively low temporal resolution, it provides whole-brain coverage and spatial resolution within the millimetre range. Functional connectivity describes statistical dependencies between regions, i.e. correlations. In fMRI words, which voxels in the brain display similar BOLD signal fluctuations over the course of a scan.

Resting-state fMRI analysis has identified reproducible brain networks that exhibit coherent fluctuations in their intrinsic, spontaneous activity. These networks closely match those engaged in specific tasks (Fox et al., 2006; Smith et al., 2009; Yeo et al., 2011), and are reproducible across subjects (Damoiseaux et al., 2006; Biswal et al., 2010). Resting-state fMRI can be employed, along with task-fMRI, to investigate functional network architecture and pathological connectivity disturbances (Centeno and Carmichael, 2014).

However, functional connectivity analyses do not consider causal interactions within the network, i.e., how information propagates through brain regions (Friston, 1994, 2009, 2011; Smith, 2012). Imagine the BOLD signal at regions 1, 2 and 3, (y1, y2 and y3 in **Figure 3.4**) are all strongly correlated; this could mean that they are connected in a number of different ways (A, B, C), or not connected at all, rather are all driven by a common input (D). In contrast, effective connectivity is defined as the directed influence one region has over another (Friston, 2009), and thus can supplement functional connectivity analyses in a complementary manner (see next paragraph).

3.3.5. Dynamic Causal Modelling -DCM

Dynamic causal modelling (DCM) is a to investigate the effective connectivity between different brain regions. Effective connectivity (EC) is defined as the influence one neural system has on another (Friston 1995).

The general idea is to estimate the parameters of a reasonably realistic neuronal system model such that the predicted blood oxygen level dependent (BOLD) signal corresponds as closely as possible to the observed BOLD time series *y*. It is important to note that the BOLD signal *y* can be considered a dependent, measurable (or observed) variable of the underlying neural activity *z* that cannot be measured with fMRI (thus, the neural activity is an example of a "hidden state variable" (Logothetis, 2008). As already expressed in paragraph 3.2, this concept is used in all general linear model-based analysis of fMRI data. DCM is simply a generalisation of the convolution models used in all GLM analyses, with the difference is that DCM allows the experimenter to additionally consider the effects of other regions on their neural model (Friston et al., 2003; Friston,2002).

In order to create a plausible model of how the observed BOLD signal *y* may be generated a number of aspects needs to be taken into account, such as: the neural activity with respect to time ($\dot{z}$) in response to some incoming signal (be it from another brain region or an exogenous environmental stimulus); the fact that possibly all) connections that exist in the brain are reciprocal; the fact that the impact of one region on another is delayed in time (Daunizeau et al., 2011a,b). The purpose of a DCM analysis is to estimate the coupling parameters of a model (the arrows in **Figure 3.4**), in order to evaluate how well a particular model (A, B, C, D in **Figure 3.4**) explains the observed data (y3 in **Figure 3.4**) to make inferences about the structure of the network and quantify the coupling strength and direction of coupling between regions.

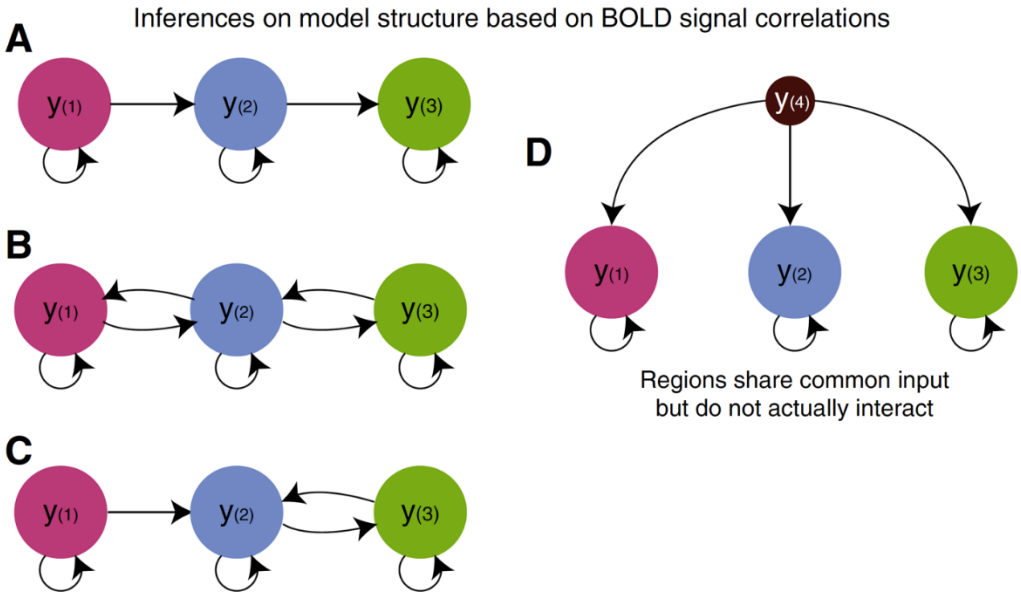

Figure 3.4 *Potential models of functional connectivity between regions.*
These three regions express highly correlated BOLD signal fluctuations, but little is known about the underlying functional architecture. Note that inferences are made at the level of the BOLD data, y, not the underlying neural activity, z (Kahan and Foltynie, 2013).

Please note that DCM has been used in the experimental study described in Chapter 10.

For a gentle but thorough introduction to the rationale behind DCM analyses please refer to Kahan and Foltynie (2013) Understanding DCM: Ten simple rules for the clinician.

Chapter 4: Combining EEG and fMRI: EEG-informed fMRI

4.1. INTRODUCTION

Functional neuroimaging aims to understand the neural basis of cognitive functions by identifying and characterizing changes in brain states, in space and in time, and their relationship to neuronal activity.

fMRI and EEG assume that brain states can be decoded by analysing the precise anatomical localization and the detailed temporal evolution of the corresponding brain activation signals.

Until the late 20th century, fMRI and EEG techniques were developed independently, with little interaction due to technological limitations. However, the advent of new systems that enable the simultaneous acquisition of EEG and fMRI data from the same subject has led to increased interest in integrated data modelling and analysis in the 21st century (Goebel and Esposito, 2022).

Initially, the idea of combining these two modalities was motivated by the desire to localize the electrical sources underlying epileptic disorders (Laufs, 2012). Later on, the multimodal approach has overcome the confinement to the epilepsy field and has been used in other areas of neuroscience, such as the study of brain functions in healthy subjects.

To combine EEG and fMRI data, researchers have developed different strategies for integrating temporal and spatial information, despite the limited temporal resolution of fMRI and limited spatial resolution of EEG.

The advantages of this approach come from the fact that by integrating EEG and fMRI spatio-temporal modelling, it is possible to detect new effects in the fMRI domain, even when the underlying event or state change occurs at very rapid temporal scales (e.g., milliseconds) or high frequency bands (above 1 Hz) (Goebel and Esposito, 2022).

Although, besides the technical challenges, such as instrumental incompatibility and artefacts, there is a need to understand and model the ongoing correlations between EEG and fMRI data.

This chapter focuses on the current methodological developments of informed EEG-fMRI analysis in epilepsy study.

4.2. EEG IN MRI ENVIRONMENT

To ensure safe and accurate simultaneous EEG-fMRI monitoring, EEG instrumentation must be carefully designed and take into account unique factors that are not relevant to traditional EEG equipment. These factors include avoiding the use of ferrous materials, limiting radiofrequency emissions to preserve image quality, and addressing static and time-varying magnetic fields that can cause EEG artifacts. The design of EEG equipment for use in the magnetic resonance (MR) scanner must consider all these factors to ensure the safety and reliability of the recording. Therefore, EEG monitoring equipment used for clinical diagnostic recordings is not appropriate for EEG-fMRI monitoring **(Figure 4.1)** (Hawsawi, et al., 2022).

***Figure 4.1**: Example of commercial EEG–fMRI instrumentation*

4.2.1. EEG Data Quality

The EEG recorded in the MR scanner is contaminated by two MRI-induced artifacts, that, if appropriately addressed, do not compromise EEG recordings.

Ballistocardiogram artefacts

The pulse artefact or ballistocardiogram, (BCG, although it may not be entirely of ballistic origin), given its non-stationary nature, is a challenging aspect of EEG-fMRI integration.

BCG is caused by multiple factors, such as such as pulse-related movement of the electrodes or blood flow in the static field (Tenforde et al., 1983; Bonmassar et al., 2002; Debener et al., 2008 Mullinger et al. 2013; Yan et al.,2010). It is typically 10–100 μV in amplitude and overlaps the EEG frequency range (Allen et al. 1998).

Ensuring the precise elimination of the ballistocardiogram (BCG) artifact while maintaining the underlying physiological EEG signal is crucial in various

applications, especially when EEG features inform BOLD-fMRI signal variations modelling, such as in mostly of the epilepsy research (Rosa et al. 2010b; Leite et al. 2013). Despite exhibiting considerably lower amplitude compared with the gradient or imaging artifact (see next paragraph), it has been proven substantially more difficult to correct for, and it is in fact widely recognized as the most challenging EEG artifact to handle in simultaneous EEG-fMRI studies (Lemieux, 2022).

The BCG artifact is roughly periodic, with artifact occurrences being approximately time-locked with the cardiac cycle; therefore, an average artifact subtraction algorithm can be employed whereby an artifact template is extracted by averaging across multiple cardiac cycles (Allen et al., 1998). Most methods for reducing pulse artifacts rely on using triggering events based on the R-peak obtained from concurrent cardiac traces recorded with the EEG-fMRI. However, caution must be exercised when using ECG in this manner, as it is distorted in the MR environment (Niendorf et al., 2012) and further degraded by the gradient artifact during fMRI acquisition, impairing the detection of R-peaks. According to a widely accepted recommendation (Mullinger et al., 2013a), a good-quality ECG signal (clean and undistorted) can be recorded from a single electrode placed at the base of the subject's back, with the corresponding lead stretched along the paravertebral line.

The BCG can also be corrected for by removing the contribution of independent components (ICs) reflecting artifact-related processes in the back-reconstruction of the EEG signal (Bénar et al., 2003; Mantini et al., 2007; Srivastava et al., 2005).

A hybrid approach that combines two methods has previously been suggested (Debener et al. 2005, 2007). In this approach, the artifact subtraction algorithm is used to remove the majority of the BCG artifact contribution, then followed by an independent component analysis (ICA) decomposition in order to eliminate any remaining artifacts. Although this approach has been effective in removing the artifact, adding an ICA-based correction could

exacerbate the unwanted reductions in physiological signals, inevitably ingrained in any artefact correction approach.

In order to reduce MR-related artifacts on the EEG, the setup of the EEG-fMRI can be optimized. This may involve using shorter and bundled EEG leads, when possible (Assecondi et al. 2016; Jorge et al. 2015b), as well as carefully placing them along the magnet bore to minimize exposure to any scanner vibrations (Mullinger et al. 2013a) and restraining head motion by means of a head-fixation system (Anami et al., 2002).

Gradient Artefact

The changing magnetic fields applied during imaging induce electromagnetic fields in the electrode lead loops (Grouiller et al., 2007). Different functional MR imaging sequences will determine how these gradients change (Niazy et al., 2005).

Amplitude of such artifact can be one hundred times higher than that of the physiological EEG, obscuring the wave forms completely (Allen et al. 2000).

Its spectral content overlapping with the EEG frequency bands makes its removal resorting to basic filtering strategies generally inappropriate. It should be noted, however, that in a few cases MR sequences can be designed such that they induce artifacts at nonessential EEG frequencies, hence allowing a Fourier domain correction (Grouiller et al., 2007; Hoffmann et al., 2000).

In the early days of this technique, t was accepted that the EEG recording during the image acquisition would be obscured, to overcome this problem, the EEG and fMRI acquisitions were interleaved in time. In studies of epilepsy, this was typically achieved by triggering fMRI acquisition immediately after observing an epileptiform spike in the EEG (Warach et al. 1996; Seeck et al. 1998).

Similarly to the BCG artifact, the gradient artifact is also roughly periodic, therefore, the development of artefact subtraction methods has now made truly simultaneous EEG and fMRI recording possible.

To date, the most frequently used approach for eliminating artifacts involves subtracting an artifact template that is created by averaging the artifact signal over several scan repetitions (Allen et al., 2000). The accuracy of this method, along with its various modifications, depends on precise calculation of the artifact template (Negishi et al., 2004; Benar et al., 2003). Moreover, as the imaging artefact contains rapidly changing components, a fast-sampling rate (5 kHz), ten times higher than the rate used in conventional EEG equipment, is required in order to capture these signals adequately (Allen et al. 2000).

Careful alignment of electrode leads can help reduce the artefact amplitude substantially (Lemieux et al., 2022).

Other artefacts

Other non-MRI induced artefacts to EEG recordings are common, including eye movements and blinks, muscle activity, and bad channels (Chaumon et al., 2015). Eye movements and blinks are more prominent in frontal electrodes and produce high-amplitude, high-frequency artifacts (Croft and Barry, 2000; Urigüen and Garcia-Zapirain, 2015). Muscle artifacts are caused by contracting muscles and can affect a wide frequency band and a large surface area due to volume conduction of myogenic activity from different head muscles (Goncharova et al., 2003; McMenamin et al., 2010 Urigüen and Garcia-Zapirain, 2015). Bad channels are characterized by uncorrelated fluctuations with the other channels and are associated with high-impedance electrodes. These types of EEG artifacts are stationary and can be removed using automatic selection and removal of artefactual ICs techniques (Chaumon et al., 2015; Urigüen and Garcia-Zapirain, 2015; Vanderperren et al., 2010.)

4.3. MRI DATA QUALITY

The EEG system can also interfere with the static and dynamic magnetic fields, affecting the quality of the MR image (Krakow et al. 2000; Mullinger et al. 2007). However, these effects can be reduced by carefully designing the EEG equipment.

The generation of electromagnetic noise by the EEG recording equipment can be mitigated through proper shielding and the use of suitable materials that are preferably diamagnetic (Krakow et al., 2000; Stevens et al., 2007). However, any electrode modifications must not compromise the overall functionality of the EEG system and must ensure patient safety, which can be achieved by incorporating current-limiting resistors (Lemieux et al., 1997). Additionally, a minimal amount of conductive gel should be applied to achieve acceptable electrode impedance while minimizing image artifacts (Krakow et al., 2000). Alhough, literature suggests that, at field strengths of 3T, negligible effects on image quality are observed when using commercially available low-density EEG caps (Mullinger et al., 2008a).

4.4. EEG-DERIVED GLM

Given that EEG-fMRI was first applied in patients with epilepsy, the initial efforts to integrate the data were focused on studying subclinical epileptic discharges that occur randomly and without observable behavioural manifestations (Centeno and Carmichael, 2014), van Graan et al., 2015).

Studying spontaneous brain activity using EEG-fMRI presents significant challenges in terms of building a general linear model (GLM). These challenges include identifying and categorizing events of interest, representing those events mathematically, selecting a basis set for the hemodynamic response function (HRF), and comparing models. Moreover, defining the baseline or control state is also difficult due to fluctuations in the background EEG.

In epilepsy EEG-fMRI studies, usually the goal is to identify regions of BOLD change that are associated with the discharges, which may aid in pre-surgical

evaluation. In this case, the timing of interictal epileptiform discharges is used in an event-related fMRI analysis to create regressors that represent the effects of interest.

The onsets of interictal epileptiform discharges, represented as delta functions (implemented a stick function of unitary amplitude), are convolved with a model of the event-related hemodynamic change in the form of a hemodynamic basis set **(Figure 4.2)**.

With each regressor corresponding to a hypothesis that according to Lemieux 2022 can be phrased as follow: "there are brain regions in which the BOLD signal change averaged across the events is nonzero".

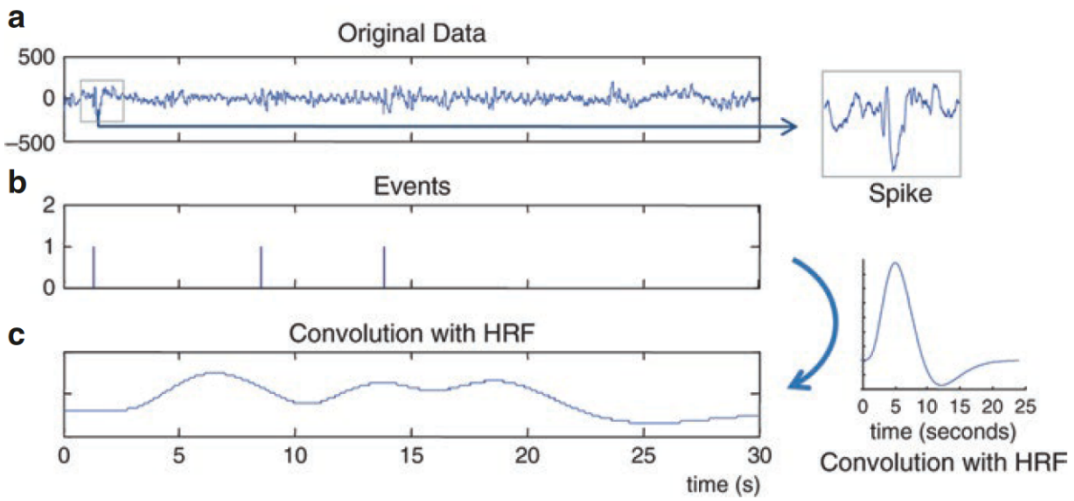

***Figure 4.2**: Modelling of fMRI signal timecourse using event timing alone and basis set consisting of a single function.*
*(**a**) Each event (here, interictal epileptic spikes) is marked by visual inspection of the EEG data recorded in the scanner. (**b**) On set vector: series of identical impulse ("delta") functions. (**c**) Corresponding regressor for a general linear model (GLM) obtained by convolving the events with a canonical HRF.*

The haemodynamic basis set can consist of a single function such as the canonical or standard HRF, or a multiplicity of functions such as assets of time-shifted standard HRFs, the finite impulse response (FIR) and Fourier basis sets (Josephs et al. 1997; Josephs and Henson 1999; Bagshaw et al.

2004). Models that rely on a single function are most effective in identifying BOLD changes that match that function. However, models that incorporate basis sets with multiple functions can be utilized to evaluate the shape of event-related BOLD changes and map interregional variations in the timecourse of these changes. Detection efficiency has been shown to be influenced by variations in the timecourse of BOLD changes related to interictal epileptiform discharges (IEDs) (Kang et al. 2003; Bagshaw et al. 2004; Lu et al. 2006; Salek-Haddadi et al. 2006; Lemieux et al. 2008; Grouiller et al. 2010; Storti et al. 2013).

This is an important aspect of fMRI modelling, as BOLD changes time-locked with EEG events have been shown to possibly appear earlier or later than predicted by the standard model, both in epilepsy and in response to normal brain rhythms (Feige et al. 2005; de Munck et al. 2007; Lemieux et al. 2008), sometimes even prior to scalp EEG changes (Hawco et al. 2007; Pittau et al. 2011).

Further research is necessary, including the use of animal and computational models, to gain a deeper understanding of the physiological processes underlying the variability of the HRF (Mirsattari et al. 2006; Vanzetta et al. 2010; Voges et al. 2012; Saillet et al. 2016).

Ultimately, the issues of HRF variability are a problem of model selection, which is a fundamental challenge in science. This problem is particularly tricky in the classical statistical framework, as it tends to favor complex models over simpler ones because the former can "mechanically" account for a larger portion of the variance.

4.4.1. EEG Spectral Analysis

The identification of brain regions that are associated with changes in brain rhythms and EEG spectral power has been one of the most significant applications of EEG-fMRI.

Typically, EEG data are filtered into short epochs of the order of a second, and power in one or more frequency bands is quantified for each epoch. In most applications, the power timeseries is convolved with the HRF (see Chapter 3, paragraph 3.2) and entered as a regressor in a GLM analysis **(Figure 4.3)** (Wirsich et al., 2022). The choice of EEG channel or group of channels for the power calculation requires careful consideration (Laufs et al., 2003) as this type of analysis is very susceptible to artefacts.

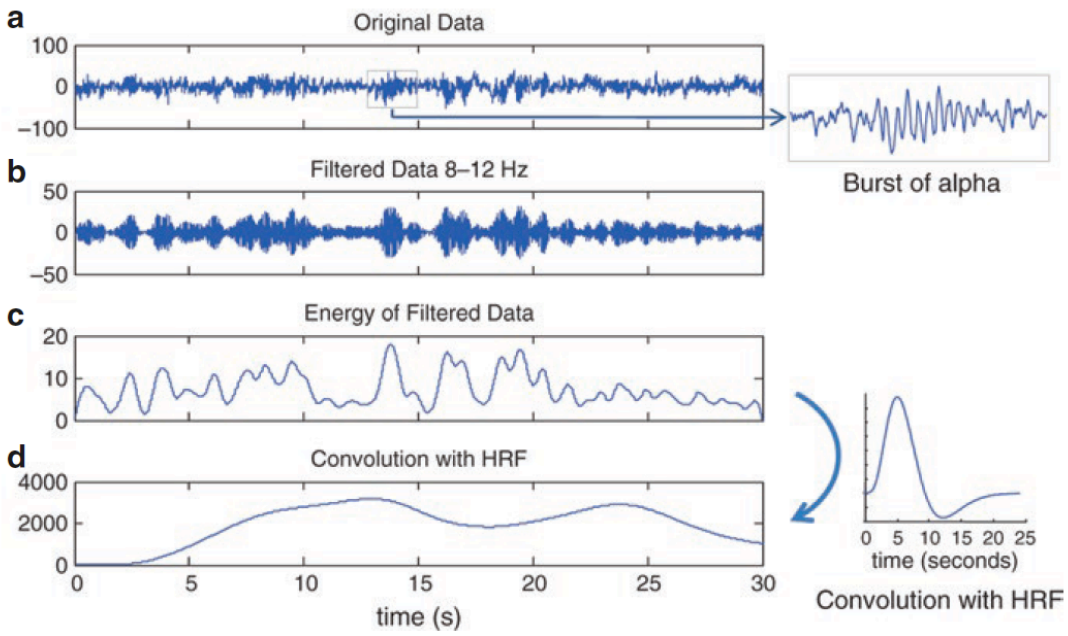

***Figure 4.3**: Modelling of fMRI timeseries using the energy within a frequency band. (**a**) Original EEG data, where several alpha wave bursts can be seen. (**b**, **c**) Energy in the 8–12 Hz band, using a sliding window Fourier transform (Goldman et al. 2002). (d) Regressor obtained by convolving energy with canonical HRF*

4.4.2. EEG-informed fMRI Functional Connectivity, PPI

The interplay between EEG frequency and BOLD activity during rest is intricate and manifested by the presence of various intrinsic functionally connected networks, known as intrinsically connected networks (ICNs) or resting state networks (RSNs).

Since fMRI-FC is generally measured by the temporal correlation over a 10–20 min resting-state recording, EEG power cannot readily be integrated by using a GLM.

To link functional connectivitty changes in a conditional setting, the psychophysiological and modulatory interactions (PPI) approach can be used (Friston et al. 1997). This allows the EEG modulation of the fluctuating connectivity changes to be investigated using a GLM.

PPI is a model of “contribution” and occupy middle ground between between models of functional vs. effective connectivity. Functional connectivity is defined as the temporal correlation between spatially separated neurophysiological events (see Chapter 3, paragraph 3.3). FC analyses are typically model-free and do not specify a direction of influence. In contrast, PPI’s are based on regression models, and therefore a direction of influence is chosen based on the model.

The interaction between the source region and experimental context (or two source regions) can be interpreted in 2 different ways: 1) as demonstrating how the contribution of one region to another is altered by the experimental context or task, or 2) as an example of how an area’s response to an experimental context is modulated by input from another region **(Figure 4.4)**.

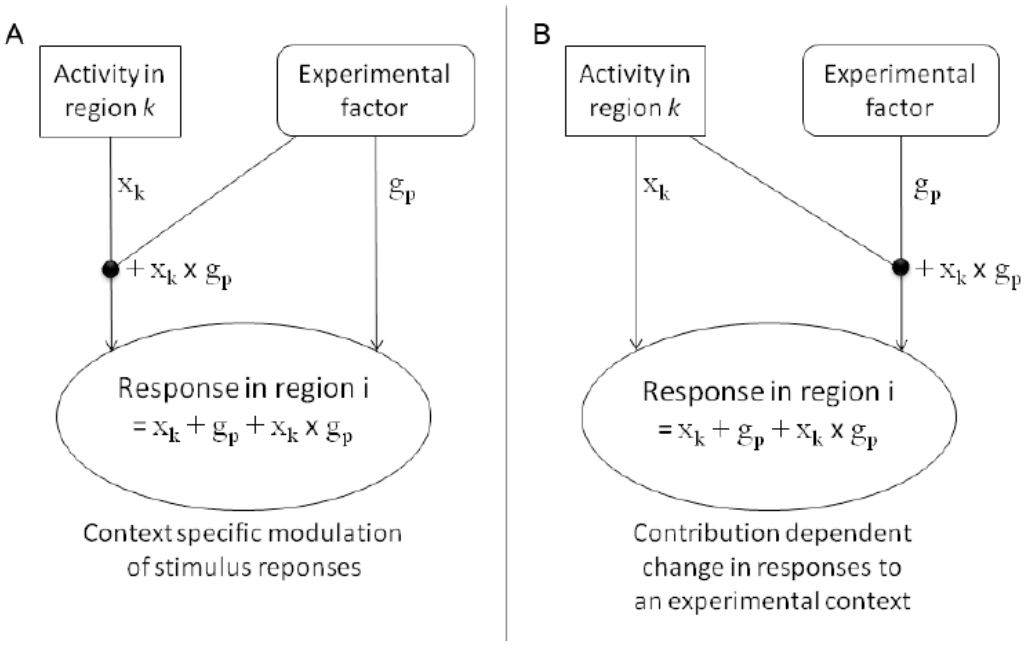

***Figure 4.4**: Two alternative interpretations of PPI effects.*
*(**A**) The contribution of one area (k) to another (i) is altered by the experimental (psychological) context. (**B**) The response of an area (i) to an experimental (psychological) context due to the contribution of region (k). (http://www.fil.ion.ucl.ac.uk/spm/doc/manual.pdf)*

Please note that PPI has been used in the experimental study described in Chapter 11.

SECTION I: REFERENCES

Akay, M., editor (2006) Wiley encyclopedia of biomedical engineering. John Wiley & Sons, Hoboken, New Jersey

Allen PJ, Josephs O, Turner R. (2000) A method for removing imaging artifact from continuous EEG recorded during functional MRI. NeuroImage. 12(2):230–239

Allen PJ, Polizzi G, Krakow K, Fish DR, Lemieux L (1998) Identification of EEG events in the MR scanner: the problem of pulse artifact and a method for its subtraction. NeuroImage. 8(3):229–239

Amzica F, Lopes da Silva FH (2018) Cellular substrates of brain rhythms. In: Schomer DL, Lopes da Silva FH (eds) Niedermeyer's electroencephalography: basic principles, clinical applications and related fields, 7th edn. Oxford University Press, Oxford, pp 20–62

Anami K, Mori T, Tanaka F, Kawagoe Y, Okamoto J, Yarita M, Ohnishi T, Yumoto M, Matsuda H, Saitoh O (2003) Stepping stone sampling for retrieving artifact-free electroencephalogram during functional magnetic resonance imaging. Neuroimage 19(2 Pt 1):281–295

Assecondi S, Lavallee C, Ferrari P et al (2016) Length matters: improved high field EEG–fMRI recordings using shorter EEG cables. J Neurosci Methods 269:74–87. https://doi.org/10.1016/j.jneumeth.2016.05.014

Babiloni F, Babiloni C, Carducci F, Romani GL, Rossini PM, Angelone LM, Cincotti F (2003) Multimodal integration of high-resolution EEG and functional magnetic resonance imaging data: a simulation study. NeuroImage 19(1):1–15

Bagshaw AP, Aghakhani Y, Benar CG, Kobayashi E, Hawco C, Dubeau F, Pike GB, Gotman J (2004) EEG-fMRI of focal epileptic spikes: analysis with multiple haemodynamic functions and comparison with gadolinium-enhanced MR angiograms. Hum Brain Mapp 22(3):179–192

Barrington SF, Koutroumanidis M, Agathonikou A, Marsden PK, Binnie CD, Polkey CE, Maisey MN, Panayiotopoulos CP (1998) Clinical value of "ictal" FDG-positron emission tomography and the routine use of simultaneous scalp EEG studies in patients with intractable partial epilepsies. Epilepsia 39(7):753–766

Benar C, Aghakhani Y, Wang Y, Izenberg A, Al Asmi A, Dubeau F, Gotman J (2003) Quality of EEG in simultaneous EEG–fMRI for epilepsy. Clin Neurophysiol 114(3):569–580

Benar CG, Schon D, Grimault S, Nazarian B, Burle B, Roth M, Badier JM, Marquis P, Liegeois-Chauvel C, Anton JL (2007) Single-trial analysis of oddball event-related potentials in simultaneous EEG-fMRI. Hum Brain Mapp 28:602–613

Beyer T, Townsend DW, Brun T, Kinahan PE, Charron M, Roddy R, Jerin J, Young J, Byars L, Nutt R (2000) A combined PET/CT scanner for clinical oncology. J Nucl Med 41(8):1369–79

Berger H (1929) Über des Elekrenkephalogramm des Menschen. Arch Psychiat Nervenkr 87:527–570

Biswal BB et al. (2010) Toward discovery science of human brain function. Proc Nat Acad Sci U S A 107:4734-4739.

Bonmassar G, Anami K, Ives J, Belliveau JW (1999) Visual evoked potential (VEP) measured by simultaneous 64-channel EEG and 3T fMRI. Neuroreport. 10(9):1893–1897

Bonmassar G, Schwartz DP, Liu AK, Kwong KK, Dale AM, Belliveau JW (2001) Spatiotemporal brain imaging of visual-evoked activity using interleaved EEG and fMRI recordings. NeuroImage. 13(6 Pt 1):1035–1043

Bonmassar G, Purdon PL, Jääskeläine IP, Chiappa K, Solo V, Brown EN, Belliveau,JW (2002) Motion and Ballistocardiogram Artifact Removal for Interleaved Recording ofEEG and EPs during MRI. NeuroImage, 16(4):1127–1141,

Brandt SA, Davis TL, Obrig H, Meyer BU, Belliveau JW, Rosen BR, Villringer A (1996) Functional magnetic resonance imaging shows localized brain activation during serial transcranial stimulation in man. Neuroreport 7:734–736

Brett, M, Penny, W, Keibel, S (2003) Introduction to Random Field Theory. In: Human Brain Mapping.

Buchner H, Fuchs M, Wischmann HA, Dössel O, Ludwig I, Knepper A, Berg P (1994) Source analysis of median nerve and finger stimulated somatosensory evoked potentials: multichannel simultaneous recording of electric and magnetic fields combined with 3D-MR tomography. Brain Topogr 6(4):299–310

Buchsbaum MS, Kessler R, King A, Johnson J, Cappelletti J (1984) Simultaneous cerebral glucography with positron emission tomography and topographic electroencephalography. Prog Brain Res 62:263–9. https://doi.org/10.1016/S0079-6123(08)62182-2. PMID: 6335920

Busch E, Hoehn-Berlage M, Eis M, Gyngell ML, Hossmann KA. (1995). Simultaneous recording of EEG, DC potential and diffusion-weighted NMR imaging during potassium induced cortical spreading depression in rats. NMR Biomed 8(2):59–64

Carmichael DW, Hamandi K, Laufs H, Duncan JS, Thomas DL, Lemieux L (2008) An investigation of the relationship between BOLD and perfusion signal changes during epileptic generalised spike wave activity. Magn Reson Imaging 26(7):870–873

Catana C, Procissi D, Wu Y, Judenhofer MS, Qi J, Pichler BJ, Jacobs RE, Cherry SR (2008) Simultaneous in vivo positron emission tomography and magnetic resonance imaging. Proc Natl Acad Sci U S A 105(10):3705–3710

Caton R (1875) The electric currents of the brain. Br Med J 2:278 Centeno M, Carmichael DW (2014) Network Connectivity in Epilepsy: Resting State fMRI and EEG-fMRI Contributions. Frontiers in neurology 5:93.

Centeno M, Carmichael DW (2014) Network connectivity in epilepsy: resting state fMRI and EEG-fMRI contributions. Front Neurol 5:93

Chang BS, Schomer DL and Niedermeyer E (2018) Epilepsy in Adults and the Elderly. In: Niedermeyer E, Lopes da Silva F (eds) Electroencephalography: basic principles, clinical applications and related fields, 6th edn. Lippincott, Williams & Wilkins, New York.

Chaumon M, Bishop DV, Busch N (2015) A Practical Guide to the Selection of Independent Components of the Electroencephalogram for Artifact Correction. Journal of Neuroscience Methods

Croft RJ and Barry RJ (2000) Removal of ocular artifact from the EEG: a review. Neurophysiologie clinique/Clinical neurophysiology, 30(1):5–19

Dale, A. M. and Halgren, E (2001) Spatiotemporal mapping of brain activity by integration of multipleimaging modalities. Current Opinion in Neurobiology, 11(2):202–208.

Damoiseaux JS, Rombouts SA, Barkhof F, Scheltens P, Stam CJ, Smith SM, Beckmann CF (2006) Consistent resting-state networks across healthy subjects. Proc Natl Acad Sci U S A 103:13848-13853.

Daunizeau J, Mattout J, Clonda D, Goulard B, Benali H, Lina JM (2006) Bayesian spatio-temporal approach for EEG source reconstruction: conciliating ECD and distributed models. IEEE Trans Biomed Eng 53(3):503–16. https://doi.org/10.1109/TBME.2005.869791

Daunizeau, J., David, O., Stephan, K.E. (2011a) Dynamic causal modelling: a critical review of the biophysical and statistical foundations. NeuroImage 58 (2):312–322

Daunizeau, Jean, et al. (2011b) Optimizing experimental design for comparing models of brain function. PLoS Comput. Biol. 7 11:e1002280

Debener S, Ullsperger M, Siegel M, Fiehler K, von Cramon DY, Engel AK (2005) Trial-by-trial coupling of concurrent electroencephalogram and functional magnetic resonance imaging identifies the dynamics of performance monitoring. J Neurosci 25:11730–11737

Debener S, Strobel A, Sorger B, Peters J, Kranczioch C, Engel AK, Goebel R (2007) Improved quality of auditory event-related potentials recorded simultaneously with 3-T fMRI: Removal of the ballistocardiogram artefact. NeuroImage, 34(2):587–597

Debener, S, Mullinger KJ, Niazy RK, Bowtell RW (2008) Properties of the ballistocardiogram artefact as revealed by EEG recordings at 1.5, 3 and 7 T static magnetic field strength. International Journal of Psychophysiology, 67(3):189–199.

de Curtis, M. and Avanzini, G. (2001) Interictal spikes in focal epileptogenesis. Progress in Neurobiology, 63(5):541–567

Deichmann R, Nöth U, Merola A, Weiskopf N (2022) The Basics of Functional Magnetic Resonance Imaging. In: Mulert C., Lemieux L (eds) EEG-fMRI: Physiological basis, Thechniques, and Applications.7th Edition. Springer Nature Switzerland https://doi.org/10.1007/978-3-031-07121-8

de Munck JC, Gonçalves SI, Huijboom L, Kuijer JP, Pouwels PJ, Heethaar RM, Lopes da Silva FH (2007) The hemodynamic response of the alpha rhythm: an EEG/fMRI study. NeuroImage 35(3):1142–1151

Feige B, Scheffler K, Esposito F, Di Salle F, Hennig J, Seifritz E (2005) Cortical and subcortical correlates of electroencephalographic alpha rhythm modulation. J Neurophysiol 93(5):2864–2872

Fox MD, Corbetta M, Snyder AZ, Vincent JL, Raichle ME (2006) Spontaneous neuronal activity distinguishes human dorsal and ventral attention systems. Proc Natl Acad Sci U S A 103:10046-10051.

Friston KJ (1994) Functional and effective connectivity in neuroimaging: a synthesis. Hum. Brain Mapp. 2 (1–2), 56–78

Friston KJ, Ashburner J, Frith CD, Poline JB, Heather JD, Frackowiak RSJ (1995) Spatial registration and normalization of images. Hum Brain Mapp 3(3):165–189

Friston KJ (1995) Functional and effective connectivity in neuroimaging: A synthesis. Human Brain Mapping, 2:56–78

Friston KJ, Williams S, Howard R, Frackowiak RS, Turner R (1996) Movement-related effects in fMRI time-series. Magn Reson Med 35(3):346–355

K.J. Friston, C. Buchel, G.R. Fink, J. Morris, E. Rolls, and R. Dolan (1997) Psychophysiological and modulatory interactions in neuroimaging. NeuroImage, 6:218–229,

Friston KJ (2002) Bayesian estimation of dynamical systems: an application to fMRI. NeuroImage 16 (2), 513–53

Friston KJ, Harrison L, Penny W (2003) Dynamic causal modelling. NeuroImage 19 (4), 1273–1302

Friston, K (2009) Causal modelling and brain connectivity in functional magnetic resonanceimaging. PLoS Biol. 7 (2), e33

Friston KJ (2011) Functional and effective connectivity: a review. Brain Connectivity 1(1):13–36

Gamma A, Lehmann D, Frei E, Iwata K, Pascual-Marqui RD, Vollenweider FX (2004) Comparison of simultaneously recorded [H215O]-PET and LORETA during cognitive and pharmacological activation. Hum Brain Mapp 22(2):83–96

Goebel R and Esposito F (2022) The Added Value of EEG-fMRI in Imaging Neuroscience. In: Mulert C., Lemieux L (eds) EEG-fMRI: Physiological basis, Thechniques, and Applications.7th Edition. Springer Nature Switzerland https://doi.org/10.1007/978-3-031-07121-8

Goldman RI, Stern JM, Engel J Jr, Cohen MS (2000) Acquiring simultaneous EEG and functional MRI. Clin Neurophysiol. 111(11):1974–1980

Goncharova I, McFarland D, Vaughan T, Wolpaw J (2003) EMG contamination of EEG: spectral and topographical characteristics. Clinical Neurophysiology, 114(9):1580–1593,

Gregory RP, Oates T, Merry RT (1993) Electroencephalogram epileptiform abnormalities in candidates for aircrew training. Electroencephalogr Clin Neurophysiol 86:75–77

Grouiller F, Vercueil L, Krainik A, Segebarth C, Kahane P, David O (2007) A comparative study of different artefact removal algorithms for EEG signals acquired during functional MRI. Neuroimage 38(1):124–137

Grouiller F, Vercueil L, Krainik A, Segebarth C, Kahane P, David O (2010) Characterization of the hemodynamic modes associated with interictal epileptic activity using a deformable model-based analysis of combined EEG and functional MRI recordings. Hum Brain Mapp 31(8):1157–1173

Hamandi K, Laufs H, Nöth U, Carmichael DW, Duncan JS, Lemieux L (2008) BOLD and perfusion changes during epileptic generalised spike wave activity. Neuroimage 39:608–618

Harel N, Lee SP, Nagaoka T, Kim DS, Kim SG (2002) Origin of negative blood oxygenation level-dependent fMRI signals. J Cereb Blood Flow Metab 22:908–917

Havlicek M, Roebroeck A, Friston KJ, Gardumi A, Ivanov D, Uludag K (2015) Physiologically informed dynamic causal modelling of fMRI data. Neuroimage 122:355–372

Hawco CS, Bagshaw AP, Lu Y, Dubeau F, Gotman J (2007) BOLD changes occur prior to epileptic spikes seen on scalp EEG. NeuroImage 35(4):1450–1458

Hawsawi HB, Allen PJ, Warbrick T, Störmer R, Iannotti G, Grouiller F, Vulliemoz S, Lemieux L (2022) EEG Instrumentation and Safety in the MRI Environment. In: Mulert C., Lemieux L (eds) EEG-fMRI: Physiological basis, Thechniques, and Applications.7th Edition. Springer Nature Switzerland https://doi.org/10.1007/978-3-031-07121-8

He, B. J., Zempel, J. M., Snyder, A. Z., and Raichle, M. E. (2010) The temporal structures and functionalsignificance of scale-free brain activity. Neuron, 66(3):353–369

Heinze HJ, Mangun GR, Burchert W, Hinrichs H, Scholz M, Munte TF, Gos A, Scherg M, Johannes S, Hundeshagen H (1994) Combined spatial and temporal imaging of brain activity during visual selective attention in humans. Nature 372:543–546

Hoffmann A, Jager L, Werhahn KJ et al (2000) Electroencephalography during functional echo-planar imaging: detection of epileptic spikes using post-processing methods. Magn Reson Med 44:791–798

Hoshi Y, Mizukami S, Tamura M (1994) Dynamic features of hemodynamic and metabolic changes in the human brain during all-night sleep as revealed by near-infrared spectroscopy. Brain Res 652(2):257–262

Huettel, S. A., Song, A.W., and McCarthy, G. (2004) Functional magnetic resonance imaging., volume 1.Sinauer Associates Sunderland

Ives JR, Warach S, Schmitt F, Edelman RR, Schomer DL (1993). Monitoring the patient's EEG during echo planar MRI. Electroencephalogr Clin Neurophysiol 87:417–420

Jorge J, Grouiller F, Ipek Ö et al (2015) Simultaneous EEG–fMRI at ultra-high field: artefact prevention and safety assessment. NeuroImage 105:132–144. https://doi.org/10.1016/j.neuroimage.2014.10.055

Josephs O, Turner R, Friston K (1997) Event-related f MRI. Hum Brain Mapp 5:243–248 Kazemi NJ, So EL, Mosewich RK et al (1997) Resection of frontal encephalomalacias for intractable epilepsy: outcome and prognostic factors. Epilepsia 38:670–677

Josephs O, Henson RN (1999) Event-related functional magnetic resonance imaging: modelling, inference and optimization. Philos Trans R Soc Lond Ser B Biol Sci 354(1387):1215–1228

Judenhofer MS, Wehrl HF, Newport DF, Catana C, Siegel SB, Becker M, Thielscher A, Kneilling M, Lichy MP, Eichner M, Klingel K, Reischl G, Widmaier S, Röcken M, Nutt RE, Machulla HJ, Uludag K, Cherry SR, Claussen CD, Pichler BJ (2008) Simultaneous PET-MRI: a new approach for functional and morphological imaging. Nat Med 14(4):459–465

Kahan J and Foltynie T (2013) Understanding DCM: Ten simple rules for the clinician. NeuroImage, 83:542–549

Kang JK, Benar C, Al-Asmi A, Khani YA, Pike GB, Dubeau F, Gotman J (2003) Using patient-specific hemodynamic response functions in combined EEG-fMRI studies in epilepsy. NeuroImage 20(2):1162–1170

Kannurpatti SS, Biswal BB (2004) Negative functional response to sensory stimulation and its origins. J Cereb Blood Flow Metab 24:703–712

Kida I, Yamamoto T, Tamura M (1996) Interpretation of BOLD MRI signals in rat brain using simultaneously measured near-infrared spectrophotometric information. NMR Biomed 9(8):333–338

Kim H, Hua Y, Chen HT, Tsai HM, Chen CT, Karczmar G, Fan X, Xi D, Xie Q, Chou CY, Kao CM (2020) Design, evaluation and initial imaging results of a PET insert based on strip-line readout for simultaneous PET/MRI. Nucl Instrum Methods Phys Res A 959:163575

Kirkpatrick PJ, Lam J, Al-Rawi P, Smielewski P, Czosnyka M (1998) Defining thresholds for critical ischemia by using near-infrared spectroscopy in the adult brain. J Neurosurg 89(3):389–394

Kleinschmidt A, Obrig H, Requardt M, Merboldt KD, Dirnagl U, Villringer A, Frahm J (1996) Simultaneous recording of cerebral blood oxygenation changes during human brain activation by magnetic resonance imaging and near-infrared spectroscopy. J Cereb Blood Flow Metab 16(5):817–826

Krakow K, Allen PJ, Symms MR, Lemieux L, Josephs O, Fish DR (2000) EEG recording during fMRI experiments: image quality. Hum Brain Mapp10(1):10–15

Krakow K, Lemieux L, Messina D, Scott CA, Symms MR, Duncan JS, Fish DR (2001a) Spatio-temporal imaging of focal interictal epileptiform activity using EEG-triggered functional MRI. Epileptic Disord 3(2):67–74

Krakow K, Messina D, Lemieux L, Duncan JS, Fish DR (2001b) Functional MRI activation of individual interictal epileptiform spikes. NeuroImage 13(3):502–505

Kwong KK, Belliveau JW, Chesler DA, Goldberg IE, Weisskoff RM, Poncelet BP, Kennedy DN, Hoppel BE, Cohen MS, Turner R, Cheng HM, Brady TJ, Rosen BR (1992) Dynamic magnetic resonance imaging of human brain activity during primary sensory stimulation. Proc Natl Acad Sci U S A 89:5675–5679

Laufs H, Kleinschmidt A, Beyerle A, Eger E, Salek-Haddadi A, Preibisch C, Krakow K (2003) EEG-correlated fMRI of human alpha activity. NeuroImage 19(4):1463–1476

Laufs H (2012) A personalized history of EEG-fMRI integration. NeuroImage 62:1056–1067. https://doi.org/10.1016/j.neuroimage.2012.01.039

Lauritzen M (2005) Reading vascular changes in brain imaging: is dendritic calcium the key? Nat Rev Neurosci 6:77–85

Leite M, Leal A, Figueiredo P (2013) Transfer function between EEG and BOLD signals of epileptic activity. Frontiers in Neurology, 4 JAN(January):1–13

Lemieux L, Allen PJ, Franconi F, Symms MR, Fish DR. Recording of EEG during fMRI experiments: patient safety. Magn Reson Med. 38(6):943–952

Lemieux L, Krakow K, Fish DR (1997) Comparison of spike-triggered functional MRI BOLD activation and EEG dipole model localization. NeuroImage. (2001a) 14(5):1097–1104

Lemieux L, Salek-Haddadi A, Josephs O, Allen P, Toms N, Scott C, Krakow K, Turner R, Fish DR (2001b) Event-related fMRI with simultaneous and continuous EEG: description of the method and initial case report. NeuroImage. 14(3):780–787

Lemieux L, Laufs H, Carmichael D, Paul JS, Walker MC, Duncan JS (2008) Noncanonical spike-related BOLD responses in focal epilepsy. Hum Brain Mapp 29(3):329–345

Lindquist MA (2008) The statistical analysis of fMRI data. Stat Sci 23(4):439–46

Liu AK, Belliveau JW, Dale AM (1998) Spatiotemporal imaging of human brain activity using functional MRI constrained magnetoencephalography data: Monte Carlo simulations. Proc Natl Acad Sci U S A 95:8945–8950

Logothetis NK, Pauls J, Augath M, Trinath T, Oeltermann A (2001) Neurophysiological investigation of the basis of the fMRI signal. Nature 412:150–157

Logothetis, NK. (2003) The underpinnings of the BOLD functional magnetic resonance imaging signal. J Neurosci 23: 3963-71.

Lopes da Silva FH (2002) Electrical potentials. In: Ramachandran VS (ed) Encyclopedia of the human brain. Elsevier, New York, pp 147–167

Lopes da Silva FH, van Rotterdam A (2018a) Biophysical aspects of EEG and magnetoencephalographic generation. In: Niedermeyer E, Lopes da Silva F (eds) Electroencephalography: basic principles, clinical applications and related fields, 6th edn. Lippincott, Williams & Wilkins, New York.

Lopes da Silva (2018b) Event-Related Potentials: General Aspects of Methodology and Quantification. In: Niedermeyer E, Lopes da Silva F (eds) Electroencephalography: basic principles, clinical applications and related fields, 6th edn. Lippincott, Williams & Wilkins, New York.

Lopes da Silva FH (2022) EEG: Origin and Measurement. In: Mulert C., Lemieux L (eds) EEG-fMRI: Physiological basis, Thechniques, and Applications.7th Edition. Springer Nature Switzerland https://doi.org/10.1007/978-3-031-07121-8

Lu Y, Bagshaw AP, Grova C, Kobayashi E, Dubeau F, Gotman J (2006) Using voxel-specific hemodynamic response function in EEG-fMRI data analysis. NeuroImage 32(1):238–247

Mackert BM, Wübbeler G, Leistner S, Uludag K, Obrig H, Villringer A, Trahms L, Curio G (2004) Neurovascular coupling analyzed non-invasively in the human brain. Neuroreport 15(1):63–66

Mantini D, Perrucci MG, Cugini S, Ferretti A, Romani GL, Del Gratta C (2007) Complete artifact removal for EEG recorded during continuous fMRI using independent component analysis. Neuroimage 34(2):598–607

Marsan CA, Zivin LS (1970) Factors related to the occurrence of typical paroxysmal abnormalities in the EEG records of epileptic patients. Epilepsia 11:361–381

McCormick DA, Contreras D (2001) On the cellular and network bases of epileptic seizures. Annu Rev Physiol 63:815–846

McDannold N, Moss M, Killiany R, Rosene DL, King RL, Jolesz FA, Hynynen K (2003) MRI-guided focused ultrasound surgery in the brain: tests in a primate model. Magn Reson Med 49(6):1188–1191

McMenamin BW, Shackman AJ, Maxwell JS, Bachhuber DRW, Koppenhaver AM, Greischar LL , Davidson RJ (2010) Validation of ICA-based myogenic artifact correction for scalp and source-localized EEG. NeuroImage, 49(3):2416–32,

McRobbie, DW, Moore EA, Graves MJ, Prince MR (2007) MRI from Picture to Proton. Cambridge university press

Mehagnoul-Schipper DJ, van der Kallen BF, Colier WN, van der Sluijs MC, van Erning LJ, Thijssen HO, Oeseburg B, Hoefnagels WH, Jansen RW (2002) Simultaneous measurements of cerebral oxygenation changes during brain activation by near-infrared spectroscopy and functional magnetic resonance imaging in healthy young and elderly subjects. Hum Brain Mapp 16(1):14–23

Mirsattari SM, Wang Z, Ives JR, Bihari F, Leung LS, Bartha R, Menon RS (2006) Linear aspects of transformation from interictal epileptic discharges to BOLD fMRI signals in an animal model of occipital epilepsy. NeuroImage 30(4):1133–1148

Moosmann M, Ritter P, Krastel I, Brink A, Thees S, Blankenburg F, Taskin B, Obrig H, Villringer A (2003) Correlates of alpha rhythm in functional magnetic resonance imaging and near infra

red spectroscopy. Neuroimage 20:145–158

Mulert C, Jäger L, Schmitt R, Bussfeld P, Pogarell O, Möller HJ, Juckel G, Hegerl U (2004) Integration of fMRI and simultaneous EEG: towards a comprehensive understanding of localization and time-course of brain activity in target detection. NeuroImage 22(1):83–94

Mulert C., Lemieux L (2022) EEG-fMRI: Physiological basis, Thechniques, and Applications.7th Edition. Springer Nature Switzerland https://doi.org/10.1007/978-3-031-07121-8

Mulert C. (2022) What Can fMRI Add to the ERP Story? In: Mulert C., Lemieux L (eds) EEG-fMRI: Physiological basis, Thechniques, and Applications.7th Edition. Springer Nature Switzerland https://doi.org/10.1007/978-3-031-07121-8

Mullinger K, Debener S, Coxon R, Bowtell R (2007) Effects of simultaneous EEG recording on MRI data quality at 1.5, 3 and 7 tesla. Int J Psychophysiol 67:178–188

Mullinger K, Brookes M, Stevenson C, Morgan P, Bowtell R (2008) Exploring the feasibility of simultaneous electroencephalography/functional magnetic resonance imaging at 7 T. Magn Reson Imaging 26(7):968–977

Mullinger, KJ, Havenhand, J, Bowtell R (2013) Identifying the sources of the pulse artefact in EEG recordings made inside an MR scanner. NeuroImage, 71:75–83

Negishi M et al (2004) Removal of time-varying gradient artifacts from EEG data acquired during continuous fMRI. Clin Neurophysiol 115(9):2181–2192

Neuner I, Warbrick T, Arrubla J, Felder J, Celik A, Reske M, Boers F, Shah NJ (2013) EEG acquisition in ultra-high static magnetic fields up to 9.4 T. NeuroImage 68:214–220

Niazy RK, Beckmann CF, Iannetti GD, Brady JM, Smith SM (2005) Removal of FMRI environment artifacts from EEG data using optimal basis sets. Neuroimage 28(3):720–737

Niedermeyer E and Schomer DL (2018) Historical Aspects of EEG In: Niedermeyer E, Lopes da Silva F (eds) Electroencephalography: basic principles, clinical applications and related fields, 6th edn. Lippincott, Williams & Wilkins, New York

Niendorf T, Winter L, Frauenrath T (2012) Electrocardiogram in an MRI environment: clinical needs, practical considerations, safety implications, technical solutions and future directions. In: Advances

Nunez PL (1995) Neocortical dynamics and human EEG rhythms. Oxford University Press, New York

Nunez, P. L. and Silberstein, R. B (2000) On the Relationship of Synaptic Activity to MacroscopicMeasurements: Does Co-Registration of EEG with fMRI Make Sense? Brain Topography, 13 (2):79–96

Obrig H, Israel H, Kohl-Bareis M, Uludag K, Wenzel R, Müller B, Arnold G, Villringer A (2002) Habituation of the visually evoked potential and its vascular response: implications for neurovascular coupling in the healthy adult. NeuroImage 17(1):1–18

Ogawa S, Lee TM, Nayak AS, Glynn P (1990) Oxygenation-sensitive contrast in magnetic resonance image of rodent brain at high magnetic fields. Magn Reson Med 14:68–78

Pittau F, Levan P, Moeller F, Gholipour T, Haegelen C, Zelmann R, Dubeau F, Gotman J (2011) Changes preceding interictal epileptic EEG abnormalities: comparison between EEG/fMRI and intracerebral EEG. Epilepsia 52(6):1120–1129

Plummer C, Vogrin SJ, Woods WP, Murphy MA, Cook MJ, Liley DTJ (2019) Interictal and ictal source localization for epilepsy surgery using high-density EEG with MEG: a prospective long-term study. Brain 142(4):932–951

Polinder-Bos HA, Elting JWJ, Aries MJ, García DV, Willemsen AT, van Laar PJ, Kuipers J, Krijnen WP, Slart RH, Luurtsema G, Westerhuis R, Gansevoort RT, Gaillard CA, Franssen CF (2020) Changes in cerebral oxygenation and cerebral blood flow during hemodialysis—a simultaneous near-infrared spectroscopy and positron emission tomography study. J Cereb Blood Flow Metab 40(2):328–340

Punwani S, Ordidge RJ, Cooper CE, Amess P, Clemence M (1998) MRI measurements of cerebral deoxyhaemoglobin concentration [dHb]—correlation with near infrared spectroscopy (NIRS). NMR Biomed 11(6):281–289

Rosa MJ, Daunizeau J, Friston KJ(2010) EEG-fMRI integration: a critical review of biophysical modelling and data analysis approaches. Journal of integrative neuroscience, 9(04): 453–476,

Sabri O, Owega A, Schreckenberger M, Sturz L, Fimm B, Kunert P, Meyer PT, Sander D, Klingelhöfer J (2003) A truly simultaneous combination of functional transcranial Doppler sonography and H215O PET adds fundamental new information on differences in cognitive activation between schizophrenics and healthy control subjects. J Nucl Med 44(5):671–681

Sadato N, Nakamura S, Oohashi T, Nishina E, Fuwamoto Y, Waki A, Yonekura Y (1998) Neural networks for generation and suppression of alpha rhythm: a PET study. Neuroreport 9(5):893–897

Saillet S, Quilichini PP, Ghestem A, Giusiano B, Ivanov AI, Hitziger S, Vanzetta I, Bernard C, Benar CG (2016) Interneurons contribute to the hemodynamic/metabolic response to epileptiform discharges. J Neurophysiol 115(3):1157–1169

Salek-Haddadi A, Diehl B, Hamandi K, Merschhemke M, Liston A, Friston K, Duncan JS, Fish DR, Lemieux L (2006) Hemodynamic correlates of epileptiform discharges: an EEG-fMRI study of 63 patients with focal epilepsy. Brain Res 1088(1):148–166

Salustri C, Chapman RM (1989) A simple method for 3-dimensional localization of epileptic activity recorded by simultaneous EEG and MEG. Electroencephalogr Clin Neurophysiol 73(6):473–478

Schomer DL and Lopes da Silva FH (2018) Niedermeyer's ElectroencephalographyBasic Principles, Clinical Applications, and Related Fields. Oxford University Press. 7th Edition.

Seeck M, Lazeyras F, Michel CM, Blanke O, Gericke CA, Ives J, Delavelle J, Golay X, Haenggeli CA, de Tribolet N, Landis T (1998) Non-invasive epileptic focus localization using EEG-triggered functional MRI and electromagnetic tomography. Electroencephalogr Clin Neurophysiol 106:508–512

Seki Y, Miyashita T, Kandori A, Maki A, Koizumi H (2012) Simultaneous measurement of neuronal activity and cortical hemodynamics by unshielded magnetoencephalography and near-infrared spectroscopy. J Biomed Opt 17(10):107001

Shin J, von Lühmann A, Kim DW, Mehnert J, Hwang HJ, Müller KR (2018) Simultaneous acquisition of EEG and NIRS during cognitive tasks for an open access dataset. Sci Data 5:180003

Shmuel A, Augath M, Oeltermann A, Logothetis NK (2006) Negative functional MRI response correlates with decreases in neuronal activity in monkey visual area V1. Nat Neurosci 9:569–577

Shmuel A and Maier A (2022) Locally Measured Neuronal Correlates of Functional MRI Signals. In: Mulert C., Lemieux L (eds) EEG-fMRI: Physiological basis, Thechniques, and Applications.7th Edition. Springer Nature Switzerland https://doi.org/10.1007/978-3-031-07121-8

Siero JCW, Hermes D, Hoogduin H, Luijten PR, Ramsey NF, Petridou N (2014) BOLD matches neuronal activity at the mm scale: a combined 7 T fMRI and ECoG study in human sensorimotor cortex. Neuroimage 101:177–184

Smith SM, Fox PT, Miller KL, Glahn DC, Fox PM, Mackay CE, Filippini N, Watkins KE, Toro R, Laird AR, Beckmann CF (2009) Correspondence of the brain's functional architecture during activation and rest. Proc Natl Acad Sci U S A 106:13040-13045

Srivastava G, Crottaz-Herbette S, Lau KM, Glover GH, Menon V (2005) ICA-based procedures for removing ballistocardiogram artifacts from EEG data acquired in the MRI scanner. NeuroImage 24(1):50–60

Stancak A, Polacek H, Vrana J, Rachmanova R, Hoechstetter K, Tintra J, Scherg M (2005) EEG source analysis and fMRI reveal two electrical sources in the fronto-parietal operculum during subepidermal finger stimulation. NeuroImage 25:8–20

Steinhoff BJ, Herrendorf G, Kurth C (1996) Ictal near infrared spectroscopy in temporal lobe epilepsy: a pilot study. Seizure 5(2):97–101

Stevens TK, Ives JR, Klassen LM, Bartha R (2007) MR compatibility of EEG scalp electrodes at 4 Tesla. J Magn Reson Imaging 25:872–877

Storti SF, Formaggio E, Bertoldo A, Manganotti P, Fiaschi A, Toffolo GM (2013) Modelling hemodynamic response function in epilepsy. Clin Neurophysiol 124(11):2108–2118

Strangman G, Culver JP, Thompson JH, Boas DA (2002) A quantitative comparison of simultaneous BOLD fMRI and NIRS recordings during functional brain activation. NeuroImage 17(2):719–731

Talairach, J, Tournoux, P (1988) Co-planar stereoaxis atlas of the human brain, Vol., Thieme, Stuttgart.

Taylor, DC, Ounsted, C. Biological mechanisms influencing the outcome of seizures in response to fever. Epilepsia 1971; 12: 33-45.

Tenforde, T.S, Gaffey, CT, Moyer, BR., and Budlnger, TF (1983) Cardiovascular alterations in Macaca monkeys exposed to stationary magnetic fields: Experimental observations and theoretical analysis. Bioelectromagnetics, 4(1):1–9,

Terborg C, Birkner T, Schack B, Weiller C, Röther J (2003) Noninvasive monitoring of cerebral oxygenation during vasomotor reactivity tests by a new near-infrared spectroscopy device. Cerebrovasc Dis 16(1):36–41

Toronov V, Webb A, Choi JH, Wolf M, Michalos A, Gratton E, Hueber D (2001) Investigation of human brain hemodynamics by simultaneous near-infrared spectroscopy and functional magnetic resonance imaging. Med Phys 28(4):521–527

Urigüen JA and Garcia-Zapirain B (2015) EEG artifact removal—state-of-the-art and guidelines. Journal of Neural Engineering, 12(3):031001

Vanderperren K, De Vos M, Ramautar JR, Novitskiy N, Mennes M, Assecondi S, Vanrumste B, Stiers P, Van den Bergh BRH, Wagemans J, Lagae L, Sunaert S, Van Huffel S (2010) Removal of BCG artifacts from EEG recordings inside the MR scanner: a comparison of methodological and validation-related aspects. NeuroImage 50:920–934. https://doi.org/10.1016/j.neuroimage.2010.01.010

van Graan LA, Lemieux L, Chaudhary UJ (2015) Methods and utility of EEG-fMRI in epilepsy. Quant Imaging Med Surg 5(2):300–312

Vanzetta I, Flynn C, Ivanov AI, Bernard C, Bénar CG (2010) Investigation of linear coupling between single-event blood flow responses and interictal discharges in a model of experimental epilepsy. J Neurophysiol 103(6):3139–3152

van Zijl PC, Hua J, Lu H (2012) The BOLD post-stimulus undershoot, one of the most debated issues in fMRI. Neuroimage 62:1092–1102

Vasios CE, Angelone LM, Purdon PL, Ahveninen J, Belliveau JW, Bonmassar G (2006) EEG/(f)MRI measurements at 7 Tesla using a new EEG cap ("InkCap"). NeuroImage 33(4):1082–1092

Villringer K, Minoshima S, Hock C, Obrig H, Ziegler S, Dirnagl U, Schwaiger M, Villringer A (1997) Comparison of near infrared spectroscopy and positron emission tomography in the assessment of frontal brain activation in humans. Adv Exp Med Biol 413:149–153

Villringer A, Mulert C and Lemieux L (2022) Principles of Multimodal Functional Imaging

Voges N, Blanchard S, Wendling F, David O, Benali H, Papadopoulo T, Clerc M, Benar C (2012) Modelling of the neurovascular coupling in epileptic discharges. Brain Topogr 25(2):136–156

and Data Integration In: Mulert C., Lemieux L (eds) EEG-fMRI: Physiological basis, Thechniques, and Applications. Springer Nature Switzerland https://doi.org/10.1007/978-3-031-07121-8

Warach S, Ives JR, Schlaug G, Patel MR, Darby DG, Thangaraj V, Edelman RR, Schomer DL (1996) EEG-triggered echo-planar functional MRI in epilepsy. Neurology 47(1):89–93

Wirsich J, Bagshaw AP, Guye G, Lemieux L, Bénar CG (2022) Experimental Design and Data Analysis Strategies. In: Mulert C., Lemieux L (eds) EEG-fMRI: Physiological basis, Thechniques, and Applications. Springer Nature Switzerland https://doi.org/10.1007/978-3-031-07121-8

Worsley KJ, Friston KJ (1995) Analysis of fMRI time-series revisited–again. NeuroImage 2(3):173–181

Worsley KJ, Liao CH, Aston J, Petre V, Duncan GH, Morales F, Evans AC (2002) A general statistical analysis for fMRI data. NeuroImage 15(1):1–15

Yan WX, Mullinger KJ, Geirsdottir GB, Bowtell R (2010) Physical modelling of pulse artefact sources in simultaneous EEG/fMRI. Human Brain Mapping, 31(4):604–620

Yeo BT, Krienen FM, Sepulcre J, Sabuncu MR, Lashkari D, Hollinshead M, Roffman JL, Smoller JW, Zollei L, Polimeni JR, Fischl B, Liu H, Buckner RL (2011) The organization of the human cerebral cortex estimated by intrinsic functional connectivity. J Neurophysiol 106:1125-1165

Zotev VS, Matlashov AN, Volegov PL, Savukov IM, Espy MA, Mosher JC, Gomez JJ, Kraus RH Jr (2008) Microtesla MRI of the human brain combined with MEG. J Magn Reson 194:115–120

Chapter 5: Epilepsy

5.1. INTRODUCTION

Epilepsy is a neurological disorder with a long-standing mythical history, with its earliest description dating back to 600BC and attributed to supernatural causes such as demons and ghosts (Reynolds and Kinnier Wilson, 2008; Wilson and Reynolds, 1990).

The term 'epilepsy' is derived from the Greek word meaning to 'seize upon', as it was believed to be acted by gods or demons upon humans. Treatments included fumigation with kindled jets and bathing new-borns in undiluted wine, with magicians and witch doctors frequently sought to ward off evil during attacks using mineral stones, camel hair, and even human blood and bones (Chaudhary et al., 2011).

However, Hippocrates was the first to dispute these supernatural explanations and suggested that epilepsy was caused by an imbalance of phlegm in the bloodstream. Although there were advances in the understanding of epilepsy in the 1700s, Sir John Hughlings Jackson's late 19th century research is considered the cornerstone of modern epileptology (Chaudhary et al., 2011). Jackson's research focused on the discharges of grey matter lesions, their localization, and the mechanisms of seizure spread, emphasizing lesion localization by semiology. He posited that the cerebral cortex's grey matter

was the origin of epilepsy while acknowledging the role of deeper grey matter structures such as the corpus striatum (Reynolds, 1988).

Curiously, Robert Bentley Todd was the pioneer of the electrical theory of epilepsy, proposing it long before Jackson's contributions. Todd saw the brain as having properties akin to a battery that, in epilepsy, triggered the sudden release of electrical energy, which he called "nervous force" (Reynolds, 1988). Despite all of his work being described in Todd's own Lumleian lectures, "On the pathology and treatment of convulsive diseases", to the Royal College of Physicians, Jackson made no reference to his work.

Currently, an epileptic seizure is defined as a sudden, abnormal, paroxysmal synchronous discharge of neuronal activity that leads to symptoms and signs representative of the area of aberrant neuronal discharge and propagation. The International League Against Epilepsy (ILAE) and the International Bureau for Epilepsy (IBE) agreed upon a definition of epilepsy as a brain disorder with a lasting predisposition to generating epileptic seizures and various neurobiological, cognitive, psychological, and social consequences (Fisher et al., 2005).

A consensus paper published in 2014 defined the operational diagnostic criteria for Epilepsy: (1) at least two unprovoked seizures occurring more than 24h apart; (2) one unprovoked (or reflex) seizure, accompanied by a likelihood of further seizures similar to the general recurrence risk (i.e., ~60% or higher) after two unprovoked seizures, occurring over the subsequent 10 years; or (3) diagnosis of an epilepsy syndrome (Fisher et al., 2014).

"Resolution" of epilepsy was defined as follows: (1) cases with an age dependent epilepsy syndrome who are past the applicable age, or for (2) individuals exhibiting a period of seizure freedom lasting longer than 10 years, and untreated with anti-epileptic medication for at least the last 5 years (Fisher et al., 2014).

5.2. EPIDEMIOLOGY AND PROGNOSIS

Epilepsy is a prevalent neurological disorder that affects 50 million people worldwide.

Annual incidence rate of 50 cases per 100,000 individuals in developed countries (Meyer et al., 2010) and similar incidence rates (43-47/100000/year across all age ranges) in Europe (Forsgren et al., 2005). Differences in incidence and prevalence are largely determined by geographic factors, with developing countries showing substantially higher incidence rates (100-190/100,000/year) due to higher incidence of neurocysticercosis and socio-economic and cultural aspects (Sander and Shorvon, 1996; Bartolini et al., 2011).

The incidence of epilepsy, however, exhibits a bimodal distribution with two peaks in the neonatal period and childhood (100-233/100,000/year) and old age (>65 years; 100-170/100,000/year).

The cumulative lifetime risks for epilepsy and unprovoked seizures are 3.1% and 4.1%, respectively (Meyer et al., 2010), while a single lifetime seizure is more common and affects approximately 5% of the adult population (Forsgren et al., 1996).

While most patients can have well-controlled seizures with anti-epileptic medication within five years of diagnosis, a subset of patients with refractory epilepsy experience continued seizures, as well as physical impairment, cognitive and language impairment, and behavioural disruption, leading to psychosocial challenges and stigmatization (de Boer et al., 2008).

Preventing and reversing these comorbidities have been identified as primary research areas at the 2007 Curing Epilepsy conference (Kelley et al., 2009).

Several studies, including the Rochester Epidemiology project, have reported a lower incidence of epilepsy and unprovoked seizures in females, while idiopathic generalized epilepsies (IGEs) are more prevalent among females.

5.3. CLASSIFICATION

With the discovery of the electroencephalogram (EEG), Gastaut's 1967, incorporating clinical features, anatomical substrates, age at onset, aetiology, ictal, and inter-ictal EEG findings, classified epilepsy into four categories: partial, generalized, unilateral, and unclassified (Gastaut, 1970).

In 1981, the International League Against Epilepsy (ILAE) developed a classification of epileptic seizures solely on the basis of retained or loss of consciousness into simple and complex partial seizures, discarded anatomical substrates, aetiology, and age at onset.

The next step involved the substitution of the terms 'primary,' 'secondary,' and 'localization-related epilepsy' by 'idiopathic,' 'symptomatic,' and 'partial' epilepsy (1985).

In 1989, epilepsy syndromes were better categorized, but the 1989 attempt was deemed inadequate for identifying subgroups of epilepsy and in 1998 four documents were proposed that were aimed at descriptive terminology for ictal phenomena (Luders et al., 1998), classification of epileptic seizures, classification of epilepsy syndromes and classification of functional disability (Engel, 1998).

Synthesis of the most recent international efforts resulted in three updated position papers by the ILAE. One in 2010 where revisions to terminology and concepts of seizure classification were proposed (Berg et al., 2010) and two in 2017, one pertaining to the classification of seizures (Fisher et al., 2017), and another one detailing the classification of the epilepsies (Scheffer et al., 2017).

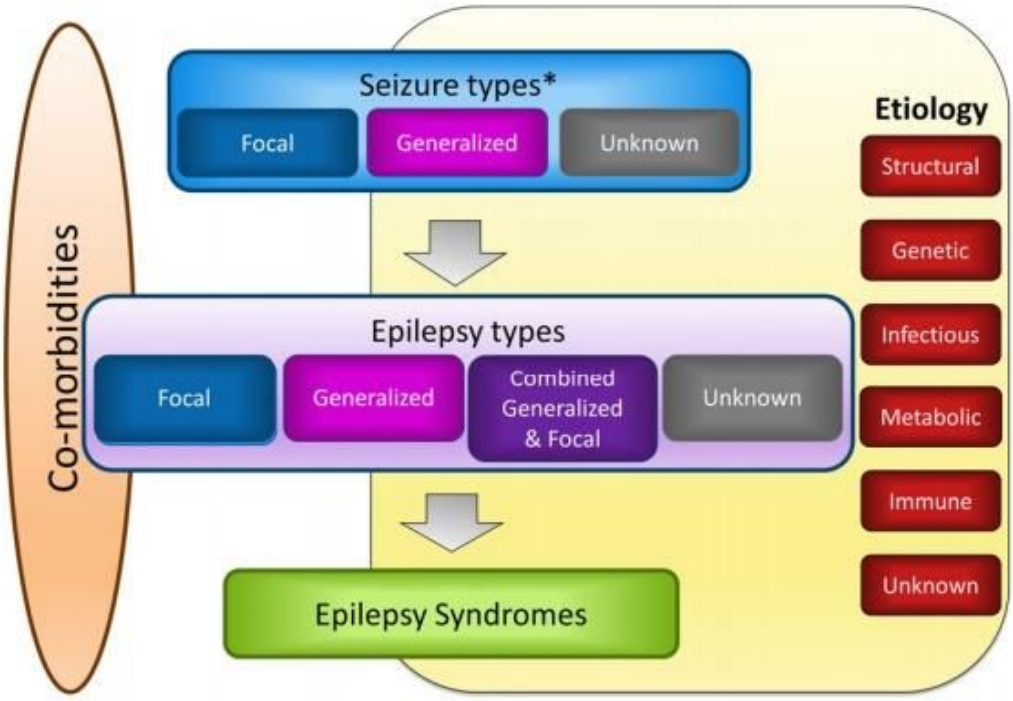

***Figure 5.1**: Framework for Classification of the Epilepsies.*
** denotes onset of seizure. (Scheffer et al., 2017– "ILAE classification of the epilepsies: Position paper of the ILAE Commission for Classification and Terminology)*

5.3.1. Seizure Types

The classification of seizures relies on the semiology and the EEG correlates.

As summarized in **Figure 5.2**, seizures are classified in:

- focal onset (previously partial): originating within networks limited to one hemisphere, with possibility of both localized and distributed intra-hemispheric networks. The "focal to bilateral tonic-clonic" wording acknowledges that focal seizures may evolve and spread to the contralateral hemisphere (previously partial onset seizures with secondary generalization);
- generalized onset: originating and/or rapidly engaging bilaterally distributed networks (Berg et al., 2010). In the 2017 classification "bilateral" is specified as more appropriate than generalized", in an

effort to distinguish focal-onset seizures from those generalized, i.e., engaging bilateral networks, from the beginning.

- unknown onset: difficult-to-ascertain patterns of onset (Fisher et al., 2017).

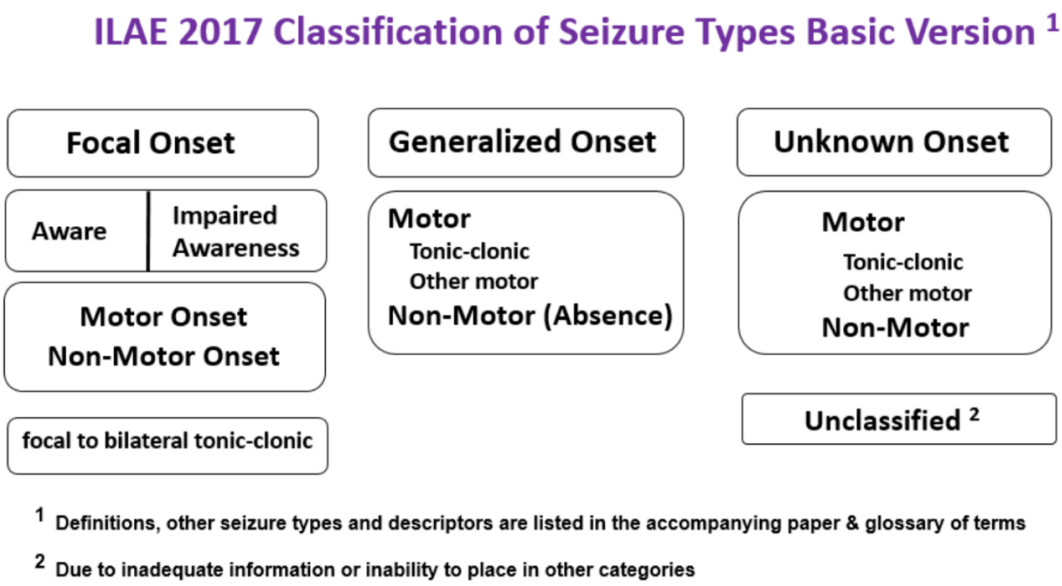

***Figure 5.2**: Seizure Classification*
(Fisher et al., 2017)

5.3.2. Epilepsy Type

This classification is strictly consequent upon seizure type (Fisher et al., 2014):

- focal epilepsies (implying the possibility of propagation to both hemispheres);
- generalized epilepsies;
- combined generalized and focal epilepsy: include cases of co-occurring focal and generalized onset seizures in the same patient (e.g., Dravet or Lennox-Gastaut syndrome);
- unknown.

5.3.3. Etiology

Before 2010, the commonly used aetiological categories were: idiopathic (no identified cause, possibly genetic), symptomatic (associated with structural or metabolic cause) and cryptogenic (likely symptomatic, but with no visible structural lesion) (ILAE, 1989).

In 2010 and 2017 (Berg et al., 2010; Scheffer et al., 2017). the following aetiological groupings were defined:

- genetic: previously defined as idiopathic, are those conditions in which a proven or presumed genetic defect is present and in which epileptic seizures are the cardinal symptom (for example, SCN1A and Dravet syndrome).
- structural/metabolic: the so-called symptomatic epilepsies, can be acquired (due to stroke, trauma, infection, tumors) or genetically determined. In this case, the genetic defect is not the direct cause of epilepsy, but there is an anatomical interposed alteration that becomes the cause of epilepsy (for example, the tubers in Tuberous Sclerosis or cortical malformations). Scheffer and colleagues propose to separate structural from metabolic causes.
- unknown cause, previously cryptogenic, are likely linked to a genetic abnormality or another alteration that is still unknown.
- immune: resulting from an immune-mediated inflammation of the central nervous system, such as anti-NMDA receptor encephalitis or anti-voltage-gated potassium channel encephalitis
- infectious: resulting from infections such as tuberculosis, HIV, cerebral malaria, neurocysticercosis, subacute sclerosing panencephalitis, cerebral toxoplasmosis

It is acknowledged that a patient's epilepsy may be concomitantly classified in more than one aetiological category (Scheffer et al., 2017).

5.3.4. Epilepsy Syndromes

Syndromes refer to a “cluster of features incorporating seizure types, EEG and imaging features that tend to occur together”, often with age-dependent features, common seizure triggers and prognostic factors (Scheffer et al., 2017).

Whilst it is emphasized that “diagnosis at all three levels” (see **Figure 5.1**) should be sought, and complemented by investigation into the aetiological underpinnings, it is also acknowledged that formal classification of syndromes by the ILAE has not yet been purported (Scheffer et al., 2017).

In addition to syndromes with recognised developmental and/or genetic components, entities not considered as electro-clinical syndromes have been defined as distinctive constellations. One such example is mesial temporal lobe epilepsy with hippocampal sclerosis (HS) (Berg et al., 2010).

Benign epilepsy with centrotemporal spikes (BECTS), that will be the focus of the study described in Chapter 11 is among the recognized electroclinical syndromes in childhood. The 2010 Berg et al. report suggested new terms to distil the elements implied in the term “benign”. Thus “benign”, as a descriptor for epilepsy, is replaced by both “self-limited” and “pharmacoresponsive”.

For the scope of this thesis, however, I will use two definitions: (a) temporal lobe epilepsy (TLE), and (b) BECTS/SeLECTS.

As the main focus of the experimental studies in this thesis will be on TLE (Chapter 9), BECTS/SeLECTS (Chapter 11) and Surgical Remediable Epilepsies (Chapter 11), the next chapters will be dedicated to a partial description of their characteristics.

Chapter 6: Temporal Lobe Epilepsy

6.1. CLINICAL ASPECTS

Temporal lobe epilepsy (TLE) is the most frequently diagnosed adult focal epilepsy, accounting for 30-35% of all epilepsy diagnoses. There are two types of TLE based on seizure onset from the mesial or lateral divisions of the temporal lobe (Wiebe, 2000; Tellez-Zenteno and Hernandez-Ronquillo, 2012) with mesial TLE comprising approximately two-thirds of TLE patients (Asadi-Pooya et al., 2017). Mesial TLE is usually linked to hippocampal sclerosis, a distinctive constellation of symptoms caused by individual genetic vulnerability or early-life cerebral injuries (Berg et al., 2010).

TLE patients may experience focal seizures with or without impaired awareness, and a variable proportion of TLE cases (around 30%) involve focal bilateral tonic-clonic seizures are considered a significant determinant of disease severity (Jobst et al., 2001; Bone et al., 2012).

Mesiotemporal seizures typically begin with an aura, followed by epigastric sensations, fear, panic, *déjà vu* or *jamais vu*, hallucinations and behavioural manifestations that may include oro-alimentary automatisms and other forms of stereotyped repetitive motor activity generally lasting less than two minutes. Ictal paresis, ipsilateral automatisms, and contralateral dystonic posturing can assist with lateralisation of seizure focus. Post-ictal confusion is common, while post-ictal aphasia often suggests involvement of the dominant hemisphere. (Williamson et al., 1998; Panayiotopoulos, 2010).

Neocortical temporal seizures are less common and tend to have different clinical features, including auras that involve auditory or vestibular sensations and complex perceptual misrepresentations. Behaviours may involve facial muscles, upper extremity dystonic posturing, and vocalizations. Seizure duration is usually shorter, secondary generalization is more common, and the typical oro-alimentary automatisms are absent (Maillard et al., 2004; Panayiotopoulos, 2010). However, early seizure propagation from lateral temporal to mesiotemporal structures or vice versa may make distinguishing between the two types difficult.

The occurrence of (secondary) generalised seizure activity is associated with an increased risk of sudden unexpected death in epilepsy (SUDEP) (Bone et al., 2012). The mechanisms underlying the spread of seizures from the temporal lobe to other brain regions are not well understood, but may involve alterations in heart rate variability and other cardiovascular markers (Toth et al., 2010).

6.2. ELECTROPHYSIOLOGY

In mesial TLE, up to a third of patients present with interictal sharp waves or spike-slow-wave complexes in the anterior temporal leads, while half of the patients have runs of temporal slow waves with lateralizing value (Williamson et al., 1993). Sleep EEG or prolonged monitoring increases diagnostic yield (Giorgi et al., 2014). The ictal pattern is characterized by rhythmic 5-9Hz activity that arises from the ipsilateral temporal lobe, leading to subjective symptoms or clinical signs after approximately 30 seconds (Wieser, 2004). In lateral TLE, unilateral or bilateral mid-temporal or posterior temporal spikes and ictal regional activity within the theta band are present, with slower ictal discharges in both delta and theta bands (Foldvary et al., 2001). Focal bilateral tonic-clonic seizures result from the transition of focal-onset seizures to widespread cortico-subcortical networks. Muscle artifacts in relation to pronounced motor manifestations often obscure scalp EEG patterns.

Intracranial EEG investigations have shown similar onset patterns in seizures with and without generalization, with more marked engagement of the posterior lateral temporal cortex in seizures leading to focal bilateral tonic-clonic seizures. (Yoo et al., 2014). The cingulate and orbito-frontal cortices were also implicated in other studies (Rektor et al., 2009).

6.3. NEUROIMAGING

In structural magnetic imaging, hippocampal sclerosis (HS) is the most frequent abnormality in mesial TL. HS is characterized by hippocampal atrophy and increased hippocampal signal in T2-weighted and a decreased signal in T1-weighted sequences. Quantification of hippocampal volumetry on T1-weighted sequences and measurement of T2 relaxation times via T2-relaxometry can aid diagnosis (Winston et al., 2013, 2017; Bernasconi et al., 2000). Other mesiotemporal lesions include DNET, astrocytic tumours (astrocytomas, gangliogliomas), and vascular abnormalities (cavernous haemangioma or malformations). Lateral TLE can result from malformations of cortical development, focal cortical dysplasia, cavernoma, or other brain tumour subtypes. However, approximately 30% of TLE cases are MRI-negative, meaning that no identifiable lesions are detected (Muhlhofer et al., 2017). Fluorodeoxyglucose PET can demonstrate ipsilateral temporal hypometabolism, while 99mTC-HMPAO SPECT can detect ictal hyper-perfusion and interictal hypo-perfusion of the epileptogenic focus.

Moreover, a recent study by our group (Ballerini et al., 2022) corroborates the involvement of the amygdala volume in temporal lobe epilepsy, particularly in mesial temporal lobe epilepsy and suggests a different amygdala subnuclei engagement depending on the aetiology and lateralization of epilepsy. Furthermore, the basolateral complex and the medial nucleus of amygdala seem to be able to differentiate temporal lobe epilepsy with hippocampal sclerosis and with MRI negative, respectively, versus controls.

6.4. NETWORK PERSPECTIVE

Studies using structural and functional magnetic resonance imaging (fMRI) have revealed extensive abnormalities in the whole-brain network architecture of patients with temporal lobe epilepsy (TLE) **(Figure 6.1)**.

Specifically, impaired functional connectivity has consistently been observed in areas belonging to the default-mode network (DMN), which is composed of mesiotemporal, mesial prefrontal, lateral, and midline parietal areas (Zhang et al., 2010a; Liao et al., 2011; Pittau et al., 2012; Voets et al., 2012; Haneef et al., 2014). The DMN is believed to play a crucial role in internally-directed activities such as memory, future planning, and mind wandering and it has been found to be disrupted by interictal spike (Andrews-Hanna et al., 2014; Kobayashi et al., 2006; Laufs et al., 2007). Patients with TLE-HS often exhibit hippocampal decoupling from anterior and posterior DMN nodes, while this is less evident in those with MRI-negative TLE (Bernhardt et al., 2016b). In addition, altered functional integration has been identified in other functional systems: sensory-motor, attentional, episodic memory, working memory, and language networks, as well as between mesiotemporal and subcortical structures such as the thalamus and cerebellum (Pittau et al., 2012; Stretton et al., 2012; Voets et al., 2012; Sidhu et al., 2013; Haneef et al., 2014; Lv et al.,2014; Voets et al., 2015).

Besides functional investigations, numerous structural studies have shown that TLE is associated with extensive abnormalities beyond the temporal lobe, such as reduced grey matter in widespread cortical areas, thalamus, and basal ganglia compared to controls and the most common site of extra-temporal atrophy is the medial dorsal thalamus (Keller and Roberts, 2008; Barron et al., 2012; Bernhardt et al., 2013b).

Left mesial TL showed cortical thinning in lateral temporal motor, medial frontal, and parietal region, while right mesial TLE exhibited abnormalities in motor regions (Whelan et al., 2018).

Morphometric studies have shown that there is reduced correlation between mesiotemporal areas and the lateral temporal, pre-frontal, fronto-central, occipito-temporal, and cingulate cortices in TLE (Bonilha et al., 2007; Bernhardt et al., 2008; Mueller et al., 2009). Additionally, thalamic atrophy is linked to cortical thinning in areas such as the entorhinal, fronto-central, and lateral temporal cortices, which suggests the involvement of the thalamus in TLE's pathological network (Mueller et al., 2010; Bernhardt et al., 2012).

Abnormal diffusion parameters were observed in the white matter of both ipsilateral and contralateral fornix, cingulum, and uncinate fasciculus (Thivard et al., 2005; Focke et al., 2008; Concha et al., 2009). Thalamic connectivity also appears to be heavily affected (Ahmadi et al., 2009; Bonilha et al., 2013; Keller et al., 2015b). These diffusion abnormalities suggest a significant restructuring of white matter architecture in TLE, with more prominent changes being observed ipsilateral to the seizure focus, but also involving the contralateral hemisphere. Left TLE appeared to be more severally affected than right TLE (Focke et al., 2008; Ahmadi et al., 2009; Besson et al., 2014).

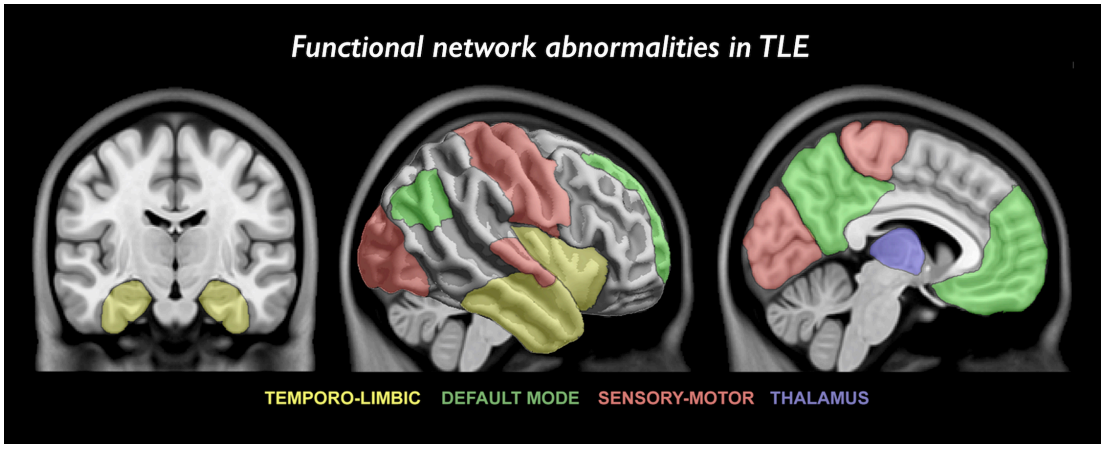

***Figure 6.1**: Summary of functional network abnormalities in TLE.*
Summary of studies reporting abnormalities of functional connectivity in TLE. Cortical and subcortical regions consistently displaying functional alterations across studies are colour-coded with respect to the associated network (Caciagli et al., Frontiers in Neuroscience 2014 (doi: 10.3389/fnins.2014.00411)).

6.5. TREATMENT

The first therapeutic intervention for TLE patients is anti-epileptic drugs (AEDs), which can result in seizure remission for approximately 50-60% of patients in monotherapy or dual therapy (Engel, 2001; Panayiotopoulos, 2010).

For patients with drug-resistant epilepsy, resective surgery is suggested. Randomized controlled trials have demonstrated that surgical interventions are more effective and superior to medical therapy (Wiebe et al., 2001; Engel et al., 2012), that's why early identification of pharmaco-resistance is critical for appropriate and timely referral to surgical centres. Please refer to Chapter 8 for further elaboration on the topic.

Chapter 7: SeLECTS

7.1. IDIOPATHIC EPILEPSIES

Idiopathic focal epilepsies comprise a group of syndromes characterized by a shared transient, age-dependent, genetically based, non-lesional and localized epileptic abnormality and for which a common functional mechanism that explains the epilepsy and abnormalities on electroencephalography (EEG) has been proposed (Guerrini et al., 2012).

They are thought to be a spectrum of disorders where the electro-clinical features make a continuum of variable severity and localization conditions within the frame of the perisylvian cognitive network (human communication).

This group includes: benign childhood epilepsy with centrotemporal spikes (BECTS), Panayiotopuolos syndrome (PS), Gastaut type childhood idiopathic occipital epilepsy, Landau - Kleffner syndrome (LKS) and Electrical Status Epilepticus in Sleep (ESES).

These epileptic syndromes are age-dependent conditions, evolving in a time-window important for the development of human communication-specific skills, have a self-limiting course, tending to resolve before adulthood with no associated severe intellectual and behavioural disorders (Pal and Ferri, 2016).

Electrical status epilepticus in sleep (ESES) is the result of the malignant, atypical evolution of idiopathic focal epilepsies, characterized by regional or global continuous IEDs during NREM sleep regardless of aetiology.

Given the complexity of the matter thorough discussion on this group of syndromes is beyond the scope of this thesis and we will only discuss benign childhood epilepsy with centrotemporal spikes (BECTS).

It is important to note that the term "benign" in BECTS implies that usually epileptic seizures do not require treatment or are easily treated, show remission before adulthood and no sequelae. Moreover, there are usually no severe seizures, and no associated severe intellectual and behavioural disorders (Guerrini et al., 2012). Although, the term “benign” is no longer recommended as it fails to acknowledge the comorbidities present in some individuals. In the same way, the term “idiopathic” is now restricted to describing the 4 syndromes termed the idiopathic generalized epilepsies. Given the typical evolution of these conditions, with age-dependent onset and remission, it has been proposed to use the term “self-limited” (Berg et al., 2010).

7.2. SELF-LIMITED ROLANDIC EPILEPSY WITH CENTRO-TEMPORAL SPIKES (SELECT)

SeLECTS is the most common form of focal epilepsy of childhood, accounting for 15% of childhood epilepsies. (Beaussart et al., 1978). In 83% of cases, it begins between the ages of 4 and 10 years, with peak onset between the ages of 5-8 years. Virtually all cases begin before 13 years of age. (Gobbi et al., 2006).

The prevalence is around 15% in children aged 1-15 years with nonfebrile seizures, and the incidence is 10-20/100,000 children aged 0-15 years. (Larsson and Eeg-Oloffson, 2006)

In 70% to 80% of cases, the clinic consists of brief, partial seizures that occur in most cases during NREM sleep. These may be the only type of seizure or may be accompanied by generalized seizures in 24-50% of cases. Most seizures are motor seizures, but sensory phenomena may also often occur (Guerrini et al., 2012).

Seizures mainly affect one side of the face (37%), the oropharyngeal muscles (53%) and less often the upper limb (20%). The lower limb is affected in only 8% of seizures. Facial seizures result in either a contraction of one side of the face,

clonic spasms of the cheek and eyelashes, or both. Oropharyngeal contractions cause guttural sounds, mouth movements, and profuse salivation. Sensory symptoms often involve either the corner of the mouth, the inside of a cheek, the tongue, or the gums. We often find speech arrest, with severe dysarthria but preserved comprehension; children know what they want to say but are unable to articulate sounds. When limbs are affected, it is often with clonic spasms, Jacksonian march is rare (Guerrini et al., 2012).

In younger children, seizures may be less localized and affect a full half of the body; they also tend to last longer. Long seizures may be followed by post-stroke hemiplegia, although these are rare cases. (Gobbi et al., 2006)

Only 5% of seizures occur exclusively during wakefulness (Guerrini et al., 2012).

The total duration of epilepsy is relatively short: <1 year in 21% of cases, 1-2 years in 18%, 2-5 years in 20%, and 3-8 years in only 7%. (Guerrini et al., 2012)

Absence of neurological or cognitive impairment is one of the criteria for clinical diagnosis of SeLECTS. However, some minor impairments may occur, for example, reversible speech disorders and small reversible deficits in cognitive performance in tests of attention. Despite this, cognitive outcomes in children with SeLECTS are within normal limits of the general population, and their social integration is equally good (Riva et al., 2007).

7.3. ELECTROPHYSIOLOGY

EEG is the first and often the only instrumental examination that allows, in patients with suspected SeLECTS, to establish the definite diagnosis. Neuroimaging is generally not necessary, since the aetiology has been recognized as genetic and not structural.

The typical pattern of focal epileptic discharges, which are found in ER, is characterized by their localization, wave shape, field of distribution, and their activation during NREM sleep.

The abnormal spike complex shows a stereotyped structure; the spikes are located in the central temporal region and typically have a bipolar distribution

potential that is negative in the centrotemporal area and positive frontally. (Guerrini et al., 2012).

The topography of these spikes has been used to distinguish between patients with good prognosis and patients with atypical SeLECTS, associated with neurological or intellectual deficits or more frequent seizures.

Van Klink et al. (Van Klink et al., 2018) studied how the presence of waves (ripples) (80-250 Hz), superimposed on the rolandic spikes in the EEG, can differentiate between different entities. The study showed how the number of waves on the rolandic tips correlated with the severity of epilepsy. Children with rolandic tips but no seizures usually do not show waves, and children with atypical ERs have a substantial number of waves. The study suggests that the number of waves might help in the decision to start drug treatment and in recognizing those atypical and more severe forms earlier.

The dipole model was used to study the neuronal origin of the discharges and it was found that the origin, in patients with typical SeLECTS, is specifically around the rolandic fissure, whereas in cases of atypical ER, the localization is less precise. This less precise localization would be due to the presence of multiple, synchronous neuronal discharges. (Gregory and Wong, 1992)

We do not have multiple spikes but frequent clustering of short bursts of 1.5-3.0 Hz. There is no relationship between the frequency and extent of spikes and the frequency of seizures or their duration. Background EEG activity is normal. In one third of cases there are bilateral spikes that can be either synchronous or asynchronous.

During slow-wave sleep, discharges tend to spread to the ipsilateral hemisphere and sometimes to the contralateral hemisphere. (Guerrini et al., 2012)

Focal seizures begin with a fast rhythm in the rolandic area contralateral to the seizures, followed by a progressive increase in amplitude of slow waves forming spike-wave complexes. Generalized seizures have a similar focal onset with secondary generalization. (Gobbi et al., 2006)

7.4. PROGNOSIS

The natural history of epilepsy is directed toward self-resolution. Even in cases of pharmacologically treated SeLECTS, where there is resistance to treatment (in about 20% of cases), resolution is guaranteed. The duration of the epilepsy syndrome, in almost all cases, is less than 3 years.

Remission occurs in 50% of patients by age 6 years, in 92% by age 12 years, and in 99.8% by age 18 years; there is a peak of remission around age 13 years. Resolution, which therefore occurs by adolescence, is definitive.

Normalization of the EEG tracing usually occurs after clinical remission. (Guerrini et al., 2012)

Thus, the prognosis is generally positive; in fact, in the majority of cases, children do not show outcomes of neurological or cognitive deficits or behavioural alterations. However, cases have been described of patients, diagnosed with SeLCTS, in whom other epileptic pictures were superimposed, such as atonic, myoclonic seizures or atypical absences. These disorders, associated with a typical ER picture, go to constitute atypical forms of SeLECTS epilepsy. In these atypical forms, resolution may not necessarily be benign; in fact, they may be associated with a worse cognitive outcome and language and learning deficits in the child (Shields and Snead, 2009).

In addition, in a small percentage of cases of children with SeLECTS there may be an evolution of ER associated with more malignant syndromes, such as Landau-Kleffner syndrome (a generalized form) or CSWS (continuous spike-wave during sleep). In these cases, the prognosis is significantly worse, with deterioration in language, social interactions, global intelligence, and motor skills. (Beaussart et al., 1978)

7.5. TREATMENT

In older texts, the use of anticonvulsants such as phenobarbital and carbamazepine was indicated as the standard treatment of SeLECTS, despite the fact that the International League Against Epilepsy (ILAE) treatment

guidelines never defined drugs with A or B levels of evidence in efficacy to treatment.

Recently, the indication has been that drug treatment should not be used in most patients.

Three features of SeLCTS support this: the first feature is that this epilepsy is not associated with any structural lesion; the second is that seizures are usually infrequent, tend to occur during sleep, and do not interfere with the child's social life; and, finally, the third is that seizures resolve by puberty and without neurological or cognitive sequelae.

This last point has been shown by several studies not to always be true, and this has led to reconsideration of the dogma of not treating SeLECTS.

The decision to treat or not to treat the patient must be based on consideration of the risk-benefit ratio.

Chapter 8: Epilepsy Surgery

8.1. INRODUCTION

Around one third of patients with epilepsy do not respond to anti-epileptic drug treatment, as per Laxer et al. (2014). For patients with temporal lobe epilepsy, anterior temporal lobe resection (ATLR) can result in remission for up to 50% of those with refractory temporal lobe epilepsy (de Tisi et al., 2011), therefore, in clinical practice, patients with focal epilepsy who do not respond to at least two anti-epileptic drugs at therapeutic doses should be directed to presurgical evaluation. Presurgical evaluations aim to determine a specific epileptogenic zone and evaluate the potential risks of surgery if it is deemed necessary.

8.2. PRE-SURGICAL EVALUATION

8.2.1. Clinical Semiology and Video Telemetry

The first step of presurgical evaluation is to take into account the patient's medical history and seizure semiology as it can help determine the localization and lateralization of the seizures. After this, the examination of the patient’s inter-ictal EEG patterns such as spike wave discharges or focal slowing can be used to infer the location and lateralization of abnormalities. Finally, video-EEG telemetry is used to capture habitual seizures for further analysis.

8.2.2. Structural Neuroimaging

In patients with epilepsy, MRI is typically the first choice of investigation if clinical and electrophysiological tests are in agreement, with the exception of those who have a confirmed diagnosis of idiopathic generalized epilepsy or other forms of epilepsy without a structural abnormality (Duncan, 1997).

Magnetic resonance imaging (MRI) at 3 Tesla is the preferred method for epilepsy imaging, as it has higher sensitivity in detecting subtle pathology such as focal cortical dysplasia compared to the conventional 1.5 Tesla MRI (Strandberg et al., 2008). Quantification techniques such as voxel-based morphometry can increase the likelihood of detecting structural abnormalities in the brain (Focke et al., 2008; Salmenpera et al., 2007). One promising imaging technique is diffusion tensor imaging, which can map white matter tracts by imaging the diffusion of water molecules. In epilepsy surgery, diffusion tensor imaging (DTI) is frequently used to map the optic radiation and pyramidal tracts, which can aid in the resection and preservation of eloquent functions. Abnormal diffusion has been detected in 50% of patients with refractory focal epilepsy, and the findings were concordant with epileptiform abnormalities on EEG (Guye et al., 2007).

8.2.3. Functional Neuroimaging

The use of functional imaging is aimed at exploring the epileptogenic zone in patients, either in cases where a structural lesion is not detected despite optimal imaging, or if an MRI lesion is inconsistent with the clinical and EEG data.

Positron emission tomography (PET) is a diagnostic tool that utilizes a positron emitting radionucleotide, such as 18F-fluoro deoxy-glucose (FDG), in conjunction with X-ray, CT-scan or MRI. Typically, it is conducted in the inter-ictal state, and hypometabolism can be observed in areas of cerebral dysfunction during interictal periods in patients with focal seizures. Research indicates that PET can detect focal areas of hypometabolism in up to 80% of

patients with interictal discharges on EEG (Theodore, 1989), and these areas are often more expansive than the region of structural pathology (Duncan, 2010).

8.2.4. Intracranial EEG

The gold-standard for pre-surgical evaluation of drug-refractory epilepsy patients is the intracranial EEG. In this invasive procedure, a grid of macro-electrodes is placed over the cortical surface (subdural electrodes) and/or on deep brain structures (depth electrodes), measuring electrical activity locally. The surgical planning is guided by the clinical history of the patient and seizure semiology.

Despite the limited spatial coverage, icEEG provides crucial information about the localization of epileptogenic brain areas when surgical treatment is being considered.

SECTION II: REFERENCES

Ahmadi ME, Hagler DJ, Jr., McDonald CR, Tecoma ES, Iragui VJ, Dale AM, Halgren E (2009) Side matters: diffusion tensor imaging tractography in left and right temporal lobe epilepsy. AJNR American journal of neuroradiology 30:1740- 1747.

Andrews-Hanna JR, Smallwood J, Spreng RN (2014) The default network and selfgenerated thought: component processes, dynamic control, and clinical relevance. Annals of the New York Academy of Sciences 1316:29-52.

Archer JS, Briellman RS, Abbott DF, Syngeniotis A, Wellard RM, Jackson GD (2003) Benign epilepsy with centro-temporal spikes: spike triggered fMRI shows somato-sensory cortex activity. Epilepsia 44:200–204

Asadi-Pooya AA, Stewart GR, Abrams DJ, Sharan A (2017) Prevalence and Incidence of Drug-Resistant Mesial Temporal Lobe Epilepsy in the United States. World Neurosurg 99:662-666.

Ballerini A, Tondelli M, Talami F et al. (2022) Amygdala subnuclear volumes in temporal lobe epilepsy with hippocampal sclerosis and in non-lesional patients. Brain Commun4(5):225. doi: 10.1093/braincomms/fcac225.

Barron DS, Fox PM, Laird AR, Robinson JL, Fox PT (2012) Thalamic medial dorsal nucleus atrophy in medial temporal lobe epilepsy: A VBM meta-analysis. Neuroimage Clin 2:25-32.

Bartolini E, Bell GS, Sander JW (2011) Multicultural challenges in epilepsy. Epilepsy Behav 20:428-434.

Beaussart M (1978) Benign epilepsy of children with Rolandic spikes. A clinical, electroencephalographic and telencephalographic study Epilepsia 15:301-315

Berg, AT, Berkovic, SF, Brodie, MJ, Buchhalter, J, Cross, JH, van Emde Boas, W, Engel, J, French, J, Glauser, TA, Mathern, GW, Moshe, SL, Nordli, D, Plouin, P, Scheffer, IE. (2010) Revised terminology and concepts for organization of seizures and epilepsies: report of the ILAE Commission on Classification and Terminology, 2005-2009. Epilepsia 51: 676-85.

Bernasconi A, Bernasconi N, Caramanos Z, Reutens DC, Andermann F, Dubeau F, Tampieri D, Pike BG, Arnold DL (2000) T2 relaxometry can lateralize mesial temporal lobe epilepsy in patients with normal MRI. In: Neuroimage, pp 739-746.

Bernhardt BC, Worsley KJ, Besson P, Concha L, Lerch JP, Evans AC, Bernasconi N (2008) Mapping limbic network organization in temporal lobe epilepsy using morphometric correlations: insights on the relation between mesiotemporal connectivity and cortical atrophy. NeuroImage 42:515-524.

Bernhardt BC, Bernasconi N, Kim H, Bernasconi A (2012) Mapping thalamocortical network pathology in temporal lobe epilepsy. Neurology 78:129-136.

Bernhardt BC, Hong S, Bernasconi A, Bernasconi N (2013) Imaging structural and functional brain networks in temporal lobe epilepsy. Front Hum Neurosci 7:624.

Besson P, Andermann F, Dubeau F, Bernasconi A (2008) Small focal cortical dysplasia lesions are located at the bottom of a deep sulcus. Brain: a journal of neurology 131:3246-3255.

Bone B, Fogarasi A, Schulz R, Gyimesi C, Kalmar Z, Kovacs N, Ebner A, Janszky Jv (2012) Secondarily generalized seizures in temporal lobe epilepsy. Epilepsia 53:817-824.

Bonilha L, Rorden C, Halford JJ, Eckert M, Appenzeller S, Cendes F, Li LM (2007) Asymmetrical extra-hippocampal grey matter loss related to hippocampal atrophy in patients with medial temporal lobe epilepsy. Journal of neurology, neurosurgery, and psychiatry 78:286-294.

Bonilha L, Helpern JA, Sainju R, Nesland T, Edwards JC, Glazier SS, Tabesh A (2013) Presurgical connectome and postsurgical seizure control in temporal lobe epilepsy. Neurology 81:1704-1710.

Boor S, Vucurevic G, Pfleiderer C, Stoeter P, Kutschke G, Boor R (2003) EEG-related functional MRI in benign childhood epilepsy with centrotemporal spikes. Epilepsia 44:688–692

Boor R, Jacobs J, Bauermann T, Scherg M, Boor S, Vucurevic G, Kutschke G, Stoeter P (2007) Combined spike-related functional MRI and multiple source analysis in the non-invasive spike localization of benign rolandic epilepsy. Clin Neurophysiol 118(4):901–909

Caciagli et al. (2014) Functional network alterations and their structural substrate in drug-resistant epilepsy. Front. Neurosci https://doi.org/10.3389/fnins.2014.00411

Chaudhary UJ, Duncan JS, Lemieux L (2011) A dialogue with historical concepts of epilepsy from the Babylonians to Hughlings Jackson: persistent beliefs. Epilepsy Behav; 21**:** 109-14.

Concha L, Beaulieu C, Collins DL, Gross DW (2009) White-matter diffusion abnormalities in temporal-lobe epilepsy with and without mesial temporal sclerosis. Journal of neurology, neurosurgery, and psychiatry 80:312-319.

de Boer HM, Mula M, Sander JW. (2008) The global burden and stigma of epilepsy. Epilepsy Behav; 12: 540-6.

de Tisi J, Bell GS, Peacock JL, McEvoy AW, Harkness WF, Sander JW, Duncan JS. (2011) The long-term outcome of adult epilepsy surgery, patterns of seizure remission, and relapse: a cohort study. Lancet 378**:** 1388-95.

Duncan JS (1997) Imaging and epilepsy. Brain 120 (Pt 2)**:** 339-77

Duncan JS (2010) Imaging in the surgical treatment of epilepsy. Nat Rev Neurol 6**:** 537-50.

Engel JJr (1998) Classifications of the International League Against Epilepsy: time for reappraisal. Epilepsia 39**:** 1014-7.

Engel JJr (2001) Mesial temporal lobe epilepsy: what have we learned? Neuroscientist 7:340-352.

Engel JJr, McDermott MP, Wiebe S, Langfitt JT, Stern JM, Dewar S, Sperling MR, Gardiner I, Erba G, Fried I, Jacobs M, Vinters HV, Mintzer S, Kieburtz K (2012) Early surgical therapy for drug-resistant temporal lobe epilepsy: a randomized trial. JAMA 307:922-930.

Fisher RS, van Emde Boas, W, Blume, W, Elger, C, Genton, P, Lee, P, Engel, J, Jr. (2005) Epileptic seizures and epilepsy: definitions proposed by the International League Against Epilepsy (ILAE) and the International Bureau for Epilepsy (IBE). Epilepsia 46: 470-2.

Fisher RS, Acevedo C, Arzimanoglou A, Bogacz A, Cross JH, Elger CE, Engel J, Jr., Forsgren L, French JA, Glynn M, Hesdorffer DC, Lee BI, Mathern GW, Moshe SL,

Perucca E, Scheffer IE, Tomson T, Watanabe M, Wiebe S (2014) ILAE official report: a practical clinical definition of epilepsy. Epilepsia 55:475-482.

Fisher RS, Cross JH, French JA, Higurashi N, Hirsch E, Jansen FE, Lagae L, Moshe SL, Peltola J, Roulet Perez E, Scheffer IE, Zuberi SM (2017) Operational classification of seizure types by the International League Against Epilepsy: Position Paper of the ILAE Commission for Classification and Terminology. Epilepsia 58:522-530.

Focke NK, Yogarajah M, Bonelli SB, Bartlett PA, Symms MR, Duncan JS (2008) Voxel-based diffusion tensor imaging in patients with mesial temporal lobe epilepsy and hippocampal sclerosis. NeuroImage 40:728-737.

Foldvary N, Klem G, Hammel J, Bingaman W, Najm I, Luders H (2001) The localizing value of ictal EEG in focal epilepsy. Neurology 57:2022-2028

Forsgren L, Bucht G, Eriksson S, Bergmark L (1996) Incidence and clinical characterization of unprovoked seizures in adults: a prospective populationbased study. Epilepsia 37:224-229.

Forsgren L, Beghi E, Oun A, Sillanpaa M (2005) The epidemiology of epilepsy in Europe - a systematic review. Eur J Neurol 12:245-253.

Gastaut H. (1970) Clinical and electroencephalographical classification of epileptic seizures. Epilepsia 11**:** 102-13.

Gobbi G, Boni A, Filippini M (2006) The spectrum of idiopathic rolandic epilepsy syndromes and idiopathic occipital epilepsies: from the benign to the disabling"; Epilepsia, 47:62-66

Gregory DL, Wong PKH (1992) Clinical relevance of dipole field in rolandic spikes. Epilepsia, 33:36-44

Guerrini R, Pellacani S (2012) Benign childhood focal epilepsies Epilepsia, 53(Suppl. 4):9-18

Guye M, Ranjeva JP, Bartolomei F, Confort-Gouny S, McGonigal A, Regis J, Chauvel P, Cozzone PJ. (2007) What is the significance of interictal water diffusion changes in frontal lobe epilepsies? Neuroimage 35**:** 28-37.

Haneef Z, Lenartowicz A, Yeh HJ, Levin HS, Engel J, Jr., Stern JM (2014) Functional connectivity of hippocampal networks in temporal lobe epilepsy. Epilepsia 55:137-145.

Jobst BC, Williamson PD, Neuschwander TB, Darcey TM, Thadani VM, Roberts DW (2001) Secondarily generalized seizures in mesial temporal epilepsy: clinical characteristics, lateralizing signs, and association with sleep-wake cycle. Epilepsia 42:1279-1287.

Kelley, MS, Jacobs, MP, Lowenstein, DH. (2009) The NINDS epilepsy research benchmarks. Epilepsia, 50: 579-82.

Keller SS, Roberts N (2008) Voxel-based morphometry of temporal lobe epilepsy: An introduction and review of the literature. Epilepsia 49:741-757.

Keller SS, Richardson MP, Schoene-Bake JC, O'Muircheartaigh J, Elkommos S, Kreilkamp B, Goh YY, Marson AG, Elger C, Weber B (2015) Thalamotemporal alteration and postoperative seizures in temporal lobe epilepsy. Annals of neurology 77:760-774

Kobayashi E, Bagshaw AP, Benar CG, Aghakhani Y, Andermann F, Dubeau F, Gotman J (2006) Temporal and extratemporal BOLD responses to temporal lobe interictal spikes. Epilepsia 47:343-354.

Kossoff EH, Los JG, Boatman DF (2007) A pilot study transitioning children onto levetiracetam monotherapy to improve language dysfunction associated with benign rolandic epilepsy", Epilepsy Behav., 11:514-517

Koutroumanidis M, Arzimanoglou A, Caraballo R, Goyal S et al. (2017) The role of EEG in the diagnosis and classification of the epilepsy syndromes: a tool for clinical practice by the ILAE Neurophysiology Task Force (Part 1)Epileptic Disorders 19(3):233-298https://doi.org/10.1684/epd.2017.0935

Koutroumanidis M, Arzimanoglou A, Caraballo R, Goyal S et al. (2017) The role of EEG in the diagnosis and classification of the epilepsy syndromes: a tool for clinical practice by the ILAE Neurophysiology Task Force (Part 2)Epileptic Disorders 19(3):233-298https://doi.org/10.1684/epd.2017.0935

Larsson K, Eeg-Oloffson O (2006) A population based study of epilepsy in children from a Sweden county", Eur J Paediatr Neurol, 10:107-113

Laufs H, Hamandi K, Salek-Haddadi A, Kleinschmidt AK, Duncan JS, Lemieux L (2007) Temporal lobe interictal epileptic discharges affect cerebral activity in "default mode" brain regions. Human brain mapping 28:1023-1032.

Laxer KD, Trinka E, Hirsch LJ, Cendes F, Langfitt J, Delanty N, Resnick T, Benbadis, SR (2014) The consequences of refractory epilepsy and its treatment. Epilepsy Behav 37: 59-70.

Lengler U, Kafadar I, Neubauer BA, Krakow K (2007) fMRI correlates of interictal epileptic activity in patients with idiopathic benign focal epilepsy of childhood. A simultaneous EEG-functional MRI study. Epilepsy Res 75:29–38

Li R, Ji GJ, Yu Y, Ding MP, Tang YL, Chen H, Liao W (2017) Epileptic discharge related functional connectivity within and between networks in benign epilepsy with centrotemporal spikes. Int J Neural Syst 27:1750018

Li R, Wang L, Chen H, Guo X, Liao W, Tang YL, Chen H (2019) Abnormal dynamics of functional connectivity density in children with benign epilepsy with centrotemporal spikes. Brain Imaging Behav 13:985–994

Liao W, Zhang Z, Pan Z, Mantini D, Ding J, Duan X, Luo C, Wang Z, Tan Q, Lu G, Chen H (2011) Default mode network abnormalities in mesial temporal lob epilepsy: A study combining fMRI and DTI. Human brain mapping 32:883- 895.

Luders, H, Acharya, J, Baumgartner, C, Benbadis, S, Bleasel, A, Burgess, R, Dinner, DS, Ebner, A, Foldvary, N, Geller, E, Hamer, H, Holthausen, H, Kotagal, P, Morris, H, Meencke, HJ, Noachtar, S, Rosenow, F, Sakamoto, A, Steinhoff, BJ, Tuxhorn, I, Wyllie, E. (1998) Semiological seizure classification. Epilepsia 39**:** 1006-13.

Maillard L, Vignal JP, Gavaret M, Guye M, Biraben A, McGonigal A, Chauvel P, Bartolomei F (2004) Semiologic and electrophysiologic correlations in temporal lobe seizure subtypes. Epilepsia 45:1590-1599.

Masterton RA, Harvey AS, Archer JS, Lillywhite LM, Abbott DF, Scheffer IE, Jackson GD (2010) Focal epileptiform spikes do not show a canonical BOLD response in patients with benign rolandic epilepsy (BECTS). Neuroimage 51:252–260

Meyer AC, Dua T, Ma J, Saxena S, Birbeck, G (2010) Global disparities in the epilepsy treatment gap: a systematic review. Bull World Health Organ 88: 260-6.

Mueller SG, Laxer KD, Barakos J, Ian C, Garcia P, Weiner MW (2009) Widespread neocortical abnormalities in temporal lobe epilepsy with and without mesial sclerosis. NeuroImage 46:353-359.

Muhlhofer W, Tan YL, Mueller SG, Knowlton R (2017) MRI-negative temporal lobe epilepsy-What do we know? Epilepsia 58:727-742.

Pal DK, Ferri C (2016) Idiopathic focal epilepsies: the lost tribe Epilectic disord, 18(3):252-88,

Panayiotopoulos CP, Micheal M, Sanders S, Valeta T, Koutroumanidis M (2008) Benign childhood focal epilepsy: assessment of established and newly recognized syndromes, Brain, 131:2264-2286

Panayiotopoulos C (2010) Epileptic Syndromes and their Treatment. Springer Healthcare, Ltd, Manchester

Pittau F, Grova C, Moeller F, Dubeau F, Gotman J (2012) Patterns of altered functional connectivity in mesial temporal lobe epilepsy. Epilepsia 53:1013- 1023.

Rektor I, Zakopcan J, Tyrlikova I, Kuba R, Brazdil M, Chrastina J, Novak Z (2009) Secondary generalisation in seizures of temporal lobe origin: Ictal EEG pattern in a stereo-EEG study. Epilepsy Behav 15:235-239.

Reynolds, EH. Todd, Hughlings Jackson, and the electrical basis of epilepsy. The Lancet 358: 575-577.

Reynolds EH (1988) Hughlings Jackson A Yorkshireman's contribution to epilepsy. Arch Neurol 45: 675-8.

Reynolds EH, Kinnier Wilson, JV. (2008) Psychoses of epilepsy in Babylon: the oldest account of the disorder. Epilepsia 49: 1488-90.

Riva D, Vago C, Franceschetti S (2007) Intelectual and language findigs and their relationship to EEG characteristics in benign childhood epilepsy with centrotemporal spikes. Epilepsy Behav 10:278-285,

Salmenpera TM, Symms MR, Rugg-Gunn FJ, Boulby PA, Free SL, Barker GJ, Yousry TA, Duncan, JS. (2007) Evaluation of quantitative magnetic resonance imaging contrasts in MRI-negative refractory focal epilepsy. Epilepsia 48: 229-37.

Sander JW, Shorvon SD (1996) Epidemiology of the epilepsies. J Neurol Neurosurg Psychiatry 61:433-443.

Scheffer IE, Berkovic S, Capovilla G, Connolly MB, French J, Guilhoto L, Hirsch E, Jain S, Mathern GW, Moshe SL, Nordli DR, Perucca E, Tomson T, Wiebe S, Zhang YH, Zuberi SM (2017) ILAE classification of the epilepsies: Position paper of the ILAE Commission for Classification and Terminology. Epilepsia 58:512-521.

Sidhu MK, Stretton J, Winston GP, Bonelli S, Centeno M, Vollmar C, Symms M, Thompson PJ, Koepp MJ, Duncan JS (2013) A functional magnetic resonance imaging study mapping the episodic memory encoding network in temporal lobe epilepsy. Brain: a journal of neurology 136:1868-1888.

Siniatchkin M, Moeller F, Jacobs J, Stephani U, Boor R, Wolff S, Jansen O, Siebner H, Scherg M (2007a) Spatial filters and automated spike detection based on brain topographies improve sensitivity of EEG-fMRI studies in focal epilepsy. Neuroimage 37:834–843

Siniatchkin M, van Baalen A, Jacobs J, Moeller F, Moehring J, Boor R, Wolff S, Jansen O, Stephani U (2007b) Different neuronal networks are associated with spikes and slow activity in Hypsarrhythmia. Epilepsia 48:2312–232

Shields WD, Snead OC (2009) Benign epilepsy with centrotemporal spikes", Epilepsia, 50(Suppl.8): 10-15

Strandberg M, Larsson EM, Backman, S, Kallen, K (2008) Pre-surgical epilepsy evaluation using 3T MRI. Do surface coils provide additional information? Epileptic Disord 10**:** 83-92.

Stretton J, Thompson PJ (2012) Frontal lobe function in temporal lobe epilepsy. Epilepsy Res 98:1-13.

Tellez-Zenteno JF, Hernandez-Ronquillo L (2012) A review of the epidemiology of temporal lobe epilepsy. Epilepsy Res Treat 2012:630853.

Theodore WH. (1989) SPECT and PET in epilepsy. Lancet 1**:** 502-3.

Thivard L, Lehericy S, Krainik A, Adam C, Dormont D, Chiras J, Baulac M, Dupont S (2005) Diffusion tensor imaging in medial temporal lobe epilepsy with hippocampal sclerosis. NeuroImage 28:682-690.

Toth V, Hejjel L, Fogarasi A, Gyimesi C, Orsi G, Szucs A, Kovacs N, Komoly S, Ebner A, Janszky J (2010) Periictal heart rate variability analysis suggests long-term postictal autonomic disturbance in epilepsy. Eur J Neurol 17:780- 787.

Tzitiridou M, Panou T, Ramantani G, Kambas A, Spyroglou K, Panteliadis C (2005) Oxcarbazepine monotherapy in benign childhood epilepsy with centrotemporal spikes: a clinical and cognitive evaluation", Epilepsy Behav., 7:458-467

Van Klink N, Klooster M, Leijten F, Jacobs J, Braun K, Zijlmans M (2016) Ripples on rolandic spikes: a marker of epilepsy severity", Epilepsia, 57(7):1179-1189

Voets NL, Beckmann CF, Cole DM, Hong S, Bernasconi A, Bernasconi N (2012) Structural substrates for resting network disruption in temporal lobe epilepsy. Brain : a journal of neurology 135:2350-2357.

Voets NL, Menke RA, Jbabdi S, Husain M, Stacey R, Carpenter K, Adcock JE (2015 Thalamo-Cortical Disruption Contributes to Short-Term Memory Deficits in Patients with Medial Temporal Lobe Damage. Cereb Cortex 25:4584-4595

Whelan CD et al. (2018) Structural brain abnormalities in the common epilepsies assessed in a worldwide ENIGMA study. Brain 141:391-408.

Wiebe S (2000) Epidemiology of temporal lobe epilepsy. Can J Neurol Sci 27 Suppl 1:S6-10; discussion S20-11.

Wiebe S, Blume WT, Girvin JP, Eliasziw M (2001) A randomized, controlled trial of surgery for temporal-lobe epilepsy. NEnglJMed 345:311-318.

Wieser HG (2004) ILAE Commission Report. Mesial temporal lobe epilepsy with hippocampal sclerosis. Epilepsia 45:695-714.

Williamson PD, French JA, Thadani VM, Kim JH, Novelly RA, Spencer SS, Spencer DD, Mattson RH (1993) Characteristics of medial temporal lobe epilepsy: II. Interictal and ictal scalp electroencephalography, neuropsychological testing, neuroimaging, surgical results, and pathology. Ann Neurol 34:781- 787.

Wilson, JV, Reynolds, EH. Texts and documents. (1990) Translation and analysis of a cuneiform text forming part of a Babylonian treatise on epilepsy. Med Hist 34: 185-98.

Winston GP, Cardoso MJ, Williams EJ, Burdett JL, Bartlett PA, Espak M, Behr C, Duncan JS, Ourselin S (2013) Automated hippocampal segmentation in patients with epilepsy: available free online. Epilepsia 54:2166-2173.

Winston GP, Vos SB, Burdett JL, Cardoso MJ, Ourselin S, Duncan JS (2017) Automated T2 relaxometry of the hippocampus for temporal lobe epilepsy. Epilepsia 58:1645-1652.

Wirrell EC, Sherman EM, Vanmastright R, Hamiwka L (2008) Deterioration in cognitive function in children with benign epilepsy of childhood with central temporal spikes treated with sulthiame", J Child Neurol, 23:14-21

Xiao F, An D, Lei L, Chen S, Wu X, Yang T, Ren J, Gong Q, Zhou D (2016) Real-time effects of centrotemporal spikes on cognition in rolandic epilepsy: an EEG-fMRI study. Neurology 86:544–551

Yoo JY, Farooque P, Chen WC, Youngblood MW, Zaveri HP, Gerrard JL, Spence DD, Hirsch LJ, Blumenfeld H (2014) Ictal spread of medial temporal lobe seizures with and without secondary generalisation: an intracranial electroencephalography analysis. Epilepsia 55:289-295.

Zhang Z, Lu G, Zhong Y, Tan Q, Liao W, Wang Z, Wang Z, Li K, Chen H, Liu Y (2010a) Altered spontaneous neuronal activity of the default-mode network in mesial temporal lobe epilepsy. Brain research 1323:152-160.

Chapter 9: Temporal Lobe Spikes Affect Distant Intrinsic Connectivity Networks

9.1. INTRODUCTION

Simultaneous EEG and fMRI (EEG–fMRI) recording is a functional neuroimaging technique that reveals cerebral hemodynamic changes related to interictal epileptiform discharges (IED) visualized on scalp EEG. It combines the temporal resolution of the EEG with the spatial resolution of MRI, offering the opportunity to define epileptogenic foci or complex epileptic networks (Krakov et al., 1999; Gotman et al., 2008). In the last 20 years, several EEG–fMRI studies have been performed in patients with epilepsy to better understand specific epileptic networks in focal and generalized epilepsies. The hemodynamic response to IED could result in BOLD increments (or fMRI activations), reflecting spike-generating fields or decrements (deactivations), which can be interpreted as areas of reduced neuronal activity, although the meaning of deactivation is still debated (Kobayashi et al., 2006; Meletti et al., 2015). In focal epilepsies, studies have detected BOLD-signal changes that are

tightly coupled with the regions generating focal IED and are concordant with intracranial EEG findings (Pittau et al., 2014). Compared to intracerebral recordings that are targeted to few cerebral structures based on a priori hypothesis, the spatial resolution of EEG–fMRI allows covering the whole brain and can highlight the involvement of deep brain structures in seizure generation or propagation, and their relationships with the cortex (Kobayashi et al., 2006). Patients with temporal lobe epilepsy (TLE) have previously been studied with EEG–fMRI (Kobayashi et al., 2006; Salek-Haddadi et al., 2006; Kobayashi et al., 2009, Fahoum et al., 2012; Pittau et al., 2012; Coan et al., 2016; Vaudano et al., 2021). Modifications of BOLD signal related to temporal IED were observed in 50–83% of the patients in the different studies, and often, but notably not only in all cases, the fMRI response was localized in the temporal lobe, ipsilateral, or/and contralateral to the IED but also in extra-temporal or subcortical structures. These findings are in line with the recent concept of "network epilepsy" applied to TLE, which has overcome the traditional hypothesis that in focal epilepsy seizure activity originates from a specific and anatomically isolated focus (Berg et al., 2010; Avanzini et al., 2012). Ideally, EEG–fMRI could represent a non-invasive way to identify the seizure onset zone as part of the presurgical evaluation, but its clinical use is still limited. Modifications of the BOLD signal in relation to IED do not distinguish between irritative zone, seizure onset zone, or propagation effect (Laufs et al., 2007). The main limitations of studies that focused on its clinical role in the presurgical evaluation were the small number of patients enrolled and the number and features of IED recorded during the scan. Efforts have been made to overcome the issue, and methods have been applied in patients without visually detectable IED on scalp EEG (Grouiller et al., 2011). A few retrospective EEG–fMRI studies on patients with TLE undergoing epilepsy surgery found that if the BOLD response was located in the area that was surgically removed (concordant fMRI response), the postsurgical outcome was better than if the BOLD response also involved regions outside the surgical resection (discordant fMRI response) (Coan et al., 2016; Thronton et al., 2010).

Studies on group analysis of EEG–fMRI data aimed to reveal common network alterations in patients with TLE. BOLD activations related to IED were found not only in the ipsilateral mesial and neocortical temporal cortex, but also in the insula and the cerebellum, while deactivations were observed in structures belonging to the default mode network (DMN) (Fahoum et al., 2012; Laufs et al., 2007), a physiological cerebral network encompassing brain areas preferentially active during conscious rest, including the precuneus and posterior cingulate, bilateral temporo-parietal, and medial prefrontal cortices (Raichle et al., 2001). Previous resting-state fMRI (rs-fMRI) studies in TLE patients showed alterations of the major intrinsic connectivity networks (ICN) (Cataldi et al., 2013). Mainly, the activity of the DMN, of attention, and of the executive control networks showed significant differences in patients with TLE when compared to healthy subjects. In the present prospective study, 33 patients with TLE undergoing EEG–fMRI as part of their presurgical workup were consecutively enrolled at the University of Modena and Reggio Emilia—Epilepsy Center. We not only aimed to verify the epileptogenic zone (EZ) through this technique but also to evaluate the patient's specific epileptic network. Specifically, we evaluated if the changes related to BOLD are triggered by interictal spikes in cortical structures that belong to physiological networks using a quantitative method. Finally, a group analysis of BOLD signal changes related to IED was conducted to search for a common network functionally altered TLE.

9.2. METHODS

9.2.1. Participants

Patients affected by TLE were prospectively included in the study: 33 concluded the EEG fMRI co-registration protocol (14 men; mean age 36 years, range 15–56 years). The inclusion criteria were (a) patients ≥14 years old with an electro-clinical diagnosis of TLE; (b) patients entering a presurgical evaluation program; and (c) no contraindication to 3T MRI scanning. This

study was approved by the local Ethical Committee (N. 322/15) and written informed consent was obtained from all participants.

Table 9.1 summarizes the main electroclinical findings of the cohort of TLE patients. In 6 patients MRI was negative for epileptogenic lesions, whereas in the remaining 27 patients an epileptogenic lesion was observed. The most frequent radiological diagnosis was hippocampal sclerosis (n = 13), followed by low-grade tumors (n = 5) and focal cortical dysplasia (n = 4).

***Table 9.1**: Electro-clinical data of patients with temporal lobe epilepsy included in the study.*

	TLE n = 33
Gender, n (%)	
female	19
male	14
Etiology, n (%)	
Hippocampal sclerosis	13
Focal cortical dysplasia	4
Scar	1
Cavernoma/vascular	4
low grade tumors	5
MRI negative	6
Lesion Side*, n (%)	
right	12
left	14
bilateral	1
MRI negative	6
Type of TLE**	
Mesial	26
Lateral	1
Age at study enrollment, years (range)	36 (15-56)
Age at epilepsy onset,years (range)	23.5 (4-49)
Duration of epilepsy,years (range)	12.6 (1-35)
Seizure frequency,n/month (range)	2.7 (0-20)
Seizures during wakefulness,n (%)	27 (82)
Seizure-Free periods***, n (%)	14 (42)

Cluster seizures,n (%)	16 (48)
Focal aware seizures,n (%)	19 (58)
Focal impaired awareness seizures, n (%)	25 (76)
Focal to generalized seizures,n (%)	25 (76)
Status Epilepticus, n (%)	1 (3)
Falls during seizures, n (%)	11 (33)

*: based on MRI findings. ··: based on clinical and radiological findings. Sz/m= number of seizures per month. N pt= number of patients ···: Period longer than 1 year without seizure recurrence

9.2.2. Video EEG-fMRI Protocol

Scalp EEG was recorded by means of a 32-channel MRIcompatible EEG recording system (Micromed, Mogliano Veneto, Italy). Electrodes were placed according to conventional 10–20 locations and the reference was FCz. ECG was recorded from two chest electrodes. Before scanning, 10min of out-of-scanner EEG data were collected. Foam pads were used to help secure the EEG leads, minimize motion, and improve the comfort of the patient. Data were transmitted via an optic fibre cable from the high-input impedance amplifier (1,024/2,048 kHz sampling rate) to a computer located outside the scanner room. Patients were also constantly observed and recorded by a small camcorder positioned on the head coil inside the scanner pointing at the patient's face to obtain a split-screen video-EEG documentation during the fMRI recording (Chaudhary et al., 2012; Ruggieri et al., 2015). Video data were used to monitor behavioural signs of sleep and movements. Functional data were acquired using a Philips Achieva system at 3T and a gradient-echo echo-planar sequence from 30 axial contiguous slices (TR = 2,000ms; in-plane matrix = 80 × 80; voxel size: 3 × 3 × 4) over one to three 8min sessions per participant (240 volumes) with continuous video-EEG recording.

The mean duration of the recording was 24min (range 8– 32min), depending on the number of acquired sessions. In particular, one patient had four

sessions recorded, 12 patients had three sessions, 18 patients had two sessions, and 2 patients had only one session. A high-resolution T1-weighted anatomical image was acquired for each participant to allow anatomical localization. The volume consisted of 170 sagittal slices (TR = 9.9ms; TE = 4.6ms; in-plane matrix = 256 × 256; voxel size = 1 × 1 × 1 mm).

9.2.3. EEG Analysis

EEG acquisition was used to identify interictal (or ictal) epileptiformactivity during the fMRI session. BrainQuick System Plus software (Micromed) was used for offline correction of the gradient artifacts and filtering of the EEG signal (Allen et al., 2000). In addition, the EEG data were exported in the .edf format and reviewed and analysed by means of the BrainVision Analyzer 2.0 software (Brain Products, Munich, Germany). After removing the gradient and mean ballistocardiographic artifacts, according to the previously published methods (Vaudano et al., 2014), two experienced electroencephalographer reviewed the preprocessed EEG recordings (LM, AEV) to identify interictal epileptiform abnormalities based on both spatial distribution and topography. When recognized, IED were marked as intervals. We classified patients as unilateral (right or left) in case of only one spike focus without contralateral spreading; bilateral, in case both temporal lobes were active simultaneously (same timing of the left and right spikes). In the latter condition, left and right IED were considered together as a single event in the GLM analysis. In patients with independent bilateral temporal IED, both right and left IED were included in the design matrix, separately.

9.2.4. Single-Subject Analysis

fMRI Analysis

The fMRI data analyses were performed using MATLAB version R2013a (The MathWorks Inc., Natick, MA, USA) and SPM12 (Wellcome Department of

Imaging Neuroscience, London, UK). Preprocessing of functional volumes included slice timing correction, realignment to the first volume acquired, normalization to the MNI (Montreal Neurologic Institute) template implemented in SPM12 and smoothing with an 8 × 8 × 8mm FWHM Gaussian kernel. The interictal (or ictal) epileptiform activity was implemented as a regressor of interest in the single patient-first level analysis. To do so, patients' IED were treated as a single event regardless of their topography or location. Their onset was exported in .mat file that describes the exact timing and duration (in seconds) of IED. The resulting timing files served as an onset for GLM, convolved with the standard hemodynamic response function (HRF) and its time and dispersion derivatives (TD, DD). Twenty-four motion parameters estimated during the realignment were included as nuisance regressors. The resulting fMRI maps (F-contrast) were estimated at the conventional statistical threshold of $p < 0.05$ at the voxel level (family-wise error (FWE)-corrected). In addition, in cases where the conventional FWE corrected statistical threshold did not show any results, the data were further explored with a less stringent statistical threshold of $p < 0.001$ (uncorrected for multiple comparisons). In the latter case we applied a small volume correction (5mmsphere) and we considered any BOLD activation/deactivation with a threshold of $p < 0.05$, FWE corrected.

This procedure reflects the standard procedure generally adopted in the previously published criteria (Siniatchkin et al., 2010; Moeller et al., 2013; Meletti et al., 2016). For each patient, specific contrasts were settled up to test the BOLD effect of IED with respect to the resting EEG background.

Identification of the Presumed EZ

The presumed EZ (pEZ) was defined based on the results of the presurgical work-up, which included video-EEG findings (interictal and ictal EEG activity and clinical ictal semiology), structural MRI scan, and interictal F-18 fluorodeoxyglucose FDG-PET when available. For each patient, this information was presented for discussion at a multidisciplinary team meeting,

resulting in a consensus EZ localization. The EZ delineation and surgical decisions were blind with respect to the EEG–fMRI results. For all patients, the presumed EZ was localized in the temporal lobe.

Evaluation of Concordance

To evaluate the concordance between the map of BOLD changes related to IED and the presumed EZ, we applied previously published criteria (Thornton et al., 2010; Markoula et al., 2018). Specifically, “Concordant” (C) refers to maps in which all the clusters (either activation or deactivation) are colocalized with the presumed EZ: within 2 cm of and in the same lobe as EZ; “Concordant Plus” (C+).

is applied to fMRI maps with some clusters of significant IED related BOLD changes colocalized with the pEZ and other significant BOLD clusters were located outside the pEZ (within or outside the temporal lobe). EEG–fMRI findings were defined “Discordant” (D) when all clusters of BOLD changes related to IED were remote from the pEZ and Null (N) where there was no cluster of significant BOLD change related to IED. For patients with mesial TLE, the presumed EZ consisted of the cerebral structures classically removed by the standard anterior temporal lobectomy (Wiebe et al., 2001), that is, 6.0–6.5 cm of the anterior lateral non-dominant temporal lobe or 4.0–4.5 cm of the dominant temporal lobe. In these cases, medially, it included the amygdala and, at a minimum, the anterior 1.0–3.0 cm of the hippocampus (most commonly, 4.0 cm). Note that the concordance between the map of BOLD changes related to IED and the presumed EZ was evaluated using nonnormalized

fMRI data.

Identification of ICN

To investigate if the cortical structures involved by the fMRI maps belonged to physiological networks (ICN), the ICN_Atlas toolbox was used to perform a

quantitative analysis (Kozák et al., 2017). This new methodology was designed to describe fMRI maps in a function-oriented way using a set of 15 metrics conceived to quantify the degree of "engagement" of ICNs for any given fMRI-derived statistical map of interest. We used the BRAINMAP20, implemented in the ICN_Atlas toolbox, as an atlas base map. It includes 18 co-activation networks and 2 artifact components, and it is based on ICA decomposition (d = 20) of the BrainMap Project large-scale neuroimaging experiment meta-analysis data (Laird et al., 2005; Laird et al., 2011). For each subject, the ICN_Atlas output can reveal the involvement of one or more than one ICN with a different degree of "engagement." The latter is reflected by a spatial involvement metric, the I_j, which expresses the ratio between the number of activated voxels in the i^{th} thresholded prototyped ICN map (ICN_i) and the volume of ICN_i (Laird et al., 2005; Laird et al., 2011).

For each patient, the spatial involvement results were visualized using rose plots (see **Figure 9.2**). The axis limit is at the maximum of the subject-specific spatial involvement metric. There are tick marks at 25, 50, and 75% of the maximum.

We have calculated how many times each ICN was engaged in the group of patients with positive fMRI findings (total number = 19 patients). For each patient, the ICNs with a spatial involvement metric lower than the patient-specific 25% were not considered. The four most frequent ICNs were the motor (6/19), the visual (7/19), the auditory/motor speech (9/19), and the default mode networks (4/19). To investigate the concordance between the most engaged ICNs (>patient-specific 25%) and ictal/postictal symptoms at the single-subject level, the corresponding ictal semiology (i.e., motor symptoms, such as tonic-clonic movements, visual auras, ictal, or postictal aphasia, impaired awareness) was examined. Ictal/postictal symptoms/signs refer both to clinical signs witnessed during video-EEG recording and to symptoms referred to by the patient in his/her recent clinical history (latest 3 months before the EEG–fMRI study).

Sensitivity, specificity, positive predictive value (PPV), and negative predictive value (NPV) of EEG–fMRI in detecting specific network alterations related to a corresponding symptom

were evaluated. Cases with an ICN involvement (i.e., motor network) and the presence of corresponding ictal/postictal semeiology (i.e., tonic-clonic seizures) were defined as true positive (TP), whereas true negative (TN) were the cases without ICNs engagement and absence of corresponding ictal/postictal semeiology (i.e., neither motor network nor motor symptoms); false positive (FP) were defined by the cases in which a specific ICN was involved but the patient did not present the corresponding clinical features (i.e., motor network involved, but absence of motor signs or symptoms), whereas false negative (FN) were defined by the cases without ICN involvement but with the presence of the

corresponding symptoms (i.e., motor network not involved but patient referring recent tonic-clonic seizures).

The mathematical definition of sensitivity is given by the ratio between TP and the sum of TP and FN cases (= TP/TP + FN). Specificity corresponds to the ratio of TN and the sum of TN and FP (= TN/TN + FP). PPV represents the proportion of truly positive cases among the positive cases detected by the test (= TP/TP + FP), and NPV represents the proportion of truly negative cases among the negative cases detected by the test (TN/TN + FN).

9.2.5. Group Analysis

To ensure a homogeneous group with all patients having the seizure focus on the same side, functional volumes of right TLE patients were right–left flipped, so the ipsilateral hemisphere was on the left in all cases. This step was done using FSL (fslswapdim tool) before the preprocessing. Using the parameter estimates obtained by single-subject analyses, we performed a second level (group) random-effect analyses on all patients with IEDs recorded during

EEG–fMRI (n = 25). A full factorial design was used, with hemodynamic shapes (HRF, TD, and DD) as levels.

Patients' age and gender were included in the model as covariates.

A double-statistical threshold (voxel-wise p < 0.001 and spatial extent of 15 voxels) was adopted to achieve a combined significance, corrected for multiple comparisons, of < 0.05, as computed by 3dClustSim AFNI routine, using the "-acf" option (https://afni.nimh.nih.gov/pub/dist/doc/program_help/3dClustSim.html).

9.3. RESULTS

In 25 patients out of 33 (75%), epileptiform activity with morphology and scalp topography typical of patients' out-of-scan IEDs was identified. A mean of 16 IEDs/run per patient was recorded (range: 2–70). The number of sessions recorded did not influence the average number of IEDs/run: patients with 1 session had a mean of 15 IEDs/run, patients with 2 sessions had a mean of 20.6 IEDs/run, patients with 3 sessions had a mean of 9.7 IEDs/run and the patient with 4 sessions recorded had a mean of 13.2 IEDs/run (p = 0.1073, two-tailed T-test between session 2 and session 3). No seizures were recorded. In the remaining eight patients, no clear epileptiform discharges were found; therefore, the fMRI analysis could not be performed. In 19 patients spike-triggered BOLD signal changes were obtained, whereas six patients had a "Null" result [Table 9.2 **(supplementary)**].

Table 9.2 (supplementary): *Single-Subject Analysis results*

Pt	Regions	BA	Lateralization	Activation (+) Deactivation (-)	MNI coordinates			Z score
					x	y	z	
MO_01 *p<0.001 unc.*	Occipital Lobe, Cuneus	30	R	+	3	-67	6	5
	Cerebellum, Declive	/			18	-70	-14	4,7
	Occipital Lobe, Middle Occipital Gyrus	19	R	+	51	-61	-6	4,5
	Temporal Lobe, Inferior Temporal Gyrus	37			51	-52	-6	4,4
	Parietal Lobe, Postcentral Gyrus	3	L	+	-33	-28	70	4,5
		2			-51	-25	42	4,3
		1			-48	-22	58	4,1
	Parietal Lobe, Postcentral Gyrus	3	R	+	51	-25	62	4
		2			60	-22	50	3,9
	Parietal Lobe, Postcentral Gyrus	4	L	+	-57	-13	34	3,4
MO_04 *p<0.001 unc*	Frontal Lobe, Paracentral Gyrus	5	L	+	15	-28	74	4,8
	Frontal Lobe, Medial Frontal Gyrus	6			-3	-19	54	4,5
	Temporal Lobe,Superior Temporal Gyrus	13	R	-	51	-40	18	4,5
	Parietal Lobe, Supramarginal Gyrus	40			48	-40	30	7,8
	Cerebellum, Declive	/	L		0	-76	-6	4,3
	Ocipital Lobe, Cuneus	23	R	+	6	-73	10	4
	Occipital Lobe, Lingual Gyrus	17	L		-12	-94	-14	4
MO_05	Caudate	/	L	+	-18	-19	22	5,2

p<0.001 unc	Thalamus		R		6	-10	22	4
	Frontal Lobe, Inferior Frontal Gyrus	47	L	-	-51	26	-18	4,1
	Temporal Lobe,Superior Temporal Lobe	38			-57	17	-30	4
	Parietal Lobe, Inferior Parietal Lobule	40	R	+	45	-43	58	4,6
	Parietal Lobe, Postcentral Gyrus	5			42	-43	58	4,4
	Parietal Lobe, Precuneus	19			27	-79	38	4,3
	Parietal Lobe, Inferior Parietal Lobule	40	L	+	-57	-58	42	4,4
	Parietal Lobe, Angular Gyrus	39			-51	-67	34	4,2
	Occipital Lobe, Superior Occipital Gyrus	19			-39	-73	22	4,1
	Parietal Lobe, Postcentral Gyrus	2	L	+	-36	-34	62	4,4
	Frontal Lobe, Precentral Gyrus	4			-36	-25	62	
MO_07	Posterior Cingulate	30	L	+	-18	-58	6	5,4
p<0.001 unc	Occipital Lobe, Cuneus	19			-15	-79	30	5
		23			-12	-70	10	4,5
	Frontal Lobe, Precentral Gyrus	4	R	+	57	-7	26	5,1
	Parietal Lobe, Postcentral Gyrus	3			57	-16	22	4,1
	Cerebellum, Posterior Lobe	/	R	-	30	-82	-34	5,1
	Frontal Lobe, Superior Frontal Gyrus	6	L	+	-3	5	62	5
	Parietal Lobe, Postcentral Gyrus	7	R	+	3	-52	70	4,7
		5	L		0	-43	70	3,9
	Ippocampi	/	L	-	-30	_	_	4,7

						25	10	
	Temporal Lobe, Sub-Gyral				-36	-31	-2	4,1
	Parietal Lobe, Postcentral Gyrus	43			-54	-7	22	4,6
	Frontal Lobe, Precentral Gyrus	6	L	+	-54	-4	30	4,5
	Parietal Lobe, Postcentral Gyrus	40			-54	-22	22	4,5
	Thalamus	/	R	-	12	-10	18	4,5
	Caudate Body				15	-1	22	4,4
	Parahippocampal Gyrus	30	L	-	-15	-37	6	4,5
	Caudate	/			-12	-22	22	4,1
MO_09 *p<0.001 unc*	Occipital Lobe, Cuneus	19	L	+	-6	-79	34	5,2
	Parietal Lobe, Postcentral Gyrus	3	R		30	-31	70	5
	Frontal Lobe, Superior Frontal Gyrus	8	R	+	27	35	50	4,3
	Temporal Lobe, Middle Temporal Lobe	21	L	+	-57	-58	6	4,3
		37			-57	-64	-2	3,9
	Thalamus	/	L	+	0	-19	10	4,1
	Cerebellum, Posterior Lobe	/	R	+	33	-76	-30	4,1
	Frontal Lobe, Middle Frontal Gyrus	10	R	+	30	44	26	4
		9			27	56	30	3,9
	Putamen	/	L	+	-24	8	-2	3,9
	Caudate Body				-15	11	6	3,6
	Frontal Lobe, Inferior Frontal Gyrus	47	L	+	-54	23	-2	3,8
		45			-51	35	2	3,6
	Temporal Lobe, Superior Temporal Gyrus	38			-57	14	-10	3,6
MO_1	Frontal Lobe, Precentral	6	R	+	54	-7	26	Inf

1 *p<0.05 FWE*	Gyrus Insula	13			36	-13	14	5,2
	Frontal Lobe, Precentral Gyrus	6	L	+	-51	-7	22	Inf
		4			-39	-19	38	7,8
	Temporal Lobe, Superior Temporal Gyrus	22			-54	-10	6	6,6
	Insula	13	L	+	-39	-10	10	5,8
	Parietal Lobe, Postcentral Gyrus	4	R	+	18	-34	58	5,2
MO_13 *p<0.001 unc*	Temporal Lobe, Middle Temporal Lobe	21	R	-	63	-40	-6	6
	Parietal Lobe, Supramarginal Gyrus	40	L	-	-54	-49	34	5
	Temporal Lobe, Superior Temporal Gyrus	13			-45	-46	22	4,8
	Temporal Lobe, Middle Temporal Lobe	21	L	-	-63	-52	-6	5
	Cerebellum, Declive	/	R	-	51	-70	-18	4,4
MO_17 *p<0.001 unc*	Temporal Lobe, Inferior Temporal Gyrus	20	L	+	-45	-13	-34	6,3
	Frontal Lobe, Middle Frontal Gyrus	10	L		-39	56	-6	5,1
	Frontal Lobe, Middle Frontal Gyrus	10	R	-	39	56	-2	5,4
		11			42	47	-10	3,6
	Frontal Lobe, Precentral Gyrus	4	L	+	-63	-7	22	5,2
	Frontal Lobe, Inferior Frontal Gyrus	9			-48	5	30	4,3
		44			-60	8	18	3,7
	Cerebellum, Posterior Lobe	/	L	+	-45	-70	-38	5,2
	Frontal Lobe, Middle Frontal Gyrus	9	R	-	48	17	30	5
		46			51	29	18	4,2
		6			45	11	46	4,2
	Frontal Lobe, Precentral	6	R	+	54	-7	30	5

	Gyrus							
	Cerebellum, Posterior Lobe	/	R	+	21	-31	-42	4,6
MO_19 *p<0.001 unc*	Parietal Lobe, SuperiorParietal Lobule	7	R	+	30	-73	46	4,3
MO_20 *p<0.05 FWE*	Frontal Lobe, Precentral Gyrus	6	L	+	-51	-7	34	Inf
		4			-45	-16	38	7,6
	Parietal Lobe, Postcentral Gyrus	3			-39	-22	58	7,4
	Parietal Lobe, Postcentral Gyrus	3	R	+	54	-10	42	Inf
	Frontal Lobe, Precentral Gyrus	6			51	-4	26	Inf
	Occipital Lobe, Cuneus	19	R	+	12	-91	22	6,9
			L		0	-76	34	6,5
		18	R		3	-76	-10	6,3
	Occipital Lobe, Inferior Occipital Gyrus	18	L	+	-39	-85	-10	6,9
	Occipital Lobe, Middle Occipital Gyrus	19			-51	-73	-6	6..85
	Occipital Lobe, Inferior Occipital Gyrus	18	R	+	42	-82	-14	6,8
	Occipital Lobe, Middle Occipital Gyrus				36	-88	-2	6,6
	Occipital Lobe, Lingual Gyrus	19			18	-43	-2	6,4
	Cerebellum, Culmen	/	R	+	15	-52	-6	5,2
	Parahippocampal Gyrus	30			9	-37	6	5
	Putamen	/	L	+	-24	5	-2	6,2
	Cerebellum, Declive	/	R	+	30	-73	-18	6
	Frontal Lobe, Medial	6	R	+	6	-1	58	6

	Frontal Gyrus							
	Occipital Lobe, Inferior Occipital Gyrus	37	R	+	54	-67	2	5,8
	Temporal Lobe, Fusiform Gyrus				51	-61	-10	4,9
	Cerebellum, Declive	/	L	+	-15	-67	-14	5,7
	Claustrum	/	R	+	36	-7	10	5,7
	Frontal Lobe, Middle Frontal Gyrus	10	R	+	30	50	18	5,6
	Temporal Lobe, Superior Temporal Gyrus	/	R	+	54	2	2	5,6
	Isula	13	L	+	-39	-1	10	5,5
	Posterior Cingulate	30	R	+	15	-61	10	5,4
	Cingulate Gyrus	24	R	+	9	-1	46	5,4
	Putamen	/	R	+	30	-16	6	5,3
MO_22 *p<0.001 unc*	Frontal Lobe, Precentral Gyrus	/	R	+	3	-19	74	3,8
MO_25 *p<0.001 unc*	Frontal Lobe, Medial Frontal Gyrus	10	L	-	0	62	2	4,8
	Frontal Lobe, Superior Frontal Gyrus				-3	68	-10	4,1
	Frontal Lobe, Superior Frontal Gyrus	9	L	-	-18	53	34	4,8
		8			-18	47	42	4
	Precuneus	31	L	-	0	-46	30	4,6
	Cingulate Gyrus				0	-58	26	4,1
MO_26 *p<0.05 FWE*	Occipital Lobe, Lingual Gyrus	17	L	-	-9	-94	-6	5,9
		18			-9	-82	-6	5,6
	Occipital Lobe, Cuneus		R		6	-85	14	5,4
	Parahippocampal Gyrus	30	L	+	-15	-40	6	5,2

	Occipital Lobe, Lingual Gyrus	19	L	-	-21	-64	-2	4,9
	Cerebellum, Culmen	/			-12	-67	-10	4,9
MO_27	Frontal Lobe, Superior Frontal Gyrus	8	R	+	24	35	54	5,4
p<0.001 unc	Precuneus				6	-58	54	5,1
	Parietal Lobe, Postcentral Gyrus	7	R	+	18	-55	70	3,3
	Parietal Lobe, Superior Parietal Lobule				15	-52	58	3,3
	Frontal Lobe, Precentral Gyrus	6	L	+	-45	-7	30	5
	Parietal Lobe, Postcentral Gyrus	3			-51	-10	50	3,9
	Parietal Lobe, Superior Parietal Lobule	7	R		30	-76	46	4,8
	Precuneus	19		+	24	-82	46	4,6
	Occipital Lobe, Cuneus	18	L		0	-79	22	4,5
	Parietal Lobe, Superior Parietal Lobule	7	L	+	-36	-49	62	4,8
	Frontal Lobe, Precentral Gyrus	6	R	+	57	-1	18	4,3
		44			60	8	6	3,7
	Parietal Lobe, Inferior Parietal Lobule	40	R	+	42	-37	54	4,1
	Parietal Lobe, Postcentral Gyrus	2			48	-28	58	4
	Occipital Lobe, Middle Occipital Gyrus	19	L	+	-57	-67	-6	4,1
	Occipital Lobe, Inferior Occipital Gyrus	19			-48	-79	-2	3,9
	Temporal Lobe, Middle Temporal Gyrus	39			-42	-70	14	3,6
	Frontal Lobe, Precentral Gyrus	6	L	+	-42	-16	62	3,9
		4			-39	-28	66	3,5

MO_28 *p<0.001 unc*	Frontal Lobe, Inferior Frontal Gyrus	45 44	L	+	-48 -45	26 17	22 14	4,1 3,9
MO_32 *p<0.001 unc*	Precuneus	7	R	+	3	-70	50	4,8
MO_33 *p<0.05 FWE*	Frontal Lobe, Precentral Gyrus Temporal Lobe, Superior Temporal Gyrus	6 22	R	+	63 51	2 -4	18 6	Inf Inf
	Brain Stem	/		+	6	-25	-34	Inf
	Frontal Lobe, Precentral Gyrus	6	L	+	-45	-10	34	Inf
	Cerebellum, Posterior Lobe	/	R	-	42	-70	-22	Inf
	Frontal Lobe, Middle Frontal Gyrus Frontal Lobe, Superior Frontal Gyrus	10	L R	-	-30 9	65 71	6 14	Inf 6,9
	Uncus	20	L	+	-24	-4	-38	Inf
	Frontal Lobe, Superior Frontal Gyrus Frontal Lobe, Middle Frontal Gyrus	8 6	R L	-	33 -33	32 5	50 58	7,6 7,4
	Occipital Lobe, Lingual Gyrus	18	R	-	6	-94	-6	7,5
	Precuneus Parietal Lobe, Superior Parietal Lobule	7	R	-	3 12	-67 -73	54 62	7,1 6,1
	Cerebellum, Posterior Lobe	/	L	-	-48	-67	-30	6,9
	Parietal Lobe, Superior Parietal Lobule Parietal Lobe, Inferior Parietal Lobule	7 40	L	-	-33 -36	-64 -49	58 58	6,6 5,8
	Insula	13	R	+	39	-10	14	6,5

	Frontal Lobe, Middle Frontal Gyrus	10	R	-	30	65	6	6,5
	Frontal Lobe, Superior Frontal Gyrus				24	53	2	5,3
	Insula	13	L	+	-42	5	-6	6,5
	Occipital Lobe, Cuneus	19	R	-	30	-88	22	6,5
	Precuneus				36	-79	34	6,1
	Temporal Lobe, Middle Temporal Gyrus	38	R	-	48	-1	-42	6,1
	Frontal Lobe, Inferior Frontal Gyrus	9	R	+	60	14	34	6
	Temporal Lobe, Middle Temporal Gyrus	21	R	-	69	-37	-6	5,9
	Occipital Lobe, Middle Occipital Gyrus	19	L	-	-51	-67	-6	5,5
	Precuneus	19	L	-	-30	-76	42	5,5
	Precuneus	23	L	-	0	-58	18	5,5
MO_34 *p<0.05 FWE*	Cerebellum, Posterior Lobe	/	R	+	42	-64	-22	5,2
	Cerebellum, Culmen				42	-49	-18	5,2
	Occipital Lobe, Lingual Gyrus	17	L	+	-9	-88	2	5,1
		18			-9	-82	-10	4,7
	Occipital Lobe, Fusiform Gyrus	19			-21	-64	-6	4,5
	Precuneus	31	R	+	6	-46	30	4,8
		7			3	-49	42	3,6
	Frontal Lobe, Precentral Gyrus	6	L	+	-63	-16	38	4,6
	Parietal Lobe, Postcentral Gyrus	1			-57	-25	38	3,6
	Frontal Lobe, Precentral Gyrus	6	R	+	54	-7	6	4,1

	Parietal Lobe, Postcentral Gyrus	1			66	-16	22	4
		43			57	-7	18	3,2
	Temporal Lobe, Superior Temporal Gyrus	41	R	+	48	-31	14	3,8
	Temporal Lobe, Middle Temporal Gyrus	21			54	-28	2	3,4
MO_35	Parietal Lobe, Postcentral Gyrus	43	L	+	-57	-7	18	4,1
p<0.001 unc	Frontal Lobe, Precentral Gyrus	6			-42	-13	34	3,8

9.3.1. Presumed EZ and BOLD Concordance

One patient, the only one with neo-cortical TLE, had a “Concordant” finding, 7 patients showed a “Concordant Plus” result and in the remaining 11 patients, fMRI maps were

“Discordant” (58%). We considered patients with C and C+ results (n = 8, 42%) as a single group. Figure 9.1 shows three exemplificative cases. Differences in clinical, radiological, aetiological, and surgery outcome data were evaluated between Concordant and Discordant patients. The only statistically significant difference (p = 0.02) regarded the antiepileptic

treatment at the time of the neuroimaging study: a higher percentage of patients (75%, n = 6 out of 8 patients) with Concordant results were taking carbamazepine as an antiseizure drug, compared to 18% of patients (n = 2 out of 11 patients) with Discordant results. At present, eight patients underwent surgery and all resulted in a good outcome (Engel class I): one had concordant and seven had discordant results [Table **9.2** ***(supplementary*** **(supplementary)**].

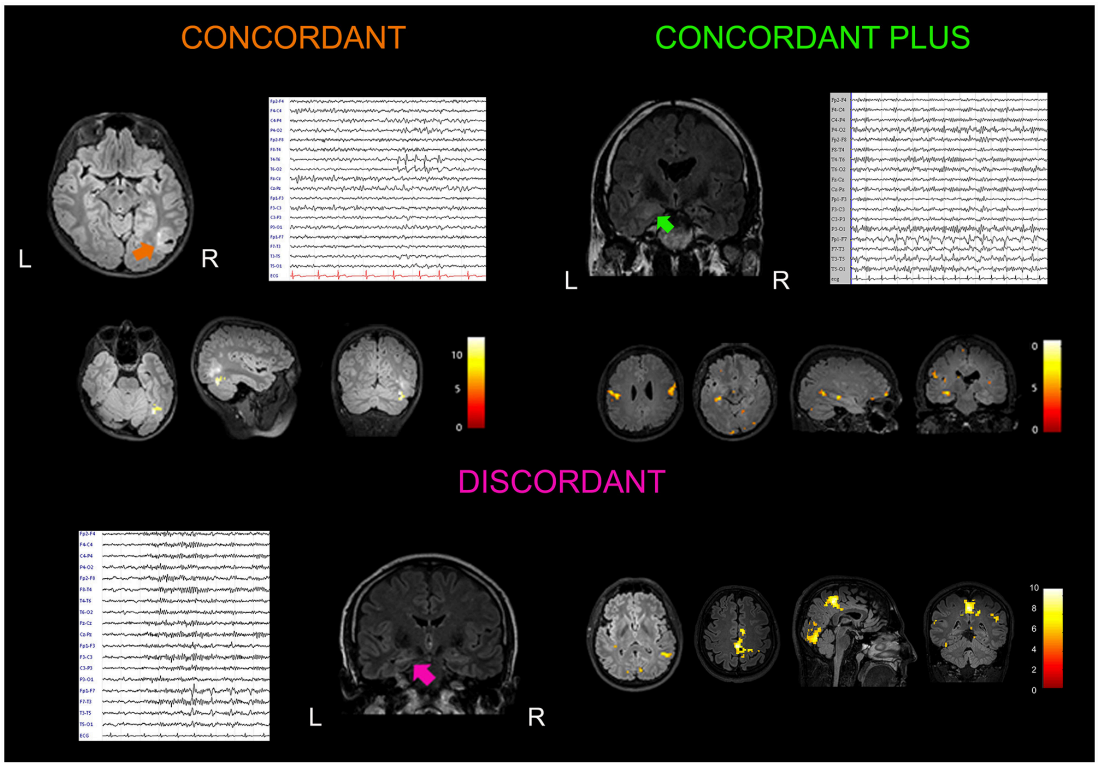

***Figure 9.1**: Examples of concordant, concordant plus and discordant EEG–fMRI findings.*
Concordant: A 15-year-old boy with a history of febrile seizures in early childhood presented with a focal to generalized seizure occurring during sleep. Brain MRI showed a lesion localized at the border of the temporal and occipital cortex on the right side (arrow). Low-amplitude spike and waves were observed in the right posterior temporal and occipital electrodes (T6, O2) on scalp EEG. He received surgery (lesionectomy) with a good outcome (Engel Class Ib at 24 months of follow up). Histological analysis documented a polymorphous low-grade neuroepithelieal tumor of the young (PLNTY). EEG–fMRI analysis guided by interictal T6 spike-and-waves showed a cluster of BOLD signal increment localized inside the tumor.
Coronal, sagittal, and axial slices of the patient's structural MRI are displayed ($p < 0.05$), FWE corrected. Concordant plus: A 37-year-old woman presented with a 6-year history of focal seizures occurring on a weekly base. She referred to two types of seizures: one with an epigastric aura ascending from the lower abdomen to the neck, nausea, and brief impairment of awareness; second seizure type was a focal aware seizure with a visual aura (visual shrinking and oscillation) with dizziness sensation. Structural MRI showed two lesions suggestive for focal cortical dysplasia localized in the right anterior mesial temporal lobe, and in the posterior part of the middle temporal cortex. EEG confirmed two epileptic foci in the right temporal lobe, one anterior temporal (F8) and the other localized in the middle posterior temporal derivations (T4, T6). The patient refused surgery after seizures improvement with pharmacological treatment. EEG–fMRI showed BOLD changes in the right temporal lobe with a cluster in the vicinity of the posterior middle-temporal lesion, plus other clusters of increased BOLD changes localized at distant cerebral structures (ipsilateral and contralateral parietal, precentral, and occipital gyrus; $p < 0.001$,

uncorrected for multiple comparisons). Discordant: A 40-year-old man with left hippocampal sclerosis presented frequent focal seizures characterized by epigastric aura, aphasia, and oral automatisms. Scalp EEG abnormalities were represented by infrequent spikes and waves visible in the anterior temporal derivations (F7, T3). Excellent seizure outcome (Engel Class Ia) was obtained after standard left anterior temporal lobectomy. EEG–fMRI showed widespread fMRI changes localized outside the left temporal lobe and involving cerebral structures belonging to the motor, visual, and DMNs (p < 0.001, uncorrected for multiple comparisons).

9.3.2. ICN Alterations Related to Spike

In every patient with an fMRI map related to spike (n = 19), at least one ICN appeared involved (**Table 9.3** and **Figure 9.2**).

The most frequent ICNs identified were, namely, motor, visual, auditory/motor speech, and DMN. The specificity of EEG–fMRI analysis in detecting alteration of an ICN in patients with corresponding ictal/postictal symptoms was high for all four ICNs investigated (all above 65%), while the sensitivity of the test was high for the motor and the language networks, and lower for the other two networks (**Table 9.4**). In particular, for the motor network, sensitivity of 57% (n◦ of TP:4) was obtained, and specificity of 83% (n◦ of TN:10) was obtained; for the language network, sensitivity of 75% (n◦ of TP:6) and specificity of 73% (n◦ of TN:8) were obtained; for the visual network, sensitivity was of 50% (n◦ of TP:1) and specificity of 65% (n◦ of TN:11), respectively, and for the DMN, the sensitivity was of 25% (n◦ of TP:3), whereas the specificity resulted in 86% (n◦ of TN:6). The positive predictive value of the test was above 67% for all networks but the visual one. Negative predictive value was above 80% in all networks, with the exception of the DMN (**Table 9.4**).

Moreover, we explored the existence of a correlation between the language network involvement and the side of TLE: the 88.9% (n = 8/9) of patients with language network involvement had TLE lateralized to the left.

***Table 9.3**: Electro-clinical and radiological features of 19 patients with positive fMRI results.*

Patient	Age (Y), sex	MRI findings	$^{18\text{-FDG}}$ PET hypo-metabolism	IEDs field	N°IEDs/run recorded	Surgery, Outcome Engel Class(follow up)	Resting State Networks (ICN_atlas)
1	37, F	R Focal cortical dysplasia	-	F8/T4	7	-	Visual
2	40, M	L Hippocampal sclerosis	-	F7/T3	23	ATL, Ia (24 months)	Visual; Motor; DMN
3	38, F	L Low grade tumor	-	F7/T3	7	Lesionectomy, Ib (12 months)	Visuospatial/ motor; DMN; interoceptive
4	36, M	L Focal cortical dysplasia	-	F7/T3	7	-	Auditory/motor speech; visual
5	29, M	R Hippocampal sclerosis	-	F8/T4	22	ATL, Ia (15 months)	Visual; motor
6	22, F	L Hippocampal sclerosis	-	F7/T3/T5	8	-	Auditory/motor speech; motor
7	37, F	MRI negative	L temporo-parietal	T3/T5	9,5	-	DMN; auditory/motor speech
8	53, F	L Hippocampal sclerosis	-	F3/T3	33,5	-	L fronto-parietal; right fronto-parietal; cerebellum
9	36, M	L Low grade tumor	-	F7/T3/C3	27,5	ATL, Ia (20 months)	Visuospatial
10	56, M	MRI negative	-	F7/T3	10,3	-	Auditory/motor speech
11	29, F	R Hippocampal sclerosis	R temporal	F8/T4	1,7	ATL, Ia (26 months)	Auditory/motor speech; motor/ visuospatial
12	40, F	L Scar	-	F7/T3	5,5	-	DMN; emotion
13	43, F	R Low grade tumor	-	T4/T6	9	Lesionectomy, Ia (27 months)	Visual
14	42, M	MRI negative	-	F7/T3	13,3	-	Visual; motor; auditory/motor speech
15	46, M	R Hippocampal sclerosis	-	F8/T4	10	ATL, Ia (15 months)	Lfronto-parietal
16	51, M	R Hippocampal sclerosis	R temporo-parietal	F8/T4/T6	10	-	Visuospatial
17	43, F	L Focal cortical dysplasia	-	F7/T3/T5	5	-	Auditory/motor speech
18	15, M	R Low grade tumor	-	T4/T6	70	Lesionectomy, Ib (23 months)	Visual

Patient	Age (Y), sex	MRI findings	$^{18\text{-FDG}}$ PET hypo-metabolism	IEDs field	N°IEDs/run recorded	Surgery, Outcome Engel Class(follow up)	Resting State Networks (ICN_atlas)
19	43, F	L Cavernoma	-	F7/T3	23	Lesionectomy , Ia (19 months)	Auditory/motor speech

F: female, M: male, R: right, L:left, ATL: anterior temporal lobectomy, FWE= Family Wise Error corrected; unc = uncorrected for multiple comparisons. DMN: Default mode network.

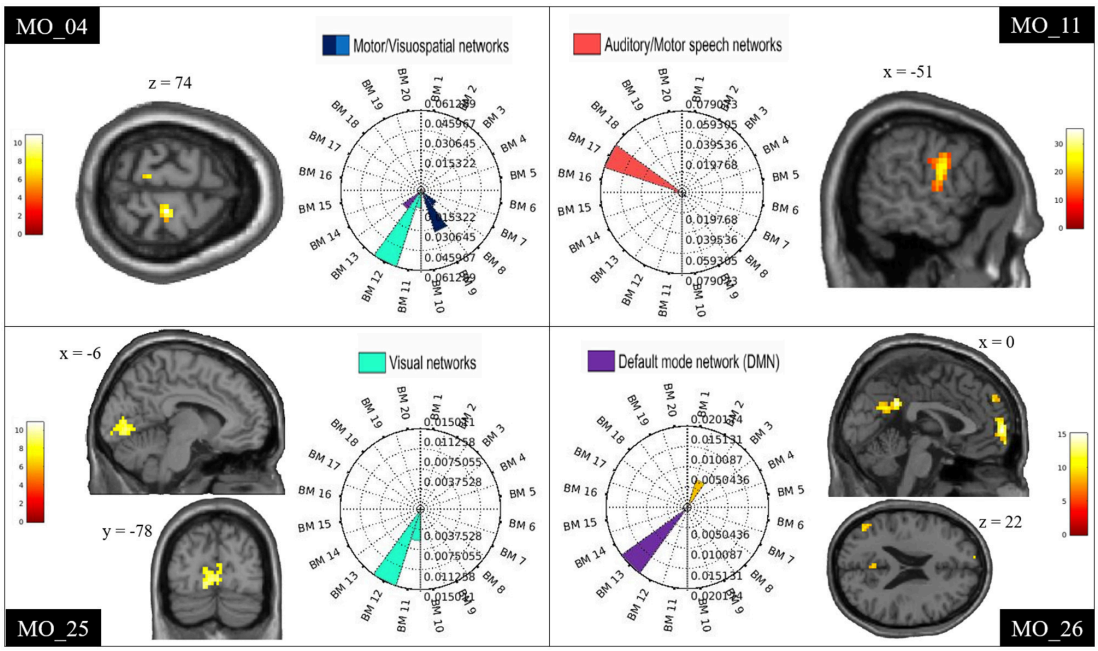

***Figure 9.2**: Examples of ICN alterations.*
Examples of single-subject results showing spike-triggered BOLD signal changes within the motor (MO_04), auditory/motor speech (MO_11), visual (MO_25), and DMN (MO_26). Clusters are shown in sagittal, coronal, and axial slices of an anatomical template as implemented in spm12.
The rose plots represent the ICN_Atlas output: the spatial involvement metric expressing the ratio between the number of activated voxels and the volume of the ICNsi. BM refers to the co-activation networks of the BRAINMAP20 atlas base map.
Table 3: Concordance between Intrinsic Connectivity Networks (ICN) related to spike and seizure semeiology.
Pt, Number of Patient; TLE, temporal lobe epilepsy; meaning of colored cells: presence of ICN involvement or presence of clinical symptom in the patient; meaning of empty cells:
absence of ICN or clinical symptom. SENS, Sensitivity; SPEC, Specificity; PPV, Positive Predictive Value; NPV, Negative Predictive Value.

***Table 9.4**: Concordance between ICN related to spike and seizure semeiology.*

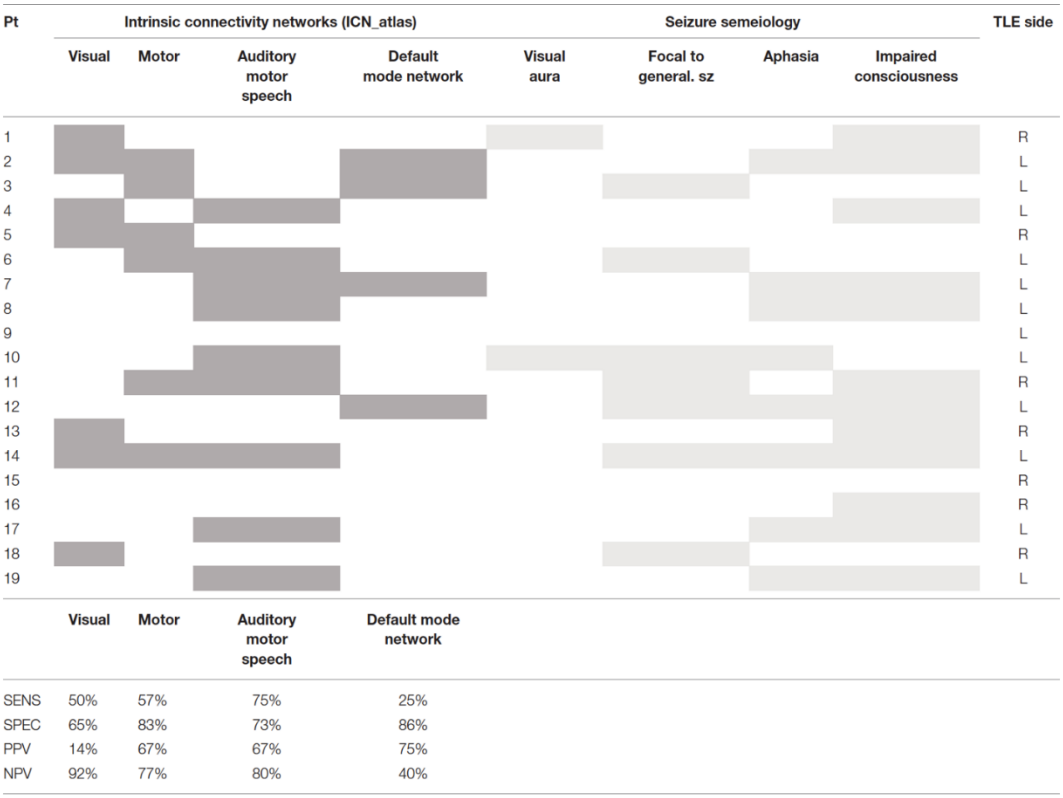

9.3.3. Group Results

The group analysis including all patients (n = 25) revealed common BOLD changes related to IED at the right precentral gyrus, supplementary motor area (SMA), and middle cingulate gyrus. Regions showing BOLD signal changes time-locked to IEDs are summarized in **Table 9.5** and Figure 9.3.

***Table 9.5**: Peak coordinates of group analysis.*

Cluster K	Brain areas	BA	Voxel level Z	MNI Coordinates		
				x	y	z
15	Precentral gyrus	4	4.64	21	-25	62
23	Middle cingulate gyrus	24	4.24	9	-4	42
	Supplementary motor area	6	4.16	0	-1	50
BA, Brodmann area						

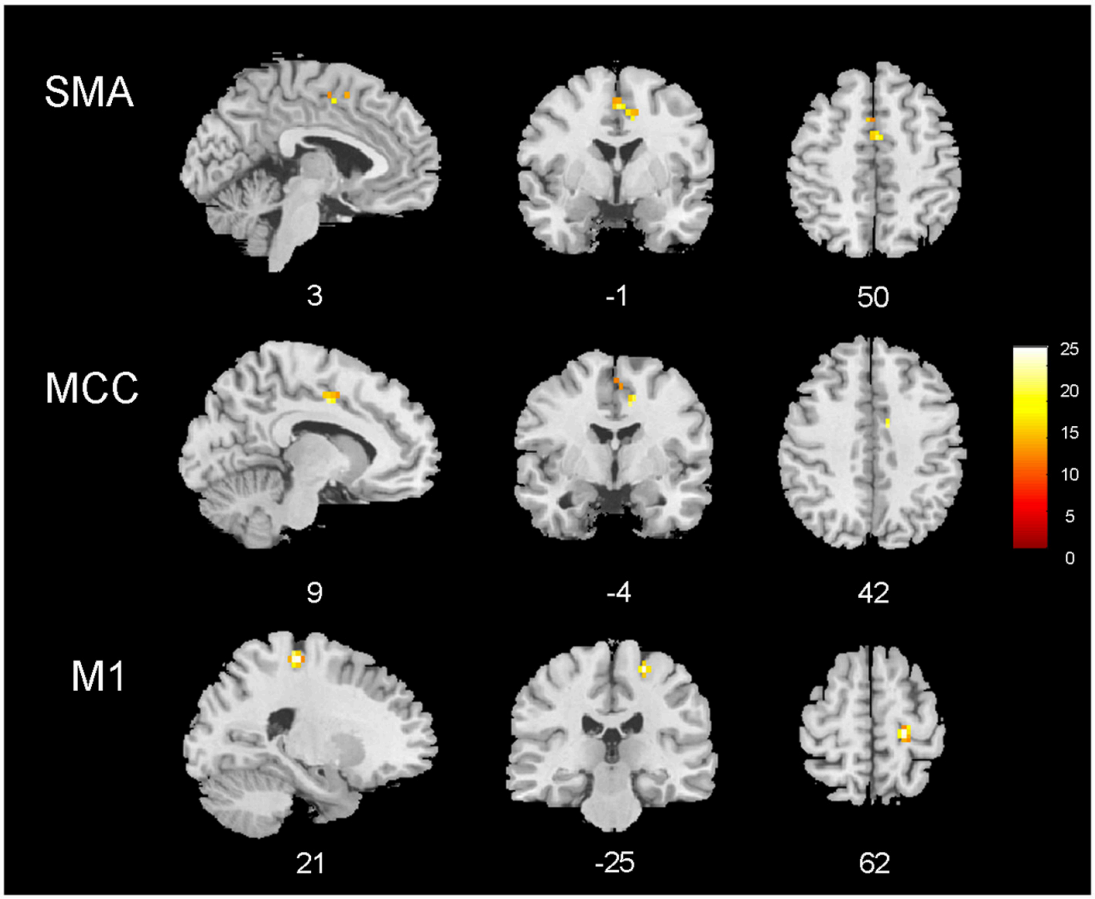

***Figure 9.3**: EEG–fMRI group analysis in 25 patients with temporal lobe epilepsy. Results of the group analysis (cluster size threshold K > 15, corrected at < 0.05). Clusters are shown in sagittal, coronal, and axial slices of an anatomical template found in the xjview toolbox (https://www.alivelearn.net/xjview). Colour bar represents t values.*

9.4. DISCUSSION

In this study, IED were recorded in 75% of the patients and in 58% a BOLD signal change was observed. These results are in line with the previous EEG–fMRI studies, confirming that a major limitation for the use of the technique in the presurgical setting in TLE patients is the low numbers of IEDs recording

during EEG–fMRI (Coan et al., 2016), and in particular, for mesial TLE, which often generates infrequent scalp-detectable IEDs (Kowalczyk et al., 2020).

We have observed BOLD maps related to IED are concordant with the EZ only in one patient, affected by neocortical temporal lobe epilepsy (Concordant case, **Figure 9.1**), whereas in the remaining patients, we detected temporal lobe activations plus extratemporal areas in 7 patients, and only extratemporal activation in 11 patients. This finding questions the clinical utility of the presurgical interictal EEG–fMRI to localize the EZ in TLE patients. Compared to other studies, we observed less concordant results (Kobayashi et al., 2006; Pittau et al., 2014; Kobayashi et al., 2009; Pittau et al., 2012). This might be related to the shorter duration (20–40min) of our recordings compared to previous works performed by other groups [recordings lasting up to 84min (Kobayashi et al., 2009)], thus reducing the chance of detecting interictal abnormalities.

These data suggest that in order to better evaluate patients with TLE, a longer EEG–fMRI session is required. In agreement with a recent retrospective review investigating the clinical impact of EEG–fMRI in the presurgical setting (Kowalczyk et al., 2020), our results suggest that in patients with TLE short EEG–fMRI recordings are not useful for the surgical decision. When a clear epileptogenic lesion is detected on structural MRI, which matches the epileptogenic focus defined by the video-EEG data, EEG–fMRI might not add information for the surgical planning.

This was the case for the 82% (n = 27) of the patients in our cohort, who had a positive MRI congruent with the electroclinical data. In the remaining six patients with a negative MRI, in three patients no IED were recorded during EEG–fMRI, and in the other three cases, the fMRI response was represented by widespread changes of the BOLD signal.

In our cohort, BOLD signal changes occurred in the temporal lobe plus in extratemporal areas in 42% of cases, whereas only extra-temporal BOLD activations or deactivations were observed in the remaining 58% of patients. When comparing the two groups (concordant or concordant plus vs.

discordant), no significant differences were found, and, in particular, no differences in seizure outcome were observed in patients who underwent surgery. This finding suggests that, at least in our series, multiple BOLD clusters related to IED involving regions outside the presumed EZ were not related to a worse surgery outcome.

To better understand the meaning of the BOLD response involving extratemporal cortical areas, we moved from a focus view to a network view, which is what a functional technique, such as EEG–fMRI, allows us to do, highlighting a patient's specific epileptic network. Indeed, advancement in functional neuroimaging leads to the observation that TLE is not only a disease of certain brain structures involved in seizures onset ("the focus") but it also affects chronically the activity of brain networks that control basic functions, such as attention, emotion, and cognition (Cataldi et al., 2013; Trimmel et al., 2021; Fadaie et al., 2021; Li et al., 2021). Moreover, recent studies on patients with drug-resistant TLE enhanced functional differences in sub-group of patients through the use of diffusion tensor imaging or rs-fMRI, i.e., with or without focal to bilateral tonic-clonic seizures (FBTCS), especially in thalamo-cortical networks (Chen et al., 2019; He et al., 2020). Intrinsic connectivity networks can be altered in patients with TLE, as previously observed at group level (Fahoum et al., 2012; Cataldi et al., 2013, Zhang et al., 2010; Liao et al., 2011; Pittau et al., 2012). In this study, we were able to define IED-related ICNs alterations at a single-subject level, and to delineate and quantify the ICNs involvement. All patients had at least one ICNinvolved, and often more than one. According to the network classification of the BrainMap20 (Kozák et al., 2017; Laird et al., 2005), the most frequent BOLD changes involved the motor network, the visual network, the auditory/speech network, and the DMN. We looked for correlations between ICN alterations and clinical data, such as ictal or postictal semiological signs, and we found that in many patients with IED-related involvement of a distant ICN, ictal/postictal semiology was concordant with the function supported by that ICN. EEG–fMRI appeared to have high specificity (above 65%) for all 4

networks, while sensitivity was high for the language network (75%) and the motor network (57%) and lower for the visual network (50%), and the DMN (25%). Positive and negative predictive values were overall high, with the exception of the PPV low for the visual network, and NPV low for the DMN.

These findings confirm the role of EEG–fMRI in highlighting physiological networks alterations in patients with TLE, which might be possibly related to the clinical semeiology of the seizures. In other words, recurrent seizures with a specific ictal semeiology (i.e., aphasia) might interfere with the corresponding network (i.e., the language network) at the individual level, as revealed by spike-triggered EEG–fMRI.

A correct clinical testing of the seizure semeiology during video-EEG monitoring might play an important role: in fact, while motor and language deficits are easily recognized, the evaluation of consciousness is more complex. This might explain a reduction in sensitivity and NPV for the DMN. Despite the relatively small number of patients enrolled, these observations represent a link between functional imaging data and the clinical seizures' phenotype. If confirmed in a larger group of patients, the research of ICN alterations through EEG– fMRI could represent complementary information to understand the fMRI maps, especially in complex cases. In particular, the finding of distant network involvement driven by interictal epileptic activity in patients with TLE, is of particular interest, underscoring the long-distance effects of interictal temporal lobe spikes.

Moreover, the correlation between the auditory/motor speech network involvement and side of TLE revealed that the great majority (n: 8/9, 88.9%) had left-side TLE. This finding suggests that patients with the epileptogenic network localized in the left temporal lobe are more prone to have an effect on the language network, confirming data from previous studies of altered functional connectivity in the language network in left TLE patients (Trimmel et al., 2018).

With a second-level group analysis, we aimed to look for common spike-triggered functional alterations in patients with TLE. No BOLD changes were

observed in the temporal structures, differently from the previous works (Kobayashi et al., 2009, Fahoum et al., 2012; Laufs et al. 2007). This finding is in line with the low frequency of temporal lobe fMRI changes observed at the single-subject level. Nevertheless, an involvement of extra-temporal structures belonging to the motor network (precentral gyrus and SMA) corroborates the alterations observed at the single-subject level in a significant proportion of cases. Since the motor network involvement is hemodynamically linked to the appearance of interictal temporal epileptic discharges on the scalp EEG, our findings suggest that IED might affect the neuronal activity of distant cerebral areas/networks subserving the sensory-motor functions. Interestingly, previous MRI morphometric studies have repeatedly reported a reduction of cortical thickness in the motor/premotor cortex in patients with TLE (Whelan et al., 2018; Bernasconi et al., 2004). Thus, the present findings might represent the functional counterpart of these structural data although further data are needed to confirm this suggestion.

Finally, we observed an alteration of the BOLD signal in the middle cingulate gyrus, as previously described (Fahoum et al., 2012). In this work, the authors observed activation of mid-cingulate gyrus bilaterally in the group analysis of patients with TLE and also frontal lobe epilepsy (FLE), suggesting that the common involvement of the mid-cingulate gyrus in both groups might result from the rapid spread of epileptic activity from temporal and frontal areas. Moreover, the reduction in grey matter volume bilaterally in the cingulate gyri was observed in patients with TLE.

In conclusion, we suggest the use of EEG–fMRI coregistration for TLE patients, not only for localizing purposes but also to investigate ICN alterations. A larger number of patients are desirable to confirm our findings.

9.4.1. Limitations of the Study

The present study presents methodological limitations that need to be underlined. First, fMRI data are driven by IED recorded from scalp EEG, not

comprising the eventual intracranial epileptic activity that does not reach the cortical surface.

This element might be considered a possible bias in the data interpretation.

As previously stated, TLE patients have infrequent IED which might be a limitation in the statistical power of the fMRI analysis: in fact, only a minority of patients presented BOLD cluster activations after FWE correction, whereas in the other patients the fMRI clusters were obtained only with $p< 0.001$ uncorrected.

In the present study, the duration of EEG–fMRI registration was also shorter compared to other studies: this represents an important limitation, and also leads to the conclusion that in this group of patients longer EEG–fMRI registrations are needed especially for localizing purposes.

Moreover, the analysis performed at the group level included patients with heterogeneous features (i.e., different epilepsy aetiologies, different disease durations, and different clinical

semiologies) that might interfere with the final findings.

Nevertheless, the results obtained in this group might represent the common epileptic network altered in TLE patients despite the heterogeneity.

Future studies including a larger number of patients might overcome these methodological limitations.

9.5. REFERENCES

Allen PJ, Josephs O, Turner R. A method for removing imaging artifact from continuous EEG recorded during functional MRI. Neuroimage. (2000) 12:230–9. doi: 10.1006/nimg.2000.0599

Avanzini G, Manganotti P, Meletti S, Moshe SL, Panzica F, Wolf P, et al. The system epilepsies: a pathophysiological hypothesis. Epilepsia. (2012) 53:771– 8. doi: 10.1111/j.1528-1167.2012.03462.x

Berg AT, Berkovic SF, Brodie MJ, Buchhalter J, Cross JH, van Emde Boas W, et al. Revised terminology and concepts for organization of seizures and epilepsies: report of the ILAE commission on classification and terminology, 2005-2009. Epilepsia. (2010) 51:676–85. doi: 10.1111/j.1528-1167.2010.02522.x

Bernasconi N, Duchesne S, Janke A, Lerch J, Collins DL, Bernasconi A. Whole-brain voxel-based statistical analysis of grey matter and white matter in temporal lobe epilepsy. Neuroimage. (2004) 23:717– 23. doi: 10.1016/j.neuroimage.2004.06.015

Cataldi M, Avoli M, de Villers-Sidani E. Resting state networks in temporal lobe epilepsy. Epilepsia. (2013) 54:2048–59. doi: 10.1111/epi.12400

Chaudhary UJ, Rodionov R, Carmichael DW, Thornton RC, Duncan JS, Lemieux L. Improving the sensitivity of EEG-fMRI studies of epileptic activity by modelling eye blinks, swallowing and other video- EEG detected physiological confounds. Neuroimage. (2012) 61:1383– 93. doi: 10.1016/j.neuroimage.2012.03.028

Chen C, Li H, Ding F, Yang L, Huang P, Wang S, et al. Alterations in the hippocampal-thalamic pathway underlying secondarily generalized tonicclonic seizures in mesial temporal lobe epilepsy: A diffusion tensor imaging study. Epilepsia. (2019) 60:121–30. doi: 10.1111/epi.14614

Coan AC, Chaudhary UJ, Grouiller F, Campos BM, Perani S, De Ciantis A, et al. EEG-fMRI in the presurgical evaluation of temporal lobe epilepsy. J Neurol Neurosurg Psychiatry. (2016) 87:642–9. doi: 10.1136/jnnp-2015-310401

Fadaie F, Lee HM, Caldairou B, Gill RS, Sziklas V, Crane J, et al. Atypical functional connectome hierarchy impacts cognition in temporal lobe epilepsy. Epilepsia. (2021) 62:2589–603. doi: 10.1111/epi.17032

Fahoum F, Lopes R, Pittau F, Dubeau F, Gotman J. Widespread epileptic networks in focal epilepsies: EEG-fMRI study. Epilepsia. (2012) 53:1618– 27. doi: 10.1111/j.1528-1167.2012.03533.x

Gotman J. Epileptic networks studied with EEG-fMRI. Epilepsia. (2008) 49:42–51. doi: 10.1111/j.1528-1167.2008.01509.x

Grouiller F, Thornton RC, Groening K, Spinelli L, Duncan JS, Schaller K, et al. With or without spikes: localization of focal epileptic activity by simultaneous electroencephalography and functional magnetic resonance imaging. Brain. (2011) 134:2867–86. doi: 10.1093/brain/awr156

He X, Chaitanya G, Asma B, Caciagli L, Basset DS, Tracy JI, et al. Disrupted basal ganglia-thalamocortical loops in focal to bilateral tonico-clonic seizures. Brain. (2020) 143:175–90. doi: 10.1093/brain/awz361

Kobayashi E, Bagshaw AP, Benar CG, Aghakhani Y, Andermann F, Dubeau F, et al. Temporal and extratemporal BOLD responses to temporal lobe interictal spikes. Epilepsia. (2006) 47:343–54. doi: 10.1111/j.1528-1167.2006. 00427.x

Kobayashi E, Grova C, Tyvaert L, Dubeau F, Gotman, J. Structures involved at the time of temporal lobe spikes revealed by interindividual group analysis of EEG/fMRI data. Epilepsia. (2009) 50:2549–56. doi: 10.1111/j.1528-1167.2009.02180.x

Kowalczyk MA, Omidvarnia A, Abbott DF, Tailby C, Vaughan DN, Jackson GD. Clinical benefit of presurgical EEG-fMRI in difficult-to-localize focal epilepsy: A single-institution retrospective review. Epilepsia. (2020) 61:49– 60. doi: 10.1111/epi.16399

Kozák LR, van Graan LA, Chaudhary UJ, Szabó ÁG, Lemieux L. ICN_Atlas: Automated description and quantification of functional MRI activation patterns in the framework of intrinsic connectivity networks. Neuroimage. (2017) 163:319–41. doi: 10.1016/j.neuroimage.2017.09.014

Krakov K, Woermann FG, Symms MR, Allen PJ, Lemieux L, Barker GJ, et al. EEG-triggered functional MRI of interictal epileptiform activity in patients with partial seizures. Brain. (1999)122:1679–88. doi: 10.1093/brain/122.9.1679

Laird AR, Fox PM, Eickhoff SB, Turner JA, Ray KL, McKay DR, et al. Behavioural interpretations of intrinsic connectivity networks. J Cogn Neurosci. (2011) 23:4022–37. doi: 10.1162/jocn_a_00077 Frontiers in Neurology | www.frontiersin.org 11 December 2021 | Volume 12 | Article 746468 Mirandola et al. Distant Effect of Temporal Spikes

Laird AR, Lancaster JL, Fox PT. BrainMap: the social evolution of a human brain mapping database. Neuroinformatics. (2005) 3:65–78. doi: 10.1385/NI:3:1:065

Laufs H, Hamandi K, Salek-Haddadi A, Kleinschmidt AK, Duncan JS, Lemieux L. Temporal lobe interictal epileptic discharges affect cerebral activity in “default mode” brain regions. Hum Brain Mapp. (2007) 28:1023– 32. doi: 10.1002/hbm.20323

Li X, Jiang Y, LiW,Qin Y, Li Z, Chen Y, et al.Disrupted functional connectivity in white matter resting-state networks in unilateral temporal lobe epilepsy. Brain Imaging Behav. (2021). doi: 10.1007/s11682-021-00506-8

Liao W, Zhang Z, Pan Z, Mantini D, Ding J, Duan X, et al. Default mode network abnormalities in mesial temporal lobe epilepsy: a study combining fMRI and DTI. Hum Brain Mapp. (2011) 32:883–95. doi: 10.1002/hbm.21076

Markoula S, Chaudhary UJ, Perani S, De Ciantis A, Yadee T, Duncan JS, et al. The impact of mapping interictal discharges using EEG-fMRI on the epilepsy presurgical clinical decision making process: A prospective study. Seizure. (2018) 61:30–7. doi: 10.1016/j.seizure.2018.07.016

Meletti S, Ruggieri A, Avanzini P, Caramaschi E, Filippini M, Bergonzini P, et al. Extrastriate visual cortex in idiopathic occipital epilepsies: The contribution of retinotopic areas to spike generation. Epilepsia. (2016) 57:896– 906. doi: 10.1111/epi.13385

Meletti S, Vaudano AE, Tassi L, Caruana F, Avanzini P. Intracranial time-frequency correlates of seizure-related negative BOLD response in the sensory-motor network. Clin Neurophysiol. (2015) 126:847–9. doi: 10.1016/j.clinph.2014.07.030

Moeller F, Stephani U, Siniatchkin M. Simultaneous EEG and fMRI recordings (EEG-fMRI) in children with epilepsy. Epilepsia. (2013) 54:971– 82. doi: 10.1111/epi.12197

Pittau F, Dubeau F, Gotman J. Contribution of EEG/fMRI to the definition of the epileptic focus. Neurology. (2012) 78:1479– 87. doi: 10.1212/WNL.0b013e3182553bf7

Pittau F, Grouiller F, Spinelli L, Seeck M, Michel C, Vulliemoz, et al. The role of functional neuroimaging in pre-surgical epilepsy evaluation. Front Neurol. (2014) 24:31. doi: 10.3389/fneur.2014.00031

Pittau F, Grova C, Moeller F, Dubeau F, Gotman J. Patterns of altered functional connectivity in mesial temporal lobe epilepsy. Epilepsia. (2012) 53:1013–23. doi: 10.1111/j.1528-1167.2012.03464.x

Raichle ME, MacLeod AM, Snyder AZ, Powers WJ, Gusnard DA, Shulman GL. A default mode of brain function. Proc Natl Acad Sci USA. (2001) 98:676–82. doi: 10.1073/pnas.98.2.676

Ruggieri A, Vaudano AE, Benuzzi F, Serafini M, Gessaroli G, Farinelli V, et al. Mapping (and modelling) physiological movements during EEG-fMRI recordings: the added value of the video acquired simultaneously. J Neurosci Methods. (2015) 239:223–37. doi: 10.1016/j.jneumeth.2014.10.005

Salek-Haddadi A, Diehl B, Hamandi K, Merschhemke M, Liston A, et al. Hemodynamic correlates of epileptiform discharges: an EEG-fMRI study of 63 patients with focal epilepsy. Brain Res. (2006) 1088:148– 66. doi: 10.1016/j.brainres.2006.02.098

Siniatchkin M, Groening K, Moehring J, Moeller F, Boor R, Brodbeck V, et al. Neuronal networks in children with continuous spikes and waves during slow sleep. Brain. (2010) 133:2798–813. doi: 10.1093/brain/awq183

Thornton R, Laufs H, Rodionov R, Cannadathu S, Carmichael DW, Vulliemoz S, et al. EEG correlated functional MRI and postoperative outcome in focal epilepsy. J Neurol Neurosurg Psychiatry. (2010) 81:922– 7. doi: 10.1136/jnnp.2009.196253

Tong X, An D, Xiao F, Lei D, Niu R, Li W, et al. Real-time effects of interictal spikes on hippocampus and amygdala functional connectivity in unilateral temporal lobe epilepsy: An EEG-fMRI study. Epilepsia. (2019) 60:246–54. doi: 10.1111/epi.14646

Trimmel K, van Graan AL, Caciagli L, Haag A, KoeppMJ, Thompson PJ, et al. Left temporal lobe language network connectivity in temporal lobe epilepsy. Brain. (2018) 141:2406–18. doi: 10.1093/brain/awy164

Trimmel K, Vos SB, Caciagli L, Xiao F, van Graan LA, Winston GP, et al. Decoupling of functional and structural language networks in temporal lobe epilepsy. Epilepsia. (2021) 62:2941–54. doi: 10.1111/epi.17098

Vaudano AE, Mirandola L, Talami F, Giovannini G, Monti G, Riguzzi P, et al. fMRI-based effective connectivity in surgical remediable epilepsies: a pilot study. Brain Topogr. (2021) 34:632–50. doi: 10.1007/s10548-021-00857-x

Vaudano AE, Ruggieri A, Vignoli A, Avanzini P, Benuzzi F, Gessaroli G, et al. Epilepsy-related brain networks in ring chromosome 20 syndrome: an EEG-fMRI study. Epilepsia. (2014) 55:403–13. doi: 10.1111/epi. 12539

Whelan CD, Altmann A, Botía JA, Jahanshad N, Hibar DP, Absil J, et al. Structural brain abnormalities in the common epilepsies assessed in a worldwide ENIGMA study. Brain. (2018) 141:391–408. doi: 10.1093/brain/awx341

Wiebe S, Blume W, Girvin JP, Eliasziv M. A randomized, controlled trial of surgery for temporal lobe epilepsy. NEJM. (2001) 345:311– 8. doi: 10.1056/NEJM200108023450501

Zhang Z, Lu G, Zhong Y, Tan Q, Liao W, Wang Z, et al. Altered spontaneous neuronal activity of the default-mode network in mesial temporal lobe epilepsy. Brain Res. (2010) 1323:152–60. doi: 10.1016/j.brainres.2010.01.042

Chapter 10: fMRI-Based Effective Connectivity in Surgical Remediable Epilepsies: A Pilot Study

10.1. INTRODUCTION

Epilepsy occurs in 0.5–1% of people and about 25% of those affected continue to have seizures following the best medical therapies (Kalilani et al. 2018). Half of the patients with Drug Resistant Epilepsy (DRE) can benefit from epilepsy surgery, which is the most effective treatment, being successful in approximately 60% of cases (Liu et al. 2018). The precise localization of the Epileptogenic Zone (EZ), described as the driving hub of abnormal activity and seizures generation, organization and propagation, is crucial for a good surgical outcome (Duncan et al. 2016; Jehi 2018). In contrast with a traditional focal model (the “zone” concept), a more dynamic concept of epileptogenic network has been progressively introduced, being defined as the set of the brain regions involved in the generation and propagation of epileptic activities (the “network” concept) (Bartolomei et al. 2017). According to the epileptogenic network view, post-operative seizure freedom might be improved by multitarget treatments alongside focal resection. This expanded concept of EZ opens the way to sophisticated non-invasive

electrophysiological and neuroimaging methods that explore the epileptogenic network, its architecture and the relationships between its nodes. Ideally, these diagnostic techniques might help us to understand the interplay between the epileptogenic tissue and the healthy brain in order to devise improved surgical strategies. However, despite advances, these approaches do not always reveal the smallest part of the cortex that require removal or disconnection, which remains the main clinical question for surgeons. The "zone" or "network" concepts of EZ are not necessarily mutually exclusive and need to be combined to achieve the best understanding of the individual EZ. Accordingly, while the epileptogenic zone is increasingly conceived as a network of nodes (sometimes even distant from each other) there is a big effort to identify the hierarchic involvement of its hubs and particularly to reveal the "leading" area/s in originating and sustaining seizures with respect to the "secondary" generators of synchronous activity. In patients with Focal Cortical Dysplasia (FCD), it was shown that within the stereo-EEG (SEEG) delineated epileptogenic network, advanced signal connectivity analyses identified the node which generates the pathological activity not only during the ictal events but also during the interictal period. In particular, this pattern was distinguished from the other cortical regions involved by ictal/interictal activity, thus clearly recognized as secondary "hubs" (Varotto et al. 2012). In clinical practice, DRE patients may undergo longterm electroencephalograph, functional imaging (fMRI, PET, ictal SPECT, MRS, or MEG) and neuropsychological testing aimed at localizing the EZ as part of a presurgical workup (Brodbeck et al. 2011; Markoula et al. 2018; Rampp et al. 2019; Duez et al. 2019). In cases in which such data are unsatisfactory, further, invasive investigations in the form of intracranial EEG recording: (icEEG) (which may be considered the "gold standard" for the EZ localization) may be performed (Vakharia et al. 2018). However, this approach is best warranted based on a solid hypothesis about the location of the epileptogenic network provided by the results of previous tests, due to the spatial sampling limitations, health risks and costs associated with icEEG (Khoo et al. 2017; Vakharia et al. 2018;

Cardinale et al. 2019). Therefore, there is a need for the development of alternative and/or complementary non-invasive image techniques to improve the localization of the EZ, and to characterize the architecture of the epileptic network.

Simultaneous scalp EEG-fMRI is a technique capable of revealing brain regions associated with interictal epileptic discharges (IED) based on local blood oxygen level dependent (BOLD) signal variations (Khoo et al. 2017; Pittau et al. 2012; Thornton et al. 2011). In surgical epilepsy, this technique has attracted interest as a preoperative diagnostic tool to localize the EZ non-invasively (Gotman and Pittau 2011). Recently, an observational prospective cohort study showed that IED-related fMRI findings can affect the clinical decision making and patients' management process in a substantial proportion of DRE cases investigated as part of their presurgical evaluation (Markoula et al. 2018).

Additionally, EEG-fMRI was shown to influence directly the decision to offer surgery in patients with focal epilepsy (Kowalczyk et al. 2020a, b). Regions of IED-related BOLD change provide useful localization information on the irritative zone, which is defined as the area of the cortex generating IED (Jehi 2018; Zijlmans et al. 2019), and which might be widespread or larger than the required resection area in focal epilepsy. For this reason, its role as a marker of the EZ is debated (Lüders et al. 2006). Nevertheless, it has been demonstrated that in many cases the regions of IED-related BOLD change are a good predictor of the seizure-onset zone (SOZ) as revealed by icEEG and/or the surgery clinical outcome (Thornton et al. 2011; Pittau et al. 2012; An et al. 2013; Coan et al. 2016; Khoo et al. 2017). Additionally, a good concordance was reported between interictal BOLD changes and ictal data (Tyvaert et al. 2008). Recently, an excellent correspondence between the region of maximum BOLD change correlated with IEDs on scalp EEG and the icEEG-defined seizure onset zone has been shown (Khoo et al. 2017, 2018), with an accuracy of more than 90% in some situations (Khoo et al. 2017). Compared to other not-invasive presurgical techniques, the presurgical IED related EEG-fMRI shows

higher specificity to identify the EZ particularly in patients with MRI negative focal epilepsy and suspected extended EZ (Rossi Sebastiano et al. 2020). However, despite encouraging results, the sensitivity and reliability of IED mapping using EEG-fMRI remains limited (Yamazoe et al. 2019). Previous EEG-fMRI studies reported that BOLD changes were able to identify accurately the EZ in a variable proportion raging between 53 and 88% of focal epilepsy patients (Pittau et al. 2012; Coan et al. 2016; Khoo et al. 2017). This high variability is thought to be related to three main factors: (a) the heterogeneity of clinical epilepsy syndromes and cohort's size; (b) differences in EEG and fMRI analysis pipelines; and (c) the definition of BOLD concordance criteria with other non-invasive and/or invasive investigations to establish the clinical relevance of the fMRI clusters' localization. While in some studies, the IED-related BOLD clusters were defined as "concordant" if the cluster with maximum t-value corresponded to the localization of the spike-field determined by scalp EEG (Pittau et al. 2012, 2017), others assessed the concordance on the primary fMRI clusters by estimating the proximity (usually within 2 cm) with the EZ as revealed by icEEG recordings (Khoo et al. 2017; Thornton et al. 2011) or the area of surgical resection (An et al. 2013; Coan et al. 2016). A common observation is that focal IED-related BOLD maps comprise two or more clusters of activations or deactivations, distributed over multiple lobes (An et al. 2013; Coan et al. 2016; Thornton et al. 2011). Furthermore, it has also been shown that the whole of any given IED-related BOLD map can contain clinically relevant information, with a degree of predictive power for the outcome of patients who subsequently underwent surgery; for example, maps with multi-lobar activations and deactivations are associated with poorer surgical prospects (An et al. 2013; Coan et al. 2016; Khoo et al. 2017; Thornton et al. 2011). Therefore, if the aim is to better identify the EZ, there is a need for more investigations on the clinical relevance of the multiple clusters that constitute many IED-related BOLD maps. In particular, we need to better understand the dynamics that underlie these BOLD maps, seen as networks, and more specifically, the possibility of

identifying the brain regions that act as 'sources' of the activity in the rest of the network. Dynamic Causal Modelling (DCM) is an analysis framework for the characterization of brain effective connectivity i.e., the causal interactions between neuronal systems (Friston et al. 2003) and hence can potentially be used to identify the neuronal drivers of pathological activity. DCM applied to fMRI allows to establish the causal influences between the activities in a set of brain regions, despite the limitation of temporal resolution inherent to this imaging technique. DCM for fMRI data, in addition to its application to task-based paradigms, has been applied to resting-state data from patients affected by generalized and focal epilepsies (Vaudano et al. 2009, 2012, 2013; Murta et al. 2012; Klamer et al. 2015, 2018; Warren et al. 2019), to identify the sources ('drivers') of the pathological activity and/or the causal connectivity between epilepsy-related BOLD clusters.

Up to now, only a few single-case reports used this methodology in surgically-remediable epilepsies (Vaudano et al. 2013; Klamer et al. 2015).

In the following, we present the results of the use of DCM on fMRI data acquired during rest to help localize the EZ in a group of consecutive patients with focal epilepsy who were candidates for surgery and in whom multiple IED-related BOLD clusters were revealed by analysis of the concurrently recorded EEG-fMRI.

10.2. METHODS

10.2.1. Study Population

From an original pool of 35 patients with surgically remediable epilepsies who consecutively underwent EEG-fMRI for mapping of their inter-ictal epileptiform activity (IED) from January 2013 to December 2017, we selected all the adult patients ($\geq$ 18 years old) who presented IED-related fMRI maps with multiple clusters, including at least one (either activation or deactivation) co-localized with the presumed EZ based on the result of the not-invasive pre-surgical workup.

The patients were collected from the two Epilepsy clinics that form the Epilepsy Surgery hub of the Emilia-Romagna Region (Italy): the Azienda Ospedaliera-Universitaria di Modena, in Modena, Italy and the IRCCS Istituto Scienze Neurologiche, AUSL Bologna, Italy. Both centers were in charge to perform the presurgical work-up. The EEG-fMRI studies were acquired and analyzed in Modena. This study was approved by the local Ethical Committee of Area Vasta Emilia Nord (N. 155/14) and written informed consent was obtained from all participants.

10.2.2. MRI and EEG-fMRI Acquisition, Processing and Analysis

The following structural MRI data were acquired using a 3 T MRI scanner (Philips Intera): a high-resolution 3D T1-weighted anatomical MR image (3D-T1) was acquired consisting of 170 sagittal slices (TR = 9.9 ms; TE = 4.6 ms; voxel size = 1 mm_3); a high-resolution 3D fluid-attenuated inversion recovery (FLAIR) (TR = 4.8 ms; TE = 3.1 ms; voxel size = 1.2 Å~ 1.2 Å~ 1.2 mm_3).

In addition, for patients who subsequently underwent resective surgery, postsurgical 3D-T1 MRI were acquired at 6 and 12 months after surgery. Scalp EEG was recorded by means of a 32-channel MRI compatible EEG recording system (Micromed, Italy) concurrently with fMRI. The fMRI data was acquired using a gradient-echo echo-planar imaging sequence (EPI) sequence from 30 axial contiguous slices (TR = 2.000 ms; voxel size: 3.75 Å~ 3.75 Å~ 4 mm) over one or two fMRI runs (240volumes/run, 8 min each run) with continuous simultaneous EEG recording. Patients were asked to remain still during the scanning with eyes closed and do not fall asleep.

After offline correction for the scanner gradient artifacts and filtering of the EEG signal, the EEG data were reviewed and preprocessed according to a previous published method (Avanzini et al. 2014). Two experienced electroencephalographers (AEV, LM) reviewed the EEG recordings independently to identify the IED. IED definition follows specific morphological and topographic criteria as recently updated by the International Federation

of Clinical Neurophysiology (Kane et al. 2017). Additionally, only IED similar to those recorded outside the scanner were marked, resulting in a set of IED event time markers, and durations for the interictal events that consist of runs of spike-wave discharges. In some
recordings, with more than one type of IED, each event was labelled according to its type. The similarity between the IED recorded inside and outside the scanner was verified visually and by analyzing the scalp topographic map. To this end, the marked spikes were averaged, and the voltage map estimated and compared to the interictal spike field observed during the clinical video-EEG monitoring. Indeed, among the established criteria to define IED, one of the best performing is represented by the inspection of the voltage topography (Kural et al. 2020).

The Matlab 15.1 and SPM12 (Wellcome Centre for Human Neuroimaging, UCL, London, UK) software were used for fMRI data analysis. Preprocessing steps consisted of: (a) slice timing correction to account of the interleaved acquisition; (b) motion correction; (c) co-registration of the 3D-T1 scan to the mean EPI fMRI; and (d) spatial smoothing with a 8-mm full-width-at-half-maximum Gaussian kernel. The six motion parameters derived from the fMRI preprocessing (translation and rotation in the X, Y, and Z direction, respectively) and a Volterra expansion of these (Friston et al. 1996) were used as covariates in the general linear model (GLM). The effects of interest consisted of the IED, each represented as either a stick function or variable-duration block, were convolved with the standard hemodynamic response function (HRF) and its temporal and dispersion derivatives (Lemieux et al. 2008; Hamandi et al. 2006; Salek-Haddadi et al. 2006). In recordings in which multiple IED types were identified, each type was included as a separate effect of interest in the GLM. The resulted fMRI maps (F-contrast) were estimated at conventional statistical threshold of $p < 0.05$ (family wise error (FWE)- corrected). In addition, in cases where conventional FEW corrected statistical threshold did not show any results, the data were further explored

with a less stringent statistical threshold of $p < 0.001$ (uncorrected for multiple comparisons).

In the latter case, we applied a small volume correction (5 mm sphere) and we considered any BOLD activation/deactivation with a cluster-level threshold at $p < 0.05$, FEW corrected. This multiple-levels statistical approach is in line with previous similar studies (Poldrack 2007; Chaudhary et al. 2012; Coan et al. 2016; Markoula et al. 2018; Rossi Sebastiano et al. 2020).

10.2.3. Identification of the Presumed EZ

The presumed EZ (pEZ) was defined based on the results of the presurgical work-up, which included: ictal clinical semiology, scalp EEG interictal spike field (i.e., the region thought to generate the IED), scalp EEG ictal activity, structural MRI scan, and interictal F-18 fluorodeoxyglucose FDG-PET when available. For each patient, the spike field was estimated at sub-lobar level by visual inspection. This information was discussed together with the other clinical and neuroradiological findings at a multidisciplinary team meeting resulting in a consensus EZ localization. The results of the EEG-fMRI analysis were not considered in the clinical evaluation or EZ localization process.

10.2.4. IED-Related BOLD Map Concordance with pEZ

In order to inspect the spatial relationship between the map of IED-related BOLD changes and the pEZ, as defined previously, we adopted the following pipeline for each patient:

1. The high-resolution anatomical 3D-T1 MRI scan underwent cortical and subcortical segmentation using a standardized image toolbox (Freesurfer, version 6.0), following standardized ENIGMA protocols for image quality check (Whelan et al. 2018). The resulting cortical and subcortical parcellation was used for anatomical labelling.
2. The FLAIR, mean EPI, PET datasets were linearly registered to the high-resolution 3D-T1 MRI using FMRIB Software Library (FSL)

(www.fmrib.ox.ac.uk/fsl/fslwiki/flirt)(six-parameter rigid-body transformation).

3. The F-map was then coregistered to the anatomical 3D-T1 MRI using the co-registration matrix derived from the registration of mean-EPI to the T1-weighted image.
4. The resulting co-registered EEG-fMRI, anatomical and PET data were visualized using the 3D Slicer software (Fedorov et al. 2012) or Freeview toolbox (https://surfer.nmr.mgh.harvard.edu/fswiki) and inspected for correct alignment and co-registration (AEV, FC).

The level of concordance/discordance between the BOLD map and the EZ was defined based on previous published criteria (Thornton et al. 2011; Chaudhary et al. 2012; Markoula
et al. 2018). Specifically, 'Concordant' (C) refers to maps in which all the clusters (either activation or deactivation) colocalized with the pEZ: within 2 cm of and in the same lobe as EZ; 'Concordant Plus' (C+) is applied to fMRI maps with some clusters of significant IED-related BOLD changes colocalized with the pEZ and other significant BOLD clusters were located within the same lobe or touching the edge of the same lobe as the pEZ; Discordant
Plus (D+) refers to the situation where some clusters of significant IED-related BOLD changes were localized within the pEZ, with other significant BOLD clusters in other lobes;
Discordant (D) where all clusters of IED-related BOLD changes were remote from the pEZ and Null (N) where there was no cluster of significant IED-related BOLD change.
For the purpose of the present study only EEG-fMRI maps labelled as C+ and D+ were further analyzed using the DCM approach. This will allow us to evaluate the results against the independently determined pEZ as part of this proof of concept study. The C, D and N maps were excluded from the DCM analysis: the C maps consisted of clusters co-localized with the pEZ

exclusively, while the D and N maps did not include any clusters co-localized with the pEZ.

10.2.5. Effective Connectivity Analysis and Interpretation

For each EEG-fMRI C+ and D+ map, DCM was used to compare competing models of the causal connectivity between the IED-related BOLD clusters. Specifically, we aimed to identify the 'source' of the recorded epileptic activity, modelled as a causal driver, in contrast to the nodes that are thought to be part of propagation pathways. DCM analyses were performed with the DCM10 module in SPM12, with models parameterized using the bilinear differential equation for fMRI in DCM (Kahan and Foltynie 2013; Friston et al. 2003). For each EEG-fMRI dataset, we devised a series of competing models clinically meaningful based on the available electro-clinical information (clinical, EEG, neuroimaging), as follows: First, a region-of-interest (ROI) (5 mm radius) was defined within the significant activation/deactivation clusters revealed by the SPM{F} contrast. The sign of the BOLD change for each cluster was determined by plotting the fitted response at the most significant voxel within the cluster. An examination of the IED-related BOLD maps was performed to identify the clusters that are candidate for EZ, and all deactivations in the Default Mode Network (DMN) were excluded as they usually do not represent realistic generator of IED. To define the DMN deactivations, the maps were first inspected visually then were labelled with BrainMap70 Atlas (Ray et al. 2013) using the ICN_Atlas tool (Koz.k et al. 2017). Second, for each selected ROI, the time series was extracted using the principal eigenvariate at the voxels surviving a threshold of $p < 0.01$ (uncorrected) or $p < 0.05$ (corrected), and adjusted using the {F} contrast of effects of interest.

Third, a family of dynamic causal models were devised consisting of all the ROIs, fully intrinsically connected (backward and forward; DCM matrix A), and with bilinear effects in the form of the modulation of connection strength

(matrix B in DCM) by the IED onsets/durations considered as the driving input (DCM matrix C) at one of the ROI's, taking each in turn. Thus, each model represents a different hypothesis concerning the driving input ('driver') that is hypothesized to perturb the neuronal activity and thereby, cause the observed IED-related BOLD changes. Fixed Effect (FFX) Bayesian Model Selection (BMS) was used to compare the models at the subject level. Each model's Free Energy, F, a lower bound of the model's logevidence, accounting for model complexity as well as data fit, was used to compare the likelihood of the different models to explain the data. Relative log-evidences, or differences in F, were converted into model posterior probabilities, p, indicating that the respective model has a probability p of being the best model/family explaining the data amongst all considered. Evidence was "strong" if $p > 0.95$ (which corresponds to a difference in F greater than 3), and "positive" if $0.75 < p < 0.95$, which stands for a difference of F between 1 and 3 (Penny et al. 2004). In the latter situation, DCM findings were classified as "inconclusive", as they did not end up with significant results (i.e., there is no single winning model).

For the cases with a conclusive DCM result, this was validated against the pEZ. DCM findings were labelled as "Concordant" if the driver identified by the connectivity approach corresponds to the pEZ as previously defined and "Discordant" otherwise.

10.2.6. Independent Validation of DCM Findings

For the patients who subsequently underwent SEEG or resective surgery a "two-step" independent validation process of the DCM findings was applied, as follows: in the first step, the winning DCM model was considered validated if the revealed source includes the contacts recording from the SOZ as revealed by visual SEEG inspection (Cardinale et al. 2019) or was comprised in the surgical resection area, and invalidated otherwise. For this purpose, the fMRI maps were visualized in relation to the SEEG electrodes position or the

resection area, by co-registering the post-implantation images [(computed tomography [CT]) (for subjects who underwent SEEG) and the postsurgical 3D-T1 MRI] and the pre-implantation anatomical 3D-T1 MRI by means of a rigid-body transformation using FSL (https://fsl.fmrib.ox.ac.uk/fsl/fslwiki/FLIRT). The positions of the SEEG recording contacts were automatically estimated using SEEGA (Narizzano et al. 2017). In the second step, the DCM result from each surgical patient was classified as confirmed or unconfirmed in consideration of the post-surgical outcome, based on the principle that a bad outcome reflects inadequate characterization of the SOZ, thus undermining the confirmation of any localization result. Outcome was defined as good for Engel's classes I–II and poor for classes III–IV at 1 year (Engel 1993).

Therefore, the possible outcomes of the two-step validation of DCM result for each patient are fourfold: (a) "SEEG/surgery-validated and confirmed" if the DCM findings was concordant with SEEG/surgery and surgical outcome was good; (b) "SEEG/surgery-validated but unconfirmed" if the DCM result was concordant with SEEG/surgery but surgical outcome was poor; (c) "SEEG/surgery-invalidated but unconfirmed" if the DCM result was discordant with SEEG/surgery and surgical outcome was poor; (d) "SEEG/surgeryinvalidated and confirmed" if the DCM result was discordant with SEEG/surgery but the surgical outcome was good.

10.3. RESULTS

10.3.1. Electro-Clinical and EEG-fMRI Characteristics

10 out of 35 patients (28%) [5 male, mean age 29.1 (SD: Å} 9.2), mean epilepsy duration 13.9 years (SD Å} 8.6)], with multiple clusters of IED-related BOLD changes as described above underwent the DCM effective connectivity analysis. See the **Figure 10.5 (supplementary)** for a schematic representation of the EEG-fMRI findings of the entire population.

Five out of 10 patients were affected by Temporal Lobe Epilepsy (TLE), 3 by Parietal Lobe Epilepsy (PLE) and 2 patients by Frontal Lobe Epilepsy (FLE). Only one patient had a normal structural MRI scan; 9 patients had a structural lesion on the MRI scan [Focal Cortical Dysplasia (FCD) in 5, perysilvian polymicrogyria in 1, Dysembryoplastic Neuroepithelial Tumors (DNET) in 1, arteriovenous malformation (AVM) in 1 and dermoid cyst in the remaining]. 6/10 patients underwent surgery with a mean follow-up of 32.8 Å} 20.7 months (range 12–72), two of which (Patients #2,3) underwent SEEG prior to surgery. Surgical outcome was classified as Engel Class I in 3 patients (Patients #2, 3, 4), II in one (Patient #8), III in the remaining two cases (Patients #7, 10). Detailed electroclinical information is provided in **Table 10.1**.

5/10 IED-related BOLD maps consisted of 2 clusters, 3/10 had three clusters and the remainder had 4 clusters (**Table 10.2**). The cluster containing the global statistical maximum matched the pEZ in 3/10 cases while for the other patients, smaller secondary clusters matched the pEZ. Four patients were labelled as C+, two of them were affected by FLE (Patients #1, 6) and two by TLE (Patients #4, 9); patient #4 underwent surgery. The remaining 6 cases were labelled ad D+: 3 had TLE (Patients #2, 5, 10) and 3 PLE (Patients #3, 7, 8), and five underwent surgery (Patients #2, 3, 7, 8, 10).

***Table 10.1**: Clinical details of patients studied with DCM based on fMRI*

Pt ID	Ictal Semiology	Interictal EEG (maximum spike distribution)	Ictal EEG (region of seizures onset)	sMRI	FDG-PET	AED/ daily dose(mg)	icEEG	Epilepsy Surgery	Pathology*	Outcome**/follow up (mo) post-surgery
1	Subjective internal tremor, loss of contact, left hand automatic gestural activity; hypermotor activity in sleep	F3; C3	F3	L Medial Frontal FCD	–	DPA/1000 LEV/1000	–	–	–	–
2	(a) Change of facial expression, staring paled, gestural bilateral purposefulness automatisms. Brief confusion afterwards; (b) sudden loss of consciousness, fall and GTC evolution	T4; T6	T6, P4	Negative	R TO and TP hypo	LEV/1500 OXC/1200	R TP and T insular, T1 and T2, TO junction implantation focus temporo-basal and temporal-occipital	R TO corticectomy plus ATL	gliosis	IA/29
3	Left arm ascending paraesthesia followed by left side mouth deviation and ideomotor slowdown	F8; T4; T6; diffuse over the right leads	Diffuse with right prevalence	R parietal perisylvian polymicrogyria	No hypo	LCS/400 LTG/150 PER/8	R P implantation revealed a focus P operculum, supramarginal gyrus, inferior parietal lobuli	R P opercolum, R supramarginal corticectomy	gliosis	IA/16

Pt ID	Ictal Semiology	Interictal EEG (maximum spike distribution)	Ictal EEG (region of seizures onset)	sMRI	FDG-PET	AED/ daily dose(mg)	icEEG	Epilepsy Surgery	Pathology*	Outcome**/follow up (mo) post-surgery
4	Subjective descending-ascending shiver sensation from the head to the stomach, loss of contact, smiling and oral automatisms. Postictal aphasia	F7; T3	–	L mesial temporal FCD	–	PB/75 PRB/225	–	L ATL	FCD IIa	IA/72
5	Subjective vertigo, visual field restriction and oscillation; rare loss of consciousness	F8; T4 T4; T6	T6, O2	R temporo-occipital cortex FCD; R parahippocampal gyrus FCD	–	CBZ/600 CLB/10	–	–	–	–
6	(a)Sleep events: scream, face redness, bilateral clonic arms movements, vocalization; (b)awake, brief epigastric subjective sensation followed by transitory loss of contact	F7; T3	F3, T3	L insular dermoid cyst	–	PRP/6 LTG/200 PB/100	–	–	–	–

Pt ID	Ictal Semiology	Interictal EEG (maximum spike distribution)	Ictal EEG (region of seizures onset)	sMRI	FDG-PET	AED/ daily dose(mg)	icEEG	Epilepsy Surgery	Pathology*	Outcome**/follow up (mo) post-surgery
7	Right foot paresthesia, tremor with spread to the homolateral shoulder followed by stiffening of the right leg and fall to the floor	Cz; C3; P3	Cz, C3, P3	L Superior Parietal FCD	–	OXC/1500 CLB/10	–	Lesionectomy	FCD IIb	III/24
8	Right visual elementary hallucinations, cephalalgia, right superior arm stiffness, stereotyped vocalizations and dizziness	P3; Pz; T5; diffuse	P3, Pz	L precuneus FCD	L precuneus hypo	LCS/400 PRP/6 LEV200	–	Lesionectomy	FCD I	IIA/24
9	Subjective muffled sound sensation, staring and oral automatisms, ideomotor slowdown	F7; T3	T3	L parahaippocampal DNET	–	CBZ/800	–	–		–

Pt ID	Ictal Semiology	Interictal EEG (maximum spike distribution)	Ictal EEG (region of seizures onset)	sMRI	FDG-PET	AED/ daily dose(mg)	icEEG	Epilepsy Surgery	Pathology*	Outcome**/follow up (mo) post-surgery
10	Subjective ascending warmth sensation and visual attraction towards surrounding stimuli, foul language, fixed gaze, facial flushing with loss of contact and brief postictal confusion	C4; P4	T4, T6, O2	R temporo-occipital AVM	–	CBZ/800	–	Lesionectomy	AVM	III/36

L left, *R* right, *mo* months, *FCD* focal cortical dysplasia, *Hypo* hypometabolism, *CBZ* carbamazepine, *LCS* lacosamide, *PRP* perampanel, *LEV* levetiracetam, *OXC* oxcarbazepine, *CLB* clobazam, *LTG* lamotrigine, *VPA* valproic acid, *PB* phenobarbital, *PRB* pregabalin, *TO* temporo-occipital, *TP* temporo-parietal, *P* parietal, *T* temporal, *ATL* anterior temporal lobectomy, *GCT* generalized tonic–clonic evolution, *AVM* arteriovenous malformation, *FCD* focal cortical dysplasia, *DNET* dysembryoplastic neuroepithelial tumors, *sMRI* structural MRI, *FDG-PET* fluorodeoxyglucose PET

(*) Pathology was defined according to Blumcke et al. 2017; (**) Outcome was defined according to the Engel Epilepsy Surgery Outcome Scale

***Table 10.2**: EEG-fMRI and DCM results.*

Pt ID	IED location/ number (type)	Presumed EZ/ EEG-fMRI concordance	Cluster 1		Cluster 2		Cluster 3		Cluster 4		DCM results	Independent Validation
			Localization	Z score	Localization	Z score	Localization	Z score	Localization	Z score		
1	F3, C3/106 (S) F3, C3/28(SW)	L Medial Frontal FCD/C+	L Superior Frontal gyrus*	7.45	L Caudal middle Frontal gyrus	6.75	–	–	–	–	Concordant	–
2	T6/98 (SW)	R temporal lateral and basal cortex (T2, TO junction)/D+	R Middle Temporal gyrus	6.67	R Middle Frontal gyrus	5.55	R Posterior Cingulate gyrus	5.60	R Superior Temporal sulcus	5.45	Concordant	Valid (SEEG & surgery) Confirmed
3	Right fronto-temporal/14 (SW)	Right polymicrogyria (post-central and parietal opercolum)/ D+	L Postcentral gyrus*	5.96	R Postcentral gyrus	5.94	R Enthorinal cortex	5.15	–	–	Concordant	Valid (SEEG & surgery) Confirmed
4**	F7, T3/19 (S)	L mesial temporal FCD/C+	L Anterior Insular cortex*	3.32	L Temporal pole	3.16	–	–	–	–	Concordant	Valid (surgery) Confirmed
5	T4, T6/33 (SW)	R temporo-occipital cortex FCD/D+	R Inferior Parietal Cortex*	5.36	R Fusiform gyrus	4.91	–	–	–	–	Concordant	–
6	F7, T3/204 (S)	L frontal opercolum/C+	L Pars triangularis*	7.39	L Anterior cingulate	6.05	–	–	–	–	Concordant	–
7	F3, C3/918 (S)	L Superior Parietal FCD/D+	L Postcentral gyrus*	4.93	L Paracentral gyrus	3.55	R Postcentral gyrus	3.68	–	–	Discordant	Invalid, (surgery) Unconfirmed
8	T3, PZ C3, P3/43 (SW)	L precuneus FCD/D+	R Superior Parietal cortex*	4.19	L Precuneus	3.26	–	–	–	–	Concordant	Valid (surgery) Confirmed
9**	F7, T3/28 (S)	L parahaippocampal DNET/C+	L Parahippocampal gyrus*	3.60	L Superior Temporal gyrus	3.34	–	–	–		Not Conclusive	–
10	C4, P4/17 (S)	R temporo-occipital MAV/D+	R Superior Temporal gyrus*	5.75	R Middle Temporal gyrus	4.59	R Cuneus	5.16	R Frontal Opercolum	5.41	Discordant	Invalid (surgery) Unconfirmed

L left, *R* right, *SW* spike-wave, *S* spikes

(*) Global maxima; (**): $p < 0.01$ uncorrected; small volume correction $p < 0.05$ FWE corrected

10.3.2. Effective Connectivity Driver Identification

In relation to the pEZ, the effective connectivity driver identified using DCM model comparison was Concordant in 7 patients (70%; Patients #1,2,3,4,5,6,8), Discordant in two cases (20%; Patients #7,10) and Inconclusive in one (10%; Patient #9) (**Table 10.2**). Among the concordant results, 2 patients were affected by FLE due to structural lesions, 3 patients by TLE (2 cases due to FCD, one subject with cryptogenic epilepsy) and 2 by PLE due to polymicrogyria and FCD respectively. The two discordant findings were both cases with focal symptomatic epilepsy: one patient with parietal FCD and one patient with temporal vascular malformation. The inconclusive result concerns a patient with a temporal mesial DNET (**Figure 10.1**). Independent validation of DCM findings was obtained in 6 patients (60%) by surgery and in two of them by surgery and SEEG (Patients #2,3). In 4 out of 6 patients (66%), DCM findings were surgery- validated (Patients #2,3,4,8), surgery-invalidated in two (33%) (Patients #7, 10). Considering the post-surgical outcome, all the validated DCM findings were confirmed (good outcome), while the two invalidated results were classified unconfirmed as the clinical outcome after surgery was poor (Engel Class III) (**Table 10.2**). **Figure 10.2** describes a representative case of concordant, SEEG/surgery-validated and confirmed DCM result, **Figure 10.3** a patient with discordant, surgery-invalidated and unconfirmed DCM result and **Figure 10.4** refers to the patient with an Inconclusive DCM result. For all the other patients, see **Figures Figure 10.6** Figure 10.7 **(supplementary)**, **Figure 10.8 (supplementary)**Figure **10.9 (supplementary)**, **Figure 10.10 (supplementary)**, **Figure 10.11 (supplementary)** and **Figure 10.12 (supplementary)**. See **Table 10.3 (supplementary)** for the details of the DCM model comparisons.

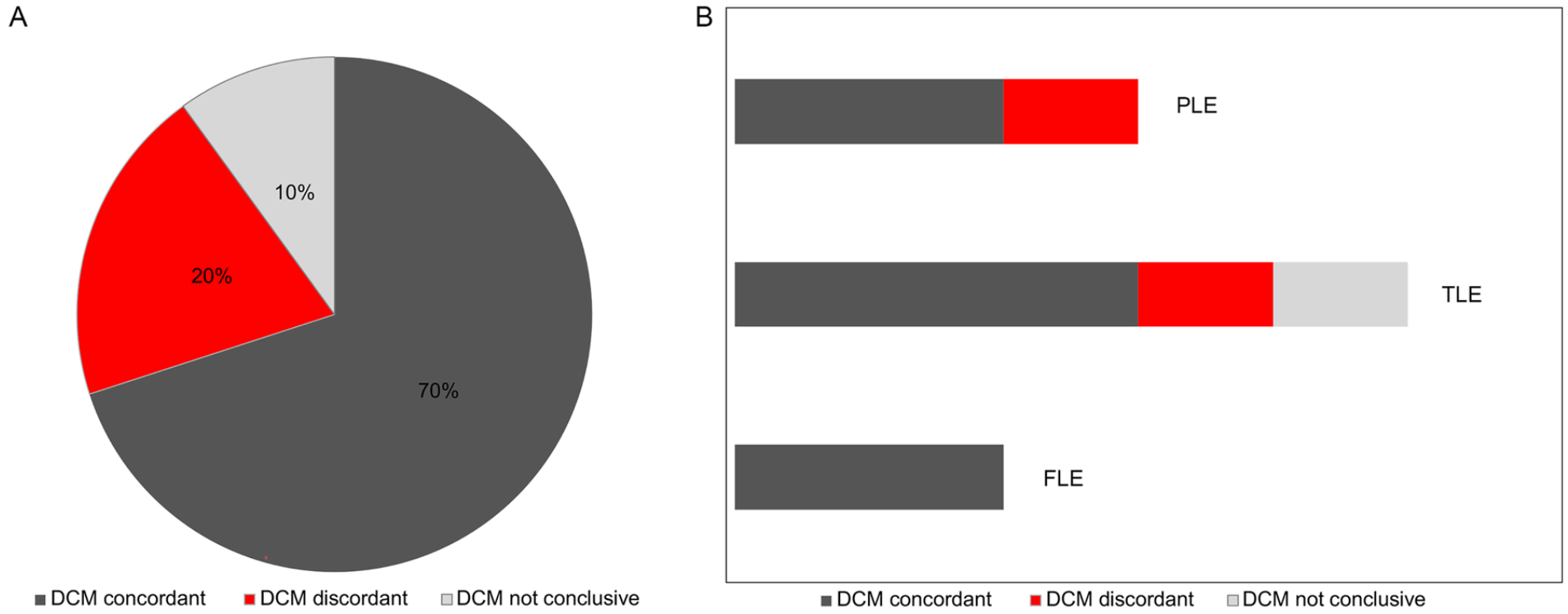

***Figure 10.1**: DCM findings.*
*(**A**) DCM findings in relation to the pEZ; (**B**) DCM findings in relation to pEZ across the different epileptic syndromes. FLE frontal lobe epilepsy; TLE temporal lobe epilepsy; PLE parietal lobe epilepsy. See text for details.*

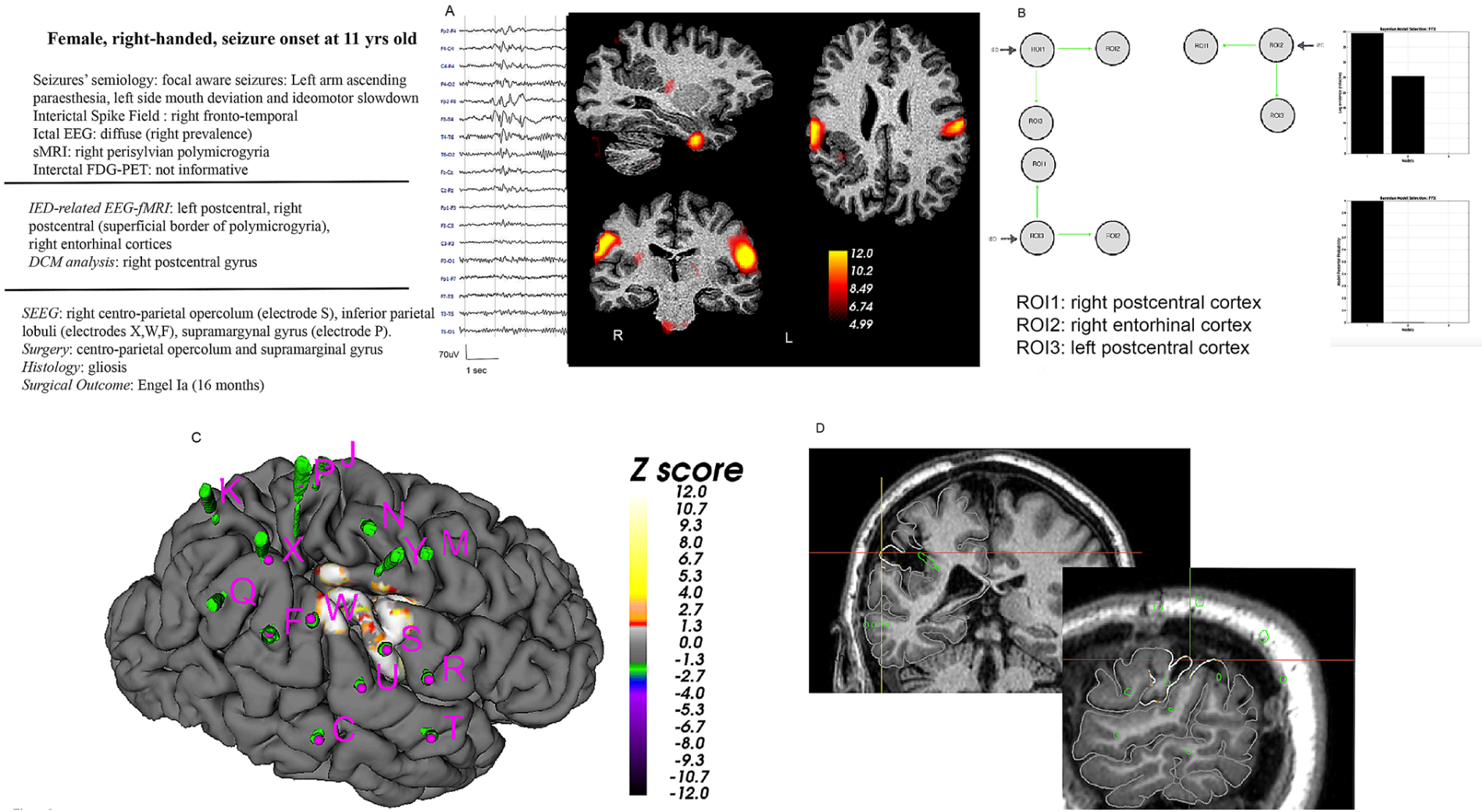

***Figure 10.2**: Example of "concordant, SEEG/surgery-validated and confirmed" DCM result.*
*Patient #3. (**A**) Left: Representative segment of scalp EEG showing IED over the right frontal and frontal–temporal leads. EEG is displayed in bipolar montage. Right: IED-related fMRI results overlaid onto high-resolution 3D T1 image (axial, coronal, sagittal slices). Three clusters of IED-related BOLD*

*signal increase (p < 0.05, FWE) in the left postcentral (global maxima), right postcentral and right entorhinal cortices. (**B**) Left: DCM model architecture: three ROIs are forward and backward connected (intrinsic connections are not shown for illustrative purposes). IED were considered as autonomous input to each of the three regions, one at a time (grey arrow). The bilinear terms are represented as solid green arrows. Right: DCM Bayesian model selection results: relative Log-evidence and Posterior Probability for the three models compared using FFX BMS show the winning model as Model 1 [p(m|Y) = 0,99]. The log-evidence difference between the three models was significant, showing a driver in the right postcentral cortex. (**C**)SEEG electrode positions and EEG-fMRI findings overlaid onto the presurgical reconstructed right hemisphere pial surface. The most active electrodes were located in the centro-parietal operculum (electrode S), supramarginal gyrus and inferior parietal lobuli (electrodes X, W, F) and anterior part of the inferior parietal lobuli (electrode P). (**D**)Post-surgical 3D-T1 MRI coronal and sagittal slices with EEG-fMRI findings and intracranial electrodes overlaid. Note that the fMRI cluster is included in the resection area. R right; L left. Rh right hemisphere; sMRI structural MRI.*

Female, right-handed, seizure onset at 5 yrs old

Seizures' semiology: focal aware seizures: paresthesia involving the right foot and homolateral shoulder, stiffening of the right leg and fall to the floor
Interictal Spike Field : left fronto-central-parietal
Ictal EEG: left fronto-central-parietal
sMRI: left superior-parietal FCD
Interctal FDG-PET: not available

IED-related EEG-fMRI: left postcentral, left paracentral gyrus, right postcentral gyrus
DCM analysis: left paracentral gyrus

Surgery: lesionectomy (left postcentral gyrus)
Histology: FCD IIb.
Surgical Outcome: Engel III (24 months)

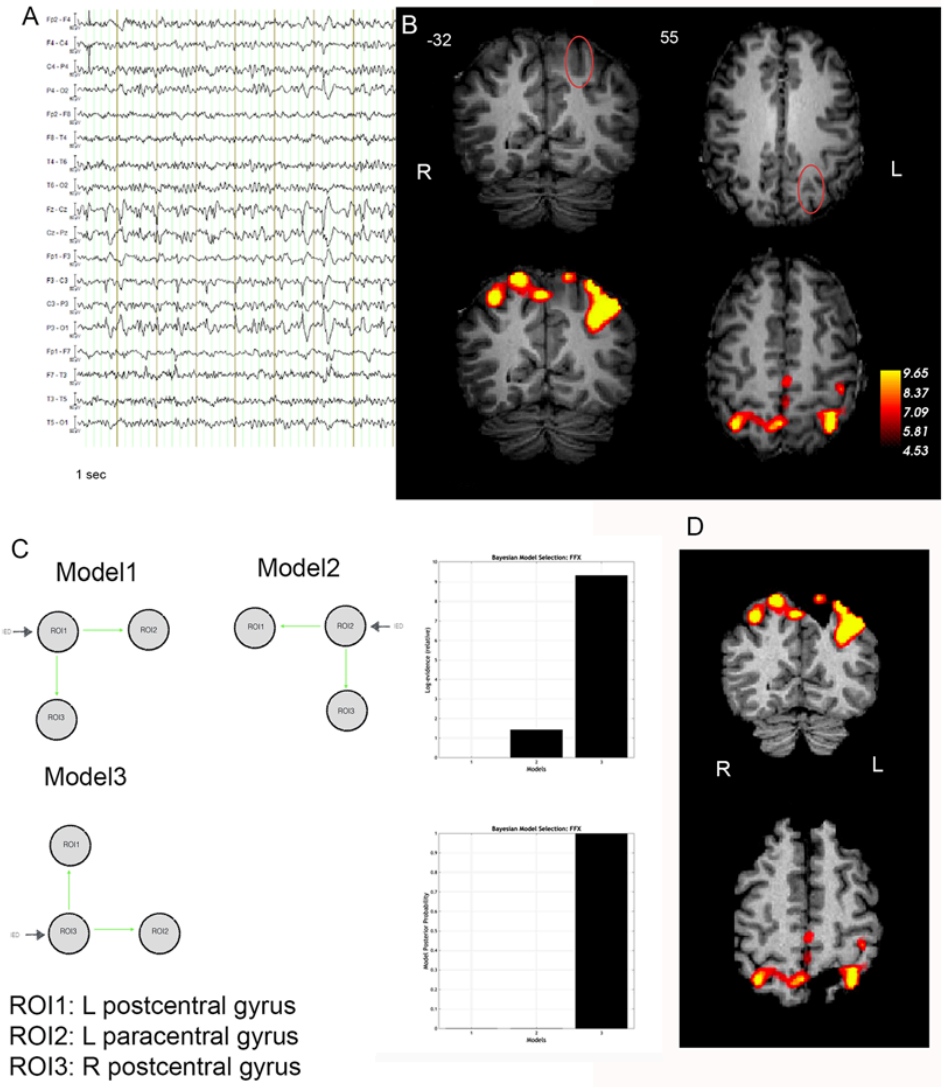

ROI1: L postcentral gyrus
ROI2: L paracentral gyrus
ROI3: R postcentral gyrus

***Figure 10.3**: Example of "discordant, surgery-invalidated but unconfirmed" DCM result.*
Patient #7. A Representative segment of scalp EEG showing IED over the left frontal-central and central-parietal regions. EEG is displayed in bipolar montage. B Top: structural MRI scan (3D-T1) shows thickening and blurring of the grey-white matter junction over the left superior parietal gyrus (red circles) suggestive of FCD. Bottom: IED-related fMRI results overlaid onto the high-resolution pre-surgical 3D-T1 image (axial and coronal slices) revealed ($p < 0.05$, small volume correction and family-wise error corrected) three main clusters of BOLD signal increase: the left post-central gyrus (global maxima), the left paracentral gyrus and the right post-central gyrus. C Left: DCM model architecture. Three ROIs are forward and backward connected (intrinsic connections are not shown for illustrative purposes). IED were considered as autonomous input to each of the three regions, one at a time (grey arrow). The bilinear terms are represented as solid green arrows. Right: DCM Bayesian model selection results: relative log-evidence and posterior probability for the three models compared using FFX BMS show the winning model as Model 3 [$p(m|Y) = 0,99$]. The log-evidence difference between these three models was significant. D Presurgical IED-related fMRI findings overlaid onto post-surgical high-resolution 3D T1scan. R right; L left. FCD focal cortical dysplasia; sMRI structural MRI.

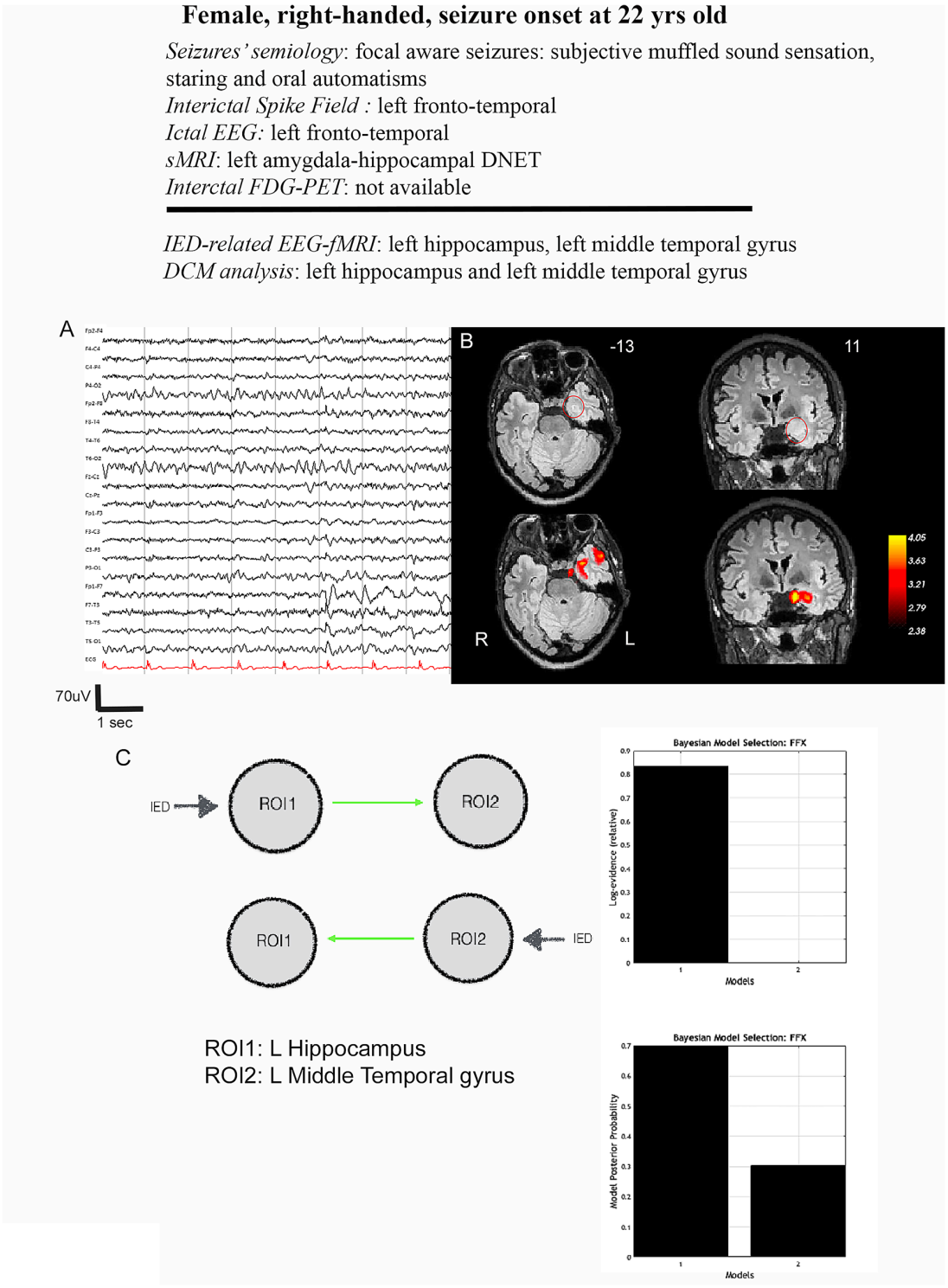

***Figure 10.4**: Example of "inconclusive" DCM result.*
*Patient #9. (**A**) Representative segment of EEG showing IED over the left frontal–temporal regions. EEG is displayed in bipolar montage. (**B**) Top: structural MRI scan (3D-T1) shows a localized left amygdala-hippocampal lesion suggestive of DNET (red circles). Bottom: IED-related fMRI results overlaid onto high-resolution presurgical 3D-T1 image (axial and coronal slices) revealed two clusters of signal increases ($p < 0.05$, small volume correction and family-wise error corrected) in the*

*left hippocampus extending to the amygdala (global maxima) and the homolateral middle temporal gyrus. (**C**) Left: DCM models' architecture: two ROIs are structurally (forward and backward) connected (intrinsic connections are not shown in the models for illustrative purposes). IED were considered as autonomous input to each of the two regions, one at a time (grey arrow). The bilinear terms are represented as solid green arrows. Right: DCM Bayesian model selection results: relative log-evidence and posterior probability for the two models compared using FFX BMS found Model 1 to be more likely [p(m|Y) = 0,70] but below the significance threshold. R right; L left; sMRI structural MRI.*

10.4. DISCUSSION

This "proof of concept" work represents the first attempt to investigate the possibility of identifying putative drivers of human focal epileptic activity using DCM on fMRI data. In order to assess the method's potential, we focused specifically on patients with surgically remediable epilepsy whose IED-related EEG-fMRI maps show widespread/multiple activations with at least one concordant with pEZ in order to elucidate the generators of interictal epileptiform discharges within the network. By comparing small sets of models of effective connectivity derived from the BOLD maps we found that the method has the capability to identify unique drivers located within the presumed epileptogenic zone in a large proportion of cases. DCM applied to fMRI data has been used successfully to investigate the effective connectivity within the epileptic networks in patients affected by generalized epilepsies (Vaudano et al. 2009; Klamer et al. 2018) and reflex epilepsies (Vaudano et al. 2012) at the group and single-subject levels. In these contexts, DCM was used to infer the causal relationship between various BOLD clusters, adding significant knowledge on the pathophysiological circuitries behind these "system epilepsy" conditions (Avanzini et al. 2012).

In potentially surgically remediable focal epilepsy, where the main clinical question is that of identifying the focus or origin of epileptic activity, the application of this methodology is even more appealing for diagnostic purposes, due to the lack of success of the EEG-fMRI approach to reveal the

EZ in a large proportion of patients (Kowalczyk et al. 2020a, b; Yamazoe et al. 2019). Nevertheless, up to date, knowledge on the technique's clinical relevance is limited due to the small number of cases studied (Hamandi et al. 2008; Murta et al. 2012; Vaudano et al. 2013; Klamer et al. 2015). To attempt to address this, we used DCM on IEDrelated fMRI maps in 10 consecutive focal epilepsy patients to investigate whether it can contribute to the localization of the EZ. Overall, our findings support the contention that DCM applied to interictal fMRI maps might contribute to identify the EZ in patients with multiple IED-related hemodynamic clusters, thus adding value to EEG-fMRI as part of epilepsy presurgical protocols.

10.4.1. Widespread IED-Related BOLD Maps in Focal Epilepsies

Previous studies have shown that fMRI mapping of IED on scalp EEG are of localizing value and predictive value for post-surgical outcome (An et al. 2013; Kowalczyk et al. 2020a, b; Markoula et al. 2018), with a concordance with the presumed EZ in up to 88% of patients (Pittau et al. 2012). However, in most studies the pool of patients with "concordance" between IED-related BOLD responses and the EZ included cases with concordant plus/discordant plus maps: i.e., with multiple clusters, including at least one co-localized with the EZ. In this work, out of a pool of 35 patients, nearly one/third (10/35, 28%) demonstrated multiple widespread IED-related BOLD clusters involving either the same hemisphere of EZ (C+, 40%) or the contralateral (D+, 60%), in line with previous reports (Thornton et al. 2011; Markoula et al. 2018). The common observation of multiple or widespread IED-related EEG-fMRI maps support the notion that this tool is perfectly suited to image the epileptic network. It has been shown that IED-related EEG-fMRI is able to identify clusters of signal increase concordant with the spike onset zone [i.e., a region where a spike is initiated, (Khoo et al. 2018)] and the regions where the spike propagate (Watanabe et al. 2017) which might be remote from the IED generator. This good performance of EEG-fMRI has been demonstrated even in cases of deep

IED sources such as in patients with mesial TLE (Yamazoe et al. 2019) and in patients with cortical malformations (Pittau et al. 2017; Thornton et al. 2011), where multiple areas of epileptogenicity can be observed. In the contest of epilepsy surgery, where the identification of the epileptic focus is required, however, these complex maps need deeper understanding to highlight the clinical relevance of each node within the revealed network and specifically to identify the generator/s of IED as often corresponding to the EZ. It has been observed that the IED-related BOLD cluster containing the voxel with highest statistical score, named “primary cluster” or “global maxima”, often has the highest localizing value with respect to the SOZ as delineated by intracranial EEG (Khoo et al. 2017). Additionally, in cases of widespread IED recorded intracranially, it has been shown that the IED recorded close to the maximum hemodynamic response are more likely to precede those recorded remotely, and that the IED delay in a particular channel is correlated with the distance between its location and the maximum hemodynamic response (Khoo et al. 2018). In our cohort, the global statistical maximum was concordant with the presumed EZ in only 3 out of 10 patients Patients #6,7 and 9). The discrepancy between our findings and previous evidences could be due partly to methodological differences. Herein, we adopted an {F} contrast to evaluate fMRI maps as best fits data in our model with canonical HRF and derivatives whereas others estimated the global maximum based on the maximum t values (Khoo et al. 2017). Furthermore, the findings in some of the patients studied here might reflect complex epileptic circuits as observed in patients with multifocal epilepsy or unknown epileptic focus (Thornton et al. 2011; Gonz.lez Ot.rula et al. 2018). Indeed, in such circumstances, it was shown that secondary clusters rather than the primary one might be consistent with the highest high-frequency-oscillation (HFO) rates recorded by SEEG (Gonz.lez Ot.rula et al. 2018). In our population however, even in highly focal cases (Patients#1, 4 and 8) in whom the totality of not-invasive investigations points toward a clear focus, the global maximum was discordant. Although we are aware that some of these patients are waiting for surgery and the

sample is small to draw conclusions, our findings suggest the importance of consider even so-called 'secondary' BOLD clusters as they might of help in identifying the epileptogenic regions in focal epilepsies.

10.4.2. Dynamic Causal Modelling

We hypothesized that DCM applied to IED-related BOLD maps can be a useful approach to infer the effective connectivity between the nodes of the epileptic networks. This is potentially highly relevant in the contest of epilepsy surgery when the IED-related BOLD maps show multiple clusters of hemodynamic changes and given the inconclusive sensitivity of the global maximum to reveal the epileptogenic focus. Generally speaking, the effective connectivity corresponds to the directed ("causal") influence that one region exerts on the activity in another, in other words: it can be used to test which brain region drives which (Kahan and Foltynie 2013). Compared to previous classical models of effective connectivity for fMRI data (like psycho-physiological interactions (PPI), or structural equation modelling (SEM)), DCM combines a neurobiologically plausible model of neural dynamics with biophysically plausible hemodynamic model that describes the transformation of neuronal activity into a BOLD response (Stephan and Friston 2010). Both sets of parameters describing the neuronal and the forward model of BOLD signal generation are estimated from each brain region included in the model using a Bayesian framework (Penny et al. 2004). This approach aims to refine the model parameters in order to produce a predicted signal that is close as possible to the observed BOLD data (Stephan and Friston 2010). In the neuronal model in DCM for fMRI data, like the approach used here, propagation delays are not modelled because fMRI data does not contain enough temporal information due to considerable inter-regional variability in hemodynamic response latencies (Kahan and Foltynie 2013). Instead, the differential latencies of the hemodynamic response are accommodated by region-specific biophysical parameters in the hemodynamic model.

Nevertheless, causality in DCM does not only rely on temporal precedence but takes into account when and where the system is perturbed by external or endogenous brain influences and the structural connectivity within the system (Friston et al. 2003; Stephan and Friston 2010). Herein, we presumed the interictal EEG activity as an extrinsic input which perturbs the investigated network. The time of IED onset is thus conceived to be the initial cause of the modelled effects as it can influence directly the neuronal states of the specified anatomical nodes. This assumption might be of concern due to such an endogenous type of activity. In addition, the IED onset as recorded from the scalp might be delayed with respect to the real interictal activity onset and represent only a fraction of what really happening inside the epileptic brain. In humans, previous applications of DCM to fMRI data in epilepsy (Hamandi et al. 2008; Klamer et al. 2015, 2018; Murta et al. 2012; Vaudano et al. 2009, 2012, 2013; Warren et al. 2019) adopted the same assumption and in some of them the DCM findings were validated against icEEG with a good agreement between the "driver" defined by the DCM and the EZ recorded by the invasive monitoring (Murta et al. 2012; Klamer et al. 2015). Additionally, there is good evidence of the validity of this approach in relation to intracerebral electrophysiology in rats (David et al. 2008). These data support the feasibility of this technique for the analysis of the temporal dynamics of the spreading of epileptic activity as recorded from the scalp.

Different concerns have been raised about DCM, particularly in relation to the model selection procedure and validation (Lohmann et al. 2012). Herein, for each patient, we built plausible models guided by the main clinical question, that is to reveal the driver of the pathological activity recorded by EEG during fMRI. Model selection was thus based on information derived from other non-invasive investigations and the clinical judgment on the localization of pEZ. In this way, we respect the premise that DCM should be used to test specific hypotheses rather that an exploratory approach (Friston et al. 2003). Accordingly, we excluded a priori any deactivated cluster within the DMN. This choice is motivated by the observation that DMN regions are not usually

considered as focus node for the IED generation. Previous EEG-fMRI studies in presurgical epilepsy population aiming to estimate the power of this method to localize the EZ have similarly excluded the DMN regions from the analysis, giving the uncertain meaning of deactivations outside the epileptic focus (An et al. 2013). Furthermore, the observations of a common pattern of IED-related co-deactivation of the DMN in patients with focal epilepsy, especially TLE, may reflect a non-specific and therefore non-localizing phenomenon (An et al. 2013; Laufs et al. 2007), albeit the causal link between IED and DMN involvement has not yet been extensively investigated. It was proposed that IED might spread from the epileptic focus to the one or more functionally interconnected regions of the DMN, perturbing its function. Activity changes in the DMN could thus be a consequence of the IED effect and have a role in decreasing the cognitive performances in TLE (Kobayashi et al. 2006a, b; Kobayashi et al. 2009; Laufs et al. 2007; McCormick et al. 2013; Cataldi et al. 2013; Coan et al. 2014).

Regarding validation of the DCM findings, for each case, we adopted a multi-level approach. Firstly, we based our assessment on the clinical judgment about the pEZ localization derived from the comprehensive presurgical workup. In clinical practice, particularly in patients with not-informative MRI scan, the clinical decision on the EZ localization is fundamental to guide the surgical plan and/ or the icEEG implantation. Thus, a comparison between the clinical and the DCM output might be of importance for evaluating the applicability of this approach for clinicians.

At this level, we found concordant findings with the DCM results in the majority of our patients (70%). Noteworthy, almost all the patients in our cohort had a structural lesion on the MRI scan which has strongly influenced and maybe simplified the clinical decision about the EZ localization. An interesting future study using DCM on fMRI would focus on a cohort of MRI negative cases in whom the EZ is for definition more complex to be localized (Rossi Sebastiano et al. 2020). Patient #2 of our cohort is a paradigmatic example (Fig. S3). In this MRI negative epilepsy case, the presurgical

investigations end up with discrepant findings: while the scalp EEG and ictal semiology point toward a temporal lateral onset, interictal FDG-PET was more consistent with a temporo-occipital focus. The EEG-fMRI demonstrated multiple areas of BOLD changes covering the temporal, frontal and parietal lobes. In this contest, the DCM approach identified correctly the epileptic nodes as subsequently validated by surgery and confirmed by the post-surgical outcome.

As a second step, the DCM findings were independently validated by comparison with the surgical data, particularly clinical outcome. Surgery was performed in 6/10 patients. The remaining 4 cases presented a clear brain lesion (2 FCD, one epidermoid cyst, one DNET) well known to be epileptogenic (Bernasconi et al. 2019; Wang et al. 2020) and in all of them, DCM revealed a driver concordant with the lesion observed in MRI. A previous EEG-fMRI study in focal epilepsy considered a focal lesion on MRI as a criterion for independent validation of fMRI findings (Pittau et al. 2012). Among the patients who underwent SEEG/surgery, a positive independent validation was obtained in the 66% (4/6) of the patients. Interestingly in two out of operated patients (Patients #7, 10) with invalid DCM results, the long-term surgery outcome (24 and 36 months respectively) was poor and the DCM findings indicated a driver outside the region of surgical resection. A possible simple explanation for this finding is that the EZ is located outside the area of resection but could correspond to the driver we identified.

10.4.3. Methodological Considerations

EEG-fMRI

We have employed a rigid and reliable approach to ensure that regional BOLD changes explained by motion are not considered as effects of interest, by incorporating these features into the GLM model.

This methodology replicates previous EEG-fMRI studies from ours (Mirandola et al. 2013; Vaudano et al. 2013; Meletti et al. 2015), and others groups in

patients with focal epilepsy (Thornton et al. 2010a, b; Thornton et al. 2011; Coan et al. 2016; Markoula et al. 2018). No dataset was discarded because of motion. The majority of our patients had structural MRI lesions, represented mostly by malformations of cortical development. Several evidences support the feasibility and reliability of the IED-related EEG-fMRI in case of FCD, with a high level of concordance between the BOLD response and the lesion (Archer et al. 2010; Tyvaert et al. 2008; Vaudano et al. 2013; Coan et al. 2016; Pittau et al. 2017) and the SOZ as revealed by icEEG (Thornton et al. 2011; Khoo et al. 2017, 2018). Similar performances were observed for patients with grey matter heterotopia (Kobayashi et al. 2006a, b; Tyvaert et al. 2008; Archer et al. 2010) and polymicrogyria (Kobayashi et al. 2005). As far as DCM on fMRI data, available published data in focal epilepsy have been performed mostly in patients with structural MRI lesion, like FCD (Vaudano et al. 2013), hypothalamic hamartoma (Murta et al. 2012) and hippocampal sclerosis (Hamandi et al. 2008). In all these cases, the DCM applied to fMRI maps demonstrated to be feasible and valid. The co-registration between EPI and anatomical images might be problematic due to the EPI signal dropout at the brain–cerebrospinal fluid–air interfaces; structural lesions could also be of concerns in relation to the coregistration process. In the present work, we addressed this issue by inspecting case by case the good performance of every co-registration step described previously, particularly the overlap between the mean EPI and the pre-operative/ post-operative 3D-T1 images. Additionally, in line with previous reports (Coan et al. 2016; Thornton et al. 2011), we allowed a distance up to 2 cm to account for displacement between the pEZ/SEEG/resections' margin and the BOLD clusters. This is motivated by the observation that although fMRI is a reliable technique, there can be a spatial difference as high as ten times its plane resolution, compared to electrophysiologically defined activity (Disbrow et al. 2000).

DCM Model Architectures

The DCM described findings are limited to the model space specified for each patient. In this regard, we opted for the minimal (from the viewpoint of competing driver hypotheses), set of models, and chose the simplest model architecture including linear and bilinear terms. The decision to include a modulator effect of IED on nodes connections (i.e., bilinear terms) is due to previous studies for our and other groups (Murta et al. 2012; Vaudano et al. 2013) in which different models (with and without modulatory effects) were compared and the bilinear models (i.e., IED act as modulator of the nodes connections) demonstrated an increased likelihood compared with the linear ones. As additional remark, we did not investigate in the models the directionality of connectivity between the nodes and we assumed that the selected ROIs are fully intrinsic connected. Measures of structural connectivity, as obtained by diffusion MRI and probabilistic tractography, have been recently used to inform the DCM structural connectivity parameters at group level with improving inference about the effective connectivity in term of models' evidence (Stephan et al. 2009; Sokolov et al. 2019). Probabilistic approaches have shown indeed that the higher the likelihood that a given connection exists anatomically, the larger the prior variance of the corresponding effective connectivity, making easier for the parameter to deviate from zero and therefore representing a stronger connection (Stephan et al. 2009). Interestingly and in support of this, previous data demonstrated a good correspondence between tractography analysis and the pathway of epileptic activity propagation as revealed by the DCM on IED-related fMRI (Hamandi et al. 2008). Up to know however, tractography information have not been used to inform the connectivity effective parameters in patients with epilepsy. Despite these preliminary evidence and proposed method (Sokolov et al. 2019), further studies are needed to implement the multimodal integration approach in the clinical setting and at individual level.

10.4.4. Limitations

Firstly, since not all the investigated patients underwent surgery and/or SEEG, the DCM findings lack validation and confirmation for these cases. Noteworthy, in the real-life scenario, when not available surgery or icEEG, the clinical judgment (based on not invasive information) is considered the gold standard for the EZ localization and it is widely used for validation of EEG-fMRI IED mapping results in terms of spatial concordance (Pittau et al. 2012; Yamazoe et al. 2019; Kowalczyk et al. 2020a, b). Secondly, the number of patients investigated with DCM is relatively small and further studies on larger groups of epilepsy patients with confirmed EZ (by SEEG/surgery and/or clinical outcome) are needed to validate our preliminary findings. Thirdly, patients are heterogenous regarding the epilepsy syndrome and related pathology, preventing to model the effective connectivity at group or subgroup level. Of note, the main aim of the present project was to test the usefulness of the DCM approach on fMRI data acquired in consecutive patients, candidate to surgery regardless the epilepsy or seizures type. In this scenario, fMRI and DCM analyses are essentially at single subject's level so the findings can be discussed in relation to the patient only. However, by collecting and analysed more fMRI datasets using a similar methodological approach would allow to speculate about the validity of the DCM in specific epilepsy clinical and aetiological subtypes.

Finally, further studies on a larger cohort of patients might address the specificity and sensibility of this approach, thus including also analyses on discordant maps.

10.4.5. Clinical Significance and Conclusion

The capability of EEG-fMRI to reveal the epileptogenic zone in focal epilepsies has already been documented. However, researchers and clinicians often deal with IED-related fMRI maps that consist of multiple and/or widespread

clusters in which the global maxima or primary cluster does not correspond to the epileptogenic zone. This is of concern specially

in patients with not-lesional MRI or inconclusive presurgical assessment. In this scenario, we propose that DCM might offer a useful approach helping to interpret these maps by inferring the causal role of its nodes. The present study is the first work that applies this approach to consecutive cases of surgically remediable epilepsies. Overall, our findings support the applicability of DCM on interictal fMRI data, therefore adding evidence on the clinical relevance of the EEG-fMRI as part of the epilepsy presurgical work-up.

Additionally, the present work underlines the potential usefulness of effective connectivity analyses to investigate the epileptic networks and to help identifying the EZ in complex

cases.

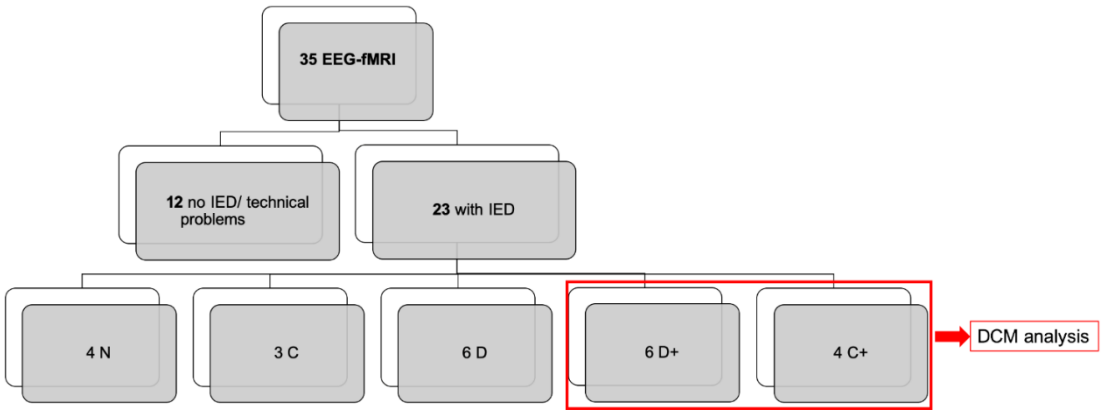

***Figure 10.5 (supplementary)**: Overview of the EEG-fMRI results.*
IED: Interictal Epileptiform Discharges; N: Null; C: Concordant; C+: Concordant Plus; D+: Discordant Plus; D: Discordant

Male, left handed, seizure onset at 22 yrs

Seizures' semiology: focal seizures with impaired awareness, left hand automatisms. Hypermotor sleep seizures
Interictal Spike Field : left fronto-central
Ictal EEG: left fronto-central
sMRI: left caudal middle frontal gyrus FCD
Interctal FDG-PET: not available

IED-related EEG-fMRI: left superior frontal gyrus, left middle frontal gyrus
DCM analysis: left middle frontal gyrus

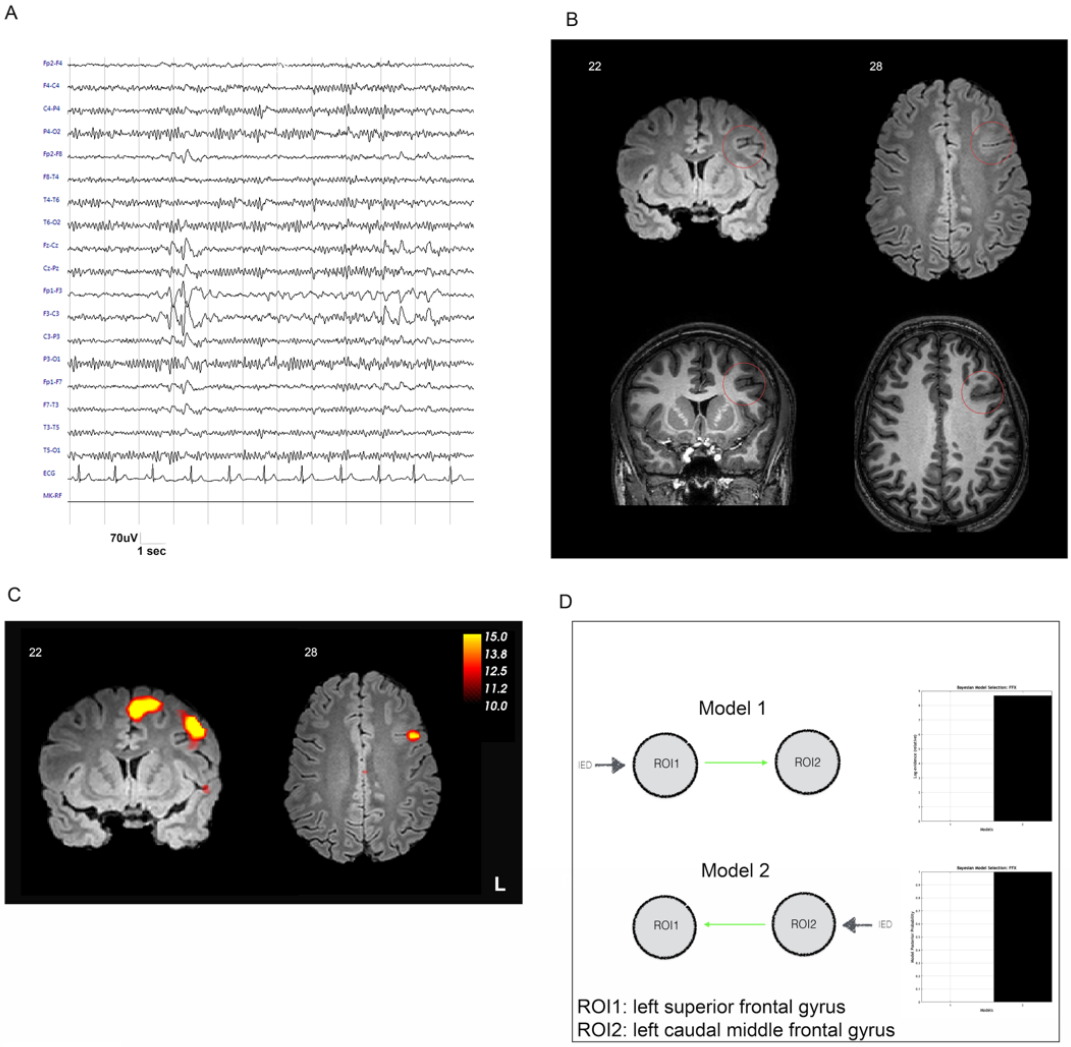

Figure 10.6 (supplementary): *Patient with "concordant" DCM result.*
*Patient #1. (**A**) Representative segment of scalp EEG showing IED over the left frontal-central regions. EEG is displayed in bipolar montage. (**B**) Structural MRI (top: high-resolution 3D FLAIR; bottom: high-resolution 3D-T1 MRI showing a deep left caudal middle frontal gyrus with blurring of the surrounding grey-white matter junction, suggestive for FCD (red circles). (**C**) IED-related fMRI results overlaid onto the high-resolution presurgical FLAIR image (axial and coronal slices) demonstrated*

*two significant (p < 0.05 FWE) clusters of signal increase: the left superior frontal gyrus (global maxima) and the homolateral middle frontal gyrus. (**D**) Left Image: DCM models' architecture: two ROIs are structurally (forward and backward) connected (intrinsic connections are not shown in the models for illustrative purposes). IED were considered as autonomous input to each of the two regions, one at a time (grey arrow). The bilinear terms are represented as solidgreen arrows. Right image: DCM Bayesian model selection results: relative log-evidence and posterior probability for the two models compared using FFX BMS show the winning model as Model 2 [p(m|Y) = 0,98]. The log-evidence difference between these two models was > 3 (hence significant). R: right; L: left; FCD: Focal Cortical Dysplasia; sMRI: Structural MRI.*

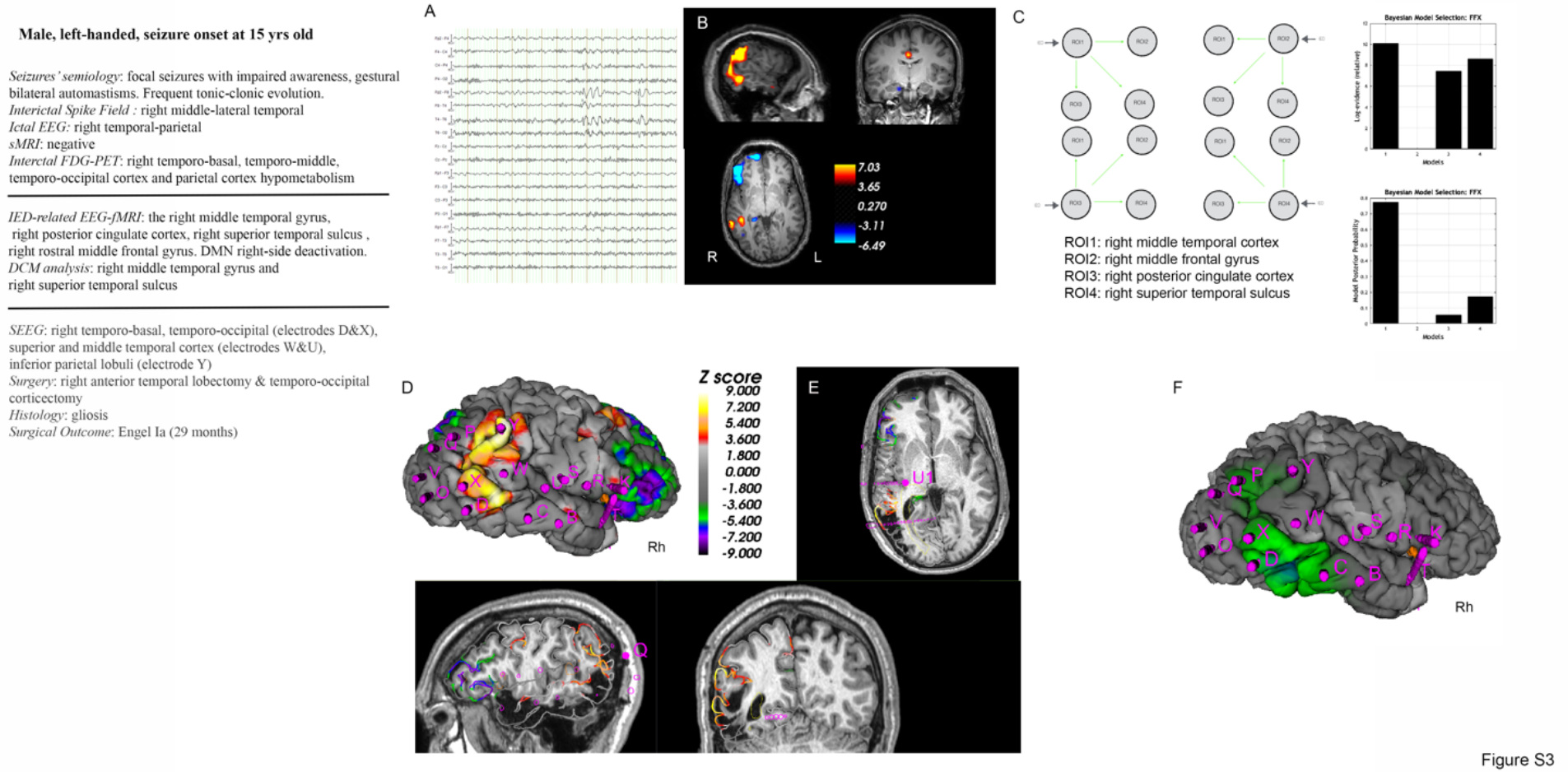

Figure 10.7 (supplementary): *Patient with "concordant, SEEG/surgery-validated and confirmed" DCM result.*
*Patient #2. (**A**) Representative segment of scalp EEG showing the marked IED over the right middle temporal regions ("s" refers to the marker of identify spikes after EEG preprocessing). EEG is displayed in bipolar montage. (**B**) IED-related fMRI results overlaid onto the high-resolution 3D-T1 (axial, coronal, sagittal slices) demonstrated a single large cluster of BOLD signal increases (p< 0.05, corrected for FWE) over the right middle*

*temporal gyrus extending toward the homolateral supramarginal gyrus and inferior parietal lobule plus smaller blobs over the right posterior cingulate cortex, right superior temporal sulcus and right rostral middle frontal gyrus. Decreases in BOLD signal changes were observed in the DMN lateralized on the right side. The cold blue color identifies BOLD signal decreases while the hot red-yellow color, BOLD signal increases. (**C**) Left: DCM models' architecture: four ROIs (derived from the activated BOLD clusters) are structurally (forward and backward) connected (intrinsic connections are not shown in the models for illustrative purposes). IED were considered as autonomous input to each of the four regions, one at a time (grey arrow). The bilinear terms are represented as solidgreen arrows. Right: DCM Bayesian model selection results: relative Log-evidence and Posterior Probability for the four models compared using FFX BMS show two winning models: Model 1 [p(m|Y) = 0,78] and Model 4 [p(m|Y) = 0,17]. The log-evidence difference between Models 1 and 4 was less than 3 (hence not significant), while the difference between Model1&4 and the Model 2&3 was > 3, hence significant. (**D**) SEEG electrodes position and EEG-fMRI findings overlaid onto the presurgical reconstructed right hemisphere pial surface. Most active electrodes explored the temporo-basal and temporo-occipital regions (D and X), superior and middle temporal cortex (W, U which corresponds to Wernicke area), and the more superficial part of the inferior parietal lobuli (Y). (**E**) Post-surgical MRI scan displayed onto 3D T1 coronal and sagittal and axial slices with overlaid the EEG-fMRI findings and intracranial electrodes. Note that the middle temporal fMRI cluster is included in the resection area. (**F**) Interictal FDG-PET overlaid onto right hemisphere pial surface together with SEEG electrodes position. The green color identifies hypometabolism. R: right; L: left; Rh: right hemisphere; sMRI: Structural MRI.*

Female, right-handed, seizure onset at 7 yrs old

Seizures' semiology: focal seizures: subjective descending-ascending shiver sensation, loss of contact, smiling and oral automatisms.
Interictal Spike Field : left anterior temporal
Ictal EEG: left anterior temporal
sMRI: left hippocampal and temporal pole FCD
Interctal FDG-PET: not available

IED-related EEG-fMRI: left temporal pole and left insular cortex
DCM analysis: left temporal pole

Surgery: left anterior temporal lobectomy
Histology: FCD type I
Surgical Outcome: Engel Ia (72 months)

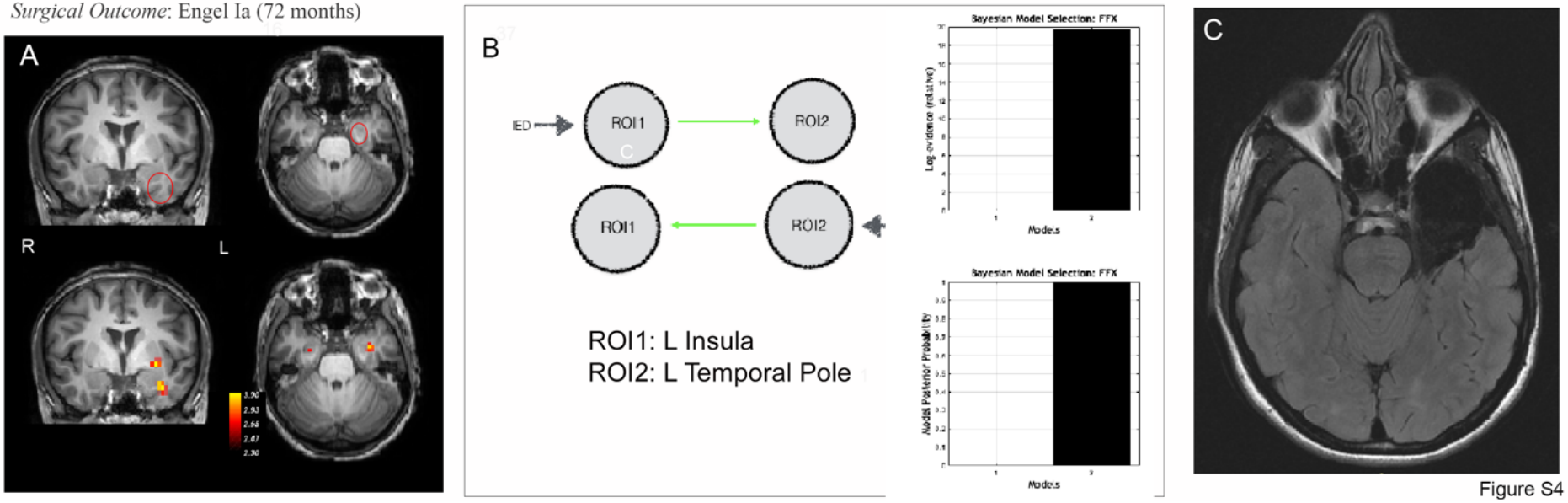

Figure S4

Figure 10.8 (supplementary): *Patient with "concordant, surgery-validated and confirmed" DCM result.*
*Patient #4. (**A**) Top: presurgical 3D-T1 shows a temporal polar and hippocampus FCD (red circles). Bottom: IED-related fMRI results overlaid onto the high-resolution presurgical 3D-T1, axial and coronal slices shown two main clusters of signal increase ($p < 0.05$, small volume correction and family-wise error corrected) in the left insular cortex (global maxima) and in the left temporal pole. (**B**) Left: DCM models' architecture: two ROIs are*

*structurally (forward and backward) connected (intrinsic connections are not shown in the models for illustrative purposes). IED were considered as autonomous input to each of the two regions, one at a time (grey arrow). The bilinear terms are represented as solidgreen arrows. Right: DCM Bayesian model selection results: relative log-evidence and posterior probability for the two models compared using FFX BMS show the winning model as Model 2 [p(m|Y) = 0,80]. The log-evidence difference between these two models was > 3 (hence significant). (**C**) Post-operative FLAIR axial image showing the resection area. R: right; L: left; sMRI: Structural MRI.*

Female, left-handed, seizure onset at 31 yrs old

Seizures' semiology: focal sensory aware seizures: vertigo, visual field restriction
Interictal Spike Field : right fronto-temporal and middle temporal
Ictal EEG: right posterior temporal
sMRI: right fusiform gyrus FCD; right parahippocampal gyrus FCD
Interctal FDG-PET: not available

IED-related EEG-fMRI: right inferior parietal gyrus, right fusiform gyrus
DCM analysis: right fusiform gyrus

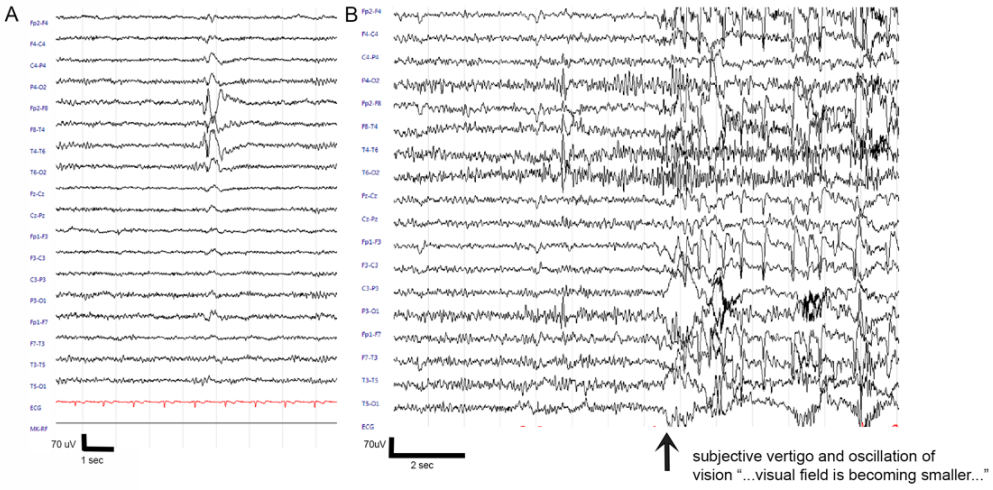

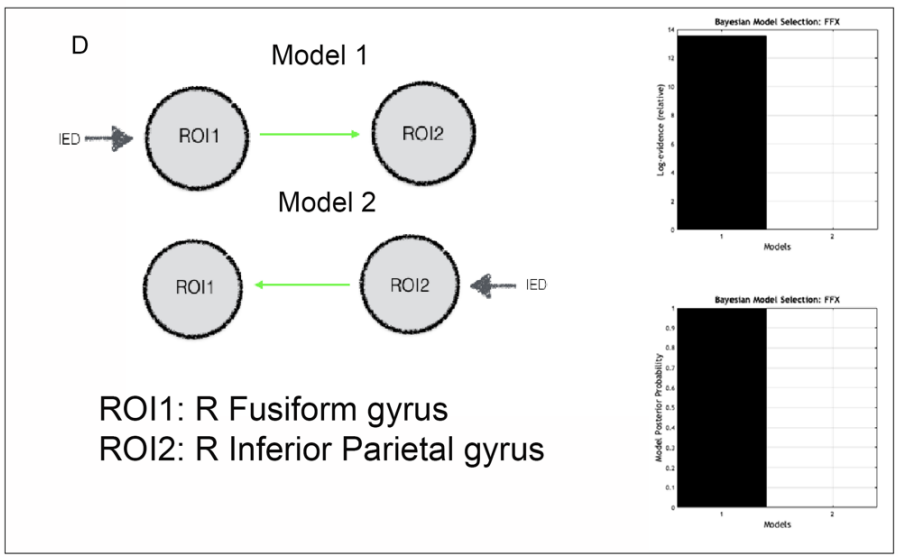

Figure 10.9 (supplementary): *Patient with "concordant" DCM result.*
*Patient #5. (**A**) Representative segment of scalp EEG showing the IED over the right fronto-temporal and middle regions. (**B**) ictal EEG shows low-voltage fast activity over the right middle and posterior temporal leads with diffusion to the homolateral parieto-occipital regions. The black arrow indicates the timing of ictal clinical semiology onset. EEGs are displayed in bipolar montage. (**C**) :Left: structural MRI (high-resolution FLAIR scan, coronal and sagittal slices) shows a right basal temporal cortex (fusiform gyrus) FCD (red circles). Right Images: IED-related fMRI results overlaid onto the high-resolution presurgical FLAIR, coronal and sagittal slices demonstrated two significant (p < 0,05 FWE) clusters of signal increase: the global maxima located in the right parietal cortex (inferior parietal gyrus) and a smaller blob in the homolateral fusiform gyrus. (**D**) Left: DCM models' architecture: two ROIs are structurally (forward and backward) connected (intrinsic connections are not shown in the models for illustrative purposes). IED were considered as autonomous input to each of the two regions, one at a time (grey arrow). The bilinear terms are represented as solid green arrows. Right: DCM Bayesian model selection results: relative log-evidence and posterior probability for the two models compared using FFX BMS show the winning model as Model 1 [p(m|Y) = 1.00]. The log-evidence difference between these two models was > 3 (hence significant). R: right; L: left; FCD: Focal Cortical Dysplasia; sMRI: Structural MRI.*

Male, right-handed, seizure onset at 31 yrs old

Seizures' semiology: (a) focal sleep-related seizures with scream, clonic arms movements; (b) awake brief epigastricsensation and loss of contact
Interictal Spike Field : left fronto-temporal
Ictal EEG: left fronto-temporal
sMRI: left anterior insular epidermoid cyst and thickening of surronding cortex
Interctal FDG-PET: not available

IED-related EEG-fMRI: left inferior frontal gyrus, left superior frontal gyrus
DCM analysis: left inferior frontal gyrus

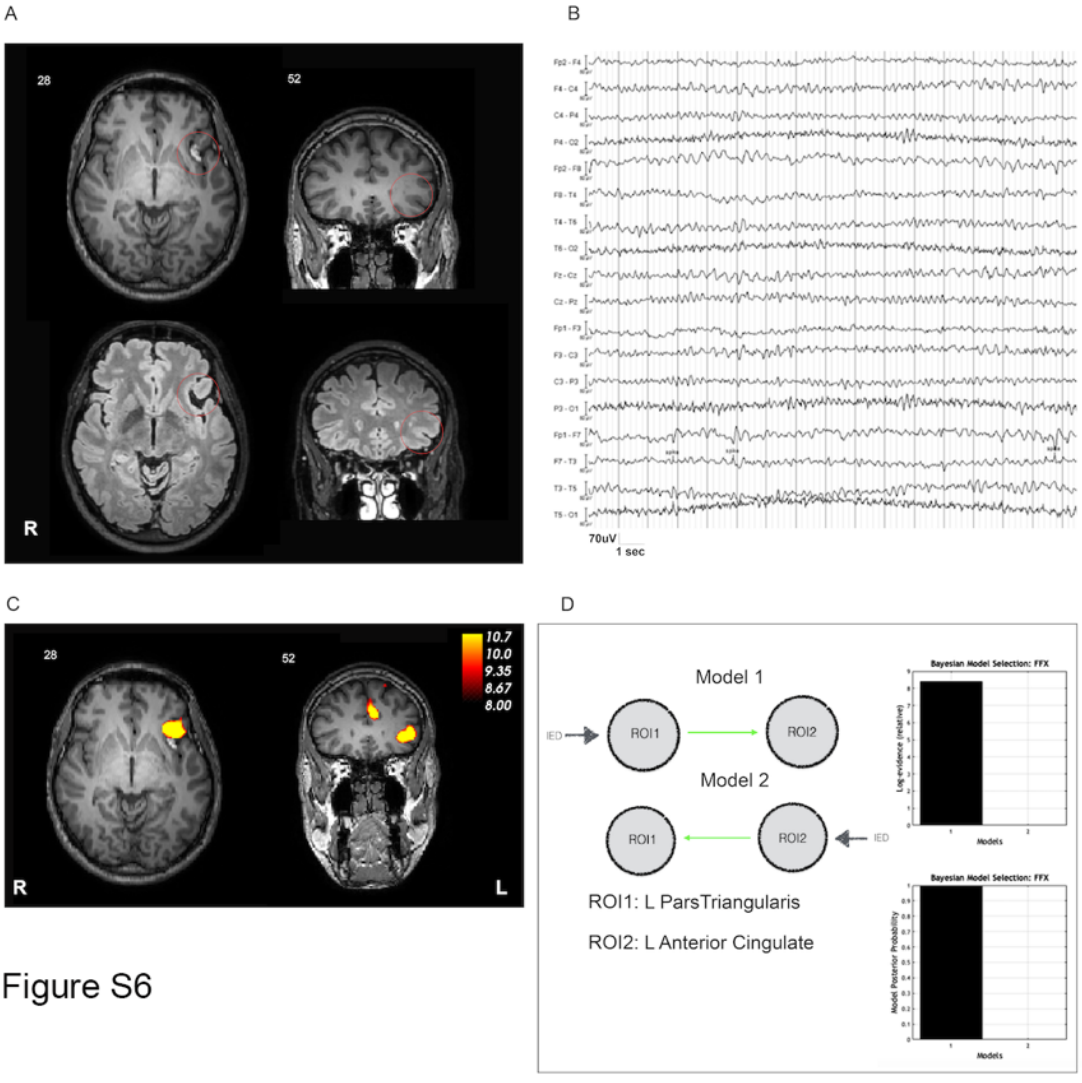

Figure S6

Figure 10.10 (supplementary): *Patient with "concordant" DCM result.*
*Patient #6. (**A**) Structural MRI (top image: high-resolution 3D-T1; bottom image: high-resolution FLAIR, axial and coronal slices) shows the left anterior insular epidermoid cyst (red circles). (**B**) Representative segment of scalp EEG showing the*

*marked IED over the left fronto-temporal regions. EEG is displayed in bipolar montage. (**C**) IED-related fMRI results overlaid onto the high-resolution presurgical 3D-T1, axial and coronal slices; demonstrated two significant (p < 0,05 FWE) clusters of signal increase: the global maxima located in the left inferior frontal gyrus (pars triangularis) and a second blob in the homolateral superior frontal gyrus. (**D**) Left: DCM models' architecture: two ROIs are structurally (forward and backward) connected (intrinsic connections are not shown in the models for illustrative purposes). IED were considered as autonomous input to each of the two regions, one at a time (grey arrow). The bilinear terms are represented as solid green arrows. Right: DCM Bayesian model selection results: relative log-evidence and posterior probability for the two models compared using FFX BMS show the winning model as Model 1 [p(m|Y) = 0,99]. The log-evidence difference between these two models was > 3, see text for details. R: right; L: left. sMRI: Structural MRI.*

Male, right-handed, seizure onset at 13 yrs old

Seizures' semiology: focal aware seizures: visual hallucinations, cephalalgia, right superior arm stiffness, stereotyped vocalizations.
Interictal Spike Field : left temporo-parietal
Ictal EEG: left parietal and parietal-central
sMRI: left precunus FCD
Interctal FDG-PET: left precuneus hypometabolism

IED-related EEG-fMRI: right superior parietal cortex, left precuneus
DCM analysis: left precuneus

Surgery: left precuneal lesionectomy
Histology: FCD I
Surgical Outcome: Engel IIa (24 months)

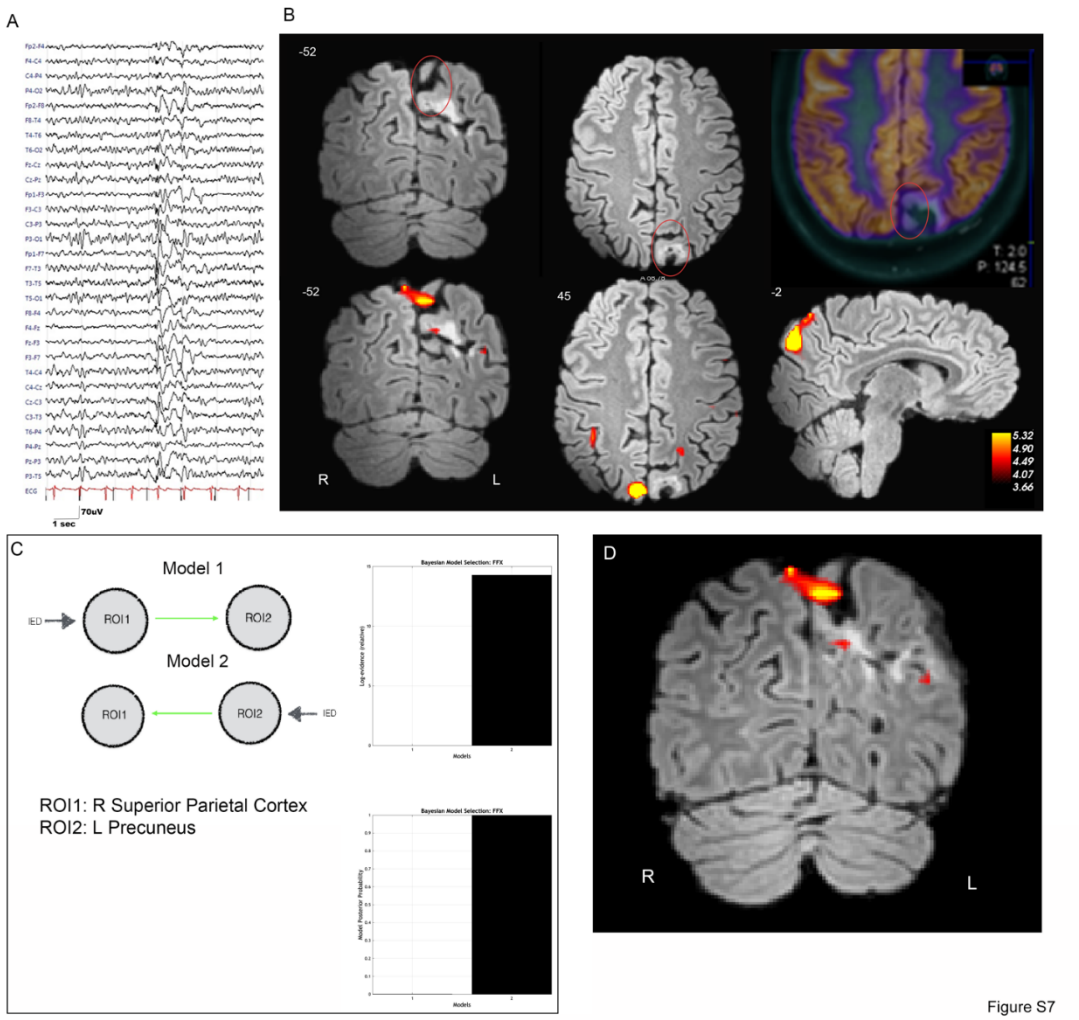

Figure S7

Figure 10.11 (supplementary): *Patient with "concordant, surgery-validated and confirmed" DCM result.*
*Patient #8. (**A**) Representative segment of scalp EEG showing diffuse IED with a clear prevalence over the left parieto-temporal leads. EEG is displayed in bipolar montage. (**B**) Top: high-resolution FLAIR coronal and axial slices showing a residual FCD around the surgical cavity involving the left precuneus concordant with interictal FDG-interictal PET findings (red circles). Bottom: IED-related fMRI results overlaid onto the high-resolution presurgical FLAIR, axial, coronal and sagittal slices revealed (p < 0.05, small volume correction and family-wise error corrected) two clusters of*

*signal increases located at the right superior parietal cortex (Global Maxima) and a smaller blob at the left precuneus. (**C**) Left: DCM models' architecture: two ROIs are structurally (forward and backward) connected (intrinsic connections are not shown in the models for illustrative purposes). IED were considered as autonomous input to each of the two regions, one at a time (grey arrow). The bilinear terms are represented as solid green arrows. Right: DCM Bayesian model selection results: relative log-evidence and posterior probability for the two models compared using FFX BMS show the winning model as Model 2 [p(m|Y) = 1]. The log-evidence difference between these two models was > 3 (hence significant). (**D**) presurgical IED-related fMRI findings overlaid onto post-surgical high-resolution FLAIR scan. R: right; L: left; FCD: Focal Cortical Dysplasia; sMRI: Structural MRI*

Male, right-handed, seizures onset at 24 yrs old

Seizures' semiology: focal seizures with impaired awareness: subjective ascending warmth sensation visual attraction towards surrounding stimuli, foul language
Interictal Spike Field : right central-parietal
Ictal EEG: right temporal-occipital, rapid diffusion
sMRI: right temporal-occipital AVM
Interctal FDG-PET: not available

IED-related EEG-fMRI: rigth superior temporal gyrus, right middle temporal gyrus (close to AVM), right cuneus, right frontal opercolum
DCM analysis: right middle temporal gyrus & right cuneus

Surgery: lesionectomy AVM
Histology: AVM
Surgical Outcome: Engel III (36 months)

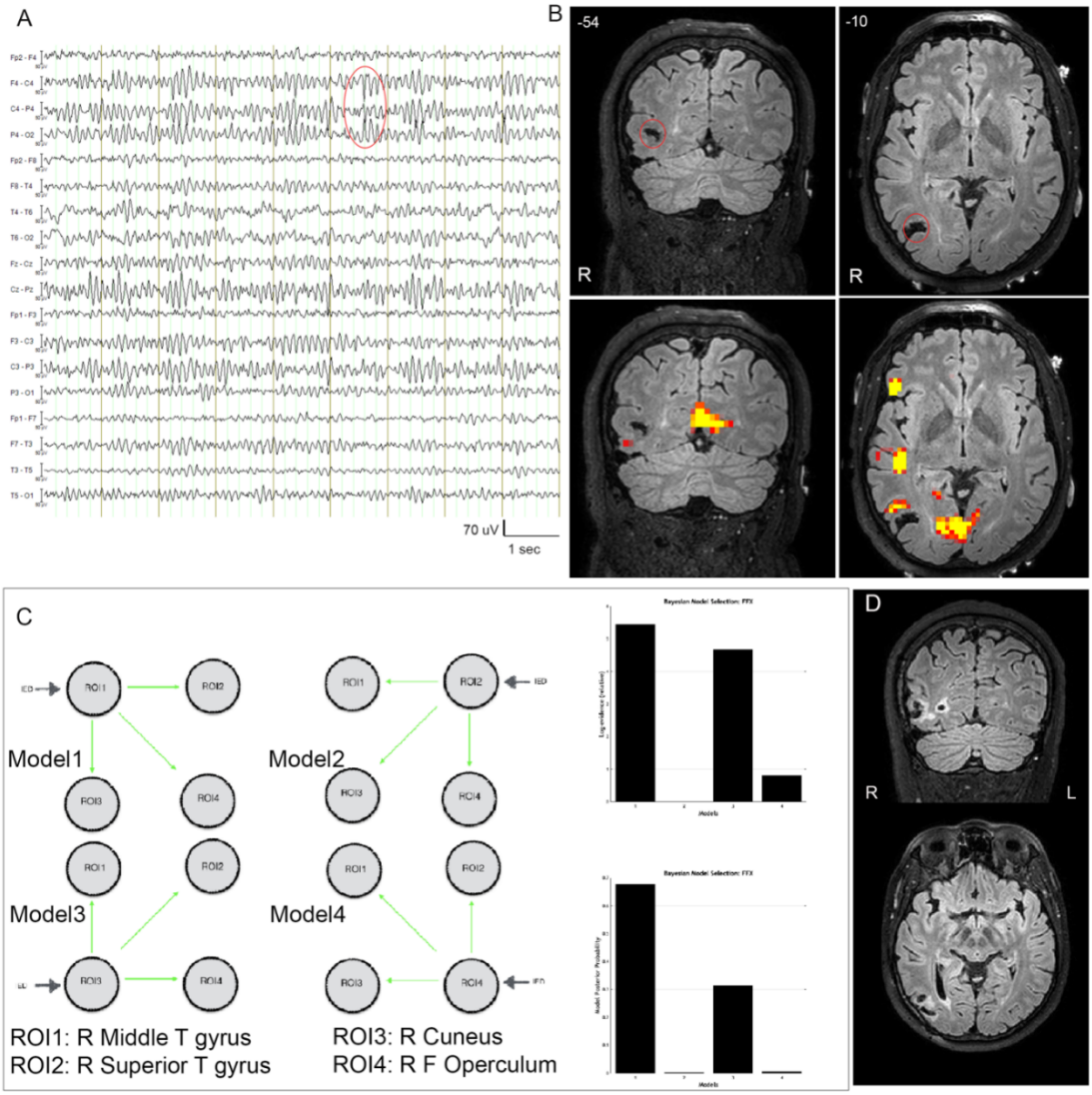

Figure 10.12 (supplementary): *Patient with "discordant, surgery invalid but unconfirmed" DCM result.*
*Patient #10. (**A**) Representative segment of scalp EEG showing focal IED located over the right fronto-central and centro-parietal leads. EEG is displayed in bipolar montage. (**B**) Top: high-resolution presurgical FLAIR coronal and axial slices show the right temporo-occipital AVM (red circles). Bottom: IED-related fMRI results*

*overlaid onto high-resolution presurgical FLAIR coronal and axial slices demonstrated (p < 0.05, FWE corrected) four principal cluster of signal increases at the right superior temporal gyrus (global maxima), right middle temporal gyrus (corresponding to the anterior border of the MAV lesion), right cuneus and right frontal operculum. (**C**) Left: DCM models' architecture: four ROIs are structurally (forward and backward) connected (intrinsic connections are not shown in the models for illustrative purposes). IED were considered as autonomous input to each of the four regions, one at a time (grey arrow). The bilinear terms are represented as solid green arrows. Right: DCM Bayesian model selection results: relative log-evidence and posterior probability for the four models compared using FFX BMS show two winning models, Model 1 [p(m|Y) = 0,68] and Model 3 [p(m|Y) = 0,31]. The log-evidence difference between these two models was < 3 (hence not significant), while the log-evidence difference between Models 1 and 3 and the others were > 3, hence significant, see text for details. (**D**) post-surgical high-resolution FLAIR scan. R: right; L: left. AVM: Arteriovenous Malformation; sMRI: Structural MRI.*

***Table 10.3 (supplementary)**: Best models for each subject are printed in bold letter. * indicates statistical significance. DCM F values (i.e., negative log-evidence) for each model at single subject*

Pt ID	DCM results	DCM Model1	DCM Model2	DCM Model3	DCM Model4
1	Concordant	-2,7749E+18	**-2,76623E+18***	-	-
2	Concordant	**-4,25053E+14***	-4,30962E+14	**-4,28434E+14***	-4,24996E+14
3	Concordant	**-3,11664E+14***	-3,13068E+14	-3,15614E+14	-
4	Concordant	-2,520029E+14	**-2,50032E+14***	-	-
5	Concordant	**-2,66267E+14***	-2,6762E+14	-	-
6	Concordant	**-2,60952E+14***	-2,61792E+14	-	-
7	Discordant	-3,16439E+03	**-**3,16296E+03	**-3.15508E+03***	-
8	Concordant	-2,76E+14	**-2,74479E+14***	-	-
9	Not Conclusive	**-2,56308E+14**	-2,56391E+14	-	-
10	Discordant	**-4,94729E+18***	-4,95273E+18	**-4,94805E+18***	-4,95193E+18

10.5. REFERENCES

An D, Fahoum F, Hall J, Olivier A, Gotman J, Dubeau F (2013) Electroencephalography/functional magnetic resonance imagingresponses help predict surgical outcome in focal epilepsy. Epilepsia54(12):2184–2194

Archer JS, Abbott DF, Masterton RAJ, Palmer SM, Jackson GD (2010)Functional MRI interactions between dysplastic nodules andoverlying cortex in periventricular nodular heterotopia. EpilepsyBehav EB 19(4):631–634

Avanzini G, Manganotti P, Meletti S, Mosh. SL, Panzica F, Wolf P et al (2012) The system epilepsies: a pathophysiological hypothesis.Epilepsia 53(5):771–778

Avanzini P, Vaudano AE, Vignoli A, Ruggieri A, Benuzzi F, Darra F et al (2014) Low frequency mu-like activity characterizes cortical rhythms in epilepsy due to ring chromosome 20. Clin Neurophysiol 125(2):239–249

Bartolomei F, Lagarde S, Wendling F, McGonigal A, Jirsa V, Guye M et al (2017) Defining epileptogenic networks: contribution of SEEG and signal analysis. Epilepsia 58(7):1131–1147

Bernasconi A, Cendes F, Theodore WH, Gill RS, Koepp MJ, Hogan RE et al (2019) Recommendations for the use of structural magnetic resonance imaging in the care of patients with epilepsy: a consensus report from the International League Against Epilepsy Neuroimaging Task Force. Epilepsia 60(6):1054–1068

Blumcke I, Spreafico R, Haaker G, Coras R, Kobow K, Bien CG et al (2017) Histopathological findings in brain tissue obtained during epilepsy surgery. N Engl J Med 377(17):1648–1656

Brodbeck V, Spinelli L, Lascano AM, Wissmeier M, Vargas MI, Vulliemoz S et al (2011) Electroencephalographic source imaging: a prospective study of 152 operated epileptic patients. Brain 134(Pt 10):2887–2897

Cardinale F, Rizzi M, Vignati E, Cossu M, Castana L, d'Orio P et al (2019) Stereoelectroencephalography: retrospective analysis of 742 procedures in a single centre. Brain J Neurol 142(9):2688–2704

Cataldi M, Avoli M, de Villers-Sidani E (2013) Resting state networks in temporal lobe epilepsy. Epilepsia 54(12):2048–2059

Chaudhary UJ, Carmichael DW, Rodionov R, Thornton RC, Bartlett P, Vulliemoz S et al (2012) Mapping preictal and ictal haemodynamic networks using video-electroencephalography and functional imaging. Brain J Neurol 135(Pt 12):3645–3663

Coan AC, Campos BM, Beltramini GC, Yasuda CL, Covolan RJM, Cendes F (2014) Distinct functional and structural MRI abnormalities in mesial temporal lobe epilepsy with and without hippocampal sclerosis. Epilepsia 55(8):1187–1196

Coan AC, Chaudhary UJ, Grouiller F, Campos BM, Perani S, De Ciantis A et al (2016) EEG-fMRI in the presurgical evaluation of temporal obe epilepsy. J Neurol Neurosurg Psychiatry 87(6):642–9

David O, Guillemain I, Saillet S, Reyt S, Deransart C, Segebarth C et al (2008) Identifying neural drivers with functional MRI: an electrophysiological validation. PLoS Biol 6(12):2683–2697

Disbrow EA, Slutsky DA, Roberts TP, Krubitzer LA (2000) Functional MRI at 1.5 tesla: a comparison of the blood oxygenation level-dependent signal and electrophysiology. Proc Natl Acad Sci USA 97(17):9718–23

Duez L, Tankisi H, Hansen PO, Sidenius P, Sabers A, Pinborg LHet al (2019) Electromagnetic source imaging in presurgicalworkup of patients with epilepsy: a prospective study. Neurology 92(6):e576–e586

Duncan JS, Winston GP, Koepp MJ, Ourselin S (2016) Brain imaging in the assessment for epilepsy surgery. Lancet Neurol15(4):420–433

Engel J (1993) Surgical treatment of the epilepsies, 2nd edn. RavenPress, New York, p 786

Fedorov A, Beichel R, Kalpathy-Cramer J, Finet J, Fillion-Robin J-C,Pujol S et al (2012) 3D Slicer as an image computing platform or the Quantitative Imaging Network. Magn Reson Imaging 30(9):1323–1341

Friston KJ, Williams S, Howard R, Frackowiak RS, Turner R (1996) Movement-related effects in fMRI time-series. Magn Reson Med 35(3):346–355

Friston KJ, Harrison L, Penny W (2003) Dynamic causal modelling. Neuroimage 19(4):1273–1302

Gonz.lez Ot.rula KA, Khoo HM, von Ellenrieder N, Hall JA, Dubeau F, Gotman J (2018) Spike-related haemodynamic responses overlap with high frequency oscillations in patients with focal epilepsy. Brain J Neurol 141(3):731–743

Gotman J, Pittau F (2011) Combining EEG and fMRI in the study of epileptic discharges. Epilepsia 52(Suppl 4):38–42

Hamandi K, Salek-Haddadi A, Laufs H, Liston A, Friston K, Duncan JS, Fish DR, Lemieux L (2006) EEG-fMRI of idiopathic and secondarily generalized epilepsies. Neuroimage 31(4):1700–1710

Hamandi K, Powell HWR, Laufs H, Symms MR, Barker GJ, Parker GJM et al (2008) Combined EEG-fMRI and tractography to visualize propagation of epileptic activity. J Neurol Neurosurg Psychiatry79(5):594–597

Jehi L (2018) The epileptogenic zone: concept and definition. EpilepsyCurr 18(1):12–16

Kahan J, Foltynie T (2013) Understanding DCM: ten simple rules forhe clinician. Neuroimage 83:542–549

Kalilani L, Sun X, Pelgrims B, Noack-Rink M, Villanueva V (2018) The epidemiology of drug-resistant epilepsy: a systematic review and meta-analysis. Epilepsia 59(12):2179–2193

Kane N, Acharya J, Beniczky S, Caboclo L, Finnigan S, Kaplan PW et al (2017) A revised glossary of terms most commonly used by clinical electroencephalographers and updated proposal for the report format of the EEG findings. Revision 2017. Clin Neurophysiol Pract 2:170–85

Khoo HM, Hao Y, von Ellenrieder N, Zazubovits N, Hall J, Olivier A et al (2017) The hemodynamic response to interictal epileptic discharges localizes the seizure-onset zone. Epilepsia 58(5):811–823

Khoo HM, von Ellenrieder N, Zazubovits N, He D, Dubeau F, Gotman J (2018) The spike onset zone: the region where epileptic spikes start and from where they propagate. Neurology 91(7):e666–e674

Klamer S, Rona S, Elshahabi A, Lerche H, Braun C, Honegger J et al (2015) Multimodal effective connectivity analysis reveals seizure focus and propagation in musicogenic epilepsy. Neuroimage 113:70–77

Klamer S, Ethofer T, Torner F, Sahib AK, Elshahabi A, Marquetand J et al (2018) Unravelling the brain networks driving spike-wave discharges in genetic generalized epilepsy-common patterns and individual differences. Epilepsia Open 3(4):485–494

Kobayashi E, Bagshaw AP, Jansen A, Andermann F, Andermann E, Gotman J et al (2005) Intrinsic epileptogenicity in polymicrogyric cortex suggested by EEG-fMRI BOLD responses. Neurology 64(7):1263–1266

Kobayashi E, Bagshaw AP, Grova C, Gotman J, Dubeau F (2006a) Grey matter heterotopia: what EEG-fMRI can tell us about epileptogenicity of neuronal migration disorders. Brain 129(2):366–374

Kobayashi E, Bagshaw AP, Grova C, Dubeau F, Gotman J (2006b) Negative BOLD responses to epileptic spikes. Hum Brain Mapp 27(6):488–497

Kobayashi E, Grova C, Tyvaert L, Dubeau F, Gotman J (2009) Structures involved at the time of temporal lobe spikes revealed by interindividual group analysis of EEG/fMRI data. Epilepsia 50(12):2549–2556

Kowalczyk MA, Omidvarnia A, Abbott DF, Tailby C, Vaughan DN, Jackson GD (2020a) Clinical benefit of presurgical EEG-fMRI in difficult-to-localize focal epilepsy: a single-institution retrospective review. Epilepsia 61(1):49–60

Kowalczyk MA, Omidvarnia A, Dhollander T, Jackson GD (2020b) Dynamic analysis of fMRI activation during epileptic spikes can help identify the seizure origin. Epilepsia 61(11):2558–2571

Koz.k LR, van Graan LA, Chaudhary UJ, Szab. .G, Lemieux L (2017) ICN_Atlas: automated description and quantification of functional MRI activation patterns in the framework of intrinsic connectivity networks. Neuroimage 163:319–341

Kural MA, Tankisi H, Duez L, Sejer Hansen V, Udupi A, Wennberg R et al (2020) Optimized set of criteria for defining interictal epileptiform EEG discharges. Clin Neurophysiol 131(9):2250–2254

Laufs H, Hamandi K, Salek-Haddadi A, Kleinschmidt AK, Duncan JS, Lemieux L (2007) Temporal lobe interictal epileptic discharges affect cerebral activity in “default mode” brain regions. Hum Brain Mapp 28(10):1023–1032

Lemieux L, Laufs H, Carmichael D, Paul JS, Walker MC, Duncan JS (2008) Noncanonical spike-related BOLD responses in focal epilepsy. Hum Brain Mapp 29(3):329–345

Liu J, Liu B, Zhang H (2018) Surgical versus medical treatment of drug-resistant epilepsy: a systematic review and meta-analysis. Epilepsy Behav 82:179–188

Lohmann G, Erfurth K, Müller K, Turner R (2012) Critical comments on dynamic causal modelling. Neuroimage 59(3):2322–2329

Lüders HO, Najm I, Nair D, Widdess-Walsh P, Bingman, W (2006) The epileptogenic zone: general principles. Epileptic Disord 8(Suppl2):S1–S9

Markoula S, Chaudhary UJ, Perani S, Ciantis AD, Yadee T, Duncan JS et al (2018) The impact of mapping interictal discharges using EEG-fMRI on the epilepsy presurgical clinical decision making process: a prospective study. Seizure 61:30–37

McCormick C, Quraan M, Cohn M, Valiante TA, McAndrews MP (2013) Default mode network connectivity indicates episodic memory capacity in mesial temporal lobe epilepsy. Epilepsia 54(5):809–818

Meletti S, Vaudano AE, Tassi L, Caruana F, Avanzini P (2015) Intracranial time–frequency correlates of seizure-related negative BOLD response in the sensory-motor network. Clin Neurophysiol 126(4):847–849

Mirandola L, Cantalupo G, Vaudano AE, Avanzini P, Ruggieri A, Pisani F et al (2013) Centrotemporal spikes during NREM sleep: the promoting action of thalamus revealed by simultaneous EEG and fMRI coregistration. Epilepsy Behav Case Rep 1:106–109

Murta T, Leal A, Garrido MI, Figueiredo P (2012) Dynamic Causal Modelling of epileptic seizure propagation pathways: a combined EEG-fMRI study. Neuroimage 62(3):1634–1642

Narizzano M, Arnulfo G, Ricci S, Toselli B, Tisdall M, Canessa A et al (2017) SEEG assistant: a 3DSlicer extension to support epilepsy surgery. BMC Bioinform 1:124

Penny WD, Stephan KE, Mechelli A, Friston KJ (2004) Comparing dynamic causal models. Neuroimage 22(3):1157–1172

Pittau F, Dubeau F, Gotman J (2012) Contribution of EEG/fMRI to the definition of the epileptic focus. Neurology 78(19):1479–1487

Pittau F, Ferri L, Fahoum F, Dubeau F, Gotman J (2017) Contributions of EEG-fMRI to assessing the epileptogenicity of focal cortical dysplasia. Front Comput Neurosci. https://doi.org/10.3389/fncom.2017.00008

Poldrack RA (2007) Region of interest analysis for fMRI. SCAN 2:67–70

Rampp S, Stefan H, Wu X, Kaltenh.user M, Maess B, Schmitt FC et al (2019) Magnetoencephalography for epileptic focus localization in a series of 1000 cases. Brain J Neurol 142(10):3059–3071

Ray KL, McKay DR, Fox PM, Riedel MC, Uecker AM, Beckmann CF et al (2013) ICA model order selection of task co-activation networks. Front Neurosci. https://doi.org/10.3389/fnins.2013.00237

Rossi Sebastiano D, Tassi L, Duran D, Visani E, Gozzo F, Cardinale F et al (2020) Identifying the epileptogenic zone by four non-invasive imaging techniques versus stereo-EEG in MRI-negative presurgery epilepsy patients. Clin Neurophysiol 131(8):1815–1823

Salek-Haddadi A, Diehl B, Hamandi K, Merschhemke M, Liston A, Friston K et al (2006) Hemodynamic correlates of epileptiform discharges: an EEG-fMRI study of 63 patients with focal epilepsy. Brain Res 1088(1):148–166

Sokolov AA, Zeidman P, Erb M, Ryvlin P, Pavlova MA, Friston KJ (2019) Linking structural and effective brain connectivity: structurally informed Parametric Empirical Bayes (si-PEB). Brain Struct Funct 224(1):205–217

Stephan KE, Friston KJ (2010) Analyzing effective connectivity with functional magnetic resonance imaging. Wiley Interdiscip Rev Cogn Sci 1(3):446–459

Stephan KE, Tittgemeyer M, Kn.sche TR, Moran RJ, Friston KJ (2009) Tractography-based priors for dynamic causal models. Neuroimage 47(4):1628–1638

Thornton R, Laufs H, Rodionov R, Cannadathu S, Carmichael DW, Vulliemoz S et al (2010a) EEG correlated functional MRI and postoperative outcome in focal epilepsy. J Neurol Neurosurg Psychiatry 81(8):922–927

Thornton RC, Rodionov R, Laufs H, Vulliemoz S, Vaudano A, Carmichael D et al (2010b) Imaging haemodynamic changes related to seizures: comparison of EEG-based general linear model, independent component analysis of fMRI and intracranial EEG. Neuroimage 53(1):196–205

Thornton R, Vulliemoz S, Rodionov R, Carmichael DW, Chaudhary UJ, Diehl B et al (2011) Epileptic networks in focal cortical dysplasia revealed using electroencephalography-functional magnetic resonance imaging. Ann Neurol 70(5):822–837

Tyvaert L, Hawco C, Kobayashi E, LeVan P, Dubeau F, Gotman J (2008) Different structures involved during ictal and interictal epileptic activity in malformations of cortical development: an EEG-fMRI study. Brain J Neurol 131(Pt 8):2042–2060

Vakharia VN, Duncan JS, Witt J-A, Elger CE, Staba R, Engel J (2018) Getting the best outcomes from epilepsy surgery: epilepsy surgery outcomes. Ann Neurol 83(4):676–690

Varotto G, Tassi L, Franceschetti S, Spreafico R, Panzica F (2012) Epileptogenic networks of type II focal cortical dysplasia: a stereo-EEG study. Neuroimage 61(3):591–598

Vaudano AE, Laufs H, Kiebel SJ, Carmichael DW, Hamandi K, Guye M et al (2009) Causal hierarchy within the thalamo-cortical network in spike and wave discharges. PLoS ONE 4(8):e6475

Vaudano AE, Carmichael DW, Salek-Haddadi A, Rampp S, Stefan H, Lemieux L et al (2012) Networks involved in seizure initiation. A reading epilepsy case studied with EEG-fMRI and MEG. Neurology 79(3):249–53

Vaudano AE, Avanzini P, Tassi L, Ruggieri A, Cantalupo G, Benuzzi F et al (2013) Causality within the epileptic network: an EEG-fMRI study validated by intracranial EEG. Front Neurol. https://doi.org/10.3389/fneur.2013.00185

Wang I, Bernasconi A, Bernhardt B, Blumenfeld H, Cendes F, Chinvarun Y et al (2020) MRI essentials in epileptology: a review from the ILAE Imaging Taskforce. Epileptic Disord 22(4):421–437

Warren AEL, Harvey AS, Vogrin SJ, Bailey C, Davidson A, Jackson GD et al (2019) The epileptic network of Lennox-Gastaut syndrome: cortically driven and reproducible across age. Neurology 93(3):e215–e226

Watanabe S, Dubeau F, Zazubovits N, Gotman J (2017) Temporal lobe spikes: EEG-fMRI contributions to the “mesial vs. lateral” debate. Clin Neurophysiol 128(6):986–91

Whelan CD, Altmann A, Bot.a JA, Jahanshad N, Hibar DP, Absil J et al (2018) Structural brain abnormalities in the common epilepsies assessed in a worldwide ENIGMA study. Brain 141(2):391–408

Yamazoe T, von Ellenrieder N, Khoo HM, Huang Y-H, Zazubovits N, Dubeau F et al (2019) Widespread interictal epileptic discharge more likely than focal discharges to unveil the seizure onset zone in EEG-fMRI. Clin Neurophysiol 130(4):429–438

Zijlmans M, Zweiphenning W, van Klink N (2019) Changing concepts in presurgical assessment for epilepsy surgery. Nat Rev Neurol

15(10):594–606

Chapter 11: The Influence Of Wakefulness On The Brain Networks Involved In Centrotemporal Spike Generation In SeLETCS

11.1. INTRODUCTION

Self-limited epilepsy with centro-temporal spikes (SeLECTS), formerly known as Benign Rolandic Epilepsy or Benign Epilepsy with Centrotemporal Spikes (BECTS), is the most common form of “self-limited focal epilepsies” (Scheffer et al., 2016; Specchio et al. 2022). The estimated incidence of SeLECTS is around 2% in children, occurring four times more frequently than typical absence epilepsy (Miziara et al. 2012; Panayiotopoulos et al., 2008). It is known to be age-dependent, to have a genetic basis occurring during crucial stages of development, with the typical age of onset is between 3 and 10 years and a peak around 6–7 years. In SeLECTS, the most frequent seizure semiology is characterized by facial sensory, oropharyngolaryngeal motor symptoms, speech arrest, and salivation, suggesting the ictal involvement of the perisylvian network (PN) and particularly of the opercular-insular regions (Guerrini et al. 2012; Halasz et al., 2020; Alving et al., 2017). Functional imaging (Archer et al. 2003, Boor et al. 2003, 2007; Lengler et al. 2007;

Siniatchkin et al. 2007a,b; Masterton et al. 2013; Xiao et al. 2016; Li et al. 2017, 2019) and EEG/MEG (Parmeggiani and Guerrini, 1999) mapping studies provided several evidences supporting this assumption. PN covers a ring of cortical regions around the sylvian fissure, including the frontal-prefrontal, temporal and temporal-occipital associative fields and harbors important cognitive functions, mainly associated with speech and reading and other essential communication capabilities (Halasz et al., 2020).

Despite the good prognosis, with recovery usually occurring before age 15–16 years (Koutroumanidis et al., 2015), SeLECTS patients have been reported to present some deficits in PN functions (Goldberg-Stern et al., 2010; Verrotti et al., 2014). Particularly, language disruption is the most prominent cognitive comorbidity (Tovia et al., 2011.) and it may be present before seizures onset and persist after seizures remission (Deonna et al., 2000; Northcott et al. 2006; Monjauze et al., 2011). Cognitive abnormalities, including language dysfunction, have been associated with abundance (or frequency) of CTS both during wakefulness and sleep (Mirandola et al., 2013; Halasz et al., 2019).

According to the AASM manual, sleep onset is defined by the first epoch scored as any stage other than stage wake (W) (generally corresponding to the first epoch of stage N1. While this approach is helpful to characterize the macrostructure of a 7–8 h of nocturnal EEG activity, it is unsatisfactory to reveal intrusions of sleep episodes into the wake state. Multispectral EEG indexes based on scalp EEG have been conceived to obtain a measurable quantification of drowsiness (Olbrich et al., 2009; Knaut et al., 2019). In healthy controls, different EEG-vigilance stages, including simple vigilance fluctuations, are associated with pronounced differences of BOLD signals as measured by EEG coregistered with fMRI (EEG-fMRI) in several brain areas (Olbrich et al., 2009, Tagliazucchi and Laufs 2013). Most of the EEG-FMRI studies, however, make the implicit assumption that all participants are in similar states of wakefulness or vigilance, but the validity of this assumption is rarely evaluated. This might be particularly important in conditions, like SeLECTS, where CTS are typically activated during drowsiness and the first

NREM sleep cycle. If the link between proper sleep and CTS occurrence have been widely investigated, the link between drowsiness and increased spiking activity in SeLECTS has not been studied extensively. In a recent paper for our group, we provided evidence about the critical role of the CTS frequency, during quiet wakefulness, to interfere with the cognitive functioning, especially language (Vaudano et al., 2019). However, we did not explore the brain endogenous state that may interfere with the CTS-related generating networks by modulating their frequency. Herein, we hypothesize that the fluctuation of the wakefulness state (i.e. drowsiness) may influence the cortico-subcortical networks involved in the CTS frequency generation. To this end, we explored by means of an EEG-fMRI approach, the relationship between CTS frequency and a multispectral EEG index of wakefulness in a homogenous population of SeLECTS. The question is not trivial because the revealed networks might involve brain regions either specifically linked to SeLECTS and/or to physiological sleep that contribute to facilitate the enhancement's phenomenon of spikes during drowsiness, potentially exportable in other clinical entities with similar behaviour of epileptiform discharges

11.2. METHODS

11.2.1. Study Population

Twenty-five SeLECTS patients [20 male; mean age, 9.8 years; median age, 9 years (range, 6-17 years) were recruited; of those, 18 patients have already been included in our previous work (Vaudano et al., 2019)]. The inclusion criteria for the present study were the following: (a) presence of CTS during the scan time (b) EEG recordings during fMRI acquisition fulfilling the American Academy of Sleep Medicine (AASM) criteria for wakefulness, while exhibiting indications of drowsiness (at a time scale below 30 s) during the recording time. i.e., light sleep (N1) as defined by the AASM-based sleep

classification (Laufs et al., 2006; Knaut et al., 2019); c) good quality EEG and fMRI.

Clinical and EEG features of the selected population are summarized in **Table 11.1**.

The human ethic committee of the University of Modena and Reggio Emilia approved this study, and written informed consent was obtained from parents and assent from patients.

11.2.2. EEG-fMRI Protocol

The EEG-fMRI protocol has been described extensively in our previous published paper (Vaudano et al., 2019). Briefly, all the recruited patients were scanned in the early afternoon, without sleep deprivation; no sedation was used. Scalp EEG (1,024Hz sampling rate, 10-20 conventional location) has been recorded by means of a 32-channel MRI compatible EEG recording system (Micromed, Mogliano Veneto, Italy). Before in-magnet EEG recording, 10min of out-of magnet EEG was collected in a room beside the scanner. Foam pads were used to help secure the EEG leads, minimize motion, and improve patient comfort. Data were transmitted via an optic fiber cable from the amplifier (1,024Hz sampling rate) to a computer located outside the scanner room. To avoid saturation, the EEG amplifiers have a resolution of 22 bits with a range of ± 25.6 mV.

Patients' behaviour has been constantly observed and recorded by means of a small camcorder positioned on the head coil inside the scanner pointing to the patients' face to obtain a split-screen video-EEG documentation during the fMRI recording. Patients were asked to remain still during the scanning with eyes closed and do not fall asleep. Functional data have been all acquired using the same Philips Intera System at 3T. fMRI data consisted of gradient-echo echo-planar sequence from 30 axial contiguous slice (TR = 3,000/2,000ms; in-plane matrix = 64 × 64; voxel size, 4 × 4 × 4) over one session of different duration according to the TR [10 minutes for a TR=3000ms

(200 volumes); 8 minutes for a TR=2000ms (240 volumes)] with continuous simultaneous EEG recording. A high-resolution T1-weighted anatomical image has been acquired to allow accurate anatomical localization of activations/deactivations. The volume consisted of 170 sagittal slices (TR=9.9ms; TE=4.6ms; in plane matrix = 256 × 256; voxel size = 1 × 1 × 1 mm).

11.2.3. EEG Preprocessing

BrainQuick System Plus software (Micromed) was used for offline correction of the gradient artifacts and filtering of the EEG signal. In addition, the EEG data were exported in .edf format and reviewed and analysed by means of the BrainVision Analyzer 2.0 software (Brain Products, Munich, Germany). After removing the gradient and mean ballistocardiographic artifacts, an independent component analysis (ICA) was performed on EEG data to isolate CTS from physiological and artifactual activities (Avanzini et al., 2014). Two experienced electroencephalographers reviewed the preprocessed EEG recordings independently (AEV, FT) to identify interictal epileptiform abnormalities based on both spatial distribution and topography. When recognized, CTS were marked at peak. We classified patients as unilateral (right or left) in case of only one spike focus without migration; bilateral in the case that both foci were active. In this latter condition, left and right CTS were considered together in further analyses. Further each EEG, once cleaned from gradient and ballistocardiographic artifacts was reviewed by expert in sleep EEG (AEV) in order to check for sleep occurrence according to the rules published by the AASM (2007).

11.2.4. fMRI preprocessing

The Matlab 7,1 and SPM12 (Wellcome Department of Imaging Neuroscience, London, UK) software were used for fMRI data preprocessing and analysis. All functional volumes were slice time corrected, realigned to the first volume acquired. Realigned fMRI data were spatially normalized to a standard EPI

template and smoothed with an 8 × 8 × 8mm full width at half maximum Gaussian kernel. The six motion parameters derived from the fMRI preprocessing (translation and rotation in the X, Y, and Z direction, respectively) and a Volterra expansion of these (Friston et al., 1996) were used as covariates in the general linear model (GLM).

11.2.5. EEG Data Analysis

Construction of the EEG wakefulness index (EWI)

We were interested to map the hemodynamic changes related to CTS (expressed by blood oxygen level-dependent-BOLD variations) in relation to fluctuations of the level of vigilance. To this end, we first construct for each patient an index of wakefulness (namely EWI, *EEG wakefulness index*) which was already applied successfully in healthy subjects as a measure of vigilance fluctuations (Knaut et al., 2019). EWI is a ratio between the power of EEG components with higher amplitude during wakefulness in the numerator (wake>drowsiness) and the power of EEG components with higher power during drowsiness in the denominator (drowsiness>wake). The higher is the EWI the more the subject is awake and vice versa. After the ICA-based rejection of residual artefact-laden and CTS-laden components, for each patient, the EWI relied on both spectral and topographical instantaneous EEG information, replicating the approach recently applied by Knaut and colleagues (2019).

The ratio (EWI) was defined as:

$$r = \frac{p(\vartheta, F_{3,4}) + p(\alpha, O_{1,2}) + p(\sigma, O_{1,2}) + p(\beta, F_{3,4})}{p(\delta, F_{3,4}) + p(\vartheta, O_{1,2}) + p(\sigma, C_{3,4}) + p(\alpha, F_{3,4}) + p(\beta, F_{3,4})}$$

where p (θ, F3,4), for example, denotes the instantaneous power in the theta frequency band, averaged across the frontal EEG channels F3 and F4. The other terms are interpreted accordingly.

The EEG frequency bands were defined as follows:

- Delta (δ): 0.5/s–4/s
- Theta (θ): 4/s–8/s
- Alpha (α): 8/s–12/s
- Sigma (σ): 12/s–15/s
- Beta (β): 16/s–30/s

Using the analytical amplitude of the individual frequency bands, the term is evaluated at each time point. The power for each frequency band was computed using a zero-phase 6^{th} order Butterworth band-pass filter and the amplitude of the filtered signal's Hilbert transform as implemented in the BrainVision Analyzer 2.0 software (Brain Products, Munich, Germany).

Construction of the CTS density regressor

Once recognized and marked on EEG, instead of treating CTS as single event, we computed the spike density, i.e., the number of ED for each time bin. As the final aim of the study was to use this information as regressor into the GLM model, the time bin was fixed equal to the subject-specific TR, i.e. 3/2s; likewise, the patient-specific EWI was down-sampled to obtain one data point per TR.

Exploration CTS-EWI relationship

In order to explore the relationship between spontaneous fluctuation in wakefulness (EWI) and the CTS frequency (number of CTS for TR), a number of exploratory analyses were implemented in Python 3.9:

a) Pearson Correlation and Local Pearson Correlation: The Pearson correlation was computed for each pair of subject-specific EWI time course and CTS density time course. To check for local multicollinearity, the Local Pearson correlation was computed for each pair of subject-specific EWI time course and CTS density time course with different

rolling windows (2s-15s). Moreover, all the subject specific EWI and CTS density time courses were normalized and concatenated and the Pearson correlation and Local Pearson correlation of the entirety normalized data was calculated.

b) Time Lagged Cross Correlation (TLCC): TLCC was computed for each pair of subject specific EWI time course and CTS density time course. TLCC involves shifting one of the signals in time relative to the other and computing the cross-correlation at each time lag. The resulting cross-correlation can be used to identify the time delay and the directionality between two signals such as a leader-follower relationship in which the leader initiates a response which is repeated by the follower. This relationship does not necessary reflect true causality, but allows to extract a sense of which signal occurs first.
c) Granger Causality: The Granger Causality test is a statistical hypothesis test for determining whether one time series is useful in forecasting. A time series X is said to Granger-Cause Y if it can be shown, through a series of t-test and F-test on lagged values of X (and with lagged values of Y also included), that those X values provide statistically significant information about future values of Y.
d) Trend Estimation: a moving average was computed to filter smooths data using a fixed window length heuristically determined.

11.2.6. EEG-fMRI data modelling, Event Related Analysis (CTS density)

First Level Analysis

After the preprocessing, for each patient we first explored the BOLD changes related to the patient's density of spikes, including the information coming from the EWI estimation. Similarly, to a previous adopted approach (Vaudano et al., 2019), the spike density regressor was convolved with the standard HRF

as provided by SPM and included in the model as effect of interest. Furthermore, in order to explore the BOLD changes related to the EWI, the down-sampled patient-specific EWI was convolved with the canonical hemodynamic response function as provided by SPM and included in the same general linear model (GLM), alongside the spike density. This allows to detect activations that are mutually exclusive to the spike density and the EWI. We then specified the 24 realignment parameters (six scan realignment parameters from image preprocessing and a Volterra expansion of these) as regressors of no interest. The threshold for statistical significance of fMRI{T} maps was set at $p < 0.001$ (uncorrected) and cluster extent of 10 voxels. All the clusters survived a correction for multiple comparison [FWE] within a 6-mmsphere ($p < .05$).

Group Level Analysis

Using the parameter estimates obtained by single-subject analyses, we performed one second level (group) random-effect analyses for “CTS density” by means of a sample T test. Subjects’ age, gender, epilepsy onset and epilepsy duration were included in the models as covariates. Statistical threshold was set at $p < 0,001$ (uncorrected) and an extent threshold of 10 contiguous voxels was applied to check for scattered BOLD changes. All the clusters survived a correction for multiple comparison [FWE] within a 6-mmsphere ($p < .05$). To map the location of BOLD signal increases and decreases clusters, MNI coordinates were converted into the Talairach space using the mni2tal Matlab algorithm.

11.2.7. Functional connectivity analysis using psychophysiological interaction

First Level Analysis

We used a psychophysiological interaction (PPI) analysis to assess the EWI-dependent whole-brain functional connectivity of the network triggered by the CTS density. Psychophysiological interactions (PPI), the form of context-dependent connectivity used in the present analysis, specifically investigate how one brain region increases or decreases its relationship with other brain regions under different contexts (Friston et al. 1997; Kim and Horwitz 2'08; O'Reilly et al. 2012).

To this end, from the CTS density-related group activation map, we chose a priori 6 seed locations: bilaterla perisylvian area, right putamen, bilateral motor cortex, insula. These regions indeed have been repetitively shown as key structures in the epileptogenic network of SeLECTS. The time series of a sphere of 8-mm radius around the group peak activity map (see **Table 11.2**) was extracted for each seed from the normalized, smoothed echo planar imaging (EPI) images (Bonelli et al., 2012).

The single-subject PPI model included three regressors: (i) the time course of the seed region (as the physiological signal); (ii) the HRF convolved EWI regressor (as the psychological context) and (iii) the interaction between the two (representing an EWI-modulated change in functional connectivity, or PPI) (Friston, 1994). This yielded a seed to voxel wise whole-brain analysis for each participant.

Group Level Analysis

Areas functionally coupled to the CTS density seeds regions were examined across the group with

one-sample t-test for each seed. Clinical variables (epilepsy duration, age at onset, age and sex) were added as covariates.

Each PPI seed region analysis can be considered to be an independent analysis, as we do not directly compare the PPI contrasts between seeds at the voxel or cluster level. Thus, a correction for the number of seed regions is not needed in this study.

Figure 11.1 summaries graphically the methodological approach adopted.

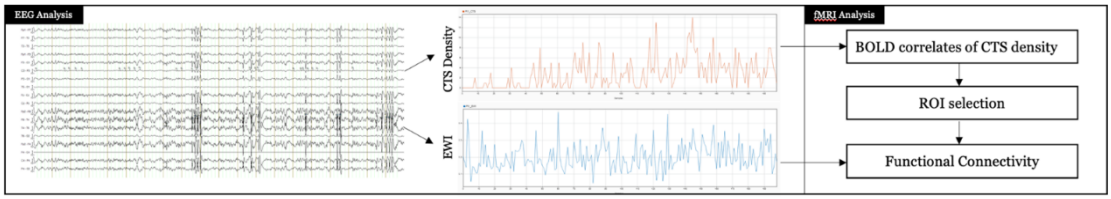

***Figure 11.1**: Workflow of the adopted methodological approach*

11.3. RESULTS

Behavioural Data

All the recruited patients completed the EEG-fMRI protocol. No subject's head motion exceeding 3mm of translation or 3◦ of rotation. All EEG studies were recorded during resting quiet wakefulness. No spindles and/or K complexes were observed. 23 patients were right-handed (Oldfield, 1971).

Disease's duration (in months) ranged between 0 and 64 months (mean, 24 months; median, 18 months). The mean full-scale IQ was equal to 96.5 ± 14.6 (range, 71–124), and mean VIQ = 99 ± 17.7 (range, 66–124). We did not observe any significant correlation between the cognitive measures and the total number of ED recorded during the fMRI experimental session ($p = 0.063$ Pearson's correlation), the CTS density parameter ($p = 0.065$), as well as duration of epilepsy ($p = 0.760$) and age at seizures' onset ($p = 0.864$). **Table 11.1** summarizes the demographic and electroclinical data of the studied population.

***Table 11.1**: Demographic and electroclinical data of SeLECTS.*

ID	EEG scoring	CTS during fMRI (n)	Handedness (Oldfield)	Gender	Age (yo)	Epilepsy Onset (yo)	Epilepsy Duration (months)	AED	IQ	VIQ
1	Wake	348	R	F	7	7	1	Naive	120	124
2	Wake	1153	R	M	6	4	32	VPA	66	N/A
3	Wake/N1	307	R	M	9	7	25.18	Naive	115	N/A
4	Wake	131	R	M	9	5	44.9	LEV+VPA	101	110
5	Wake	77	R	M	9	8	9	LEV+CLB	79	78
6	Wake	158	R	F	13	10	30.8	Naive	106	103
7	Wake/N1	125	R	M	8	8	24	Naive	100	102
8	Wake	51	R	M	11	11	3.9	OXC	104	101
9	Wake	1600	R	M	12	10	24.28	Naive	93	N/A
10	Wake	300	L	M	11	11	2	Naive	97	97
11	Wake	251	R	M	17	13	36	VPA	73	69
12	Wake	1237	R	M	15	8	77	VPA	95	N/A
13	Wake	422	R	M	7	6	0.15	Naive	81	89
14	Wake	497	R	M	7	5	19.3	LEV	109	123
15	Wake/N1	530	R	M	9	7	24	OXC	N/A	N/A
16	Wake	1633	R	M	8	6	15.14	CBZ	89	75
17	Wake	540	R	M	10	7	27.22	LEV	110	91
18	Wake/N1	84	R	F	8	7	12	Naive	95	N/A

19	Wake	1607	R	M	6	6	0.16	Naive	124	115
20	Wake	83	R	M	13	-	-	OXC	95	95
21	Wake/N1	185	R	F	10	-	-	Naive	106	N/A
22	Wake	47	L	M	13	-	-	Naive	84	77
23	Wake/N1	477	R	M	6	2	45.9	Hydr+VPA+CBZ	84	102
24	Wake	83	R	M	10	8	9.22	Naive	100	108
25	Wake	22	R	F	10	-	64	VPA+LEV	75	66

Mean age of epilepsy onset: 7 years; median age: 7 years (range, 2-13 years); mean epilepsy duration: 24 months; median epilepsy duration: 18 months (range, 1-64 months)].

M, male; F, female; R, right; L, left; n, number; yo, years old; VPA, valproic acid; LEV, levetiracetam; OXC, oxcarbazepine; ESM, ethosuximide; Hydr, hydrocortisone; CBZ, carbamazepine. Spikes during fMRI sessions are described based on total number.

11.3.1. Exploration CTS-EWI relationship, EEG analyses

None of the patients showed significant correlation between CTS density and EWI. Specifically, no correlation was found between the normalized and concatenated EWI time-course and CTS-density time-course (r=0.03, p=0.004). Moreover, Local Pearson Correlation did not identify any pairs that were independent globally but correlated locally, regardless of the windows length. It was not possible to identify the directionality between the two signals, no significant leader-follower relationship was identified by means of TLCC. Moreover, neither EWI granger caused the CTS density, neither the other way around. One possible explanation of these negative findings, might be linked to the variance of EWI and CTS density which might be too small to yield a significant effect, considering the short duration of each EEG-fMRI session (8/10 minutes). Thus, to verify our suggestion, for each patient recruited, we checked for clinical EEG acquired outside the MRI scan as a standard clinical practice for diagnostic purpose. Out of twenty-five SeLECTS, for a subset of 9 patients, we had access to the clinical EEG, acquired as a standard clinical practice for diagnostic purpose outside the MRI (Nihon Kohden Neurofax EEG-1200, Mod JE-120). Clinical EEG data (18 channels, 10-20 montage) were then exported in .edf format and reviewed and analysed by means of the BrainVision Analyzer 2.0 software (Brain Products, Munich, Germany). Two experienced electroencephalographers reviewed the EEG recordings independently (AEV, EM) to identify interictal epileptiform abnormalities based on both spatial distribution and topography. When recognized, CTS were marked at peak. An expert in EEG and sleep scoring (AEV) reviewed all the EEG data following the rules published by the AASM (2007). In case of proper sleep (N2-N3 NREM), the EEG was cut after the last N1 epoch, before N2 appeared for the first time. The mean duration of the resulting datasets was on average 17 minutes. **Figure 2.1** describe the trend estimation related to the relationship between EWI and CTS density in one representative SeLECTS patients.

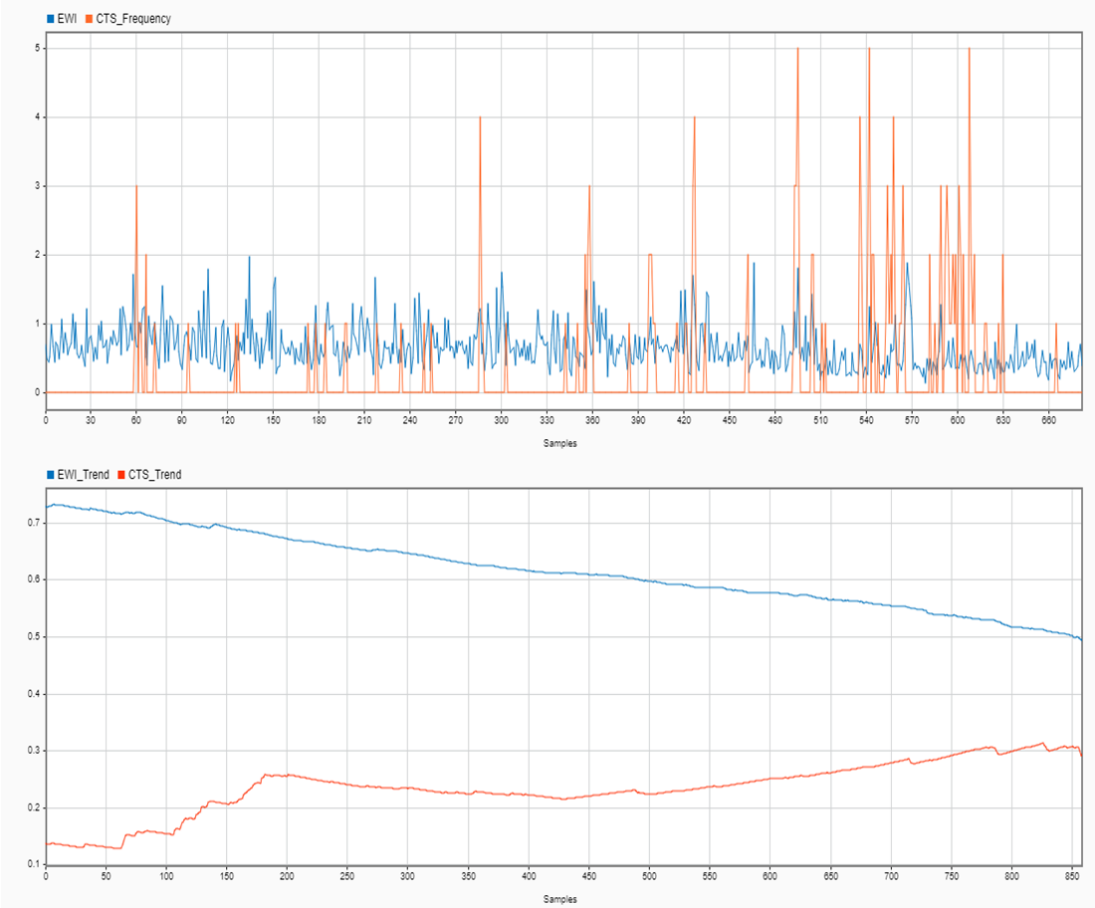

***Figure 11.2**: 20 minutes long Clinical EEG showed an anti-correlated trend between CTS density and EWI. Ordinate = time (1 value every 2 seconds); Abscissa = EWI and CTS density values.*

11.3.2. EEG-fMRI Group Analysis

BOLD Signal Changes Related to CTS density

CTS density group analysis reveals the involvement of a network encompassing the bilateral putamen, sensory-motor cortex (B4), temporal cortex (BA22), left perisylvian areas (BA42), right insula (BA13), left supplementary motor area (BA6), right middle and inferior frontal gyrus (BA8 and BA47) and left cingulate gyrus (BA23) (Figure 3; **Table 11.2**).

***Table 11.2**: Peak coordinates of CTS density group analysis (p<0.001 uncorrected, 10 voxel extent threshold).*

Cluster				**Voxel level**	**MNI Coordinates**		
K	**Brain areas**	**R/L**	**BA**	**Z**	**x**	**y**	**z**
420	Transverse Temporal Gyrus	L	42	4.72	-64	-14	14
	Frontal Lobe, Precentral Gyrus		6/4	3.69	-60	0	16
63	Superior Temporal Gyrus	R	22	3.79	62	4	-4
228	Middle Frontal Gyrus	R	8	3.67	56	10	40
	Precentral Gyrus		4	3.63	50	-4	42
155	Middle Temporal Gyrus	R	21	3.66	62	-48	-4
130	Putamen	R	-	3.56	26	-8	10
41	Superior Frontal Gyrus	L	6	3.53	-6	24	58
57	Insula	R	13	3.51	38	-18	6
51	Putamen	L	-	3.44	-30	-10	8
12	Middle Temporal Gyrus	L	20	3.41	-56	-38	-8
75	Cingulate Gyrus	L	23	3.38	0	-14	28
12	Inferior Frontal Gyrus	R	47	3.35	48	34	-6
61	Precentral Gyrus	L	4	3.33	-42	-2	56

BA, Brodmann area

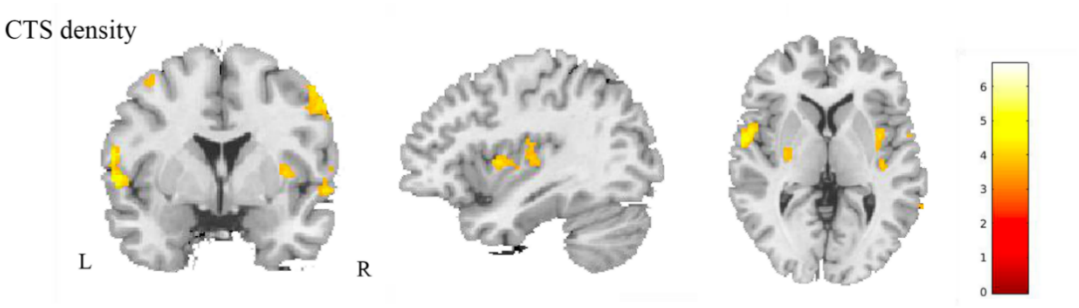

***Figure 11.3**: BOLD-related map of CTS density at group level.*
The clusters of activation are overlaid onto the canonical template as implemented by SPM12. L=Left; R=Right.

Functional Connectivity Analysis using PPI

There was significant functional connectivity between the peak CTS density-related activation in left perisylvian area seed and left frontal operculum (**Table 11.3**; **Figure 11.4**).

***Table 11.3**: Peak coordinates of PPI group analysis*

ROI	Cluster				Voxel level	MNI Coordinates		
	K	Brain areas	R/L	BA	Z	x	y	z
L Perisylvian	34	Inferior Frontal Lobe	L	47/11	3.39	-34	24	-14

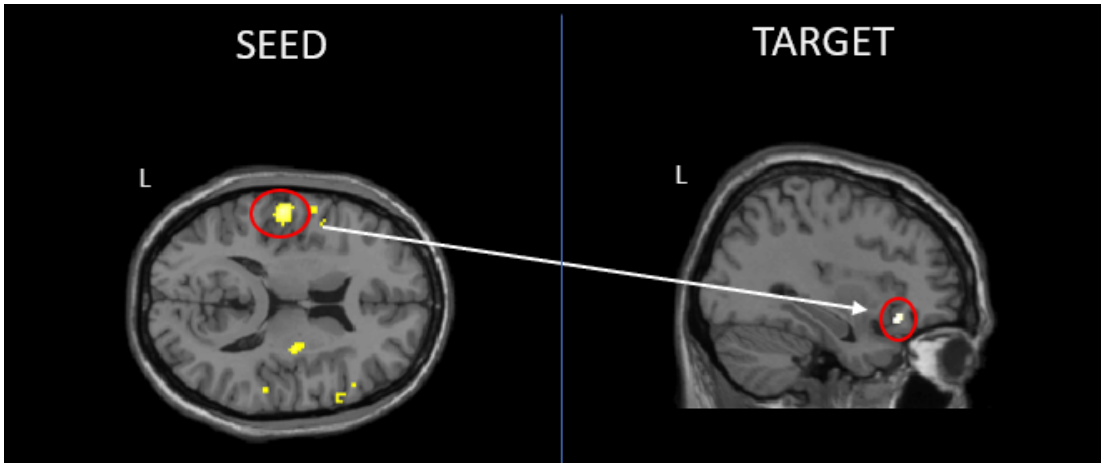

***Figure 11.4**: BOLD-related map of PPI at group level.*
The clusters of activation are overlaid onto the canonical template as implemented by SPM12. L=Left

11.4. DISCUSSION

The present report is, to our knowledge, the first study that explore the relationship between CTS generated networks and drowsiness in a homogenous population of SeLECTS using an EEG-fMRI approach. We parameterized the fluctuations of wakefulness by adopting a multispectral EEG index (i.e. EWI) already applied with similar purposes in healthy controls who exhibit signs of drowsiness (N1 NREM) but not deep sleep during EEG recordings (Knaut et al., 2019). Fluctuations in wakefulness are in fact derived from EEG features (a ratio of linear combinations of different frequency band powers, including topographic information) thought to gradually change with increasing or decreasing wakefulness.

Our analyses provide two main results: a) EWI fluctuations and CTS density appear to be independent from each other when observed over a short time period (8/10 minutes). By contrary, when longer recordings are considered (longer than 15 minutes), EWI fluctuations and CTS density exhibit an anticorrelated trend (i.e. when the frequency of spikes shows a positive trend,

EWI level shows a negative trend); b) the relationship between the brain circuitries involved in the generation and modulation of CTS frequency and drowsiness relies on the engagement of the left frontal operculum, a region mainly associated with speech and reading and other essential communication functions.

11.4.1. EWI fluctuation and CTS density: insight from the EEG analysis

The exploration of the relationship between EWI and CTS density didn't reveal any fined grained dynamics, as they did not exhibit any correlation, cross-correlation, or Granger causality. However, when longer portion of the time series were considered, it was possible to appreciate an anticorrelated trend between them. This may be due to the fact that, in longer routinary clinical recordings, patients actually fell asleep reaching deeper sleep stages (N2, N3) and the signal was cut after the last N1 epoch, before N2 appeared for the first time. In awake/drowsy subjects, not falling asleep, the variance of EWI might have been too small to yield a significant direct effect on CTS density measure. Therefore, the covariation of EWI and CTS density seems to be a net effect of a gross state change and not high local synchrony. This can be seen in analogy to the described tonic firing mode of thalamic neurons during wakefulness versus the more burst-like activity during deeper sleep (Weyand et al., 2001). Thalamic activity, in fact, varies with early changes of wakefulness (Knaut et al., 2019), as a result of a net change in state of vigilance (wakefulness versus sleep) and not a continuous gradual shifting (Knaut et al., 2019).

Analysis of the slight fluctuations between wakefulness and light sleep by means of EEG power bands in 10/8 minutes EEG dataset, may not be sensitive enough for the detection of thalamic mode switches. Our data seem to confirm the need for the involvement of the thalamic mechanisms of synchronization in order to appreciate a direct relationship between CTS

density and EWI (Nobili et al., 2001). In 2013, our group published a case report on a 13-years old with learning disability and bilateral independent CTS, importantly enhanced during NREM sleep. fMRI in wakefulness revealed a focal increment of the BOLD signal in the bilateral sensory-motor cortex while in NREM N2 sleep, a widespread CTS-related cortical-subcortical network over the perisylvian cortex and the thalamus was observed (Mirandola et al., 2013).

11.4.2. EWI fluctuation and CTS density: insight from the fMRI connectivity analysis

Although the relationship between CTS and EWI doesn't seem to be straightforward, the PPI results suggest that either the influence of the CTS-related network on brain activity in the left FO is modulated by different wakefulness-dependent brain states, or the response of the left FO to fluctuations in wakefulness are modulated by activity in the CTS network. Therefore, the left FO may be a key element in the relationship between CTS and wakefulness-dependent brain states.

In fact, given spontaneous fluctuations in wakefulness, SeLECTS displayed increased functional connectivity between the left PN seed and left frontal operculum. Moreover, seeding from the left motor cortex involved functional connectivity with the left middle frontal gyrus and superior temporal gyrus.

A number of imaging studies reported altered connectivity between sensorimotor and left frontal opercolum. Besseling and colleagues (2013a,b,c) revealed a decrease in fMRI resting state connectivity between the left inferior frontal gyrus and motor regions in children with SeLECTS, while another study indicated an increase in regional fMRI homogeneity in left frontal regions (Zeng et al., 2015). We previously described CTS density being related to hemodynamic changes within the language network, likely interfering on the cognitive profile of CECTS (Vaudano et al., 2019). Further, a recent EEG study, despite lacking the spatial resolution of fMRI, described increases in functional

connectivity between left frontal and bicentral electrodes, before and after CTS events (Goad et al., 2022).

11.4.3. Methodological considerations

It has been shown that fluctuations of physiological rhythms can have an impact on the results of EEG-fMRI studies (Tyvaert et al. 2008). In particular, for epileptic spikes, there seems to be a complex relationship between spikes density and arousal or sleep stages, fluctuations of physiological rhythms can be a confounding effect as the response could originate from regions involved in the fluctuation of the arousal level.

Lastly, from a methodological point of view, these results are a good example of how EEG-fMRI can theoretically enhance our understanding of brain function, as a new effect became detectable in the fMRI, even when the original electrophysiological events didn't show any relationship in the time domain. The relationship between EWI and CTS is, in fact, not straightforward as measured by EEG, but, stressing the issue of reciprocal relationships between brain regions by means of fMRI data, it was possible to test whether the regression slope between the seeds in CTS density network and the rest of the brain was modulated by the strength of EWI oscillations.

It goes without saying that this exploration was possible only by characterizing time-relevant changes, as measured by the EEG, in the space domain, as measured by the fMRI.

11.5. CONCLUSION

The study explores the relationship between networks generated by benign epilepsy with centro-temporal spikes (CTS) and drowsiness in a homogenous population of patients using EEG-fMRI approach.

Our findings suggest that fluctuation of wakefulness modulates the connectivity between the brain networks engaged by the CTS occurrence and the anterior language network in CECTS.

Moreover, the exploration of the complex relationship between the CTS density measure and the wakefulness measure suggests the need for a net change in state of vigilance (wakefulness versus sleep) for an anticorrelated trend to emerge.

11.6. REFERENCES

Archer JS, Briellman RS, Abbott DF, Syngeniotis A, Wellard RM, Jackson GD (2003) Benign epilepsy with centro-temporal spikes: spike triggered fMRI shows somato-sensory cortex activity. Epilepsia 44:200–204

Beelke M, Nobili L, Belietto MG, et al. Relationship of sigma activity to sleep interictal epileptic discharges: a study in children affected by benign epilepsy with occipital paroxysms. Epilepsy Res 2000;40(2-3):179–86.

Besseling RMH, Jansen JFA, Overvliet GM, van der Kruijs SJM, Ebus SCM, de Louw A,Hofman PAM, Vles JSH, Aldenkamp AP, Backes WH, Wilke M (2013a) Reduced structural connectivity between sensorimotor and language areas in rolandicepilepsy. PLoS ONE;8(12):e83568.

Besseling RMH, Jansen JFA, Overvliet GM, van der Kruijs SJM, Vles JSH, Ebus SCM, Hofman PAM, Louw Ad, Aldenkamp AP, Backes WH. (2013b) Reduced functional integration of the sensorimotor and language network in rolandic epilepsy. NeuroImage Clin 2:239–46.

Besseling RMH, Overvliet GM, Jansen JFA, van der Kruijs SJM, Vles JSH, Ebus SCM, Hofman PAM, de Louw AJA, Aldenkamp AP, Backes WH (2013c) Aberrant functional connectivity between motor and language networks in rolandic epilepsy. Epilepsy Res 107(3):253–62.

Besseling RMH, Jansen JFA, Overvliet GM, van der Kruijs SJM, Ebus SCM, de Louw AJA, Hofman PAM, Aldenkamp AP, Backes WH. Delayed convergence between brain network structure and function in rolandic epilepsy. Front Hum Neurosci 2014;8. https://doi.org/10.3389/fnhum.2014.00704.

Bonelli SB, Thompson PJ, Yogarajah M et al. (2012) Imaging language networks before and after anterior temporal lobe resection: Results of a longitudinal fMRI study. Epilepsia, 53(4):639–650, 2012 doi: 10.1111/j.1528-1167.2012.03433.x

Boor S, Vucurevic G, Pfleiderer C, Stoeter P, Kutschke G, Boor R (2003) EEG-related functional MRI in benign childhood epilepsy with centrotemporal spikes. Epilepsia 44:688–692

Boor R, Jacobs J, Bauermann T, Scherg M, Boor S, Vucurevic G, Kutschke G, Stoeter P (2007) Combined spike-related functional MRI and multiple source analysis in the non-invasive spike localization of benign rolandic epilepsy. Clin Neurophysiol 118(4):901–909

Clemens B, Majoros E (1987) Sleep studies in benign epilepsy of childhood with rolandic spikes. II. Analysis of discharge frequency and its relation to sleep dynamics Epilepsia 28(1):24-7. doi: 10.1111/j.1528-1157.1987.tb03617.x.

Deonna T, Zesiger P, Davidoff V, Maeder M, Mayor C, Roulet E, et al. (2000) Benign partial epilepsy of childhood: a longitudinal neuropsychologica and EEG study of cognitive function. Dev Med Child Neurol. 42(09):595–603.

Friston KJ (1994) Functional and effective connectivity in neuroimaging: A synthesis. Human Brain Mapping. 2:56-78 https://doi.org/10.1002/hbm.46002010

Friston KJ, Williams S, Howard R, Frackowiak RS, Turner R. (1996) Movement related effects in fMRI time-series. Magn Reson Med. 35:346–55. doi: 10.1002/mrm.1910350312

Friston, K., Buechel, C., Fink, G., Morris, J., Rolls, E., & Dolan, R. (1997). Psychophysiological and modulatory interactions in neuroimaging. Neuroimage, 6, 218–229.

Goad BS, Lee-Messer C, He Z, Porter BE, Baumer FM (2022) Connectivity increases during spikes and spike-free periods in self-limited epilepsy with centrotemporal spikes. Clinical Neurophysiology 144:123–134. https://doi.org/10.1016/j.clinph.2022.09.015

Goldberg-Stern H, Gonen OM, Sadeh M, Kivity S, Shuper A, Inbar D. (2010) Neuropsychological aspects of benign childhood epilepsy with centro-temporal spikes. Seizure 19(1):12–6

Halász P, Kundra O, Rajna P, Pál I, Vargha M (1979) Micro-arousals during nocturnal sleep. Acta Physiologica Academiae Scientiarum Hungaricae, 54(1):1-12.

Halász P, Kelemen A, Rosdy B, Rásonyi G, Clemens B, Szűcs A (2020) Perisylvian epileptic network revisited. Seizure: European Journal of Epilepsy. 65: 31–41. https://doi.org/10.1016/j.seizure.2018.12.003

Ibrahim GM, Cassel D, Morgan BR, Smith ML, Otsubo H, Ochi A, et al. (2014) Resilience of developing brain networks to interictal epileptiform discharges is associated with cognitive outcome. Brain J Neurol. 137:2690–702. doi: 10.1093/brain/awu214

Knaut P, von Wegner F, Morzelewski A, Laufs H (2019) EEG-correlated fMRI of human alpha (de-)synchronization. Clinical Neurophysiology. 130:1375–1386. https://doi.org/10.1016/j.clinph.2019.04.715

Kim, J., & Horwitz, B. (2008). Investigating the neural basis for fMRI-based functional connectivity in a blocked design: Application to interregional correlations and psycho-physiological interactions. Magnetic Resonance Imaging, 26, 583–593.

Koutroumanidis M, Arzimanoglou A, Caraballo R, Goyal S et al. (2017) The role of EEG in the diagnosis and classification of the epilepsy syndromes: a tool for clinical practice by the ILAE Neurophysiology Task Force (Part 1) Epileptic Disorders 19(3):233-298https://doi.org/10.1684/epd.2017.0935

Koutroumanidis M, Arzimanoglou A, Caraballo R, Goyal S et al. (2017) The role of EEG in the diagnosis and classification of the epilepsy syndromes: a tool for clinical practice by the ILAE Neurophysiology Task Force (Part 2) Epileptic Disorders 19(3):233-298https://doi.org/10.1684/epd.2017.0935

Lengler U, Kafadar I, Neubauer BA, Krakow K (2007) fMRI correlates of interictal epileptic activity in patients with idiopathic benign focal epilepsy of childhood. A simultaneous EEG-functional MRI study. Epilepsy Res 75:29–38

Li R, Ji GJ, Yu Y, Ding MP, Tang YL, Chen H, Liao W (2017) Epileptic discharge related functional connectivity within and between networks in benign epilepsy with centrotemporal spikes. Int J Neural Syst 27:1750018

Li R, Wang L, Chen H, Guo X, Liao W, Tang YL, Chen H (2019) Abnormal dynamics of functional connectivity density in children with benign epilepsy with centrotemporal spikes. Brain Imaging Behav 13:985–994

Masterton RA, Harvey AS, Archer JS, Lillywhite LM, Abbott DF, Scheffer IE, Jackson GD (2010) Focal epileptiform spikes do not show a canonical BOLD response in patients with benign rolandic epilepsy (BECTS). Neuroimage 51:252–260

Mirandola L, Cantalupo G, Vaudano AE, Avanzini P, Ruggieri A, Pisani F, et al. (2013) Centrotemporal spikes during NREM sleep: The promoting action of thalamus

revealed by simultaneous EEG and fMRI coregistration. Epilepsy Behav Case Rep. 1:106–9. doi: 10.1016/j.ebcr.2013.06.005

Monjauze C, Broadbent H, Boyd SG, Neville BGR, Baldeweg T. (2011) Language deficits and altered hemispheric lateralization in young people in remission from BECTS. Epilepsia. 52(8):e79–83

Nobili, L, Ferrillo, F, Baglietto, MG, Beelke, M, De Carli, F, De Negri, E, Schiavi, G, Rosadini, G, De Negri, M,1999a. Relationship of sleep interictal epileptiform discharges to sigma activity (12–16 Hz) in Benign Epilepsy of Childhood with Rolandic Spikes. Clin. Neurophysiol. 110, 39–46.

Nobili, L, Ferrillo, F, Baglietto, MG, Beelke, M, De Carli, F, De Negri, E, Rosadini, G, De Negri, M, 1999. Modulation sleep interictal epileptiform discharges in partial epilepsy of childhood. Clin. Neurophysiol. 110, 839– 845.

Nobili, L, Ferrillo, F, Baglietto, MG, Beelke, M, De Carli, F, De Negri, E, Rosadini, G, De Negri, M, 1999b. Modulation sleep interictal epileptiform discharges in partial epilepsy of childhood. Clin. Neurophysiol. 110, 839– 845.

Nobili L, Baglietto MG, Beelke M, De Carli F, De Negri E, Gaggero R, Rosadini G, Veneselli E, Ferrillo F (2001) Distribution of epileptiform discharges during nREM sleep in the CSWSS syndrome: relationship with sigma and delta activities. Epilepsy Research 44:119–128

Northcott E, Connolly AM, McIntyre J, Christie J, Berroya A, Taylor A, et al. (2006) Longitudinal assessment of neuropsychologic and language function in children with benign rolandic epilepsy. J Child Neurol.21(6):518–22.

Olbrich S, Mulert C, Karch S, Trenner M, Leicht G, Pogarell O, Hegerl U (2009) EEG-vigilance and BOLD effect during simultaneous EEG/fMRI measurement. Neuroimage 45:319–332

O'Reilly, J. X., Woolrich, M. W., Behrens, T., Smith, S. M., & Heidi, J.-B. (2012). Tools of the trade: Psychophysiological interactions and functional connectivity. Social Cognitive and Affective Neuroscience, 7, 604–609.

Parmeggiani L, Guerrini R. (1999) Idiopathic partial epilepsy: electroclinical demonstration of a prolonged seizure with sequential rolandic and occipital involvement. Seizure spread due to regional susceptibility? Epileptic Disord. 1(1):35–40

Şanlıdağ B, Köken ÖY et al. (2020) Benign epilepsy with centrotemporal spikes: Is there a thalamocortical network dysfunction present? Seizure 79:44-48 https://doi.org/10.1016/j.seizure.2020.04.003

Siniatchkin M, Moeller F, Jacobs J, Stephani U, Boor R, Wolff S, Jansen O, Siebner H, Scherg M (2007a) Spatial filters and automated spike detection based on brain topographies improve sensitivity of EEG-fMRI studies in focal epilepsy. Neuroimage 37:834–843

Siniatchkin M, van Baalen A, Jacobs J, Moeller F, Moehring J, Boor R, Wolff S, Jansen O, Stephani U (2007b) Different neuronal networks are associated with spikes and slow activity in Hypsarrhythmia. Epilepsia 48:2312–232

Tagliazucchi E, Laufs H (2014) Decoding wakefulness levels from typical fMRI resting-state data reveals reliable drifts between wakefulness and sleep. Neuron 82(3):695–708

Tononi G, Cirelli C. (2003) Sleep and synaptic homeostasis: a hypothesis. Brain Research Bull. 62:143–50. doi: 10.1016/j.brainresbull.2003.09.004

Tovia E, Goldberg-Stern H, Ben Zeev B, Heyman E, Watemberg N, Fattal-Valevski Kramer U (2011)The prevalence of atypical presentations and comorbidities of benign childhood epilepsy with centrotemporal spikes. Epilepsia 52:1483–8

Tyvaert L, Levan P, Grova C, Dubeau F, Gotman J (2008) Effects of fluctuating physiological rhythms during prolonged EEG-fMRI studies. Clin Neurophysiol 119(12):2762–2774

Vaudano AE, Avanzini P, Cantalupo G, Filippini M, Ruggieri A, Talami F et al. (2019) Mapping the Effect of Interictal Epileptic Activity Density During Wakefulness on Brain Functioning in Focal Childhood Epilepsies With Centrotemporal Spikes. Frontiers in Neurology. 10:1316. doi: 10.3389/fneur.2019.01316

Verrotti A, Filippini M, Matricardi S, Agostinelli MF, Gobbi G. (2014) Memory impairment and Benign Epilepsy with centrotemporal spike (BECTS): a growing suspicion. Brain Cogn 84(1):123–31

Weyand TG, Boudreaux M, Guido W. (2001) Burst and tonic response modes in thalamic neurons during sleep and wakefulness. J Neurophysiol 85(3):1107–18

Xiao F, An D, Lei L, Chen S, Wu X, Yang T, Ren J, Gong Q, Zhou D (2016) Real-time effects of centrotemporal spikes on cognition in rolandic epilepsy: an EEG-fMRI study. Neurology 86:544–551

Zeng H, Ramos CG, Nair VA, Hu Y, Liao J, La C, Chen Li, Gan Y, Wen F, Hermann B, Prabhakaran V (2015) Regional homogeneity (ReHo) changes in new onset versus chronic benign epilepsy of childhood with centrotemporal spikes (BECTS): A resting state fMRI study. Epilepsy Res 116:79–85.